

**PREPARATION, CHARACTERIZATION AND CATALYTIC APPLICATIONS OF  
PILLARED CLAY ANALOGUES AND CLAY-POLYMER COMPOSITE MATERIALS**

***A THESIS***

*Submitted by*

**PURABI KAR**

*for the award of the degree*

*of*

**DOCTOR OF PHILOSOPHY**



**DEPARTMENT OF CHEMISTRY  
NATIONAL INSTITUTE OF TECHNOLOGY, ROURKELA  
ROURKELA - 769 008, ODISHA**

**NOVEMBER 2014**

*Dedicated to*  
**My PARENTS**

**Dr. Braja Gopal Mishra**  
**Associate Professor**  
**DEPARTMENT OF CHEMISTRY**  
**NIT, Rourkela-ODISHA**



---

## **THESIS CERTIFICATE**

This is to certify that the thesis entitled “**PREPARATION, CHARACTERIZATION AND CATALYTIC APPLICATIONS OF PILLARED CLAY ANALOGUES AND CLAY-POLYMER COMPOSITE MATERIALS**” submitted by **Purabi Kar** to the National Institute of Technology, Rourkela for the award of degree of Doctor of Philosophy is a bonafide record of research work carried out by her under my supervision. I am satisfied that the thesis has reached the standard fulfilling the requirements of the regulations relating to the nature of the degree. The contents of this thesis in full or in parts have not been submitted to any other Institute or University for the award of any degree or diploma.

Rourkela-769 008

Research Guide

Date:

**(Dr. B. G. Mishra)**

# ACKNOWLEDGEMENT

During my research period I came across with a great number of humble and wonderful people whose efforts helped me in many ways. I devote my sincere thanks to all of them.

I take this opportunity to express my sincere gratitude to all of them.

First and foremost acknowledgement goes to my research mentor **Prof. Braja Gopal Mishra** for his endless and untiring effort, constant encouragement and valuable suggestions. I feel fortunate myself as I got the opportunity to work under him. His vast scientific knowledge and technical suggestions had given a proper direction to my research work. I express my deep obligations to him as his patience and encouragement had supported me a lot and nourished my enthusiasm. Without his immense effort and guidance this work would not be accomplished. I express my sincere thanks to his family members for their hospitality and care during my stay.

Besides my advisor, I express my deep sense of gratitude to all of my doctoral committee members **Prof. R. K. Patel** (Chairman), **Prof U. Subuddhi**, **Prof. S. Patel** and **Prof. S.K. Pratihar** for their valuable, constructive and friendly advice. I convey my heartfelt thanks to **Prof. R. K. Patel** (Chairman DSC) for his useful suggestions.

I am very much thankful to Head of the Department, **Prof. N. Panda** for providing the necessary infrastructure and facilities to carry out this work.

I am indebted to all the faculty members and staff of Department of Chemistry for their essential help during my research work.

I am sincerely obliged to **Prof. S. K. Pratihar**, HOD, Department of Ceramic Engineering, NIT Rourkela and **Prof. D. K. Bishoyi**, HOD, Department of Physics for allowing me to avail the instrumental facilities for analytical purpose.

I am using this opportunity to thank **Pratap Behera** for helping me in acquisition of NMR data of the synthesized organic compounds.

I am very much thankful to all labmates, **Dr. Satish Samantaray, Sagnika Pradhan** and **Jagyan Prakash Bhoi** for their support and co-operation during my work as well as during my stay period in the lab. I am deeply indebted to Dr.Satish Samantaray for his guidance during the initial stages of my experimental work.

I am very much pleased to express my heartfelt gratitude to my friends **Swati, Pranati, Lipeeka, Subhraseema, Prakash, Sandip, Saswati, Dinesh, Raghavendra** and **Jyoti** for their encouragement and companionship.

I am indebted and cannot express enough obligations to my parents, brother and my other beloved family members for their constant support and inspiration that boosted my energy during my work.

Last but not the least I am glad to acknowledge Department of Chemistry, NIT Rourkela for giving me infrastructure and other facilities needed for the work. I am also thankful to NIT Rourkela for providing me the financial help.

**Purabi Kar**

## ABSTRACT

**KEYWORDS:** *Clay, Cr-Pillared clay, Al-pillared clay, Zr-pillared clay, Xanthene derivatives, dihydropyridines, tetrahydropyridines, hexahydropyrimidines, hydrodehalogenation, multicomponent condensations, bimetallic particles, FE-SEM, XRD, FTIR, Microwave, Solventfree synthesis*

Cr-pillared montmorillonite clay (Cr-P) was prepared by intercalation of chromium oxyhydroxy cationic clusters into the clay interlayer and subsequent thermal activation. The Cr-P material was characterized by XRD, FTIR, UV-Vis and sorptometric techniques. The expansion in the clay lattice as a result of pillaring was confirmed from the XRD study. The UV-Vis study of the pillared clay revealed the presence of Cr<sup>3+</sup> species as Cr<sub>2</sub>O<sub>3</sub> nanoclusters inside the clay interlayer. The IR study was employed to show the presence of acidic and non-acidic hydroxyl groups in the pillared clays. The Cr-P material was used as an efficient heterogeneous catalyst for the synthesis of benzoxanthenes and octahydroxanthenes. The benzoxanthenes were synthesized by condensation of two mole of β-naphthol with one mole of benzaldehyde. Similarly, the octahydroxanthenes were synthesized by the condensation of two mole of dimedone with one mole aryl aldehydes. Structurally diverse xanthene derivatives were synthesized under solvent free conditions and microwave irradiation using Cr-P as heterogeneous catalyst. The Cr-P clay was used further as support for dispersion of silicotungstic acid (STA). The STA particles were dispersed in the micropores of Cr-P clay by wet impregnation method. The synthesized materials were characterized by XRD, FTIR, UV-Vis, sorptometric, TGA, SEM and TEM techniques. IR and UV-Vis study illustrates the structural integrity of the STA particles in the micropores of the pillared clay. N<sub>2</sub> adsorption/ desorption shows that the synthesized materials are microporous in nature. The catalytic activity of the STA/Cr-P materials was evaluated for synthesis of 1,4-dihydropyridines (DHPs) by multicomponent reaction of aldehydes/chalcones, ethylacetoacetate and ammonium acetate. Structurally diverse DHPs are prepared by using aryl aldehydes and chalcones as starting materials.

A series of Zr-pillared clay (Zr-P)-polyphosphoric acid (PPA) and Zr-pillared clay-sulfonated polyvinyl alcohol (SPVA) composites were synthesized by adopting different preparative strategies. Initially, the polymeric species were intercalated to the clay matrix with and without the use of structure expanding agent (CTAB). In case of PPA based composites, the PPA-clay was pillared with Zr-polycation to form the composite materials. In an alternate approach, Zr-pillared clay was synthesized by insertion of Zr-polycation, which was subsequently used for

dispersion of PPA moiety. For composites involving SPVA polymer, two set of materials were synthesized by insertion of the sulfonated PVA and PVA species into the interlayer space of clay and Zr-P material. The PVA containing materials were sulfonated in situ to generate the SPVA polymers inside the interlayer space. The synthesized composites are characterized by XRD, TGA, FTIR, UV-vis, EDX, FE-SEM and sorptometric techniques. XRD study indicated an expansion in the clay structure after intercalation of polymeric species as well as the Zr-polycations. The FTIR spectra exhibited characteristic vibrational features of the clay sheet and the polymeric moieties indicating structural stability of the composite materials. The phosphorous and sulfur content in the composite samples was analyzed using EDX study. FE-SEM study indicated morphological changes upon intercalation of polymeric species and Zr-polycations to the clay matrix. The catalytic activity of the Zr-P-PPA composite catalysts was examined for the synthesis of tetrahydropyridines by one pot multicomponent condensation of  $\beta$ -dicarbonyl compounds, substituted anilines and substituted benzaldehydes. The ZrP-SPVA materials were used as efficient catalyst for synthesis of hexahydropyrimidines by multicomponent condensation of  $\beta$ -dicarbonyl compounds, substituted aniline and formaldehyde. Structurally diverse tetrahydropyridines and hexahydropyrimidines were obtained in high yield and purity using the Zr-P-polymeric composite materials.

The Al-pillared clay was prepared by insertion of  $[\text{AlO}_4\text{Al}_{12}(\text{OH})_{24}(\text{H}_2\text{O})_{12}]^{7+}$  clusters into clay interlayer and subsequent thermal activation. Palladium (Pd) and Palladium-Nickel (Pd-Ni) nanoparticles dispersed in the micropores of Al-pillared clay was prepared by chemical reduction method. The pillared clay supported systems (Pd/Al-P and Pd-Ni/Al-P) were characterized using XRD, IR, UV-Vis, SEM, TEM and sorptometric technique. The expansion of the interlayer space as a result of pillaring was noted for Pd-M/Al-P system from the XRD study. The TEM study of the supported system indicated well dispersion of the metallic species with particle size in the range of 5–30 nm. The supported Pd and Pd-Ni bimetallic nanoparticles were used as an efficient heterogeneous catalyst for the hydrodehalogenation of halogenated organics under hydrogen transfer condition using hydrazine hydrate as hydrogen donating agent. The effect of various reaction parameters such as temperature, time, and nature of support, type of hydrogen transfer agents and functionality of substrate was studied in details. The catalytic study clearly indicated superior catalytic activity of the supported Pd based metallic systems in presence of hydrazine hydrate as hydrogen donating agent. The Al-pillared clay as support influences the dispersion and catalytic activity of the supported Pd nanoparticles.

## TABLE OF CONTENTS

	<b>Page No.</b>
<b>ACKNOWLEDGEMENTS</b> .....	i
<b>ABSTRACT</b> .....	iii
<b>TABLE OF CONTENTS</b> .....	v
<b>LIST OF TABLES</b> .....	xi
<b>LIST OF FIGURES</b> .....	xiii
<b>ABBREVIATIONS</b> .....	xvii
<b>NOTATIONS</b> .....	xix
<b>CHAPTER 1            INTRODUCTION</b>	
1.1        General Introduction.....	1
1.2        Structure and classification of clay materials.....	2
1.3        Acidic and catalytic properties of clay materials.....	6
1.4        Disadvantages of clay materials as catalysts.....	9
1.5        Modification of clay materials.....	10
1.6        Pillaring of clay by inorganic polycations.....	11
1.7        Al-Pillared clays (Al-PIL).....	15
1.8        Effect of synthetic conditions on the property of Al-pillared clay.	18
1.9        Catalytic applications of Al-Pillared clay.....	21
1.10       Al-Pillared clay as support.....	23
1.11       Zr-Pillared clay.....	30
1.12       Zr-Pillared clay as catalyst and support.....	33
1.13       Cr-Pillared clays.....	37
1.14       Objectives of the present study.....	42



## CHAPTER 2 MATERIALS AND METHODS

2.1	Preparation of clay based catalytic materials.....	45
2.1.1.	Preparation of Cr-Pillared clay (Cr-P) based catalytic materials...	45
2.1.1.1.	Preparation of Cr-Pillared clay (Cr-P).....	45
2.1.1.2	Preparation of silicotungstic acid dispersed in the matrix of Cr-Pillared clay (STA/Cr-P).....	46
2.1.2	Preparation of Zr-Pillared clay based catalytic materials.....	46
2.1.2.1	Preparation of Zirconia Pillared clay (Zr-P).....	46
2.1.2.2	Preparation of polyphosphoric acid-clay and polyphosphoric acid-Zr-P composite materials.....	47
2.1.2.2.1	Preparation of polyphosphoric acid dispersed in Zr-pillared clay matrix (ZrP-PPA).....	47
2.1.2.2.2	Preparation of polyphosphoric acid dispersed in parent clay matrix (PPA-Clay).....	47
2.1.2.2.3	Preparation of polyphosphoric acid intercalated clay using CTAB as a structure expansion agent (PPA-CTAB-Clay).....	47
2.1.2.2.4	Preparation of polyphosphoric acid-clay composite pillared with Zr-polycations (PPA-ZrP).....	48
2.1.2.3	Preparation of sulfonated polyvinyl alcohol-clay and sulfonated polyvinyl alcohol-Zr-P composite materials.....	48
2.1.2.3.1	Preparation of sulfonated polyvinyl alcohol (SPVA).....	48
2.1.2.3.2	Preparation of sulfonated PVA-clay composite material (Clay-SP).....	49
2.1.2.3.3.	Preparation of SPVA-clay composite using CTAB as a structure expansion agent (CTAB-Clay-SP).....	49
2.1.2.3.4	Preparation of SPVA-Zr-Pillared clay composite material (ZrP-SP).....	50
2.1.2.3.5	Preparation of PVA intercalated clay followed by in situ sulfonation (Clay-PIS).....	50
2.1.2.3.6	Preparation of PVA intercalated CTAB-Clay followed by in situ sulfonation (CTAB-Clay-PIS).....	50
2.1.2.3.7	Preparation of PVA dispersed in Zr-Pillared clay matrix followed by in situ sulfonation (ZrP-PIS).....	51

2.1.4	Preparation of Al-Pillared clay based catalytic materials.....	51
2.1.4.1	Preparation of Al-Pillared clay (Al-P).....	51
2.1.4.2	Preparation of palladium nanoparticles supported over Al-Pillared clay (Pd/Al-P).....	52
2.1.4.3	Preparation of palladium based bimetallic nanoparticles supported over Al-Pillared clay (Pd-M/Al-P where M= Cu and Ni).....	52
2.2	Characterization methods.....	53
2.2.1	Powder X-Ray diffraction (XRD).....	53
2.2.2	Infra-red spectroscopy (FTIR).....	53
2.2.3	UV-VIS spectroscopy.....	54
2.2.4	Thermogravimetric analysis.....	54
2.2.5	Sorptometric Studies.....	54
2.2.6	Scanning electron microscopy (SEM).....	54
2.2.7	Field emission scanning electron microscopy (FE-SEM).....	55
2.2.8	Transmission electron micrographs (TEM).....	55
2.2.9	Surface acidity measurement.....	55
2.2.9.1	Non-aqueous titration method.....	55
2.2.9.2	TG analysis of adsorbed n-Butylamine.....	55
2.2.10	Gas chromatography (GC).....	56
2.2.11	NMR spectroscopy.....	56
2.3	Catalytic activity study.....	56
2.3.1	Synthesis of octahydroxanthenes catalyzed by Cr-P material.....	56
2.3.2	Synthesis of benzoxanthenes catalyzed by Cr-P material.....	57
2.3.3	Synthesis of 1,4-dihydropyridines catalyzed by STA/Cr-P material.....	57
2.3.4	Synthesis of tetrahydropyridines catalyzed by PPA-ZrP composite materials.....	58

2.3.5	Synthesis of hexahydropyrimidines catalyzed by SPVA–Zr-P composite materials.....	58
2.3.6	Hydrodehalogenation (HDH) of haloenated aromatic compounds catalyzed by Pd/Al-P and Pd-M/Al-P (M= Cu and Ni) materials.....	59

### **CHAPTER 3 CATALYTIC APPLICATIONS OF Cr-PILLARED CLAY BASED MATERIALS**

#### **PART A: Synthesis of xanthene derivatives catalyzed by Cr-pillared clay**

3.1	Introduction.....	61
3.2	Results and Discussion.....	65
3.2.1	XRD Study.....	65
3.2.2	FTIR Study.....	66
3.2.3	UV-VIS Study.....	68
3.2.4	Thermogravimetric analysis.....	70
3.2.5	Sorptometric Study.....	71
3.2.6	Catalytic activity Study.....	72
3.2.6.1	Synthesis of octahydroxanthenes.....	72
3.2.6.2	Synthesis of benzoxanthenes.....	78

#### **PART B: Synthesis of 1,4-dihydropyridines catalyzed by silicotungstic acid particles dispersed over Cr-Pillared clays**

3.3	Introduction.....	83
3.4	Results and Discussion.....	87
3.4.1	XRD Study.....	87
3.4.2	FT-IR Study.....	88
3.4.3	UV-VIS Study.....	89
3.4.4	Thermogravimetric analysis.....	91
3.4.5	Sorptometric Study.....	92
3.4.6	SEM Study.....	93

3.4.7	TEM Study.....	94
3.4.8	Catalytic activity for the synthesis of 1,4-dihydropyridines.....	95
3.5	Conclusions.....	104

**CHAPTER 4                    SYNTHESIS AND CATALYTIC APPLICATIONS OF Zr-PILLARED CLAY-POLYMER COMPOSITE MATERIALS**

**PART A:        Synthesis of tetrahydropyridines using polyphosphoric acid–Zr-Pillared clay composite materials as catalyst**

4.1	Introduction.....	106
4.2	Results and Discussion.....	108
4.2.1	XRD Study.....	108
4.2.2	FTIR Study.....	111
4.2.3	UV-VIS Study.....	113
4.2.4	Thermogravimetric analysis.....	114
4.2.5	FE-SEM Study.....	116
4.2.6	Catalytic studies for synthesis of tetrahydropyridines.....	118

**PART B:        Synthesis of hexahydropyrimidines using Zr-P-sulfonated PVA composite as heterogeneous catalyst**

4.3	Introduction.....	127
4.4	Results and Discussion.....	131
4.4.1	XRD Study.....	131
4.4.2	FT-IR Study.....	135
4.4.3	UV-VIS Study.....	137
4.4.4	FE-SEM Study.....	139
4.4.5	Catalytic studies for synthesis of hexahydropyrimidines.....	141
4.5	Conclusions.....	148

**CHAPTER 5 CATALYTIC APPLICATION OF Pd AND Pd BASED BIMETALLIC PARTICLES SUPPORTED ON Al-PILLARED CLAY**

**PART A: Hydrodehalogenation of halogenated phenols over Pd/Al-Pillared clay**

5.1	Introduction.....	150
5.2	Results and Discussion.....	152
5.2.1	XRD Study.....	152
5.2.2	FTIR Study.....	154
5.2.3	Sorptometric Study.....	155
5.2.4	FE-SEM Study.....	156
5.2.5	TEM Study.....	157
5.2.6	Catalytic activity of Pd/Al-P materials for hydrodehalogenation (HDH) reaction.....	158

**PART B: Hydrodehalogenation of halogenated anilines over Pd-M (M= Cu and Ni)/Al-Pillared clay**

5.3	Introduction.....	165
5.4	Results and Discussions.....	167
5.4.1	XRD Study.....	167
5.4.2	UV-VIS Study.....	168
5.4.3	FE-SEM Study.....	170
5.4.4	TEM Study.....	171
5.4.5	Catalytic activity for hydrodehalogenation of organic compounds.....	172
5.5	Conclusions.....	179

**CHAPTER 6 SUMMARY AND CONCLUSIONS ..... 180**

**REFERENCES..... 184**

**LIST OF PUBLICATIONS..... 208**

## LIST OF TABLES

Table	Title	Page No.
1.1	Classification of clay minerals.....	5
1.2	Different types of pillaring species used for preparation of pillared clays.....	13
1.3	Properties of the parent clay before and after pillaring .....	14
1.4	Catalytic applications of Al-pillared clay based catalytic materials.	28
1.5	Catalytic applications of Zr-pillared clay based catalytic materials.	36
1.6	Catalytic applications of Cr-pillared clay based catalytic materials.	41
3.1	Physicochemical characteristics of parent clay and calcined Cr-P material.....	65
3.2	Calcined Cr-P catalyzed synthesis of octahydroxanthenes under solvent free conditions and microwave irradiation .....	74
3.3	Comparison of the catalytic activity of Cr-P with other catalytic system reported in literature for synthesis of octahydroxanthenes...	75
3.4	Cr-P catalyzed synthesis of benzoxanthenes under solvent free condition and microwave irradiation .....	80
3.5	Comparison of the catalytic activity of Cr-P with other catalytic systems reported in literature for synthesis of benzoxanthenes.....	81
3.6	Physicochemical characteristics and catalytic activity of different clay materials studied for the synthesis of 1,4-Dihydropyridines by multicomponent condensation of benzaldehyde, ethylacetoacetate and NH <sub>4</sub> OAc.....	97
3.7	STA/Cr-P catalyzed one pot synthesis of dihydropyridines by condensation of arylaldehydes (1mmol), ethylacetoacetate (2 mmol) and ammonium acetate (1 mmol).....	100
3.8	STA/Cr-P catalyzed one pot synthesis of dihydropyridines by condensation of chalcones (1mmol), ethylacetoacetate (1mmol) and ammonium acetate (1mmol).....	102
3.9	Comparison of the catalytic activity of STA/Cr-P with other catalytic systems reported in literature for synthesis of	103

dihydropyridine.

4.1	Basal spacing and surface area of different clay-PPA composite catalysts.....	111
4.2	Physicochemical characteristics and catalytic activity of the clay-PPA composite materials.....	119
4.3	Catalytic activity of PPA-ZrP composite materials for the synthesis of tetrahydropyridines by one-pot multicomponent reaction of aryl aldehydes, substituted anilines and ethylacetoacetate.....	122
4.4	Comparison of the catalytic activity of PPA-ZrP with other catalytic systems reported in literature for synthesis of tetrahydropyridines....	124
4.5	Physicochemical characteristics and catalytic activity of ZrP-sulfonated PVA composite catalysts for the synthesis of hexahydropyrimidines by multicomponent condensation of ethylacetoacetate (1mmol), aniline (2 mmol) and formaldehyde (3 mmol).....	133
4.6	Catalytic activity of ZrP-SP composite material for synthesis of hexahydropyrimidines by multicomponent condensation of $\beta$ -dicarbonyl compounds substituted aniline and formaldehyde.....	145
4.7	Comparison of the catalytic activity of ZrP-SP with other catalytic systems reported in literature for synthesis of hexahydropyrimidines.	146
5.1	Physicochemical properties of parent clay, Al-P and Pd/Al-P.....	154
5.2	Dehydrohalogenation of different halogenated organic compounds using Pd/Al-P as catalyst after 30 minutes reaction time.....	163
5.3	Physicochemical characteristics of Pd-M/Al-P catalyst.....	168

## LIST OF FIGURES

Figure	Title	Page No.
1.1	Silicate sheet of a clay mineral formed from corner sharing of SiO <sub>4</sub> unit	2
1.2	Alumina octahedral sheets in clay mineral.....	3
1.3	Structure of 2:1 clay mineral montmorillonite.....	4
1.4	Hydration sphere of metal ion in the clay interlayers.....	7
1.5	Type of hydroxyl groups and their IR band positions in clay structure	8
1.6	Protonation of clay sheets and generation of Brønsted acidity.....	8
1.7	Arrangement of clay sheets in a clay particles (house of card model)...	10
1.8	Schematic representation of the process of pillaring of the clay sheets.	12
1.9	The structure of [Al <sub>13</sub> O <sub>4</sub> (OH) <sub>24</sub> (H <sub>2</sub> O) <sub>12</sub> ] <sup>7+</sup> ion. ....	16
1.10	The process of crosslinking of the pillar and the clay sheet.....	17
1.11	Structure of the [Zr <sub>4</sub> (OH) <sub>8</sub> (H <sub>2</sub> O) <sub>16</sub> ] <sup>8+</sup> pillaring polycation .....	30
3.1	XRD profiles of (a) clay and (b) calcined Cr-P.....	66
3.2	FT-IR spectra of (a) clay, (b) air dried Cr-P and (c) calcined Cr-P.....	67
3.3	UV-vis absorbance spectra of (a) clay, (b) air dried Cr-P and (c) calcined Cr-P.....	68
3.4	Thermogravimetric analysis of the air dried Cr-P material.....	70
3.5	N <sub>2</sub> sorption isotherm of (a) Parent Clay and (b) Cr-P material.....	71
3.6	Effect of various reaction parameters on the yield of the product for the reaction of benzaldehyde (1 mmol) with dimedone (2mmol) (I) Effect of reaction time (900 W and 50 mg of catalyst), (II) Effect of catalyst amount (900 W for 15 minutes duration), (III) Effect of microwave power (50 mg catalyst for 15 minutes duration).....	73
3.7	Structure of keggin anion.....	84



3.8	XRD patterns of (a) Clay, (b) Cr-P and (c) STA/Cr-P.....	87
3.9	FTIR spectra of (a) Parent clay, (b) air dried Cr-P, (c) calcined Cr-P and (d) STA/Cr-P (Panel III, inset (e) bulk STA).....	88
3.10	UV-Vis spectra of (a) parent clay, (b) Cr-P calcined, (c) STA/Cr-P and (d) bulk STA.....	90
3.11	TGA/DTG profile of 10STA/CrP material.....	91
3.12	N <sub>2</sub> sorption isotherm of (a) STA/Cr-P and (b) Cr-P.....	92
3.13	Scanning electron micrograph of (a) Cr-P air dried, (b) Cr-P calcined and (c) STA/Cr-P.....	93
3.14	Transmission electron micrographs of (a) STA/Cr-P and (b) STA/Clay.....	94
3.15	Effect of microwave exposure time on the yield of 1,4-dihydropyridines synthesized by condensation of benzaldehyde (1mmol), ethylacetoacetate (2 mmol) and NH <sub>4</sub> OAc (1mmol) . (-•-) STA/Cr-P, (-■-) Cr-P, (-▲-) AAM, and (-••) STA/Clay.....	98
3.16	Effect of catalyst weight on the yield of of 1,4-dihydropyridines synthesized by condensation of benzaldehyde (1mmol), ethylacetoacetate (2 mmol) and NH <sub>4</sub> OAc (1mmol) using STA/Cr-P catalyst.....	99
4.1	XRD patterns of (a) parent clay, (b) air dried Zr-P, (c) calcined Zr-P, (d) PPA- Clay, (e) PPA-ZrP and (f) ZrP-PPA.....	109
4.2	FTIR Spectra of (a) parent clay, (b) PPA-clay (c) CTAB-PPA-clay (d) ZrP-PPA and (e) PPA-ZrP (panel I and panel II in the range of 4000-3000 cm <sup>-1</sup> and 1700-400 cm <sup>-1</sup> , respectively).....	112
4.3	UV-Vis spectra of (a) parent clay, (b) PPA-clay, (c) ZrP-PPA and (d) PPA-ZrP. ....	114
4.4	Thermogravimetric profiles of (I) Zr-P, (II) PPA-Clay and (III) ZrP-PPA materials.....	115
4.5	FE-SEM images (a) PPA-ZrP and (b) ZrP-PPA.....	117
4.6	Effect of catalyst amount, temperature and solvent on the yield of the tetrahydropyridine synthesized by one-pot multicomponent reaction of benzaldehyde, aniline and ethylacetoacetate.....	120

4.7	XRD patterns of (a) Clay-SP, (b) CTAB-Clay-SP, (c) ZrP-SP.....	132
4.8	XRD patterns of (a) Clay-PIS, (b) ZrP-PIS.....	134
4.9	FTIR spectra of (a) Clay, (b) Clay-SP, (c) CTAB-Clay-SP, (c) ZrP-SP...	136
4.10	FTIR spectra of (a) Clay-PIS, (b) CTAB-Clay-PIS, (c) ZrP, (d) ZrP-PIS.	137
4.11	UV-Vis spectra of (a) Clay, (b) Zr-P, (c) ZrP-SP, (d) ZrP-PIS.....	138
4.12	FE-SEM image of (a) Clay-SP, (b) Clay-PIS, (c) ZrP-SP and (d) ZrP-PIS.....	140
4.13	Effect of catalyst amount and microwave power on the catalytic activity of ZrP-SP catalyst for the synthesis of hexahydropyrimidines by multicomponent condensation of ethylacetoacetate (1mmol), aniline (2 mmol) and formaldehyde (3 mmol).....	143
4.14	Effect of temperature and reaction media on the catalytic activity of ZrP-SP catalyst for the synthesis of hexahydropyrimidines obtained by multicomponent condensation of ethylacetoacetate (1mmol), aniline (2 mmol) and formaldehyde (3 mmol).....	144
5.1	XRD patterns of (a) Clay, (b) Al-P and (c) Pd/Al-P.....	153
5.2	FTIR Spectra of (a) Pd/Al-P, (b) Al-P and (c) clay.....	155
5.3	N <sub>2</sub> adsorption desorption isotherms of (a) Al-P and (b) Pd/Al-P .....	156
5.4	FE-SEM images of (a) Al-P and (b) Pd/Al-P.....	157
5.5	Transmission electron micrograph of Pd/Al-P.....	157
5.6	Effect of different supports used for dispersion of 5 wt% Pd particles on the HDC activity for p-Chlorophenol.....	159
5.7	Effect of (a) different hydrogen transfer reagents and (b) hydrazine hydrate as hydrogen donors on the catalytic activity of Pd/Al-P for the hydrodechlorination of p-chlorophenol.....	160
5.8	Effect of temperature on the hydrodechlorination activity of p-chlorophenol catalysed by Pd/Al-P catalyst.....	161
5.9	Effect of t molar ratio of p-chlorophenol and hydrazine hydrate on the hydrodechlorination activity of p-chlorophenol catalysed by Pd/Al-P.....	162
5.10	Activity of Pd/Al-P catalyst for the hydrodechlorination of different halogenated organic compounds at 30 °C.....	163

5.11	Catalytic activity of Pd/Al-P catalyst for the hydrodechlorination of mono- and di- chlorinated phenols at 30 °C.....	164
5.12	XRD patterns of (a) Pd-Ni(1:1)/Al-P and (b) Pd-Cu(1:1)/Al-P.....	168
5.13	UV-Vis spectra of (a) PdCl <sub>2</sub> , (b) Pd nanoclusters, (c) Clay and (d) Al-P (panel I) and (e) Pd/Al-P, (f) Pd-Ni(1:1)/Al-P and (g) Pd-Cu(1:1)/Al-P (panel II).....	169
5.14	FE-SEM images (a) Pd-Ni (1:1)/Al-P and (b) Pd-Cu(1:1)/Al-P.....	171
5.15	TEM images (a) Pd/Al-P and (b) Pd-Ni(1:1)/Al-P.....	172
5.16	Time vs conversion profile of Pd-Cu(1:1)/Al-P and Pd-Ni(1:1)/Al-P materials for hydrodechlorination of 4-Chloroaniline at 40 °C. ....	173
5.17	(I) Effect of molar ratio of Pd:Ni on the catalytic activity of Pd-Ni/Al-P catalyst, (II) catalytic activity of Pd/Al-P, for the hydrodechlorination of 4-Chloroaniline.....	174
5.18	Effect of various hydrogenating agents on the hydrodechlorination activity of 4-Chloroaniline for Pd-Ni(1:1)/Al-P catalyst.....	175
5.19	Effect of temperature on hydrodechlorination of 4-Chloroaniline after 1 h of reaction time for Pd-Ni(1:1)/Al-P catalyst.....	176
5.20	Effect of molar ratio of 4-Chloroaniline and hydrazine hydrate on the hydrodechlorination of 4-Chloroaniline after 1 h of reaction time for PdNi(1:1)/Al-P catalyst at 40 °C.....	177
5.21	Catalytic activity of Pd-Ni(1:1)/Al-P catalyst for the hydrodechlorination of different substituted anilines at 40 °C.....	178
5.22	Catalytic activity of Pd-Ni(1:1)/Al-P catalyst for the hydrodechlorination of 4-Chlorophenol and 4-Chlorotoluene at 40 °C....	178

## ABBREVIATIONS

CT	: Charge Transfer
DRS	: Diffuse Reflectance Spectroscopy
FID	: Flame Ionization Detector
GC	: Gas Chromatography
FE-SEM	: Field Emission Scanning Electron microscopy
SEM	: Scanning Electron Microscopy
TEM	: Transmission Electron Microscopy
XRD	: X-Ray Diffraction
FT-IR	: Fourier Transform Infrared Spectroscopy
PILC	: Pillared Interlayer Clay
TG	: Thermogravimetry
EDAX	: Energy Dispersive X-Ray Analysis
Cr-P	: Chromium Pillared Clay
STA	: Silicotungstic Acid
STA/Clay	: Silicotungstic acid supported over Parent clay
STA/Cr-P	: Silicotungstic Acid Dispersed in the Matrix of Cr-Pillared Clay
AAM	: Acid Activated Montmorillonite
DHP	: Dihydropyridines
Zr-P	: Zirconium Pillared Clay
HPA	: Heteropoly Acid
PPA	: Polyphosphoric Acid
CTAB	: Cetyl Trimethyl Ammonium Bromide
ZrP-PPA	: Polyphosphoric Acid Dispersed in Zr-Pillared Clay Matrix
PPA-Clay	: Polyphosphoric Acid Dispersed in Parent Clay Matrix

PPA-CTAB-Clay:	Polyphosphoric Acid Intercalated Clay using CTAB as a Structure Expansion Agent
PPA-ZrP	: Polyphosphoric Acid-Clay Composite Pillared with Zr-Polycations
THP	: Tetrahydropyridines
PVA	: Polyvinyl Alcohol
SPVA	: Sulfonated Polyvinyl Alcohol
Clay-SP	: Sulfonated PVA-Clay Composite Material
CTAB-Clay-SP	: SPVA-Clay Composite Using CTAB as a Structure Expansion Agent
ZrP-SP	: SPVA-Zr-Pillared Clay Composite Material
Clay-PIS	: PVA Intercalated Clay Followed by In Situ Sulfonation
CTAB-Clay-PIS	: PVA Intercalated CTAB-Clay Followed by In Situ Sulfonation
ZrP-PIS	: PVA Dispersed in Zr-Pillared Clay Matrix Followed by In Situ Sulfonation
HHP	: Hexahydropyrimidines
Al-P	: Aluminium Pillared Clay
Pd/Al-P	: Palladium Nanoparticles Supported over Al-Pillared Clay
Pd-M/Al-P	: Palladium Based Bimetallic Nanoparticles Supported over Al-Pillared Clay
(M: Cu and Ni)	
HDC	: Hydrodechlorination
HDH	: Hydrodehalogenation

## NOTATIONS

eV	:	Electronvolt
m <sup>2</sup> /g	:	Square meter per gram
K	:	Kelvin
g	:	Gram
Hz	:	Hertz
nm	:	Nanometer
Å	:	Angstrong
d	:	Interplanner spacing
cm	:	Centimetre
h	:	Hour
$\theta$	:	Bragg angle
$\nu$	:	Frequency
cc	:	Cubic centimetre

# CHAPTER 1

## INTRODUCTION

### 1.1 GENERAL INTRODUCTION

Clays are the most common mineral on earth's surface and have been used by mankind for centuries. These materials are highly versatile and are used in millions of tons in different areas of application. Clays find wide applications in building ceramics, paper coating and filling, drilling muds, foundry moulds, and pharmaceuticals. These materials are also the most primitive materials to be used as adsorbents and catalysts for various industrial applications (Pinnavia, 1983; Adams and McCabe, 2006; Bhattacharyya and Sen Gupta, 2008; Ruiz-Hitzky *et al.*, 2010). The high surface area and polarity of the clay structure helps in retaining ionic species such as  $K^+$  and  $Ca^{2+}$  which are vital for the plant growth (Carvalho *et al.*, 2003). Clay minerals are also known as very good adsorbents for toxic organic chemicals such as chlorinated compounds, heavy metal ions (eg.  $Pb^{2+}$ ,  $Hg^{2+}$ ) and nuclear waste (Boonamnuayvitaya *et al.*, 2004; Sdiri *et al.*, 2011; Sis and Uysal, 2014; Nascimento and Masini, 2014;). Acid treated clays have been used extensively as cracking catalysts before introduction of zeolites in petroleum industries. The first hydrocracking process came on stream with acid treated clays in 1936 (Occelli and Rennard, 1988, Klopogge *et al.*, 2005; Centi and Perathoner, 2008). However, after the advent of zeolites and aluminosilicates these materials were replaced in 1964. Acid treated clays are still used in some cases for cracking of heavy fraction of the crude oil (M.F. Rosa-Brussin, 1995). Salt loaded, acid-treated and ion exchanged clays have been found to be efficient catalysts for many organic reactions (Pinnavia, 1983; Mc Cabe, 1996; Chitnis and Sharma, 1997; Cheng, 1999; Vaccari, 1999; Thomas *et al.*, 2011; Chmielarz *et al.*, 2012; Jha *et al.*, 2013; Zhao *et al.*, 2013). Recently, the clay-polymer nanocomposites and clay based nanohybrids have been investigated extensively for possible application as adsorbents, heterogeneous catalysts, structural materials and frame

retardants (Pavlidou and Papaspyrides, 2008; Hetzer *et al.*, 2008; Tămășan *et al.*, 2013; Tokarský *et al.*, 2013). Clays are divided into two main groups: cationic and anionic clays (Rajamathi *et al.*, 2001). The cationic clays are widely available in nature and contain negatively charged alumino-silicate layers (Vaccari, 1998; Centi and Perathoner, 2008). The negative charge in the layer is balanced by the presence of cations in the interlayer of these materials. These materials exhibit surface acidic properties due to the presence of structural hydroxyl groups. The anionic clays on the other hand, are relatively rare in nature but simple and inexpensive to synthesize (Rajamathi *et al.*, 2001; Nethravathi *et al.*, 2011). These materials have positively charged metal hydroxide layers with balancing anions and water molecules located interstitially. The work described in the thesis mainly concerned with the structural modification and catalytic application of the cationic clays.

## 1.2 STRUCTURE AND CLASSIFICATION OF CLAY MATERIALS

Clays are two dimensional hydrous layer silicates belonging to the phyllosilicate family (Mott, 1988; Klopogge *et al.*, 2005; Zhang *et al.*, 2010). The basic framework of clay consists of silicate layers formed from the condensation of the extremely stable  $\text{SiO}_4$  tetrahedral units. The  $\text{SiO}_4$  tetrahedra share three basal oxygen atoms by corner sharing to form the silicate layer. The oxygen atoms which can be imagined as being at the base of the equilateral triangle form a repeating pattern of regular hexagons. The structure of a typical silicate plane of a clay mineral is shown in Fig.1.1.

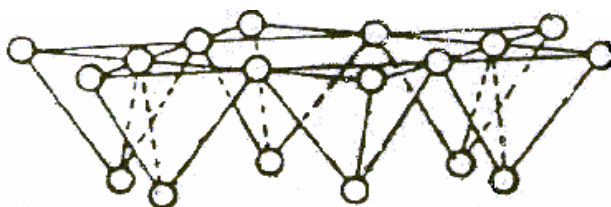


**Figure 1.1 Silicate sheet of a clay mineral formed from corner sharing of  $\text{SiO}_4$  unit.**



Each tetrahedron in the silicate layer has a spare oxygen atom which is unshared and pointed normally away from the tetrahedral siloxane sheet. These silicate planes then condense with different octahedral planar units through the unshared oxygen atoms to form different classes of clay materials. The octahedral layer is formed from the edge sharing of the  $MO_6$  ( $M= Al, Mg$  etc.) octahedra. The  $MO_6$  octahedra are polymerized in the plane by sharing four of its edges to form the octahedral layer (Mott, 1988; Brigatti *et al.*, 2013). Each octahedron in the layer contains two unshared oxygen atoms pointing normally above and below the plane of polymerization. This results in the generation of two negative charges to be satisfied by the metal cations. This is why trivalent aluminium occupies only two third of the available octahedral holes and forms dioctahedral clay minerals whereas magnesium occupy all the octahedral holes to form trioctahedral clay minerals. The structure of an alumina layer is shown in the Fig 1.2.

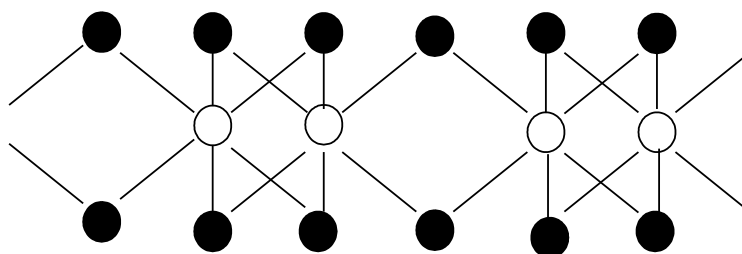


**Figure 1.2 Alumina octahedral sheets in clay mineral.**

The most widely used clay material in catalysis is montmorillonite. The structure of montmorillonite consists of an alumina layer sandwiched between two-silicate layers. The tetrahedral sheet of the polymerized  $SiO_4$  unit and the octahedral sheet of the polymerized  $AlO_6$  unit are the basic building blocks of the montmorillonite clay. The alumina plane condensed with two silicate planes to form the clay sheet. These clay sheets are then stacked in the z-direction to form the structure of montmorillonite. The structure of montmorillonite clay is shown in Fig 1.3. The space between each sheet of clay is called the interlayer

spacing. Isomorphous substitution of  $\text{Al}^{3+}$  ion by lower valent ions such as  $\text{Fe}^{2+}$ ,  $\text{Mg}^{2+}$  in the octahedral layer of clay sheet is a common phenomenon in clay minerals. This results in the development of negative charge in the clay sheet, which is usually satisfied by cations of alkali and alkaline earth metals. These charge-compensating cations are found in the interlayer and are easily exchangeable with other cationic species.

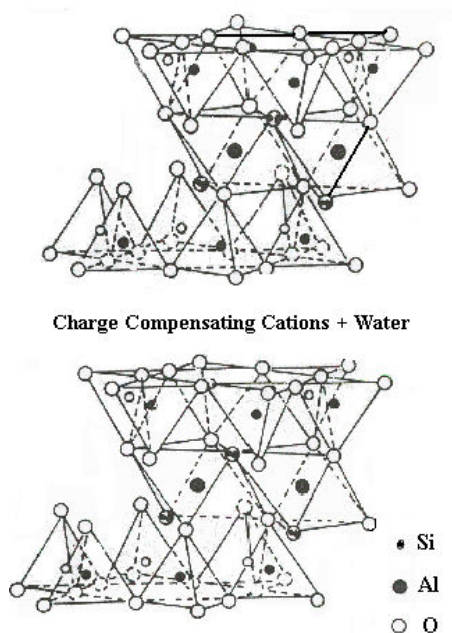


**Figure 1.3 Structure of 2:1 clay mineral montmorillonite.**

The total amount of negative charge originated as a result of isomorphous substitutions is called the cation exchange capacity (CEC) of the clay material (Figueras, 1988; Bergaya *et al.*, 2006a; Brigatti *et al.*, 2013). The montmorillonite type clay minerals are called 2:1 clay minerals. The other possibility is that one silicate layer can condense with one alumina layer. Such clay minerals are called 1:1 clay minerals (Mott, 1988; Brigatti *et al.*, 2013). One such clay mineral used in catalysis is Kaonilite. Clay minerals have been divided into several groups, sub-groups and species depending upon the layer type, charge and occupancy and the type of charge compensating cations. Some of the important groups of clay minerals are listed in Table 1.1.

**Table 1.1 Classification of clay minerals**

<b>Group Name</b>	<b>Layer Type</b>	<b>Charge (x)</b>	<b>Interlayer Type</b>	<b>Octahedral Occupancy</b>	<b>Subgroup</b>	<b>Species</b>
Serpentine-Kaolin	1:1	very low or zero	---	Tri -- Di --	Serpentines Kaolins	Chrysotile Kaolinite
Talc-Pyrophyllite	2:1	zero	---	Tri -- Di --	Talcs Pyrophyllite	Talc Pyrophyllite
Smectite	2:1	low ( $0.6 < x < 1.2$ )	hydrated cation (Na)	Tri -- Di --	Saponites Montmorillonite	Saponite Beidellite
Vermiculite	2:1	medium ( $1.2 < x < 1.8$ )	hydrated cation (Mg)	Tri -- Di --	Tri-vermiculites Di-Vermiculites	Tri-vermiculites Di-Vermiculites
Mica	2:1	high ( $x \approx 2$ )	Unhydrated cation (K)	Tri -- Di --	Tri-Mica Di-Mica	Biotite Illite
Brittle Mica	2:1	very high ( $x \approx 4$ )	Unhydrated cation (Mg)	Tri -- Di --	Tri-Brittle Mica Di-Brittle Mica	Clintonite Margarite
Chlorite	2:1	variable	Octahedral layer	Tri -- Di --	Tri-Chlorites Di-Chlorites	Chlinochlore Donbassite
Sepiolite-Palygorskite	2:1	variable	Any	Tri -- Di --	Sepiolites Palygorstites	Sepiolites Palygorstites

### 1.3 ACIDIC AND CATALYTIC PROPERTIES OF CLAY MATERIALS

Cationic clays are used as solid catalysts for several acid catalysed reactions. The acidic property of the clay surface has been studied using several methods such as surface conductivity (Fripiat *et al.*, 1965), Linear free energy relationship of H/D exchange of substituted benzenes (Gonçalves *et al.*, 2007), Hammett indicator, diffuse reflectance Fourier transform infrared spectroscopy (Benesi, 1956; Liu *et al.*, 2011), temperature programmed desorption (Arena *et al.*, 1998; Okada *et al.*, 2006), first principles molecular dynamics simulations (Liu *et al.*, 2014), microcalorimetry (Jerónimo *et al.*, 2007) and temperature programmed desorption (TPD) and FTIR spectra of adsorbed probe molecules (Bodoardo *et al.*, 1994; Mokaya and Jones, 1995; Akcay, 2005; Liu *et al.*, 2013). The acidity observed in the clay materials is mostly Brønsted in nature. However, it is possible to generate Lewis acidity by suitable thermal treatment. The structural and environmental factors govern the degree of presence of these sites and normally one type predominates under a given set of conditions (Pinnavia, 1983; Morikawa, 1992; McCabe, 1996; Akcay, 2005). The Lewis acidity is mainly associated with the exposed  $Al^{3+}$  ions at the broken crystallite edges. Such sites can be created by heat treatment of the clay materials at higher temperatures. However, the heat treatment results in the removal of interlayer and coordinated water and irreversible collapse of the clay structure.

The origin and nature of Brønsted acidity in clay have been studied by several authors (Mortland *et al.*, 1963; Fripiat *et al.*, 1965; Frenkel, 1974; Bodoardo *et al.*, 1994; Akcay, 2005; Azzouz *et al.*, 2006; Tyagi *et al.*, 2006; Ravindra Reddy *et al.*, 2007; 2009; Liu *et al.*, 2013). The most important source of Brønsted acidity in case of clay materials is due to the dissociation of water molecules in the hydration sphere of the interlayer exchangeable cations. The water molecules in the primary coordination sphere of the interlayer ion are highly polarized and sterically hindered (Fig.1.4). These water molecules under the influence

of the “negative” potential of the clay sheet dissociate to form protons which act as a source of acidity.

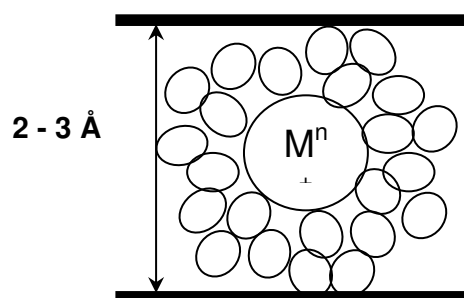


**Figure 1.4** Hydration sphere of metal ion in the clay interlayers

The generation of acidity by water dissociation process depends upon its content in the clay and the ionic charge of the interlayer cation. When the water content in the clay is low, the Brønsted acidity is maximized because of less dissipation of ionic charge of the interlayer cation by water molecules (Bodoardo *et al.*, 1994). Similarly, when the interlayer  $\text{Na}^+$  and  $\text{Ca}^{2+}$  ions are exchanged with highly polarizing cations such as  $\text{M}^{3+}$ , the dissociation of the water molecules in the coordination sphere is facilitated (Mc Cabe, 1996). The Brønsted acidity of the clay materials can be optimized by suitable choice of the pretreatment temperature or dehydrating the clay particles under vacuum. However, care has to be taken not to overheat the samples as this may lead to the collapse of the clay structure.

The other source of acidity of the clay materials is the structural hydroxyl groups present in the octahedral layers. These hydroxyl groups protrude through the hexagonal rings of the silicate layer into the clay interlayer. Several varieties of hydroxyl groups have been identified on the clay layers by FTIR spectroscopy (Bodoardo *et al.*, 1994; Liu *et al.*, 2013). These hydroxyl groups differ in the chemical environment around them and consequently exhibit acidic property of different strength (Fig. 1.5).

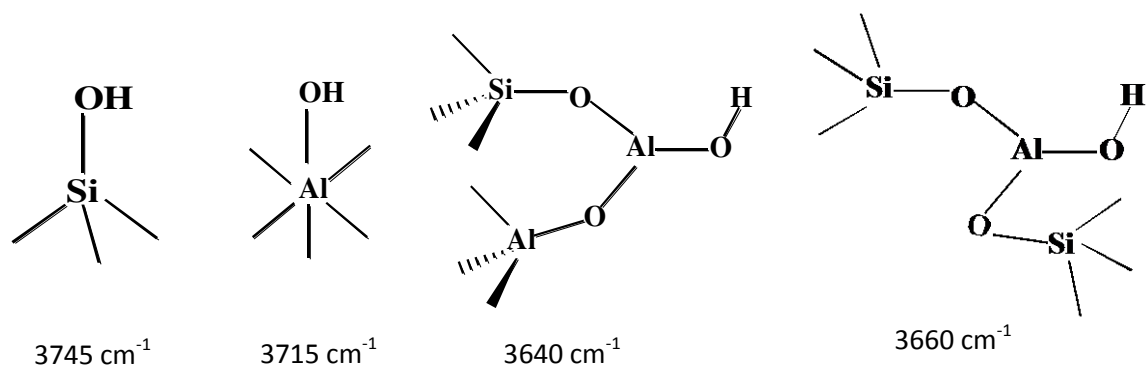


**Figure 1.5** Type of hydroxyl groups and their IR band positions in clay structure (Bodoardo et al., 1994).

The number of hydroxyl groups in the clay octahedral layer can be increased by preparing proton exchanged clays. The clay materials can be exchanged with ammonium ions which upon heat treatment at 200-300°C expels ammonia to form proton exchanged clay. The exchanged protons can migrate into the octahedral vacancies of the dioctahedral clays and protonate the bridging oxygens in the clay resulting in structural hydroxyl groups (Azzouz *et al.*, 2006; Elkhalfah *et al.*, 2013) (Fig. 1.6).

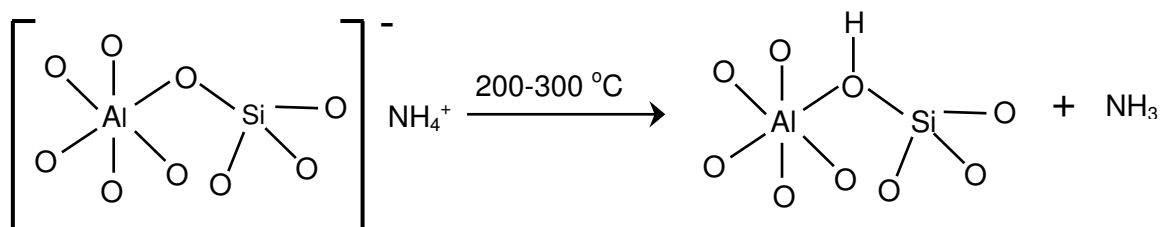


**Figure 1.6** Protonation of clay sheets and generation of Brønsted acidity.

Clay minerals have been used as solid acid catalysts for a variety of organic transformations (Mc Cabe, 1996; Varma, 2002; Adams *et al.*, 2006). The inherent Brønsted acidic nature of clay combined with the restricted environment in the clay interlayer has been used to carry out many shape selective reactions. Reactions requiring both Lewis and Brønsted acidic sites are catalyzed by clay materials. Clays intercalated with transition metal cations can also catalyze redox and photochemical transformations. As pointed out before, both the structural

hydroxyl groups and the interlayer water molecules act as source of acidity for clay materials. Ion exchanged and protonated clays have been used as catalysts for several organic reactions requiring Brønsted acidic sites (Vaccari, 1999). Montmorillonite clay containing  $Zn^{2+}$ ,  $Al^{3+}$  and  $Fe^{3+}$  ions in the interlayer had been utilized as catalyst for hydroxyalkylation of p-cresol by formaldehyde (Jha *et al.*, 2013). Shimizu *et al.* had synthesized different cation exchanged K-10 montmorillonite clay and examined their catalytic activity for acetylation of alcohol (Shimizu *et al.*, 2008). Clay containing  $M^{3+}$  type ions ( $Ce^{3+}$ ,  $Al^{3+}$ ,  $Fe^{3+}$ ) in the interlayer have been demonstrated as efficient catalyst for acetalization of carbonyl compounds with methanol (Thomas *et al.*, 2011). Further the ion exchanged montmorillonite have been effectively used for ring-opening polymerization of lactones (Hachemaoui and Belbachir, 2005). Clays treated with mineral acids have been used as solid acid catalysts for glycerol dehydration (Zhao *et al.*, 2013), isomerisation of  $\alpha$ -pinene (Yadav *et al.*, 2004) and selective catalytic reduction of nitric oxide (Chmielarz *et al.*, 2012). **Vijay kumar and Ranga rao have utilized the montmorillonite K-10 as support for  $ZrOCl_2 \cdot 8H_2O$ . The prepared catalyst had been catalytically examined for the synthesis of 3,4-dihydropyrimidin-2(1H)-ones/thiones (VijayKumar and RangaRao 2012a).** Beside the above mentioned reactions clays have been used for a number of reactions requiring Brønsted acid sites such as Beckmann rearrangement (Mitsudome *et al.*, 2012), formation of cyclic anhydrides (Mc Cabe, 1996), heterocyclic synthesis (Varma, 2002) and Claisen rearrangements (Castanheiro *et al.*, 2009).

#### **1.4 DISADVANTAGES OF CLAY MATERIALS AS CATALYSTS**

Although clay materials are used as solid acid catalysts for variety of organic reactions, they possess certain inherent disadvantages, which limit their application in heterogeneous catalysis (Figueras, 1988; Gil *et al.*, 2000a). Extensive dehydration of the clay sheets takes place at high temperatures leading to the loss in Brønsted acidity. This limits their application as catalysts at higher temperatures. The forces between individual clay sheets are purely

electrostatic and Van der Waals type. These forces are very weak in nature and cannot retain the interlayer space at high temperatures. At elevated temperatures complete collapse of clay structure takes place resulting in the loss of Brønsted acidity and shape selective property. The interlayer dimension of the clay materials are typically between 3-5 Å, which is smaller than the kinetic diameter of most of the bulky reactant molecules. This results in diffusional constraints and most of the interlayer catalytically active sites remain unutilized during catalysis. Although the clay sheets are stacked along the z-axis in clay crystallite, the orientation of the crystallites in the clay particles are highly haphazard which is described by house of card model shown in Fig. 1.7. During the catalytic processes, only the sites in the periphery of the particles are effectively used whereas the sites in the bulk remain unutilized due to diffusional constraints. The disorder in the clay structure also results in a decrease in the crystallinity of the clay materials and when used under hydrothermal conditions these materials are rapidly deactivated due to structural instability.

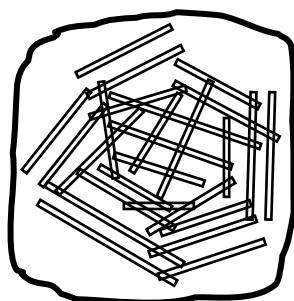


**Figure 1.7** Arrangement of clay sheets in a clay particles (house of card model).

## **1.5 MODIFICATION OF CLAY MATERIALS**

In last two decades, different types of surface as well as interlayer modifications have been done to increase the thermal stability, acidity and catalytic properties of clay materials. The most important modifications reported in literature are the exchange of interlayer cations by inorganic and organic cationic species (McCabe, 1996; Thomas *et al.*, 2011; Dultz *et al.*, 2012), acid treatment (Chitnis and Sharma, 1997, Komadel and Madejova 2006), supporting



active species on clay surface for catalysis (Rhodes and Brown, 1993; Garrido-Ramirez *et al.*, 2012; Meshram *et al.*, 2012), pillaring by inorganic polycations (Gil *et al.*, 2010) and preparation of clay-polymer nanocomposite materials (Pavlidou and Papaspyrides, 2008). While the first three processes essentially increase the acidity and catalytic activity, the pillaring of clay by inorganic polycations provides a multitude of advantages in terms of increasing surface area, microporosity, thermal stability, acidity and catalytic activity. The clay-polymer nanocomposites are relatively new class of materials whose catalytic potential is yet to be explored fully. However, these materials are known to exhibit superior physical, chemical and mechanical properties. The research work reported in this thesis deals with the catalytic application of pillared clay based materials and their modified analogues. The following sections provide a detail description of the synthetic methods adopted for pillared clay synthesis and their application in various heterogeneous catalytic processes.

## **1.6 PILLARING OF CLAY BY INORGANIC POLYCATIONS**

Pillared clays are a class of microporous materials studied extensively in the last decade as catalysts and supports for various organic transformations. These materials are prepared by exchanging the interlayer cations of the clay materials by inorganic polyoxocationic clusters of few molecular dimension (Cool and Vansant, 1998; Vaccari, 1999; Bergaya *et al.*, 2006b; Gil *et al.*, 2008; 2010). The intercalated polycations increase the basal spacing of the clays and upon heat treatment they are converted to stable metal oxide clusters. These oxide clusters called pillars hold the individual clay sheets and prevent them from collapsing during high temperature applications. Two important properties of clay materials are responsible for pillaring process to occur.

1. *Swelling in polar solvent:* As mentioned previously, the forces between clay layers are purely electrostatic. When clay particles are dispersed in polar solvents such as water, solvent

molecules enter into the interlayer of clay and reduce the electrostatic forces. Under such conditions the individual clay layers move apart resulting in the swelling of clay minerals.

2. *Exchangeability of the interlayer cations*: The negative charges in the clay sheet originate from isomorphous substitution in the octahedral layer. However, these charges are not point charges but delocalised over the oxygen plane. In the polar solvent, charge delocalisation provides considerable mobility to the interlayer cations which can be exchanged by other cations. The process of pillaring is shown schematically in Fig. 1.8.

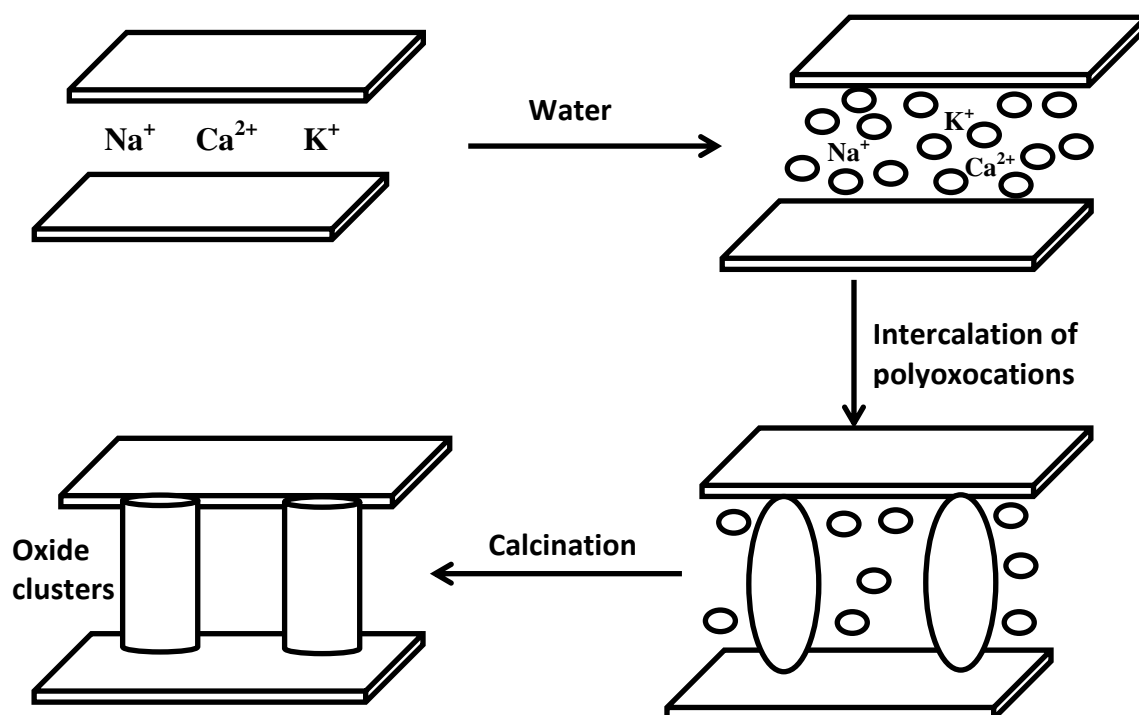


**Figure 1.8** Schematic representation of the process of pillaring of the clay sheets.

The parent clay containing  $\text{Na}^+$ ,  $\text{Ca}^{2+}$  and  $\text{K}^+$  ions in the interlayer are initially dispersed in polar solvent such as water which results in the swelling of clay. Under such conditions, the inorganic cationic clusters are intercalated into the clay layers. The cationic clusters replace the interlayer cations and give rise to the intercalated clay (Gil *et al.*, 2008). Upon calcination, the inorganic polyoxoclusters present inside the clay interlayer are converted into

stable oxide clusters. The oxide clusters are chemically bonded to the adjacent clay sheets acting as nano-pillars and generate a three dimensional structure with open channels.

Clay pillared with a variety of inorganic polycations of Al (Letaief *et al.*, 2003; Tomul and Balci, 2009; León *et al.*, 2014; Zhou *et al.*, 2014), Zr (Cool and Vansant, 1996; Gil *et al.*, 2000b; Colín *et al.*, 2005; Zhou *et al.*, 2010; Gil *et al.*, 2011), Ti (Jagtap and Ramaswamy, 2006; Bineesh *et al.*, 2011), Cr (Pinnavia *et al.*, 1985; Akçay, 2004), Fe (Akçay, 2004; Hadjltaief *et al.*, 2013), Ta (Guiu *et al.*, 1997); V (Choudary and Valli, 1990); Ga (Duong *et al.*, 2005); Si (Li *et al.*, 2011) and Nb (Gallo *et al.*, 2006) have been reported in literature. These polycations are generally prepared by controlled hydrolysis of the corresponding metal cations in solutions (Figueras, 1988). The final property of the pillared clay depends largely upon the nature of the polycations which in turn depend upon the method of preparation (Figueras *et al.*, 1988; Gil *et al.*, 2000a; Bergaya *et al.*, 2006b). The different types of polycations used for the preparation of the pillared clays are given in Table 1.2.

**Table 1.2 Different types of pillaring species used for preparation of pillared clays.**

Pillar type	Pillaring species	Reference
Al	$[Al_{13}O_4(OH)_{24}(H_2O)_{12}]^{7+}$	Shabtai <i>et al.</i> , 1984; León <i>et al.</i> , 2014
Zr	$[Zr_4(OH)_8(H_2O)_{16}]^{8+}$	Cool and Vansant, 1996; Zhou <i>et al.</i> , 2010
Fe	$[Fe_3(OAC)_7OH.2H_2O]^+$	Mishra <i>et al.</i> , 1996; Hadjltaief <i>et al.</i> , 2013
Ti	$[TiO(OH)_x]^{x+}$	Kooli <i>et al.</i> , 1997; Jagtap and Ramaswamy, 2006
Ga	$[Ga_{13}O_4(OH)_{24}(H_2O)_{12}]^{7+}$	Bradley and Kydd, 1993a; Duong <i>et al.</i> , 2005
Cr	$[Cr_4O(OH)_5(H_2O)_{10}]^{5+}$	Pinnavia <i>et al.</i> , 1985a; Akçay, 2004
Ta	$[Ta_8O_{10}(OR)_{20}]$	Guiu <i>et al.</i> , 1997

The characteristic changes that occur as a result of pillaring include an increase in thermal stability, microporosity, surface area and acidic properties of the parent clay. Table 1.3 shows a general comparison of the properties of the parent clay and pillared clay materials often observed in the literature.

**Table 1.3 Properties of the parent clay before and after pillaring.**

<b>Physical and chemical properties</b>	<b>Parent clay</b>	<b>Pillared clay</b>
Interlayer spacing	2-3 Å	8-15 Å
Surface area	30-60 m <sup>2</sup> /g	200-350 m <sup>2</sup> /g
Pore size	4-8 Å	16-25 Å
Micropore volume	< 0.02 cm <sup>3</sup> /g	> 0.10 cm <sup>3</sup> /g
Brønsted acidity	0.1-0.2	0.4 - 0.6 mmol H <sup>+</sup> /g
Lewis acidity	0.05-0.1 mmol/g	0.6-0.8 mmol/g
Thermal stability	< 300°C	< 800°C

The evidence of the intercalation of the inorganic polycations into the clay interlayer can be obtained from the X-ray diffraction study. Since the size of the polycation (10-15 Å) is higher than the individual interlayer ions, the intercalation of the former results in the expansion of clay structure in z-direction (Gil *et al.*, 2000a). This expansion results in a shift of the d<sub>001</sub> reflections to lower 2θ value. Considerable expansion and desegregation of the of the clay materials takes place during pillaring process resulting in materials with high surface area and pore volume. It is evident from Table 1.3 that nearly five times increase in the surface area is observed for pillared materials. Pillared clays are generally microporous in nature. The adsorption isotherm observed for the pillared clays is type-I according to Brunauer, Deming, Deming and Teller (BDDT) classification which indicate the presence of micropores (Gil *et*

*al.*, 2000a, Sowmiya *et al.*, 2007; Gil *et al.*, 2011; Jalil *et al.*, 2014). The acidic property of pillared clay have been studied by several methods such as TPD of ammonia (Arena *et al.*, 1998), FTIR of the adsorbed basic probe molecules (Bodoardo *et al.*, 1994; Gil and Montes, 1997), and Breen's method (Breen, 1991; Mokaya and Jones, 1995). The general conclusions arrived at from these studies are: (i) pillared clays are more acidic compared to the parent clay materials both in terms of the strength and number of acidic sites; (ii) the oxide clusters (pillars) in the clay interlayer are highly defective and contains acidic centres; (iii) pillared clay offers both Lewis and Brønsted acidic sites while the parent clay contains mostly Brønsted acid sites and (iv) most of the Lewis acid sites are associated with the pillars. IR Spectroscopy has been used to discriminate the acidic and nonacidic –OH groups in clay minerals. The acidic sites are identified with careful experiments using basic probe molecules and deuterium exchange reactions (Bodoardo *et al.*, 1994; Gonçalves *et al.*, 2007). A gradual evolution of the Lewis acidic sites with thermal treatment has also been monitored employing suitable probe molecule such as pyridine (Gil and Montes, 1997). The Lewis acidic sites in the clay are mostly associated with the pillared oxides and the unsaturated cations present in the broken edges of the clay. The present work deals with the catalytic application of Al-, Zr- and Cr-pillared clay based materials. The following section provides a detail description of basic understanding as well as recent progress in the catalytic application of these pillared clay materials.

## **1.7 AI-PILLARED CLAYS (AI-PIL)**

Among all pillared clay materials, the Al-pillared clay is the most extensively investigated system reported in literature. The pillaring solution for the Al-pillared clay contains  $[\text{Al}^{\text{IV}}\text{Al}^{\text{VI}}_{12}\text{O}_4(\text{OH})_{24}(\text{H}_2\text{O})_{12}]^{7+}$  polycationic species (Vaccari, 1999; Bergaya *et al.*, 2006b). These polycations are prepared by the partial base hydrolysis of a dilute solution of aluminium chloride. In case of Al-pillared clay, it has been clearly demonstrated that the

preparation and concentration of  $[\text{Al}_{13}\text{O}_4(\text{OH})_{24}(\text{H}_2\text{O})_{12}]^{7+}$  polycation in the pillaring solution depends upon several parameters such as degree of hydrolysis, temperature, time of aging, concentration of the ion in solution, type of counter ion and method of preparation of the pillaring solution (Gil, 2000a; Vicente *et al.*, 2013). The precise control of these parameters is necessary to get reproducible results. The  $[\text{Al}_{13}\text{O}_4(\text{OH})_{24}(\text{H}_2\text{O})_{12}]^{7+}$  polycation has a Keggin ion type structure in which one  $\text{AlO}_4$  tetrahedra is symmetrically surrounded by twelve  $\text{AlO}_6$  octahedra in a dodecahedral coordination (Fig.1.9) (Bergaya *et al.*, 2006b). A moderate temperature of 60-80°C, relatively higher (2.5 M) concentration of aluminium ion and  $\text{OH}/\text{Al} \sim 2$  favors the formation of this cation in solution (Mrad *et al.*, 1997).

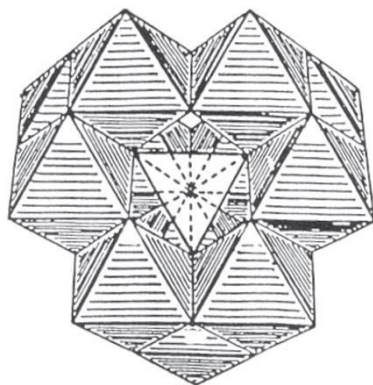


**Figure 1.9** The structure of  $[\text{Al}_{13}\text{O}_4(\text{OH})_{24}(\text{H}_2\text{O})_{12}]^{7+}$  ion.

The bonding interaction between the pillars and the clay layers have been studied extensively for the Al-pillared clay.  $^{27}\text{Al}$  and  $^{29}\text{Si}$  solid state NMR study of clay materials have been quite versatile in depicting the structural changes and bonding interactions between the clay sheets and pillars (Pinnavia *et al.*, 1985b, Fripiat, 1988; Occelli *et al.*, 2000; Salerno and Mendioroz, 2002 ). In case of alumina pillared clay,  $^{27}\text{Al}$  NMR study indicates that the origin of the layer charge (from octahedral or tetrahedral layer) is very crucial for the pillaring process. Plee *et al* (1985) have studied the process of pillaring in two different clays, beidellite,  $[\text{Na}_{0.91}(\text{Si}_{7.09}\text{Al}_{0.91})^{\text{IV}}(\text{Al}_4)^{\text{VI}}\text{O}_{20}(\text{OH})_4]$  and hectorite,  $[\text{Li}_{1.6}(\text{Li}_{1.6}\text{Mg}_{4.4})^{\text{VI}}(\text{Si}_8)^{\text{IV}}\text{O}_2(\text{OH})_4]$ . In case of hectorite, the layer charge originates from the octahedral layer and is highly

delocalised while in case of beidellite the layer charge originates from the tetrahedral layer and is considered as point charge. The downfield shift of the Al octahedral resonance to + 6.8 ppm in case of pillared hectorite has been interpreted as further polymerization of  $Al_{13}$  polycation due to its mobility in the clay interlayer facilitated by charge delocalization. In pillared beidellite, on the other hand, the moment of the  $Al_{13}$  polycations are restricted due to point charges, which results in an Al octahedral resonance at +3 ppm observed normally for the  $Al_{13}$  polycations. The bonding interactions between the pillars and clay sheet have also been studied by  $^{29}Si$  NMR. These studies indicate that the intercalation of pillars from solution is purely an electrostatic process and cannot be considered really crosslinked. However, heat treatment at higher temperature results in the formation of covalent bonds between the pillars and the clay sheets. It has been proposed that during the process of crosslinking, some of the  $SiO_4$  tetrahedra in the clay structure undergo structural inversion to accommodate the  $Al_{13}$  polycationic species (Fig. 1.10) (Ocelli *et al.*, 2000).

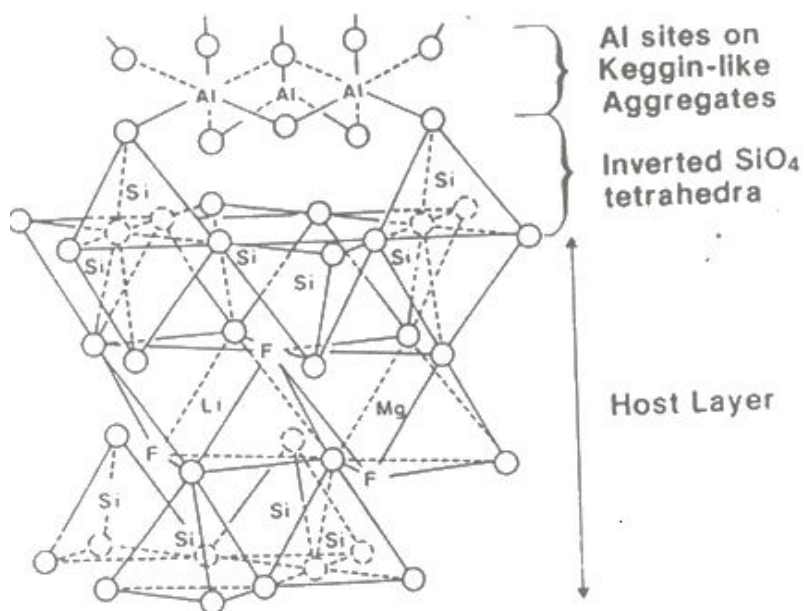


**Figure 1.10** The process of crosslinking of the pillar and the clay sheet (Ocelli *et al.*, 2000).

## 1.8 EFFECT OF SYNTHETIC CONDITIONS ON THE PROPERTY OF Al-PILLARED CLAY.

The effect of synthetic parameters on the physicochemical properties of the Al-pillared clay has been studied by several authors in literature. Since the synthesis process of pillared clay involve multiple steps such as clay dispersion, intercalation of pillaring species, washing, drying and calcination steps, each step has to be controlled precisely to get reproducible results. Thermally stable Al-P have been obtained using pillaring solution prepared from  $\text{AlCl}_3$  as precursor salt and Al/OH ratio of 2 - 2.5 (Mrad *et al.*, 1997; Zuo and Zhou, 2008; Zuo *et al.*, 2011). At lower pH the pillaring solution comprises of monomers and dimers along with oligomeric species. At higher pH the precipitation of  $\text{Al}(\text{OH})_3$  occurs (Hutson *et al.*, 1999; Gil *et al.*, 2000b; Zuo and Zhou, 2008;) . Hence the final pH of the pillaring solution was maintained around 5.6 (Mrad *et al.*, 1997; Gil *et al.*, 2000b).

Three different preparative strategies have been used for the synthesis of  $\text{Al}_{13}$  polycations in literature (Vicente *et al.*, 2013).

(A) The  $\text{Al}_{13}$  polycations have been mostly obtained by partial base hydrolysis of  $\text{AlCl}_3$  salt solution using NaOH or  $\text{Na}_2\text{CO}_3$  as base (Gil *et al.*, 2000b; Sivaiah *et al.*, 2010). Aluminium Nitrates and sulphates have also been used as precursor for synthesis of  $\text{Al}_{13}^{7+}$  species (Moreno *et al.*, 1997a; Barrera-Vargas *et al.*, 2005). Apart from sodium bases other bases such as  $\text{K}_2\text{CO}_3$  can also be used for hydrolysis. This method is most commonly used in Al-P synthesis.

(B) The dissolution of Al metal in the acidic medium such as HCl or acidic  $\text{AlCl}_3$  solution can produce  $\text{Al}_{13}$  polycations. Presence of interfering ions can be prevented by using this method.



(C) Electrolysis of  $\text{AlCl}_3$  can yield pure  $\text{Al}_{13}$  at OH/Al ratio at 2.4 (Akitt and Farthing, 1981).

The intercalation of oligomeric species other than  $\text{Al}_{13}$  has also been reported for synthesis of Al-pillared clay. Vaughan *et al* have reported the synthesis of Al-pillared clay by intercalation of  $\text{Al}_{24}$  and  $\text{Al}_{26}$  oligomeric clusters inside the clay interlayer. The  $\text{Al}_{24}$  species have been synthesized by prolonged thermal aging of Al-pillaring solution whereas  $\text{Al}_{26}$  was synthesized under ammonia hydrolysis condition that results in condensation of two  $\text{Al}_{13}$  units (Vaughan *et al.*, 1988).

The intercalation of the pillaring cations inside the clay interlayer is an important step which can influence the physicochemical characteristics of the Al-pillared clay. The intercalation of the pillaring species is mainly carried out in dilute solution by mixing a clay suspension with the pillaring solution and mechanically stirring the mixture for extended period of time. Different variations have been studied in literature to optimize the pillaring process. Since the intercalation is a diffusion dependant process, the use of microwave as well as ultrasound can expedite the intercalation of the polyoxocation inside the clay interlayer (Katdare *et al.*, 2000; Olaya *et al.*, 2009a, 2009b; Sivaiah *et al.*, 2010). Katdare *et al.* have employed ultrasonic method for the synthesis of Al-pillared clay from Na, Ca, and La ion-exchanged clay. The ultrasonic method allows faster intercalation of Al-polyoxocations. It was observed that intercalation of Al-polycations is faster in Na-clay as compared to other ion exchanged clays which is related to the extent of electrostatic interaction between the clay sheet and the interlayer cation (Katdare *et al.*, 2000). Similarly, the use of microwave for efficient intercalation of the pillaring cations inside the clay interlayer has been reported. The use of microwave method considerably shortens the pillaring time (Olaya *et al.*, 2009a, 2009b).

A minimum of three washing is required for the better intercalation of the Al-polycations into the clay interlayers (Hutson *et al.*, 1999; Aouad *et al.*, 2005; Moronta *et al.*, 2008). Use of other precursor salt such as sulphate and nitrate causes incomplete intercalation of the cationic species (Mrad *et al.*, 1997). Calcination temperature varies with type of clay material used. Hutson *et al.* have studied the effect of various preparative parameters on the microporosity of the Al-pillared clay. The microporosity of the Al-P strongly depends on the pH of the pillaring solution, calcination temperature and the cation exchange capacity (CEC) of the parent clay. At high calcination temperature, sintering and agglomeration of Al<sub>2</sub>O<sub>3</sub> pillars takes place resulting in a decrease in microporosity. Clay having higher CEC such as Cheto bentonite displays well defined microporosity and superior bimodal pore size distribution as compared to clay with lower CEC like Wyoming bentonite which is related to the pillar density in the clay interlayer (Hutson *et al.*, 1999).

In recent years, in order to develop commercial processes for synthesis of Al-pillared clay, pillaring in concentrated medium has been studied by many authors (Guo *et al.*, 2009; Sanabria *et al.*, 2009a; 2009b). The main approach has been to synthesize the Al-polycation from concentrated metal salt solutions for subsequent utilization in Al-pillared clay synthesis (Aouad *et al.*, 2006; Chen *et al.*, 2007; Guo *et al.*, 2009; Olaya *et al.*, 2009c; Sanabria *et al.*, 2009b). Guo *et al.* have synthesized highly concentrated 80% ε-Al<sub>13</sub> oligomeric species using base hydrolysis and membrane distillation concentration process. The initial pH of the pillaring solution used in the concentration process affects the final concentration of the ε-Al<sub>13</sub> species. The initial pH of 5.00 favours the formation of ε-Al<sub>13</sub> species (Guo *et al.*, 2009). The use of concentrated clay dispersions and microwave or ultrasound irradiation during the intercalation step have been performed to yield Al-pillared clay with superior physicochemical properties (Olaya *et al.*, 2009a; Sanabria *et al.*, 2009a; Yapar *et al.*, 2009). Olaya *et al.* have studied the use of microwave and ultrasound methods for the synthesis of

Al-Fe and Al-Fe-Ce pillared clays. The preparation of pillaring solution and their subsequent intercalation in to the clay interlayer was carried out in presence microwave and ultrasonic waves. The method developed by these authors is found to be advantageous in terms of minimum use of water, efficient uptake of Fe and Ce ions and less intercalation time (Olaya *et al.*, 2009c). Aouad *et al.* have performed pillaring process using a mixture of concentrated chlorhydrol pillaring solution and montmorillonite in dialysis bag. The mixture was dialysed with minimum amount of deionized water thereby introducing the Al-polyoxocations into the interlayers of the clay material. This method is found to yield Al-pillared clay with enhanced microporosity and is advantageous in terms of the use of less amount of solvent (Aouad *et al.*, 2005).

## **1.9 CATALYTIC APPLICATIONS OF Al-PILLARED CLAY**

The Al-pillared clay material because of its higher surface area, uniform microporosity and thermal stability has been employed as catalyst for several organic transformation reactions. The inherent acidic property of the Al-pillared clay is capable of promoting acid catalyzed reactions. Moreover, mixed cationic pillaring with Al- as major component and transition metal and lanthanides as minor component has been studied extensively in literature (Gil *et al.*, 2000a; 2010a, Vicente *et al.*, 2009; Timofeeva *et al.*, 2011a). The mixed cation pillared clay materials have been investigated as catalyst for mineralization of organic pollutants from aqueous sources. The interaction of the transition metal with the Al-pillars and the restricted environment present inside the clay interlayer have been found to be crucial for the catalytic activity displayed by these materials (Herney-Ramirez *et al.*, 2010). Galeano *et al.* has synthesized Al-Fe, Al-Cu and Al-Fe-Cu mixed cation pillared clays, and studied their catalytic activity for catalytic wet peroxide oxidation of methyl orange from aqueous solutions (Galeano *et al.*, 2010). The presence of Fe in the microenvironment of the pillared

clay significantly enhances the wet oxidation process. The interaction between the pillars and the  $\text{Fe}^{3+}$  ions is crucial for site isolation and their catalytic activity. Pillared clays with uniform micropores can be considered as large pore zeolites to carry out many shape selective reactions involving large reactant molecules. Alumina pillared clay based catalytic systems have been studied for several reactions such as catalytic wet peroxide oxidation, CO oxidation, hydroxylation of benzene, hydroformylation of alkenes, epoxidation of cyclooctene, oxidation of propene, hydrodechlorination of 4-chlorophenol, hydrogenation, and hydrodesulfurization of dibenzothiophene. (Kaspar *et al.*, 1992; Pan *et al.*, 2008; Ramaswamy *et al.*, 2008 ; Mata *et al.*, 2009; Gil *et al.*, 2009; Tomul and Balci, 2009; Figueiredo *et al.*, 2009; Galeano *et al.*, 2010; Molina *et al.*, 2010; Aznárez *et al.*, 2011; Romero-Pérez *et al.*, 2012). In addition to their catalytic properties the pillared clay materials have also been evaluated as hydrogen storage materials and as efficient adsorbents for removal of dye from aqueous solutions (Gil *et al.*, 2009; 2011). Moronta *et al.* had compared the catalytic activity of Al- and Fe- ion exchanged clay with that of Al/Fe-mixed cation pillared clays for isomerisation of 1-butene. The Al/Fe-P exhibit superior catalytic activity compared to the ion exchanged clays which have been ascribed to its higher surface area and greater acidic strength. The Alumina-iron oxide pillars contain defect centres that contribute to the acidity of the material (Moronta *et al.*, 2008). Timofeeva *et al.* have studied the synthesis of propylene glycol methyl ether by condensation of methanol and propylene oxide in presence of Al-pillared clay. The activity and the selectivity of the reaction has been correlated to the number of acidic sites which in turn depends on the amount of the Al-content in the pillared clay (Timofeeva *et al.*, 2011b). Tomul and Balci have carried out CO oxidation using Al, Cr and Cr/Al pillared clays as catalyst. They observed that the Al/Cr-mixed pillared clay is highly active for the reaction and presence of Cr as minor component enhances the number of acidic sites in the pillared clay catalyst (Tomul and Balci, 2009). The

catalytic wet peroxidation of toluene had been performed using Al/Cu pillared clays. The presence of Cu in the pillared clay microenvironment significantly enhances the toluene oxidation. Copper being strong electron oxidant favours the homolytic cleavage of H<sub>2</sub>O<sub>2</sub> thereby enhancing the degradation of toluene (Mojović *et al.*, 2009). Al-Cu, Al-Fe, Al-Cu-Fe PILC had been utilized as catalyst for deep oxidation of 4-Chlorophenol. The second metal plays an important role in selectivity of the product (Zhou *et al.*, 2014). The oxidation of industrial dyes reactive black 5 and reactive blue 19 has been reported using Al- Cu PILC as catalyst under mild condition. The mixed cation pillared clay shows stable catalytic activity without any appreciable leaching of the copper ions. The interaction between the alumina pillars and the Cu species has been crucial for the catalytic stability of the pillared clay catalyst (Kim and Lee, 2004). Mixed Al-Fe and Al-Fe-Ce pillared clays have also been evaluated for the phenol oxidation reaction in diluted aqueous medium (Letai'ef *et al.*, 2003; Olaya *et al.*, 2009c). The incorporation of low quantities of Ce and Fe has a beneficial effect on the crystallinity, surface area, porosity and catalytic activity of the Al-pillared clay (Olaya *et al.*, 2009c). The Fe-Al and Cu-Al pillared clays are also found to be active catalysts for deep oxidation of phenols (Barrault *et al.*, 2000). The leaching of copper during the reaction was very low for the Cu-Al pillared clays indicating the strong interaction between the copper and Al-pillars.

### **1.10 Al-PILLARED CLAY AS SUPPORT**

Al-Pillared clay due to its high surface area and uniform pore structure have been used as effective supports for catalytically active components such as oxides, metals and organometallic complexes (Ramaswamy *et al.*, 2002; Issaadi *et al.*, 2006; Sowmiya *et al.*, 2007; Molina *et al.*, 2009a; 2009b; Kanda *et al.*, 2009; Molina *et al.*, 2010; Aznárez *et al.*, 2011). The surface acidic property of Al-pillared clay combined with the supported metallic

particles has been used for bifunctional catalysis. (Ramaswamy *et al.*, 2002; Gil *et al.*, 2006; Achma *et al.*, 2008; Bineesh *et al.*, 2013; Pizarro *et al.*, 2014). In the past few years there have been extensive studies on the preparation, characterization and catalytic activity of supported mono and bimetallic systems on Al-pillared clays (Gil *et al.*, 2001; Louloudi *et al.*, 2003; Mishra and RangaRao, 2007; Molina *et al.*, 2009a; 2009b; Gil *et al.*, 2001; Moronta *et al.*, 2006; Ranga Rao and Mishra, 2007; Barama *et al.*, 2009; Molina *et al.*, 2010). Many of these studies point to the fact that the catalytic efficiency of metallic particles is enhanced significantly when disperse in the Al-pillared clay matrix. The interaction between the metal and alumina pillar in the clay microenvironment has been crucial for the stabilization of the metal particles (Mishra and Ranga Rao, 2007; Molina *et al.*, 2010). The other factor which considerable influence the catalytic activity is the dispersion of the metallic particles in the Al-pillared clay matrix. The uniform dispersion of the metallic particles exposes more number of active metallic sites for catalysis. Pan *et al* studied the catalytic activity of Cu particles supported on Al-PILC for hydroxylation of benzene to phenol. The Al-PILC due to its large internal surface and porosity facilitates well dispersion of the Cu metallic species exposing more numbers of active metallic sites for the reaction. In comparison with a series of conventional support such as silica, alumina and clay, the pillared clay supported catalyst show highest catalytic activity (Pan *et al.*, 2008). Ni-metal supported on Al-pillared montmorillonite and saponite has been studied for hydrogenation of benzene (Louloudi *et al.*, 2003) and CO<sub>2</sub> reforming of methane to form synthesis gas (Wang *et al.*, 1998). The Ni particles present near the acidic sites of the pillared clays are highly active for the hydrogenation of benzene. Al-Pillared clay supported noble metals such as Pd, Pt and Rh have been explored as catalyst for catalytic reduction of nitric oxide, propene combustion, combustion of methyl ethyl ketone, hydrogenation of phenyl alkyl acetylenes, hydrogenation of adipic ester, oxidation of aromatic VOCs and deep oxidation of benzene (Gil *et al.*, 2001;

Marín-Astorga *et al.*, 2005; Zuo and Zhou, 2006; Figueiredo *et al.*, 2008; Oliveira *et al.*, 2008; Molina *et al.*, 2009b; Aznárez *et al.*, 2011). The catalytic activity of Rh/Al-PILC has been studied for the hydrodechlorination of 4-Chlorophenols using molecular hydrogen and formic acid as hydrogen source. The Rh/AL-P material shows well dispersion of the metallic species and stable catalytic activity upto 3 cycles without leaching of the Rh metal during the hydrodechlorination process (Molina *et al.*, 2010). Pd/Al-PILC modified with 1 wt% CeO<sub>2</sub> has been employed as catalyst for the combustion of propene. Ceria as additive partially blocks the microporous volume of the catalyst and interacts with the Pd to form new metallic species that enhance the catalytic property of the Al-PILC supported Pd metal (Aznárez *et al.*, 2014a). Gold nanoparticles supported over mixed Ce-Fe-Al-pillared clay materials have been studied as catalyst for CO oxidation. The size of the gold particles on the pillared clay depends on the nature of clay used. Among different clay materials studied the Al-pillared bentonite show well dispersed gold nanoparticles of smaller size and enhanced catalytic activity for CO oxidation (Álvarez *et al.*, 2012). Fontana *et al.* have carried out the hydrogenation of dimethyl adipate using Ru-Sn bimetallics particles supported over different reducible oxides and Al-pillared clay. Among different supported system, the Al-pillared clay supported system exhibited highest catalytic activity however the selectivity for  $\gamma$  – caprolactone is compromised due to side reactions. The formation of undesired products was suppressed to a greater extent by deposition of barium on the RuSn/Al-PILC catalyst (Fontana *et al.*, 2011). Barama *et al.* had performed reforming of methane with carbon dioxide to synthesis gas using 3-10 wt% Rh, Ni, Pd, Ce metal oxide supported on Al-pillared clays. The CO<sub>2</sub> reforming of methane proceeds effectively on 3% Rh/AL-PILC and 10% Ni/Al-PILC catalysts. The activity of catalysts has been be correlated with the accessible metal surface area. The Al-pillared clay as support stabilizes the metallic or oxidic sites, which in turn are responsible for catalyst activity (Barama *et al.*, 2009). Aznárez *et al.* had studied the catalytic

activity of Pd/Al-P and Pt/Al-P for the oxidation of chlorobenzene. The Pd/Al-P was less active for combustion of chlorobenzene and more selective to CO and oxychlorination reaction, than their Pt/Al-PILC counterparts. The 0.1 wt% Pt/Al-PILC shows high conversion of PhCl with better selectivity compared to other supported catalyst studied for this reaction (Aznárez *et al* 2014b).

Pillared clays have also been used as supports for several catalytically active metal oxides which include MnO<sub>2</sub> (Gandia *et al.*, 2002), MoO<sub>3</sub> (Saleno *et al.*, 2001), V<sub>2</sub>O<sub>5</sub> (Vicente *et al.*, 2003; Bineesh *et al.*, 2011), V<sub>2</sub>O<sub>5</sub> -WO<sub>3</sub> (Long and Yang, 2000) and CoO (Hayashi *et al.*, 1999). The dispersion of the oxide components and their catalytic activity depend upon the type of clay material and the pillaring species used. (Salerno *et al.*, 2001; Gil *et al.*, 2006; Zuo *et al.*, 2009; Bineesh *et al.*, 2013; Zhang *et al.*, 2013b). Gandia *et al.* (2002) have studied complete oxidation of acetone over MnO<sub>2</sub> catalyst supported on a series of Al- and Zr-pillared montmorillonites and saponites. The MnO<sub>2</sub> catalyst supported on montmorillonite clay invariably shows better catalytic activity compared to saponite. Alumina pillared clay has been examined as possible support for MoO<sub>3</sub> based HDS catalysts (Saleno *et al.*, 2001). A strong interaction between Mo species and alumina pillared clay has been observed in the TPR study of the catalyst material. The catalytic activity of sulfated tin oxide particles (STO) supported on Al-pillared clay have been studied for the solvent-free synthesis of 3,4-dihydropyrimidin-2(1H)-ones, thiochromans, and coumarins (Sowmiya *et al.*, 2007). The STO particles are present in a well dispersed form in the pillared clay matrix and acidic properties of the pillared clay have been found to supplement the catalytic activity of the supported catalyst. Bineesh *et al* have performed a comparative study of the catalytic activity of vanadia nanoparticles supported over Ti-, Zr-, Fe- and Al- pillared clays for selective H<sub>2</sub>S oxidation. Among the four pillared clay employed as support, the vanadia



particles supported on Al-pillared clay show highest activity and selectivity of elemental sulphur (Bineesh *et al.*, 2013).

The Al-Pillared clay has also been used as an efficient support to anchor catalytically active organometallic complexes (Ramaswamy *et al.*, 2002; Costa *et al.*, 2004; Biernacka *et al.* 2007). Ramaswamy *et al.* have employed ultrasonic technique for immobilising copper-tetra decachlorophthalocyanine (Cu-Cl<sub>14</sub>Pc) complex into the matrix of the Al-pillared clay. Ultrasonication method is found to be more effective for immobilization of complex than normal agitation method as the former helps in better dispersion of the Cu-complex in the pores of the Al-pillared clay. The copper phthalocyanine complexes display excellent catalytic activity for hydroxylation of phenol to catechol and hydroquinone. The isolated copper species present in the pores of Al-PILC serve as active sites to carry out the hydroxylation process (Ramaswamy *et al.*, 2002). Immobilisation of Mn(III) salen complexes into Al-pillared clay following different methodologies has also been reported. The catalytic activity of the Mn(III) salen complex immobilized Al-PILC has been examined for the epoxidation of styrene with iodosylbenzene acting as the oxygen source. The catalytic material prepared by direct immobilisation method shows greater catalytic efficiency and can be reused for several times without leaching of the active phase (Biernacka *et al.* 2007). Table 1.4 summarizes some of the recent catalytic studies performed using Al-pillared clay materials and their modified analogues.

**Table 1.4 Catalytic applications of Al-pillared clay based catalytic materials.**

<b>Catalyst</b>	<b>Interlayer spacing (Å)</b>	<b>Surface area (m<sup>2</sup>/g)</b>	<b>Reaction</b>	<b>Reference</b>
Fe-Al-P	16.7	210	4-chlorophenol oxidation	Zhou <i>et al.</i> , 2014
Pd/Al-P	--	172	HDC/HDN of 4-chloronitrobenzene	Pizarro <i>et al.</i> , 2014
Ce-Pd/Al-P	--	58	Combustion of propene	Aznárez <i>et al.</i> , 2014a
Al-P	18.5	279	Thiabendazole removal	Jalil <i>et al.</i> , 2014
Cr-Al -P	9.8	84	Oxidative dehydrogenation of propane	León <i>et al.</i> , 2014
Fe <sub>2</sub> O <sub>3</sub> /Al-laponite	--	413	Oxidation of H <sub>2</sub> S	Zhang <i>et al.</i> , 2013b
V <sub>2</sub> O <sub>5</sub> /Al-P	17.6	170	Oxidation of H <sub>2</sub> S	Bineesh <i>et al.</i> , 2013
Au/Ce-Fe-Al -P	18.3	104	CO oxidation	Álvarez <i>et al.</i> , 2012
Al-P	18.0	203	Synthesis of propylene glycol methyl ether	Timofeeva <i>et al.</i> , 2011b
Rh/Al-P	19.2	205	HDC of 4-chlorophenol	Molina <i>et al.</i> , 2010
Cu-Al-P	15.8	--	Toluene oxidation	Mojović <i>et al.</i> , 2009
Pd/Al-P	18.6	182	HDC of 4-chlorophenol	Molina <i>et al.</i> , 2009a
Cr-Al-P	17.2	96	CO oxidation	Tomul and Balci, 2009
Ni-Al-P	18.0	113	Reforming of methane	Barama <i>et al.</i> , 2009

Al-P	16.4	176	Isomerisation of 1-butene	Moronta <i>et al.</i> , 2008
Cu/Al-P	18.2	123	Wet H <sub>2</sub> O <sub>2</sub> oxidation of tyrosol	Achma <i>et al.</i> , 2008
Pt/Al-P	18.0	162	Hydrogenation of adipic ester	Figueiredo <i>et al.</i> , 2008
Cr/Al-P	17.1	156	Oxidation of chlorobenzene or xylene	Oliveira <i>et al.</i> , 2008
CuPd/Al-P	18.2	--	Nitrate reduction	Ranga Rao and Mishra, 2007
MnO <sub>2</sub> /Al-P	20.5	280	Oxidation of acetone	Gil <i>et al.</i> , 2006
Pd-Ce/Al-P	18.2	238	Oxidation of benzene	Zuo and Zhou, 2006
CoMo/Al-P	16.0	84	Dehydrogenation of ethylbenzene	Moronta <i>et al.</i> , 2006
Pd/Al-P	17.0	154	Hydrogenation of phenyl alkyl acetylenes	Mar'in-Astorga <i>et al.</i> , 2005
Cu-Al-P	18.0	147	Reactive dyes oxidation	Kim and Lee, 2004
Al-P Wyoming montmorillonite	17.5	297	Hydroxylation of phenol	Letai'ef <i>et al.</i> , 2003
Al-P bentonite	17.5	205	Hydroxylation of phenol	Letai'ef <i>et al.</i> , 2003
phthalocyanine/Al-P	19.3	135	Hydroxylation of phenol	Ramaswamy <i>et al.</i> , 2002
Pt/Al-P	--	132	Combustion of methyl-ethyl-ketone	Gil <i>et al.</i> , 2001

## 1.11 Zr-PILLARED CLAY

The Zr-pillared clay is another class of pillared clay material which has been extensively investigated as catalyst and support for carrying out a variety of organic transformation (Gand'ia *et al.*, 2002; Jinjun *et al.*, 2005; Sadykov *et al.*, 2006; Mnasri-Ghnimi and Frini-Srasra, 2014). The Zr-pillared clays are generally prepared by intercalation of  $[\text{Zr}_4(\text{OH})_8(\text{H}_2\text{O})_{16}]^{8+}$  oligomeric cationic species into the clay interlayer. The aqueous chemistry of zirconium salt solutions has been studied earlier by many authors (Muha and Vaughan, 1960; Clearfield, 1964; Singhal *et al.*, 1996). Zirconium ion is known to form stable tetrameric species in moderately concentrated and acidic solutions with structural formula  $[\text{Zr}_4(\text{OH})_8(\text{H}_2\text{O})_{16}]^{8+}$  and size  $0.89 \times 0.89 \times 0.58 \text{ nm}^3$  ((Fig. 1.11).

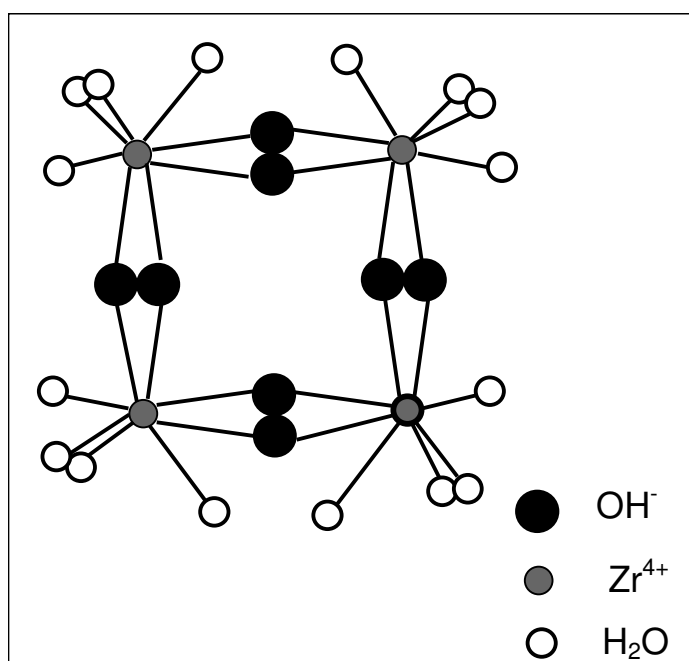


**Figure 1.11** Structure of the  $[\text{Zr}_4(\text{OH})_8(\text{H}_2\text{O})_{16}]^{8+}$  pillaring polycation

These tetrameric species are well characterized in solution and are considered to be the major oligomeric species present in the pillaring solution (Vaccari, 1998; Cool and Vansant, 1996; Singhal *et al.*, 1996). The structure of the complex ion in solution is described as square

planar with  $Zr^{4+}$  ions located at the corners of the square which are joined by two bridging  $OH^-$  ions along each edge (Muha and Vaughan, 1960; Bartley, 1988; Mompean *et al.*, 2005). The eight-fold coordination of  $Zr^{4+}$  ion is satisfied by the oxygen atoms of four surrounded water molecules. Zirconium ions form larger polymeric species in solution upon aging at elevated temperature under mild acidic condition (Baes and Mesmer, 1976; Yamanaka and Brindley, 1979; Farfan-Torres *et al.*, 1992; Chaabene *et al.*, 2004). It has been observed that further hydrolysis of the tetrameric species takes place at elevated temperature to generate larger cationic clusters. This aspect of zirconium ion aqueous chemistry has been exploited in pillared clay synthesis to generate Zr-pillared clay materials with different gallery height and porosity. Zr-pillared clay with different degree of hydrothermal stability, crystalline nature and interlayer expansion have been prepared by using thermally aged, refluxed and hydrothermally treated Zr-pillaring solutions (Ohtsuka *et al.*, 1993; Cool and Vansant, 1996, Mishra and Ranga Rao, 2003; Bineesh *et al.*, 2012). The physiochemical properties of the Zr-pillared clay material depends on several factors such as the genesis of the polycation, method and pH of intercalation, Zr/Clay molar ratio used in intercalation process, washing, drying and calcination steps (Bartley, 1988; Awate *et al.*, 2001; Mishra and Ranga Rao, 2003; Guerra *et al.*, 2008; Mnasria and Frini-Srasra, 2013). It has been observed that thermally stable Zr-pillared clay can be synthesized using pillaring solution with pH  $\sim 2.7$ . When the pillaring is performed under highly acidic condition, delamination of the clay occurs which prevents the fixation of the pillars to the clay sheet (Sun Kou *et al.*, 1998; Klopogge, 1998; Mnasria and Frini-Srasra, 2013). Similarly, the Zr/clay ratio used in pillaring process has an impact on the final properties of the Zr-pillared clays (Sun Kou *et al.*, 1998; Guerra *et al.*, 2008). If the Zr/clay ratio is  $< 2\text{ meq/g}$ , then uneven distribution of the pillars in the clay matrix takes place resulting in material with low thermal stability. Similarly, for Zr/clay ratio  $> 20\text{ meq/g}$  of clay, delamination of the clay takes place and instead of pillaring, amorphous

zirconia particles are intercalated into the clay (Sun Kou *et al.*, 1998). The ageing temperature and time of the pillaring solution is a crucial factor which influences the porosity as well as interlayer spacing of the Zr-pillared clay (Farfan-Torres *et al.*, 1992; Mishra and Ranga Rao, 2003; Chaabene *et al.*, 2004). As stated earlier further hydrolysis and polymerization of the tetrameric species takes place at elevated temperature. Upon aging the pillaring solution at elevated temperature, Zr-pillared clay with different gallery height has been synthesized (Ohtsuka *et al.*, 1993; Mishra and Ranga Rao, 2003). Tomul had synthesized cerium modified Zr pillared clays by following conventional as well as ultrasonic intercalation methods. The ultrasonic treatment considerably decreases the time period for Zr-P synthesis. Nevertheless the textural characteristics of the pillared clays obtained from both methods are similar. It is observed that on modification with Ce, the Ce-Zr-P prepared by ultrasonic method shows higher number and strength of acidic sites as compared to Ce-Zr-P prepared using conventional method (Tomul, 2011). The intercalation time can also be reduced by applying microwave radiation. Zr-pillared clay with well-ordered structure has been synthesized by MW induced intercalation of the pillaring species with in an exposure time of 10-30 min. However, MW irradiation does not have significant impact over the textural and chemical properties of the Zr-P (Fetter *et al.*, 2003). Drying of the as synthesized pillared clay materials have been done using freeze, vacuum and air drying. The drying and washing steps also influences the physicochemical properties of the pillared clay. The Zr-P materials with greater microporosity and higher basal spacing have been synthesized, when methanol is used as a solvent to remove excess water during washing step followed by drying at lower temperature. The methanol treatment promotes stacking of the polymeric clusters in the clay interlayer (Bartley, 1988).

## 1.12 Zr-PILLARED CLAY AS CATALYST AND SUPPORT

Zr-pillared clay and their modified analogues due to high surface area, uniform pore size distribution, and acidic property have been investigated as catalyst and support for several organic transformations (Awate *et al.*, 2001; Molina *et al.*, 2006; Anisia and Kumar, 2007; Guerra *et al.*, 2008). The catalytic efficiency of Zr-pillared clays has been modified by mixed cation pillaring, grafting sulphate ions and supporting various metallic and oxidic phases (Gand'ia *et al.*, 2002; Sadykov *et al.*, 2006; Jinjun *et al.*, 2005; Samantaray *et al.* 2011; Mnasri-Ghnimi and Frini-Srasra, 2014). The mixed cationic pillaring offers advantages in terms of increase in its thermal stability as well as number of acidic sites (Hao *et al.*, 2003; Molina *et al.*, 2006; Guerra *et al.*, 2008b). Grafting sulphate species onto the zirconia nanopillars enhances significantly the acidic property of the pillared clay material (Chaabene *et al.*, 2004; Samantaray *et al.* 2011; Fatimah *et al.*, 2014). Guerra *et al.* have studied the alkylation of benzene using olefins as alkylating agent over Zr-pillared clay materials prepared from Brazilian montmorillonite and Wyoming clays. The TPD study of Zr-P materials indicates that the pillared montmorillonite has less number of acidic sites as compared to pillared Wyoming clay material. The Zr-pillared Wyoming clay shows higher selectivity for the monoalkylated products (Guerra *et al.*, 2008). The catalytic activity of Al-Zr-mixed pillared vermiculite materials have been studied for isomerization and hydrocracking of n-decane. The mixed pillared vermiculite obtained by subjecting the parent vermiculite to hydrothermal treatment followed by intercalation of Al-Zr mixed polycations are thermally stable and display excellent catalytic activity (Campos *et al.*, 2008). The catalytic application of various Zr-pillared clay based materials is presented in Table 1.5.

In addition to synthesis of molecules with industrial utility, Zr-pillared clay materials have also been used as catalyst for synthesis of bioactive molecules and heterocycles. Singh *et al.* have studied the synthesis of tetrahydropyrans by cyclization of various symmetrical 1,n-

diols using Zr-pillared clay as catalyst following conventional method as well as microwave irradiation. The Zr-P material was more active compared to KSF and K-10 catalyst. The elimination of diffusional constraints due to structural expansion and the increase in number of Lewis acidic sites due to pillaring has been proposed to be responsible for higher catalytic activity (Singh *et al.*, 2004b). Similarly, the synthesis of biologically important dihydropyrimidinone (DHPM) moieties by multicomponent one pot condensation of aryl aldehyde, ethyl acetoacetate and urea is catalysed by Zr-pillared clay. The enhanced acidity of the clay material achieved due to pillaring has been responsible for the catalytic activity (Singh *et al.*, 2006). Samantaray *et al* have studied the synthesis of  $\beta$ -aminocarbonyl compounds by multicomponent condensation of aryl aldehydes, substituted aniline and acetophenone over modified zirconia pillared clay in aqueous media. It has been observed that treatment of the Zr-pillared clay material with mild sulphuric acid followed by supporting phosphomolybdic acid over the surface of Zr-pillared clay significantly enhances its catalytic activity (Samantaray *et al* 2011). Mnasri-Ghnimi and Frini-Srasra have studied the catalytic activity of the  $Ce^{3+}$  intercalated mixed Al-Zr pillared clay for 1,3-dioxolane synthesis from the reaction between ethylene glycol and acetone. The pillared clays containing Zr-polyoxocations as major pillaring species have greater catalytic efficiency than that of Al-pillared clays. The addition of  $Ce^{3+}$  to the Zr pillared clays increases the yield of the product which is correlated with the acidity of the pillared clays (Mnasri-Ghnimi and Frini-Srasra, 2014). The ensuing discussion on the catalytic application of Zr-pillared clay indicate that, these materials have promising application potential in catalysis involving synthesis of biologically important molecules.

Beside the application of Zr-Pillared clay as catalyst, it has also been used as an efficient support for catalytically active phases. In many cases, the acidic sites of the Zr-pillared clay work synergistically with catalytically active phases. The Zr-pillared clay has been used as



support for noble and transition metal, oxides, sulphides and organometallic complexes (Hao *et al.*, 2003; Coli'n L. *et al.*, 2005; Anisia and Kumar, 2007; Shen *et al.*, 2014). Hao *et al.* have studied the catalytic reforming of methane with carbon dioxide using nickel particles supported over Zr-pillared laponite clay. The Zr-pillared clay material was synthesized from a structurally expanded clay material where polyethylene oxide is used as structure expansion agent. The Zr-pillared clay prepared by this method show enhanced surface area and pore volume compared to conventional Zr-pillared clays. The Ni/Zr-P material show higher initial conversion and long-term stability for the reforming reaction (Hao *et al.*, 2003). Molybdenum sulfide ( $\text{MoS}_2$ ) particles supported over Al- and Zr-pillared clays ( $\text{MoS}_2/\text{Zr-P}$ ) have been evaluated as catalyst for hydrogenation of naphthalene.  $\text{MoS}_2$  catalysts supported on Zr-pillared clays were more active than the samples supported on Al-pillared clays and pure alumina support. The higher hydrogenation activity of the  $\text{MoS}_2/\text{Zr-P}$  has been ascribed to the presence of small  $\text{MoS}_2$  nanoparticles particles interacting strongly with the zirconia pillars (Coli'n L. *et al.*, 2005). Issaadi and Garin have compared the catalytic activity of palladium particles supported over sulphated Zr-pillared clay, Al-pillared clay and alumina for hydroisomerisation of hexane. The Pd/SZr-P material found to exhibit highest catalytic activity with >98% selectivity to isomerized product. The synergetic effect between the acidic site of the support and the active Pd species has been invoked to explain the catalytic activity (Issaadi and Garin, 2003). Similarly, vanadia particles supported over Zr-pillared clay show excellent catalytic activity for the oxidation of hydrogen sulphide with good selectivity to elemental sulphur (Bineesh *et al.*, 2012).

**Table 1.5 Catalytic applications of Zr-pillared clay based catalytic materials.**

Catalyst	Basal spacing (Å)	Surface area (m <sup>2</sup> /g)	Catalytic study	Reference
SO <sub>4</sub> <sup>2-</sup> /Zr-P	--	287	conversion of citronellal to isopulegol	Fatimah <i>et al.</i> , 2014
Ce-Zr-P	19.3	180	synthesis of 1,3-dioxolane	Mnasri-Ghnimi and Frini-Srasra, 2014
V <sub>2</sub> O <sub>5</sub> /Zr-P	~46	228	Oxidation of H <sub>2</sub> S	Bineesh <i>et al.</i> , 2012
H <sub>3</sub> PMo <sub>12</sub> O <sub>40</sub> /SZr-P	18.8	132	synthesis of β-minocarbonyl compounds	Samantaray <i>et al.</i> , 2011
Zr-P (Brazilian clay)	23	206	Alkylation of benzene	Guerra <i>et al.</i> , 2008
Zr-P (Wyoming clay)	23.2	217	Alkylation of benzene	Guerra <i>et al.</i> , 2008
Fe-Cu /Zr-P	--	99	Oxidation of cyclohexane	Anisia and Kumar, 2007
Zr-P	21	224	Synthesis of dihydropyrimidinones	Singh <i>et al.</i> , 2006
Zr-P	1.77	192	Catalytic wet peroxide oxidation of phenol	Molina <i>et al.</i> , 2006
Fe-Zr-P	1.83	211	Catalytic wet peroxide oxidation of phenol	Molina <i>et al.</i> , 2006
Pt-Cu/Zr-P	-	-	NOx selective catalytic reduction by propylene and decane	Sadykov <i>et al.</i> , 2006
Ce-Zr-P	19.2	117	cyclohexanol dehydration	Mishra and Ranga Rao, 2005
Pd/Zr-P (laponite)	-	474	oxidation of benzene	Jinjun <i>et al.</i> , 2005
Zr-P	21	224	acylation of 1,n-diols	Singh <i>et al.</i> , 2004b
Zr-P	21	224	monotetrahydropyranylation of diols and alcohols	Singh <i>et al.</i> , 2004a
SO <sub>4</sub> <sup>2-</sup> /Zr-P	-	267	isopropanol dehydration and isomerization of n-hexane	Chaabene <i>et al.</i> , 2004

Ni/Zr-P	-	371.9	methane reforming with carbon dioxide	Hao <i>et al.</i> , 2003
MnO <sub>2</sub> /Zr-P (saponite)	-	280	oxidation of acetone	Gand'ia <i>et al.</i> , 2002
Zr-P	17	272	Phenol hydroxylation	Awate <i>et al.</i> , 2001
V <sub>2</sub> O <sub>5</sub> / Zr-P	11.6	99	Oxidative dehydrogenation of propane	Bahranowski <i>et al.</i> , 2000

### 1.13 Cr-PILLARED CLAYS

The previous sections described the physicochemical properties and catalytic application of Al- and Zr-pillared clay materials. The other class of pillared clay material which has attracted significant attention from researchers is chromia-pillared clay for their wide application in catalysis (Skoularikis *et al.*, 1988; Storaro *et al.*, 1997; Akçay, 2004; Gyftopoulou *et al.*, 2005; Mata *et al.*, 2007; Tomul and Balci, 2009; León *et al.*, 2014). Cr-pillared clay is prepared by intercalating hydroxy chromium oligomeric cationic clusters into the interlayer of the clay material. The physicochemical characteristics of Cr-P is tailored by various factors such as methods of preparation, type of clay used, strength of the base used, stoichiometry ratio of base to Cr ions (n), stoichiometric coefficient of Cr ion to clay and the ageing temperature and time (Pinnavaia *et al.*, 1985a; Tzou and Pinnavaia, 1988; Volzon *et al.*, 1993, Kirksi *et al.*, 1997; Akçay, 2004). Various salts of chromium such as chloride, nitrate, acetylacetonate, acetate and chlorite have been widely used as precursor for preparation of the chromium pillaring solution (Lopez *et al.*, 1993; Mata *et al.*, 2007; Yurdakoc *et al.*, 2008; Arafoui *et al.*, 2009). Base hydrolysis of the chromium salt leads to formation of different types of polyoxocations such as  $[\text{Cr}_2(\text{OH})_2(\text{H}_2\text{O})_8]^{4+}$  (dimer),  $[\text{Cr}_3(\text{OH})_4(\text{H}_2\text{O})_9]^{5+}$  (trimer),  $[\text{Cr}_4(\text{OH})_6(\text{H}_2\text{O})_{11}]^{6+}$  (open tetramer)  $[\text{Cr}_4(\text{OH})_5\text{O}(\text{H}_2\text{O})_{10}]^{5+}$  (closed tetramer), or even hexamers (Carr, 1985; Toranzo *et al.*, 1997; Mata *et al.*, 2007). Non complexing bases such as NaOH and Na<sub>2</sub>CO<sub>3</sub> have been used to carry out the partial

base hydrolysis of the Cr salt solution (Sychev *et al.*, 1997a; Kirksi *et al.*, 1997; Dubbin *et al.*, 1999; Roulia 2005). However use of strong base such as NaOH causes precipitation of Cr(OH)<sub>3</sub> phase. Precipitation of chromium hydroxide in the pillaring solution can be prevented by using milder base such as Na<sub>2</sub>CO<sub>3</sub> or by decreasing the concentration of NaOH (Tzou and Pinnavaia, 1988). The extent of formation and size of the oligomeric cluster in the pillaring solution depends on the ageing time and temperature. The hydrolysis of the Cr ions is a slow process at room temperature. However, at elevated temperature (60-90°C), the hydrolysis process is completed within one or two days (Tzou and Pinnavaia, 1988; Drljaca *et al.*, 1997; Sychev *et al.*, 1997a; Arafoui *et al.*, 2009). Pillaring solution containing larger oligomeric clusters in significantly higher amount can be obtained by carrying out the hydrolysis under reflux condition using mild base as hydrolysing agent (Pinnavaia *et al.*, 1985a; Lopez *et al.*, 1993). The Cr-polyoxocations have also been prepared by quick addition of both NaOH and HClO<sub>4</sub> to a Cr salt solution followed by refluxing to generate higher amount of oligomeric clusters in the pillaring solution (Drljaca *et al.*, 1997; Roulia, 2005). Other acids such as HCl and HNO<sub>3</sub> have also been used in place of HClO<sub>4</sub> (Roulia, 2005). The addition of both base and acid reduces the ageing period. The base/Cr (n) ratio regulates the hydrolysis process and generation of the polycationic species (Brindley and Yamanaka, 1979; Carr, 1985). Pillared clays with high interlayer spacing (23-27.6 Å) are obtained when the base/Cr ratio in the range of 1.5-2.5 is used in hydrolysis process (Tzou and Pinnavaia, 1988; Arafoui *et al.*, 2009). The effect of stoichiometric coefficient (mmol Cr/clay) on the textural properties of Cr-pillared clay has been studied by several authors (Volzone, 1995; Gyftopoulou *et al.*, 2005). Cr-pillared smectites have been synthesized using Cr/Clay molar ratio in the range 0.5- 20 mmol/g. With increase in Cr/clay ratio, thermal stability and basal spacing of the Cr-P was found to increase with an optimum value of 20.7 Å obtained at 20 mmol Cr/g of clay (Volzone, 1995). Tzou and Pinnavia have synthesized Cr-P clay with basal

spacing of 27.6 Å using the Cr/clay ratio of 50 mmol/g from a thermally aged (95°C) pillaring solution (Tzou and Pinnavaia, 1988). Clay materials differing in composition, structure and layer charge density have been used for the preparation of the Cr-pillared clays (Volzone, 2001; Gyftopoulou *et al.*, 2005; Yurdakoc *et al.*, 2008; Tomul and Balci, 2009). The Cr uptake depends significantly on the layer charge density which in turn affects the thermal stability and textural property of the Cr-pillared clay material (Tomul and Balci, 2009).

Cr-pillared clays display Lewis acidic centres as well as enhanced microporous character compared to other pillared clay materials (Auer and H. Hofmann, 1993; Sychev *et al.*, 1997b; Akçay, 2004). These properties of Cr-pillared clay have been exploited for its application as heterogeneous solid acid catalyst for various organic transformations. Cr-pillared clays have been used as catalyst to carry out various shape selective reactions such as methylation of toluene, hydrocracking of heavy fuels, propene oxidation, n-decane cracking, acylation of alcohol, oxidation of chlorinated hydrocarbon and carbon monoxide (Skoularikis *et al.*, 1988; Storaro *et al.*, 1997; Akçay, 2004; Gyftopoulou *et al.*, 2005; Mata *et al.*, 2007; Binitha and Sugunan, 2008; Tomul and Balci, 2009). The sulfidation of the Cr-pillared clay has also been done to generate sulfided chromium pillared clays which has been employed as catalyst for the hydrodesulfurization of thiophene and hydrogenation of butane (Sychev *et al.*, 1995). Sychev *et al.* observed that sulfided Cr-pillared bentonite shows better catalytic activity than Cr-pillared sulfided K-10 catalyst (Sychev *et al.*, 1995). Gyftopoulou *et al.* have studied the catalytic activity of Cr-pillared laponites and montmorillonite clay for hydrocracking of coal derived hydrocarbons. The open channels of the pillared clay combined with the expanded interlayer facilitate the diffusion of bulky substrate molecules to the reactive sites in the clay interlayer (Gyftopoulou *et al.*, 2005). The synergistic effect between the active sites of the chromia pillars and clay layers have been invoked to explain the activity for hydrocracking

process (Bodman *et al.*, 2003, Gyftopoulou *et al.*, 2005). Binitha and Sugunan have carried out shape selective toluene methylation using Cr-pillared and mixed Cr/Zr-P, Cr/Al-P and Cr/Ti-Al-P as catalyst. The pillared clay materials are more selective towards the p-xylene which has been explained in terms of restricted lateral space between the pillars. The thermal stability and recyclability of the chromium pillared clays is enhanced in presence of Zr, Al, Ti as second pillaring component (Binitha and Sugunan, 2008). Tomul and Balci have employed Cr/Fe bentonites for wet peroxide oxidation of phenol. The catalytic activity of the Fe/Cr-pillared bentonites is regulated by the number and distribution of the active sites on the surface of the catalyst (Tomul and Balci, 2009). Leon *et al* have observed that the Cr-Al-mixed pillared clays show excellent catalytic activity for propane dehydrogenation. They have identified the Cr-Al-O bond at the pillar-clay junction as the active sites which are highly selective for propylene formation (Jibril, 2004; León *et al.*, 2014). Vicente *et al.* have studied the dehydrogenation of ethylbenzene employing Al-Cr-pillared saponites as catalyst. The catalyst activity of the mixed cation pillared clay correlate well with the Al/Cr ratio in the interlayer. The introduction of the mixed cation pillars increases the surface area of the saponite clay, thereby exposing the Brønsted and Lewis acidic sites for the substrate molecules. Increase in Al content in the pillars enhances the selectivity towards styrene, whereas increase in Cr content leads to cracking activity (Vicente *et al.*, 2002). Mishra and Parida prepared sulphate grafted Fe-Cr mixed pillared clay and examined their catalytic activity for methanol dehydration. At a sulphate loading of  $\leq 2\text{wt}\%$ , new Lewis acidic sites of higher strength are generated in the pillared clay leading to improved catalytic activity. When the sulphate loading is increased further, partial blocking of the pores of the pillared clay was observed with a consequent decrease in surface area and catalytic activity of the pillared clay (Mishra and Parida, 2006). The catalytic applications of various Cr-pillared clay based materials are listed in Table 1.6.

**Table 1.6 Catalytic applications of Cr-pillared clay based catalytic materials.**

Catalyst	Basal spacing (Å)	Surface area (m <sup>2</sup> /g)	Catalytic study	Reference
Cr-P	9.5	57	oxidative dehydrogenation of propane	León <i>et al.</i> , 2014
Al-Cr-P	18	257	CO oxidation	Tomul and Balci, 2009
Zr-Cr-P	20.4	125	toluene methylation	Binitha and Sugunan, 2008
Al-Cr-P	17.2	240	propene oxidation	Mata <i>et al.</i> , 2007
Cr-P	15.9	-	Hydrocracking of heavy liquid fuels	Gyftopoulou <i>et al.</i> , 2005
SO <sub>4</sub> <sup>2-</sup> /Fe-Cr P	18.1	228	Methanol conversion	Mishra and Parida, 2006
Fe-Cr-P	10.5	67.6	Acylation of alcohols with acetic acid	Akçay, 2004
Al-Cr-P	19.9	310	Dehydrogenation of ethylbenzene	Vicente <i>et al.</i> , 2002
Cr <sub>2</sub> S <sub>3</sub> -P	26.3	278	thiophene hydrodesulfurization	Sychev <i>et al.</i> , 1997
Cr-P	15.2	353	deep oxidation of methylene chloride	Storaro <i>et al.</i> , 1997
Cr-P	17.8	286	Nitration of chlorobenzene	Mishra <i>et al.</i> , 1997
Cr-P	-	279	toluene disproportionation	Auer and Hofmann, 1993
Cr-P	-	200	Cumene conversion	Bradley and Kydd, 1993b
Cr-P	-	200	Dehydrocyclodimerization of propane	Bradley and Kydd, 1993a
Cr-P	23.6	-	Benzylic Oxidation and Oxidative Deprotection reactions	Choudary <i>et al.</i> , 1992
Cr-P	27	353	Dehydrogenation of cyclohexane	Pinnavaia <i>et al.</i> , 1985a

The literature survey on the three classes of pillared clay (Al-, Zr- and Cr-) presented in the preceding sections clearly points to the fact that they are promising catalytic materials for

activation and chemical transformation of a variety of small molecules with industrial utility. However, the catalytic potential of pillared clay materials in organic synthesis involving bulky heterocyclic compounds is yet to be explored fully. The interlayer space of pillared clay (~ 1 nm) intermediate between the micropore and mesopore range is ideal for construction of bulky molecules. Moreover, the number of acidic sites in pillared clay matrix can be enhanced by supporting catalytically active phases as well as by forming nanocomposites. In this work, the specific issues concerning enhancement of acidic property of pillared clays and their utilization in synthesis of biologically important heterocyclic compounds have been addressed. Catalytically active phases with well-defined acidic properties such as silicotungstic acid, Sulfonated polyvinyl alcohol and polyphosphoric acid have been dispersed in the pillared clay matrix and their interactions with clay structure have been investigated. The pillared clay based composite systems have been investigated as heterogeneous catalysts for synthesis of biologically important heterocyclic molecules using multicomponent condensation approach.

#### **1.14 OBJECTIVES OF THE PRESENT STUDY**

*General objective:*

The broad objective of this study is to apply pillared clays and their novel derivatives for the synthesis of the biological important molecules and for detoxification of waste water containing halogenated aromatics.

*Specific objectives:* The specific objectives of this work is

1. To evaluate the applicability of Cr-pillared clay material as heterogeneous catalyst for synthesis of biologically potent xanthene derivatives.
2. To disperse silicotungstic acid nanoclusters (STA) in the micropores of Cr-pillared clays (Cr-P) and to evaluate the catalytic activity of the composite catalytic system (STA/Cr-P) for synthesis of structurally diverse dihydropyridine molecules.



3. To prepare and characterize novel Zr-pillared clay-polyphosphoric acid (ZrP-PPA) and Zr-pillared clay-sulfonated poly vinyl alcohol (ZrP-SPVA) composite catalytic system.
4. Evaluation of catalytic activity of the ZrP-PPA and ZrP-SPVA nanocomposites for synthesis of biologically important tetrahydropyridines and hexahydropyrimidines molecules, respectively.
5. Investigation of the catalytic activity of the Pd based mono and bimetallic (Pd-Ni and Pd-Cu) nanoparticles supported over Al-pillared clay for hydrodehalogenation of halogenated aromatic organic pollutants from aqueous phase.

The results obtained in this investigation are described in the following chapters.

**Chapter 1:** This chapter describes the present understanding as well as recent developments in synthesis and catalytic application of various pillared clays. Different preparatory strategies adopted in literature for the synthesis of alumina, zirconia and chromia pillared clays and their impact on the physicochemical characteristics of the pillared clays has been presented. The utility of the pillared clay materials in the field of catalysis have been emphasized with suitable examples.

**Chapter 2:** This chapter presents the detail experimental procedure adopted for the synthesis of chromia, zirconia, alumina pillared clays and their modified analogues. The instrumental techniques used for the studying physicochemical characteristics of the prepared materials and the method of analysis are briefly explained in this chapter. The experimental method employed for synthesis of octahydroxanthenes, benzoxanthenes, dihydropyridines, tetrahydropyridines, hexahydropyrimidines and hydrodechlorination of organic pollutants from aqueous phase are described. The product analysis protocols are also outlined.

**Chapter 3:** This chapter describes the physicochemical characterization and catalytic applications of Cr-pillared clay based materials. This chapter is divided into two parts. Part A comprises of characterization and catalytic activity of the Cr-pillared clay. The study of

physicochemical properties of the Cr-pillared using XRD, FTIR, UV-Vis, TGA and sorptometric method is described. The catalytic activity data for the synthesis of octahydroxanthenes and benzoxanthene have been presented. Part B deals with the characterization and catalytic application of silicotungstic acid nanoclusters supported on Cr-pillared clay materials. The catalytic activity of the supported system has been studied for the synthesis of dihydropyrimidones.

**Chapter 4:** A detail study of synthesis, characterization and catalytic application of Zr-pillared clay based composite materials are presented in this chapter. The chapter contains the catalytic results of two composite catalytic systems based on zirconia pillared clay. Part A deals with study of polyphosphoric acid–Zr pillared clay composite materials and their catalytic application for synthesis of tetrahydropyridines. Part B describes the synthesis and characterization of sulfonated polyvinyl alcohol (SPVA)-Zr-P composite materials. The catalytic application of SPVA-ZrP composite material for the synthesis of hexahydropyrimidines is presented.

**Chapter 5:** In this chapter the applicability of Al-pillared clay as support for catalytically active palladium and palladium based bimetallic particles has been examined and their catalytic application in environmental catalysis is presented. The chapter includes two parts. Part A deals with characterization and catalytic application of Pd nanoparticles supported on Al-pillared clay (Pd/Al-P). Part B of this chapter explains the effect of second metallic component on the catalytic property of supported Pd nanoparticles on Al-pillared clay. The catalytic test results for both mono and bimetallic particles supported on Al-P for hydrodehalogenation of a variety of halogenated organic compounds is outlined in this chapter.

**Chapter 6:** The summary of results obtained from various investigations and the major conclusions drawn from these studies are presented in this chapter.

## CHAPTER 2

### MATERIALS AND METHODS

#### 2.1 PREPARATION OF CLAY BASED CATALYTIC MATERIALS

Na-montmorillonite  $[(\text{Na}_{0.35}\text{K}_{0.01}\text{Ca}_{0.02}) (\text{Si}_{3.89}\text{Al}_{0.11})_{\text{tet}} (\text{Al}_{1.60}\text{Fe}_{0.08}\text{Mg}_{0.32})_{\text{oct}} \text{O}_{10}(\text{OH})_2 \cdot n\text{H}_2\text{O}]$  (Kunipia-F) obtained from Kunimine industries, Japan was used in all the studies reported in this thesis. The clay was used as received without any further purification. The cation exchange capacity of the clay material was 120 mequiv/100 g clay, which was determined by the method described by Fraser and Russel (Fraser and Russell, 1969).

#### 2.1.1 PREPARATION OF Cr-PILLARED CLAY (Cr-P) BASED CATALYTIC MATERIALS

##### 2.1.1.1 PREPARATION OF Cr-PILLARED CLAY (Cr-P)

The Cr-pillared clay material was synthesized by intercalation of chromium cationic oligomeric clusters into the clay interlayer and subsequent thermal activation. The Cr-pillaring solution was prepared by partial base hydrolysis of chromium nitrate ( $\text{Cr}(\text{NO}_3)_3 \cdot 9\text{H}_2\text{O}$ ) (S.D. Fine chemicals Ltd, India) solution using sodium carbonate as base to obtain an OH/Cr molar ratio of 2.0 (Pinnavaia *et al.*, 1985a; Sychev *et al.*, 1997a). The resulting solution was aged at 90°C for 24 h before using in the pillaring process. In a typical pillaring procedure, 2 g of the montmorillonite clay was dispersed in 200 ml of deionized water to form 1.0 wt% clay slurry. The pillaring solution was then added dropwise (50 ml/h) to the clay slurry under continuous stirring to obtain Cr/montmorillonite ratio of 40 mmol/g of clay. The mixture was kept under constant stirring for 24 h at room temperature, filtered, washed with deionized water (6 times with 200 ml portions), centrifuged, dried in hot air oven and calcined at 500°C for 1 h to obtain Cr-pillared clay (Cr-P).

### **2.1.1.2 PREPARATION OF SILICOTUNGSTIC ACID DISPERSED IN THE MATRIX OF Cr-PILLARED CLAY (STA/Cr-P).**

The Cr-pillared clay was used as carrier for catalytically active silicotungstic acid (STA). The silicotungstic acid was obtained from Loba chemie Pvt. Ltd., India. The 10 wt% STA/Cr-P catalyst was prepared by wet impregnation method. Required amount of STA was dissolved in 50 ml of double distilled water and to this solution 2.0 g of Cr-pillared clay was added. The resulting aqueous suspension was stirred for 3 h at room temperature. The temperature was then raised to 90°C and was heated continuously under stirring to remove the excess water. The resulting material was dried in air at 120°C followed by calcination at 250°C for 1 h to obtain the STA/Cr-P material.

## **2.1.2 PREPARATION OF Zr-PILLARED CLAY BASED CATALYTIC MATERIALS**

### **2.1.2.1 PREPARATION OF ZIRCONIA PILLARED CLAY (Zr-P)**

The Zr-pillared clay material was synthesized by intercalation of the zirconium cationic oligomeric clusters into the clay interlayer and subsequent thermal activation. Zirconium oxychloride (S. D. Fine Chemicals, India) was used as source for zirconium polycations. The 0.1 M  $ZrOCl_2 \cdot 8H_2O$  solution was prepared by dissolving the required amount of salt in double distilled water. The solution was aged at 50°C for 24 h to prepare the pillaring solutions. In a typical procedure for synthesis of Zr-pillared clay, 5 gm of clay was dispersed in 250 ml of double distilled water to form clay slurry. To ensure well dispersion, the clay suspension was stirred at room temperature for 2 h followed by sonication for 15 minutes. The pillaring solution was then added dropwise to the clay suspension at the rate of 50 ml per hour under continuous stirring at room temperature. The mixture was left for stirring under room temperature for 24 h

which was subsequently filtered and washed six times with deionised water to remove the chloride ions. The obtained gel was air dried at 120°C followed by calcination at 450°C for 2 h to obtain the Zr-Pillared clay (Zr-P).

## **2.1.2.2 PREPARATION OF POLYPHOSPHORIC ACID-CLAY AND POLYPHOSPHORIC ACID-Zr-P COMPOSITE MATERIALS**

### **2.1.2.2.1 PREPARATION OF POLYPHOSPHORIC ACID DISPERSED IN Zr-PILLARED CLAY MATRIX (ZrP-PPA)**

2 gm of Zr-pillared clay was dispersed in 50 ml of distilled water and sonicated for 15 minutes. 0.4 ml of PPA was added to the Zr-P clay slurry under vigorous stirring. Stirring was continued for 6 h at room temperature. The solvent was evaporated by heating under vacuum and the obtained solid particles were subsequently air dried at 120°C to obtain the ZrP-PPA clay.

### **2.1.2.2.2 PREPARATION OF POLYPHOSPHORIC ACID DISPERSED IN PARENT CLAY MATRIX (PPA-Clay)**

2 gm of clay material was dispersed in 50 ml of deionized water to form clay slurry. The slurry was sonicated for 15 minutes for better dispersion of the clay platelets. 0.4 ml of PPA was added to the clay suspension and the suspension was allowed to stir for 6 h. After stirring for the required amount of time, the excess water was removed by heating under vacuum. The resulting material was air dried at 120°C and grinded to obtain the polycrystalline powder of PPA-Clay.

### **2.1.2.2.3 PREPARATION OF POLYPHOSPHORIC ACID INTERCALATED CLAY USING CTAB AS A STRUCTURE EXPANSION AGENT (PPA-CTAB-Clay)**

5 gm of montmorillonite clay was dispersed in 100 ml of double distilled water followed by stirring for 2 h at room temperature and sonication for 15 minutes to prepare clay slurry. 5 mmol

of CTAB was completely dissolved in 50 ml of distilled water under sonication for 20 minutes. The CTAB solution was added drop wise to the clay slurry under continuous stirring at room temperature. The resulting suspension was stirred for 12 h. The ensuing solid material was filtered, washed three times with distilled water and then air dried at 110°C overnight to obtain CTAB intercalated clay material (CTAB-Clay). 2 gm of CTAB-Clay was subsequently dispersed in 50 ml of distilled water to which required amount of PPA (0.4 ml) was added. The resulting slurry was kept under continuous stirring for 12 h which was then centrifuged, washed and dried overnight at 120°C to obtain the CTAB-PPA-Clay.

#### **2.1.2.2.4 PREPARATION OF POLYPHOSPHORIC ACID-CLAY COMPOSITE PILLARED WITH Zr-POLYCATIONS (PPA-ZrP)**

The Zr-pillaring solution was prepared as per the procedure described in section 2.1.2.1. To a 2 gm clay suspension in 50 ml water, 0.4 ml of PPA was added and stirred at room temperature for 6 h. 100 ml of Zr-pillaring solution was added drop wise to the same pot at the rate of 50 ml per hour under continuous stirring. The mixture was then allowed for stirring at room temperature for another 12 h. The resulting particles were centrifuged and washed with deionized water. The obtained solid was air dried at 110°C overnight, and heated at 300°C for 2 h to obtain the PPA-ZrP clay material.

#### **2.1.2.3 PREPARATION OF SULFONATED POLYVINYL ALCOHOL-CLAY AND SULFONATED POLYVINYL ALCOHOL-Zr-P COMPOSITE MATERIALS.**

##### **2.1.2.3.1 PREPARATION OF SULFONATED POLYVINYL ALCOHOL (SPVA)**

4.4 gm of polyvinyl alcohol (PVA) (Molecular weight: 14000) (Sigma-Aldrich limited) was dissolved in 15 ml of pyridine and refluxed for 2 h at 80°C. The polymeric solution was

subsequently cooled in an ice bath and stored in a freezer. 8 ml of chlorosulfonic acid was added dropwise for 30 min to another 15 ml of portion of pyridine which was previously kept in an ice bath. The resulting yellow solid was stored in a freezer. During the sulfonation process, the yellow solid was dissolved in 15 ml of pyridine by warming at 60°C. The solution was then added dropwise to the polymeric solution under cold condition. The resulting solution was refluxed at 80°C for 4 h to obtain the sulfonated PVA. The sulfonated polymer was filtered, washed using acetone and purified by precipitation from hot water.

#### **2.1.2.3.2 PREPARATION OF SULFONATED PVA-CLAY COMPOSITE MATERIAL (Clay-SP)**

2 gm of clay material was dispersed in 200 ml of deionized water to form clay slurry. The slurry was sonicated for 15 min for better dispersion of the clay platelets and then stirred at 60 °C for 2 h. 2 gm of SPVA was dissolved in 50 ml of hot water. The polymeric solution was added dropwise to the clay slurry under constant stirring. The resulting suspension was stirred for 12 h at 60°C and then cooled to ice temperature. The suspension was filtered, washed with cold water and dried at 120°C in a hot air oven to obtain the Clay-SP material.

#### **2.1.2.3.3 PREPARATION OF SPVA-CLAY COMPOSITE USING CTAB AS A STRUCTURE EXPANSION AGENT (CTAB-Clay-SP)**

CTAB intercalated clay was prepared using the procedure described in section 2.1.2.4. 2 gm of CTAB-Clay was subsequently dispersed in 100 ml of distilled water, to which the SPVA solution (2 gm in 50 ml of hot water) was added dropwise under constant stirring. The resulting suspension was stirred for 12 h at 60°C and then cooled near to ice temperature. The suspension was filtered, washed with cold water and dried at 120°C in a hot air oven to obtain the CTAB-Clay-SP material.

#### **2.1.2.3.4 PREPARATION OF SPVA-Zr-PILLARED CLAY COMPOSITE MATERIAL (ZrP-SP)**

The Zr-pillared clay described in section 2.1.2.1 was used for the preparation of the ZrP-SP. 2 gm of Zr-P was dispersed in 100 ml of distilled water, to which the SPVA solution (2 gm in 50 ml of hot water) was added dropwise under constant stirring. The resulting suspension was stirred for 12 h at 60°C and then cooled near to ice temperature. The suspension was filtered, washed with cold water and dried at 120°C in a hot air oven to obtain the ZrP-SP catalyst.

#### **2.1.2.3.5 PREPARATION OF PVA INTERCALATED CLAY FOLLOWED BY IN SITU SULFONATION (Clay-PIS)**

2 gm of clay material was dispersed in 100 ml of double distilled water to form clay slurry. 2 gm of PVA was dissolved in 50 ml of hot water. The polymeric solution was added dropwise to the clay slurry. The resulting suspension was stirred at 60°C for 12 h which was subsequently filtered, washed with hot water and dried in hot air oven at 120°C overnight to obtain PVA intercalated clay. 2 gm of PVA intercalated clay was dispersed in 15 ml of pyridine to which required amount of chlorosulfonic acid dissolved in pyridine was added dropwise and the mixture was refluxed at 80°C for 12 h. The solid particles were filtered, washed with acetone and dried overnight in a hot air oven at 120°C to prepare the Clay-PIS material.

#### **2.1.2.3.6 PREPARATION OF PVA INTERCALATED CTAB-CLAY FOLLOWED BY IN SITU SULFONATION (CTAB-Clay-PIS)**

The CTAB-Clay described in section 2.1.2.4 was used for the preparation of CTAB-Clay-PIS. 2 gm of CTAB-clay material was dispersed in 100 ml of double distilled water to form CTAB-clay slurry. 2 gm of PVA was dissolved in 50 ml of hot water. The polymeric solution was added dropwise to the CTAB-clay slurry. The resulting suspension was stirred at 60°C for 12 h which



was subsequently filtered, washed with hot water and dried in a hot air oven at 120°C overnight to obtain PVA intercalated CTAB-clay. 2 gm of PVA intercalated CTAB-clay was dispersed in 15 ml of pyridine to which required amount of chlorosulfonic acid dissolved in pyridine was added dropwise and the mixture was refluxed at 80°C for 12 h. The solid particles were filtered, washed with acetone, dried overnight in a hot air oven at 120°C to prepare CTAB-Clay-PIS material.

#### **2.1.2.3.7 PREPARATION OF PVA DISPERSED IN Zr-PILLARED CLAY MATRIX FOLLOWED BY IN SITU SULFONATION (ZrP-PIS)**

The Zr-pillared clay described in section 2.1.2.1 was used for the preparation of the ZrP-PIS. 2 gm of Zr-P was dispersed in 100 ml of double distilled water to form Zr-P clay slurry. 2 gm of PVA was dissolved in 50 ml of hot water. The polymeric solution was added dropwise to the Zr-P slurry. The resulting suspension was stirred at 60°C for 12 h which was subsequently filtered, washed and dried at hot air oven at 120°C overnight to obtain PVA intercalated Zr-P. 2 gm of PVA intercalated Zr-P was dispersed in 15 ml of pyridine to which required amount of chlorosulfonic acid dissolved in pyridine was added dropwise and the mixture was refluxed at 80°C for 12 h. The solid particles were filtered, washed with acetone, dried overnight in a hot air oven at 120°C to prepare the ZrP-PIS material.

#### **2.1.4 PREPARATION OF Al-PILLARED CLAY BASED CATALYTIC MATERIALS**

##### **2.1.4.1 PREPARATION OF Al-PILLARED CLAY (Al-P)**

The Al-pillared clay material was synthesized by intercalation of the aluminium cationic oligomeric clusters into the clay interlayer and subsequent thermal activation. The Al-pillaring solution was prepared by partial base hydrolysis of a 0.2 M aluminum chloride ( $\text{AlCl}_3 \cdot 6\text{H}_2\text{O}$ )

(S.D. Fine chemicals limited) solution using 0.2 M sodium hydroxide solution as base to obtain OH/Al molar ratio of 2.0. The resulting solution was aged at 50°C for 24 h before using in the pillaring process. In a typical pillaring procedure, 2 g of the montmorillonite clay was dispersed in 200 ml of deionised water to form clay slurry. The pillaring solution was then added drop wise (50 ml/h) to the clay slurry under continuous stirring. The mixture was kept at constant stirring for 24 h at room temperature, filtered, washed with hot deionised water (6 times with 200 ml portions), dried overnight in hot air oven at 120°C and calcined at 500°C for 2 h to obtain Al-pillared clay (Al-P).

#### **2.1.4.2 PREPARATION OF PALLADIUM NANOPARTICLES SUPPORTED OVER Al-PILLARED CLAY (Pd/Al-P)**

The 5 wt% Pd/Al-P catalyst was prepared by wet impregnation method. Required amount of palladium chloride (Merck India Limited) was dissolved in 25 ml of water and then added dropwise to the Al-pillared clay slurry. After 15 minutes of stirring, in situ chemical reduction was carried out by dropwise addition of 10 ml mixture of formaldehyde and 1 N sodium hydroxide. The resulting suspension was stirred for 6 h. It was then filtered and dried in a hot air oven at 120°C for 12 h to obtain the Pd/Al-P. Using similar procedure, 5 wt% Pd metal supported on CTAB intercalated clay (Pd/CTAB-Clay) and zirconium pillared clay (Pd/Zr-P) were also prepared for comparative study.

#### **2.1.4.3 PREPARATION OF PALLADIUM BASED BIMETALLIC NANOPARTICLES SUPPORTED OVER Al-PILLARED CLAY (Pd-M/Al-P WHERE M= Cu and Ni)**

A total of 5 wt% of the bimetallic particles was supported over the Al-P. In a typical synthesis procedure, required amount of PdCl<sub>2</sub> and Cu(NO<sub>3</sub>)<sub>2</sub> [or Ni(NO<sub>3</sub>)<sub>2</sub>] was dissolved in 25 ml of

water and then added dropwise to the Al-pillared clay slurry. After stirring for 15 minutes, in situ chemical reduction was carried out by dropwise addition of 10 ml mixture of formaldehyde and 1N sodium hydroxide. The resulting suspension was stirred for 6 h. It was then filtered and dried in a hot air oven at 120°C for 12 h to obtain the Pd-M/Al-P catalyst. Using the above procedure Pd-Ni (molar ratio 1:3, 1:1 and 3:1)/Al-P and Pd-Cu (1:1)/Al-P materials were prepared.

## **2.2 CHARACTERIZATION METHODS**

### **2.2.1 POWDER X-RAY DIFFRACTION (XRD)**

The X-ray diffraction patterns of various clay based catalysts were recorded using a Rigaku Ultima-IV diffractometer using Ni filtered  $\text{CuK}\alpha_1$  ( $\lambda=1.5405 \text{ \AA}$ ) radiation. The XRD measurements were carried out in the  $2\theta$  range of  $1\text{-}15^\circ$  with a scan speed of 1 degree per minute using Bragg –Brantano configuration. Since clays and pillared clays show broad low angle XRD patterns, oriented specimens were prepared for basal spacing determination. 2 wt% slurry of different clay samples in water were spread on a glass slide and dried in air at room temperature. The slides were then equilibrated with ethylene glycol for 12 h to obtain the oriented specimen. For this purpose small strips of filter paper were soaked with ethylene glycol and warped around the glass slide and kept for 12 h. The excess of ethylene glycol was removed from the slide by gentle contact with dry filter papers and XRD measurements were performed within 1 hour of the sample preparation.

### **2.2.2 INFRA-RED SPECTROSCOPY (FTIR)**

The FTIR spectra of different clay samples (as KBr pellets) were obtained using a Perkin-Elmer Infrared spectrometer with a resolution of  $4 \text{ cm}^{-1}$  in the range of  $400 \text{ cm}^{-1}$  to  $4000 \text{ cm}^{-1}$ . Nearly, 3-4 mg of the sample was mixed thoroughly with 30 mg of oven dried KBr and made into pellets

by using a hydraulic press. The pallets were stored in vacuum desiccators and exposed to IR lamp for 1 minute prior to the FTIR measurement.

### **2.2.3 UV-VIS SPECTROSCOPY**

The UV-Visible absorbance spectra of the clay based materials were recorded using Shimadzu spectrometer model 2450 with BaSO<sub>4</sub> coated integration sphere in the range of 200-800 nm. The selected recording parameters comprised of spectral bandwidth of 4 nm and data point distance of 1nm. The spectra were recorded at ambient condition in air.

### **2.2.4 THERMOGRAVIMETRIC ANALYSIS**

Thermogravimetric analysis of the samples were performed using Netzsch, Model 449C apparatus in air (30 ml per min) with linear heating rate (10°C per min) from room temperature to 800°C. For the determination of the acidity of the clay catalysts by TGA of adsorbed n-butyl amine (discussed in section 2.2.10.2) nitrogen atmosphere was used and TG analysis was performed from room temperature to 550°C at a linear heating rate of 20°C per minute.

### **2.2.5 SORPTOMETRIC STUDIES**

The specific surface areas of the clay based materials were determined by BET method using N<sub>2</sub> adsorption/desorption at 77 K on a Quantachrome Autosorb gas sorption system. The samples were degassed at 120 °C for 5 h prior to the sorptometric studies.

### **2.2.6 SCANNING ELECTRON MICROSCOPY (SEM)**

Scanning electron micrograph (SEM) of the pillared clay samples were recorded using JEOL JSM-6480 LV microscope (acceleration voltage 15 kV). Prior to the SEM analysis, the clay particles were dispersed in water and sonicated for 30 minutes. One drop of the aqueous clay suspension was then mounted over a small glass slide and spread uniformly. The glass slide was subsequently air dried and used for SEM analysis

## **2.2.7 FIELD EMISSION SCANNING ELECTRON MICROSCOPY (FE-SEM)**

FE-SEM studies were performed using a Nova Nano SEM/FEI microscope operating at 5 kV accelerating voltage. Prior to FE-SEM analysis, sample powder was deposited on a carbon tape. In order to reduce the charge developed on the sample, gold/platinum sputtering was done for 3 minutes on all the samples.

## **2.2.8 TRANSMISSION ELECTRON MICROGRAPHS (TEM)**

Transmission electron micrographs of the clay materials were recorded using PHILIPS CM 200 equipment operating at 100 kV accelerating voltage. Samples for TEM analysis were prepared by dispersing the powdered sample in ethanol by sonication and then drop drying on a copper grid (400 mesh) coated with carbon film.

## **2.2.9 SURFACE ACIDITY MEASUREMENT**

### **2.2.9.1 NON-AQUEOUS TITRATION METHOD**

0.5 gm of the clay based material was kept in contact with a standard n-butylamine solution (0.025 M in benzene) for 24 h in a sealed container. A 5 ml portion of the supernatant solution was pipetted out and titrated against trichloroacetic acid solution (0.025 M), using neutral red as indicator (Ranga Rao *et al.*, 2003). The total acidity was computed from the volume of n-butylamine consumed and the value was expressed in millimoles per gram of the catalyst.

### **2.2.9.2 TG ANALYSIS OF ADSORBED n-BUTYLAMINE**

The Brønsted acidity of the clay based materials was also obtained following the method described by Breen (Breen, 1991). Pillared clay samples were exposed to the reagent grade n-butyl amine for 48 h in a desiccator. Thermogravimetric analysis of the samples was then performed in nitrogen atmosphere from room temperature to 550°C at a rate of 20°C per minute.

The percentage weight loss corresponding to the temperature range 350-450°C were calculated

and the proton acidity is obtained assuming each base molecule interact with a single proton site in the clay. Prior to the thermogravimetric analysis the samples were flushed with nitrogen gas for 30 minutes at room temperature to remove the physisorbed n-butyl amine molecules.

#### **2.2.10 GAS CHROMATOGRAPHY (GC)**

The GC analysis of the reaction mixture was performed by Nucon 5765 equipment fitted with a FID detector and different packed as well as capillary column. Depending on the sample type, different column have been used for analysis.

#### **2.2.11 NMR SPECTROSCOPY**

<sup>1</sup>H NMR spectra were recorded using Bruker spectrometer at 400 MHz using TMS as internal standard.

### **2.3 CATALYTIC ACTIVITY STUDY**

#### **2.3.1 SYNTHESIS OF OCTAHYDROXANTHENES CATALYZED BY Cr-P MATERIAL**

The synthesis of octahydroxanthenes was carried out under solvent free condition using microwave as an energy source. A neat mixture of dimedone (2 mmol), aromatic aldehyde (1mmol) and 50 mg of Cr-P catalyst in a beaker was exposed to microwave radiation for the required amount of time. The reaction mixture was irradiated at 900 W for the specified time with an intermittent cooling interval of 60 s after every 60 s of microwave irradiation. The reaction was monitored by TLC. After the completion of the reaction, the reaction mixture was treated with 10 ml of ethyl acetate and the catalyst was filtered. The final product was recovered by vacuum drying of the ethyl acetate solution followed by recrystallization from ethanol to afford the pure product. The used catalyst was regenerated by washing three times with 10 ml portions of methanol followed by heat treatment at 450 °C for 2 h.

### **2.3.2 SYNTHESIS OF BENZOXANTHENES CATALYZED BY Cr-P MATERIAL**

The catalytic activity of Cr-P material was also examined for the synthesis benzoxanthenes. A neat mixture of benzaldehyde (1 mmol),  $\beta$ -naphthol (2 mmol) and Cr-P material (50 mg) in a 20 ml beaker was exposed to microwave radiation for the required amount of time. The reaction mixture was irradiated at 900 W for the specified time with an intermittent cooling interval of 60 s after every 60 s of microwave irradiation. After the completion of the reaction, the reaction mixture was transferred to 10 ml of ethyl acetate, stirred for 15 min, filtered and the reaction product was recovered from the solution and recrystallized. The used catalyst was regenerated by washing three times with 10 ml portion of methanol followed by heat treatment at 450°C for 2 h.

### **2.3.3 SYNTHESIS OF 1,4-DIHYDROPYRIDINES CATALYZED BY STA/Cr-P MATERIAL**

A neat mixture of benzaldehyde (1 mmol), ethylacetoacetate (2 mmol),  $\text{NH}_4\text{OAc}$  (1 mmol) and 0.1 g of STA/Cr-P in a 20 ml beaker was exposed to microwave radiation for the required amount of time. The reaction mixture was irradiated at 900 W for the specified time with an intermittent cooling interval of 60 s after every 60 s of microwave irradiation. The progress of the reaction was monitored by TLC. After the completion of the reaction, the reaction mixture was transferred to 10 ml of ethyl acetate, stirred for 15 min, filtered and the reaction product was recovered from the ethyl acetate solution and recrystallized. The used catalyst was regenerated by washing three times with 10 ml portions of ethyl acetate followed by heat treatment at 250 °C for 1 h. The reaction rates over different clay catalysts were calculated with respect to the conversion of the benzaldehyde in the reaction mixture. The percentage conversion of benzaldehyde was calculated from the GC analysis of the reaction mixture using a EC-Wax column and FID detector. The dihydropyridines were also synthesized by using chalcones as

substrates in place of aryl aldehydes. Similar protocol and work up conditions was used except in this case the molar ratio of chalcone, ethyl acetoacetate and ammonium acetate was 1:1:1.

#### **2.3.4 SYNTHESIS OF TETRAHYDROPYRIDINES CATALYZED BY PPA-ZrP COMPOSITE MATERIALS**

The catalytic activity of the polyphosphoric acid-Zr pillared clay composite materials was evaluated for the synthesis of tetrahydropyridines. The synthesis of tetrahydropyridines was carried out by stirring a mixture of aryl aldehyde (2 mmol), ethylacetoacetate (1 mmol), aniline (2 mmol) and 50 mg of different synthesized catalysts in acetonitrile solvent at 50°C. The reaction was monitored by TLC. Catalytic activity was also examined at different temperatures and in different solvent media. After the completion of the reaction, the reaction mixture was filtered to separate the catalyst. The final product was recovered from the acetonitrile solution and recrystallized from ethanol to acquire the pure product. The used catalyst was regenerated by washing three times with 10 ml portion of ethanol and subsequent heat treatment at 300°C for 2 h.

#### **2.3.5 SYNTHESIS OF HEXAHYDROPYRIMIDINES CATALYZED BY SPVA-Zr-P COMPOSITE MATERIALS**

##### **Method A:** *Microwave irradiation method*

The catalytic activity of the SPVA-Zr-P composite materials was evaluated for the synthesis of hexahydropyrimidines by multicomponent condensation of 1,3-dicarbonyl compounds, substituted anilines and formaldehyde under solvent free condition using microwave as energy source. Typically, a mixture of 1,3-dicarbonyl compounds (1 mmol), aniline (2 mmol), formaldehyde (3 mmol) and 50 mg of ZrP-SP composite materials was exposed to microwave for the desired amount of time with an intermittent cooling interval of 120 s after every 60 s of



exposure time. The reaction was monitored by TLC. After the completion of the reaction, 10 ml of ethanol was added to the reaction mixture and the content was stirred for 30 minutes. The ethanoic suspension was subsequently filtered to separate the catalyst. The final product was recovered from the ethanol solution and recrystallized to acquire the pure product.

**Method B:** *Conventional heating method*

Hexahydropyrimidines were also synthesized by conventional heating in a thermostatic oil bath at 70°C. Typically, a mixture of ethylacetoacetate (1mmol), aniline (2mmol), formaldehyde (3mmol) and 50 mg of ZrP-SP composite catalysts in 5 ml ethanol was heated under stirring at 70°C for required period of time. The progress of the reaction was monitored by TLC. After completion of reaction, an additional 5 ml of ethanol was added to the reaction mixture and catalyst particles were filtered out. The ethanolic solution was dried under reduced pressure to recover the product and recrystallized. The used catalyst was regenerated by washing three times with 10 ml portion of ethanol and subsequent drying in a hot air oven at 150°C for 2 h.

All the synthesized compounds described in section 2.31-2.3.5 are known compounds and are characterized by comparing their melting points, IR, <sup>1</sup>H NMR spectroscopic data with those reported in literature.

**2.3.6 HYDRODEHALOGENATION (HDH) OF HLAOGENATED AROMATIC COMPOUNDS CATALYZED BY Pd/Al-P AND Pd-M/Al-P (M= Cu and Ni) MATERIALS**

The aqueous phase hydrodehalogenation of a variety of halogenated aromatics including 4-Chlorophenol, 4-Fluorophenol, 2-Chlorophenol, 4-Chloroanilines, 4-Chlorotoluene, 2,4-disubstituted as well as 2,6-disubstituted products was carried out using Pd/Al-P and Pd-M/Al-P as catalyst under hydrogen transfer conditions. In a typical experimental procedure, 3 mmol of p-

chlorophenol was dispersed in 10 ml water and stirred for 30 min at 30°C. 50 mg of Pd/Al-P catalyst was added to the solution followed by stirring for another 15 minutes. Hydrazine hydrate was used as hydrogen transfer agent to carry out the hydrodehalogenation of the substrate. The initial molar ratio of substrate to hydrogenating agent of 1:8 was used in the study. The hydrazine hydrate was added dropwise to the reaction mixture under constant stirring. The reaction mixture was allowed to stir for 5 h at 30°C. Periodically, a small aliquot of the reaction mixture was taken out from the reaction mixture and analysed by gas chromatography using a FID detector and OV-101 column.

# CHAPTER 3

## CATALYTIC APPLICATIONS OF Cr-PILLARED CLAY BASED MATERIALS

### PART A: SYNTHESIS OF XANTHENE DERIVATIVES CATALYZED BY Cr-PILLARED CLAY

#### 3.1 INTRODUCTION

Porous solids with uniform pore size in the micro- (< 2 nm) and mesopore (2-50 nm) range are extensively used in industrial catalytic processes. These materials possess high surface area, thermal stability, uniform pore structure and tunable acid-base and redox properties (Taguchi and Schuth, 2005; Chidambaram and Biswanathan, 2007; Berlier *et al.*, 2008; El-Rassy *et al.*, 2009; Dutta *et al.*, 2012; Valtchev and Tosheva, 2013). The acid-base property of the porous materials in combination with the supported metallic particles has been used as bifunctional catalysts for several important reactions (Lee *et al.*, 2008; Kim *et al.*, 2008) Similarly, redox property can be generated by incorporation of transition metals into the three dimensional frame work (Grieken *et al.*, 2009; Akondi *et al.*, 2012). Among various porous materials, pillared clays are increasingly investigated in recent years because of their acidic property, thermally stable three dimensional pore structures akin to zeolites and shape selective catalysis (Gil *et al.*, 2000a; Cool *et al.*, 2002; Jagtap and Ramaswamy, 2006; Gil *et al.*, 2008; Gil *et al.*, 2010; Bineesh *et al.*, 2011). The pore size of pillared clays (10-20 Å) intermediate between the micro and mesoporous materials is suitable for reactivity of large reactant molecules (Sowmiya *et al.*, 2007; Mnasri-Ghniemi and Frini-Srasra, 2014). Moreover, the interlayer space of the pillared clays is ideal for construction of bulky heterocyclic compounds (Sowmiya *et al.*, 2007; Dar *et al.*, 2013). Among the pillared clays, clay pillared with inorganic polycations of Al and Zr has been most widely

investigated because of its simple and reproducible way of preparation, and high thermal stability (Cool *et al.*, 2002; Mishra and Ranga Rao, 2003; Colin L. *et al.*, 2005; Timofeeva *et al.*, 2011a). The other pillared clay material of interest is the Cr-pillared clay where Cr<sub>2</sub>O<sub>3</sub> nanoclusters as pillars have been intercalated into the clay interlayer (Volzone, 2001; Gyftopoulou *et al.*, 2005; Yurdakoc *et al.*, 2008; Tomul and Balci, 2009). The Cr-pillaring solutions are generally prepared by partial base hydrolysis of the chromium salt solution. The nature and geometry of the Cr ions present in the Cr-salt solution can be established from the UV-DRS study. The Cr<sup>3+</sup> ions in partially hydrolyzed state exhibit charge transfer transition and d-d transitions. The polymerization of the Cr<sup>3+</sup> ions can be illustrated from the shifting of the absorption bands due to Cr<sup>3+</sup> toward higher wavelength (Charan and Ranga Rao 2013). Cr-pillared clays have been used to carry out various organic transformations such as methylation of toluene, hydrocracking of heavy fuels, propene oxidation, acylation of alcohol, chlorinated hydrocarbon oxidation, propane dehydrogenation and CO oxidation (Storaro *et al.*, 1997; Akçay, 2004; Gyftopoulou *et al.*, 2005; Mata *et al.*, 2007; Binitha and Sugunan, 2008; Tomul and Balci 2009; León *et al.*, 2014). Although, there are many investigations on the catalytic properties of the pillared clay materials, most of these works are related to their applications in industrial catalysis. There is a vast scope to study the applicability of these materials as catalyst for synthesis of fine chemicals more so in reference to bioactive materials. Recently, Mishra et al have studied the application of modified Al- and Zr-pillared materials for synthesis of biologically important molecules including β-aminocarbonyl compounds, dihydropyrimidines, coumarins and thiochromans (Sowmiya *et al.*, 2007; Samantaray *et al.*, 2011). Phosphomolybdic acid supported over sulphate grafted Zr-pillared clay has been employed as catalyst for the synthesis of β-aminocarbonyl molecules in aqueous media (Samantaray *et al.*, 2011). In this work, we have studied the catalytic application

of Cr-pillared clay material for synthesis of octahydroxanthenes and benzoxanthenes under solventfree condition using microwave radiation as energy source. The Cr-pillared clays have been chosen for synthesis of xanthene derivatives because of their higher surface area compared to other pillared clay materials, presence of predominantly Bronsted acidic sites which are the active sites for xanthene synthesis as well as their enhanced gallery height which is conducive for construction of bulky heterocyclic compounds.

Xanthenes are an important class of biologically active heterocycles with potential applications as antibacterial, anti-inflammatory and antiviral agents (Poupelin *et al.*, 1978; Bekaert *et al.*, 1992). They also exhibit promising activity in photodynamic therapy and agricultural bactericide (Poupelin *et al.*, 1978). In addition to their biological and pharmacological applications, xanthenes are also used as dyes, fluorescent probes for detection of biomolecules and in laser technologies (Bekaert *et al.*, 1992). In past years, many synthetic methods have been reported for preparation of xanthenes which include reaction of  $\beta$ -Naphthol with aldehydes or acetals under acidic conditions, cyclocondensation between 2-hydroxyaromatic aldehydes and 2-tetralone, cyclodehydrations, alkylations  $\gamma$  to the heteroatoms, and intramolecular phenyl carbonyl coupling reactions of benzaldehydes and acetophenones (Bekaert *et al.*, 1992; Wang and Harvey, 2002; Jha and Beal 2004). However, most of these synthetic procedures involve conventional methods and suffer from drawbacks such as longer reaction times, low yields, harsh reaction conditions and utilization of excess of reagents and catalysts. Recently, improved protocols have been formulated for the synthesis of xanthenes which involves the condensation of  $\beta$ -naphthol and aromatic aldehydes in presence of acidic catalysts. Several acidic catalysts such as sulfamic acid, molecular iodine, cellulose sulfuric acid,  $\text{BF}_3 \cdot \text{SiO}_2$ , Dow-ex-50W,  $\text{HClO}_4 \cdot \text{SiO}_2$ , ammonium dihydrogen phosphate supported over silica

( $\text{NH}_4\text{H}_2\text{PO}_4/\text{SiO}_2$ ), ceric ammonium nitrate (CAN), dipyridine cobalt chloride and  $\text{Yb}(\text{OTf})_3$  has been utilized for this condensation reactions (Shakibaei *et al.*, 2007; Mirjalili *et al.*, 2008; Su *et al.*, 2008; Madhav *et al.*, 2009; Mahdavinia *et al.*, 2009; Kumar *et al.*, 2010). However, many of these catalyzed processes are homogeneous in nature and leads to tedious work up and difficulty in separation and handling of the catalysts.

Xanthene derivatives particularly, 1,8-Dioxo-octahydroxanthenes have been found as a substructure in a large number of naturally occurring molecules. Because of their biological activity, 1,8-dioxo-octahydroxanthenes and their derivatives occupy a prominent position in medicinal chemistry (Kantevari *et al.*, 2007). The most efficient way of synthesizing octahydroxanthenes involves the condensation of dimedones with aryl aldehydes in presence of acidic catalysts. The various catalytic systems employed for this condensation reaction include among others  $\text{HClO}_4/\text{SiO}_2$ , 3-(N,N-dimethyldodecylammonium) propanesulfonic acid hydrogen sulfate [DDPA][ $\text{HSO}_4$ ], ionic liquids, polyaniline p-toluenesulphonate,  $\text{NaHSO}_4/\text{SiO}_2$ , dowex 50w, molecular iodine,  $\text{TMCl}$ , 1-methylimidazolium trifluoroacetate ([Hmim]TFA) (Kantevari *et al.*, 2007; Dabiri *et al.*, 2008; Karthikeyana and Pandurangana, 2009; Pore *et al.*, 2010; Fang *et al.*, 2011; Mulakayala *et al.*, 2012; Hasaninejad *et al.*, 2012; Dadhania *et al.*, 2012). Most of the used catalysts are either homogeneous catalysts or supported reagents or polymers which suffer from deactivation, regeneration and handling of the catalyst. A stable heterogeneous catalyst which is reusable and efficient for the synthesis of this important class of compounds is highly desirable.

## 3.2 RESULTS AND DISCUSSION

### 3.2.1 XRD STUDY

The XRD patterns of the Cr-P material along with the parent clay is presented in Fig. 3.1. The corresponding basal spacing values obtained from the XRD study are presented in Table 3.1. The parent clay shows a sharp and intense reflection at  $2\theta=6.8^\circ$  corresponding to the reflection from the (001) planes of the layered material (Fig. 3.1 a). The basal spacing of the clay material is found to be 12.9 Å (Table 3.1). Montmorillonite clay is a dioctahedral clay material with a layer height of 9.6 Å, the interlayer spacing of the parent clay is calculated to be 3.3 Å. The insertion of the Cr-oligomeric cationic clusters into the clay interlayer resulted in an expansion of the clay interlayer. The calcined Cr-P material shows a  $d_{001}$  spacing of 20.8 Å (Fig. 3.1 b). The preparation and characterization of the Cr-pillared clay materials have been studied earlier by different authors in the literature (Pinnavaia *et al.*, 1985a; Sychev *et al.*, 1997a; Gyftopoulou *et al.*, 2005; Yurdakoc *et al.*, 2008; Tomul and Balci, 2009).

**Table 3.1 Physicochemical characteristics of parent clay and calcined Cr-P material.**

Clay sample	Basal spacing (Å )	Interlayer spacing (Å )	Surface area (m <sup>2</sup> /g)	Pore volume (cc/g)	Acidic sites (mmol/g)
Clay	12.9	3.3	30.1	0.06	0.15
Calcined Cr-P	20.8	11.2	272.0	0.22	0.42

The Cr-pillaring species are generally prepared by the partial base hydrolysis of Cr(III) ions at moderately concentrated aqueous solutions. The type of the Cr salt precursor used and the temperature of hydrolysis have been found to be crucial for the formation of Cr-oligomeric clusters. It has been reported that Cr ions form larger polycations upon base hydrolysis at elevated temperatures (95 °C) (Pinnavaia *et al.*, 1985a). The basal spacing value observed in

this study is in accordance with the earlier literature reported value for Cr-pillared clay materials (Roulia, 2005; Tomul and Balci, 2009).

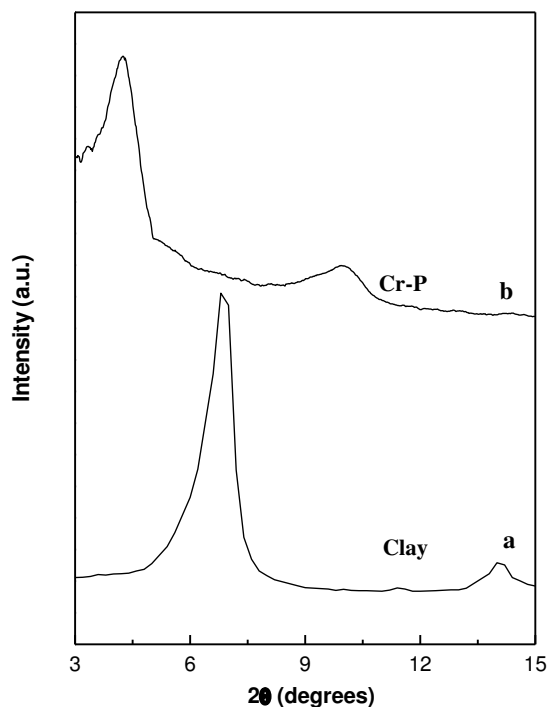


**Figure 3.1** XRD profiles of (a) clay and (b) calcined Cr-P.

### 3.2.2 FTIR STUDY

The FT-IR spectra of the Cr-P material before and after calcination along with the parent clay are presented in Fig. 3.2. The parent montmorillonite shows a prominent band at  $3630\text{ cm}^{-1}$  along with a broad less intense peak at  $3456\text{ cm}^{-1}$  in the stretching frequency region of the spectrum (Fig. 3.2, Panel I). These peaks correspond to the O–H stretching from the structural hydroxyl group and water molecules present in the interlayer space of the clay materials (Sposito *et al.*, 1983; Bodoardo *et al.*, 1994; Mishra and Ranga Rao, 2005). The pillaring of the clay materials results in an enhancement of the intensity of these bands. It is apparent from the IR spectra that pillaring of the clay increases the water retention capacity of the clay materials. Moreover, the



oxyhydroxy cationic clusters can contribute to the enhancement of the intensity of the bands corresponding to the structural hydroxyl groups.

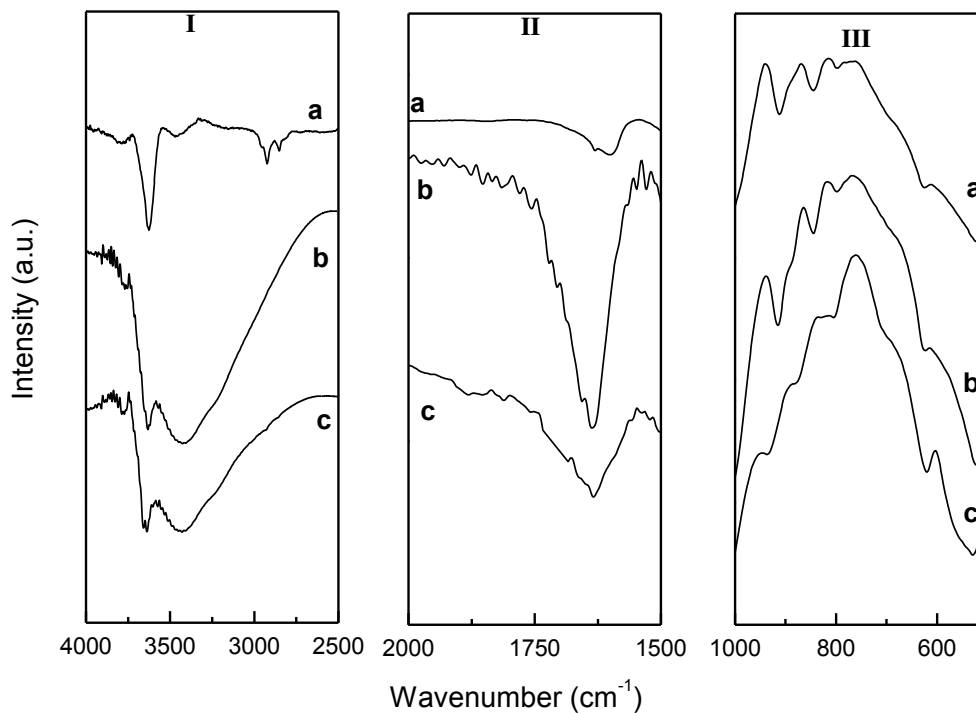


**Figure 3.2** FT-IR spectra of (a) clay, (b) air dried Cr-P and (c) calcined Cr-P.

In the bending mode region, the pillared materials as well as the parent clay show a prominent band  $1630\text{ cm}^{-1}$  (Fig. 3.2, Panel II). This band has been assigned to the OH bending vibration. Montmorillonite clay is known to possess two kinds of water molecules, namely the loosely bonded water molecules present in the interlayer and the strained water molecules present in the 1<sup>st</sup> coordination sphere of the interlayer cations. The latter type contributes to the acidity of the material and has been known to contribute significantly to the peak at  $1630\text{ cm}^{-1}$  (Sposito *et al.*,1983). The intense band observed at  $1630\text{ cm}^{-1}$  for the Cr-pillared clay suggests the possibility of an enhancement of acidity due to the pillaring process. In the frequency region of  $600\text{--}1000\text{ cm}^{-1}$ , the clay material shows a series of discrete peaks depending upon the cation

composition in the octahedral sheet. In the present study, three bands were observed at 915, 845 and 805  $\text{cm}^{-1}$  for all the clay samples (Fig. 3.2, Panel III). These bands have been assigned to the bending vibration modes of Al–Al–OH, Al–Mg–OH and Mg–Mg–OH groups in the octahedral layer of the montmorillonite clay (He *et al.*, 2001).

### 3.2.3 UV-VIS STUDY

The UV–Vis spectra of the as synthesized and calcined Cr-P material along with the parent clay are presented in Fig. 3.3. The parent clay shows a characteristic broad band with a maximum at 245 nm (Fig. 3.3a). This band is assigned to the ( $\text{Fe}^{3+} \leftarrow \text{O}^{2-}$ ,  $\text{OH}^-$  or  $\text{OH}_2$ ) charge transfer transition for the structural iron present in the octahedral layer of the clay mineral (Mishra and Ranga Rao, 2004).

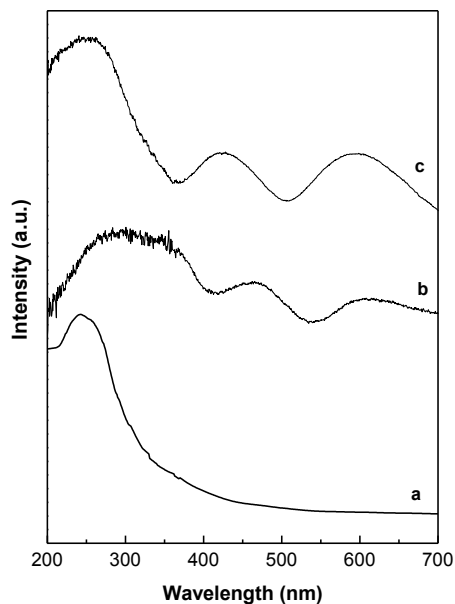


**Figure 3.3** UV-vis absorbance spectra of (a) clay, (b) air dried Cr-P and (c) calcined Cr-P.

The basic structural units of tetrahedral silicate layers in the clay lattice do not absorb UV light in the range of 200–800 nm except when the transition metal ions are exchanged in the interlayers or present in the silicate structure. The intercalation of the chromium oxyhydroxy clusters into the clay interlayer resulted in significant change in the absorption feature of the clay material. The as synthesized Cr-P clay material shows a broad peak spanning from 250 to 380 nm. In addition, two well defined bands with maxima around 450–470 nm and 580–600 nm are observed in the absorption spectrum (Fig. 3.3b). The latter two peaks can be assigned to the  $A_{2g} \rightarrow T_{1g}$  and  $A_{2u} \rightarrow T_{2g}$  transitions characteristics of Cr(III) in octahedral symmetry (Mishra and Parida, 1998; Rossi *et al.*, 1998; Thomas *et al.*, 2002; Rombia *et al.*, 2006). The broad peak observed in the high energy region seems to be a composite peak with contribution from the absorption from the clay lattice as well as pillars. It has been reported that in the charge transfer region, two bands at 260–280 nm and 370–380 nm are characteristic of the presence of Cr(VI) ions (Rossi *et al.*, 1998; Rombia *et al.*, 2006). It is likely that some of the chromium ions can exist as Cr(VI) and contribute to the absorption feature of the material. Heat treatment at higher temperature resulted in the disappearance of the peak corresponding to the Cr(VI) ions, simultaneously, the peaks due to the Cr(III) ions gained intensity (Fig. 3.3c). It has been reported that during thermal treatment, the chromium oligomeric clusters undergo further hydrolysis and polymerization to form bigger clusters inside the clay interlayer (Sychev *et al.*, 1997a). Moreover, the thermal transformation of the chromium hydroxide gel to chromia particles is known to occur through the formation of CrO<sub>3</sub> particles (Mishra and Parida, 1998; Rossi *et al.*, 1998). In the present case, it is believed that the air dried as synthesized materials contain oxyhydroxy clusters of both Cr(VI) and Cr(III) ions. The calcination of the pillared clay materials lead to the formation of stable Cr<sub>2</sub>O<sub>3</sub> nanoclusters inside the clay interlayer.

### 3.2.4 THERMOGRAVIMETRIC ANALYSIS

The thermal transformation of the air dried pillared clay material is studied by TG analysis. The TG profile along with the derivative plot for the air dried Cr-P is presented in Fig. 3.4. A major weight loss region is observed in the range of 50-200°C corresponding to the loss of the physisorbed and loosely bonded water molecules in the clay interlayer. Beyond 200°C the weight loss is more gradual. However, two broad weight loss regions can be observed in Fig. 3.4. The weight loss corresponding to the temperature range of 300-450°C can be ascribed to the loss of water molecules coordinated to the pillars whereas between 500-650°C corresponds to the dehydration and dehydroxylation of the clay sheets and pillars (Sychev *et al.*, 1997b; Mishra and Ranga Rao, 2004).

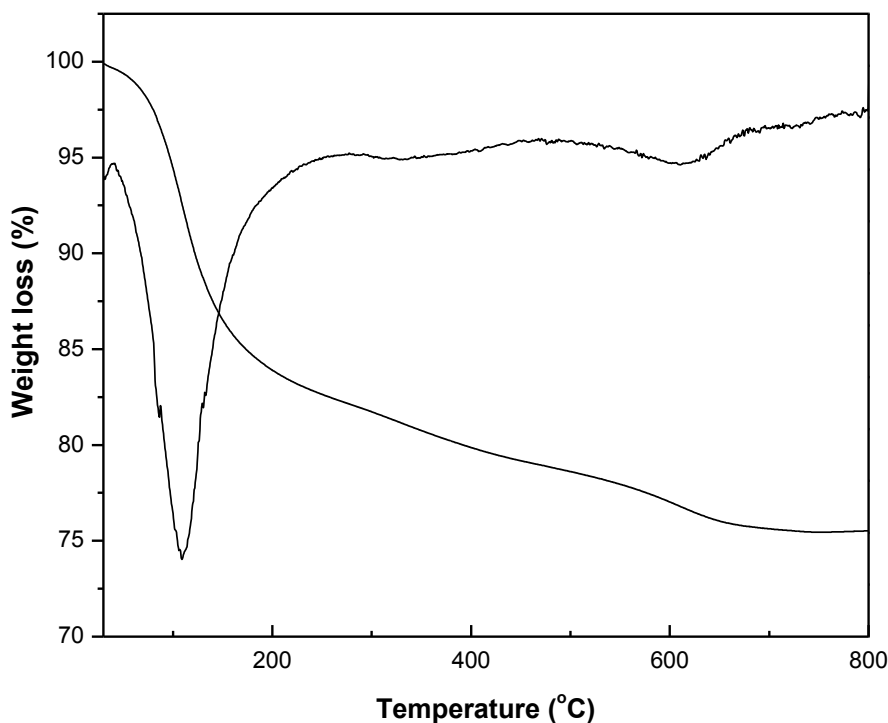


**Figure 3.4** Thermogravimetric analysis of the air dried Cr-P material.

### 3.2.5 SORPTOMETRIC STUDY

The surface area and pore volume of the calcined Cr-P material are evaluated using N<sub>2</sub> sorption at 77 K. The N<sub>2</sub> sorption isotherm of the parent clay along with the Cr-P material is presented in Fig. 3.5. The Cr-P material exhibits high initial adsorption with a nearly horizontal plateau up to relative pressure of ~0.9 (Fig. 3.5 b). This behaviour is characteristic of microporous solids (Gregg and Sing, 1982). The sorption isotherms observed for the parent clay as well as Cr-P material is type I according to the BDDT classification indicating the presence of micropores. The hysteresis found in the adsorption isotherm is H3 type (Fig. 3.5) according to IUPAC classification, and attributed to slit shaped pores or plate like particles with space between the parallel plates. A similar observation has been noted earlier for the Cr-pillared montmorillonite clay materials (Pinnavaia *et al.*, 1985a; Tzou and Pinnavaia, 1988; Sychev *et al.*, 1997a; Roulia, 2005).

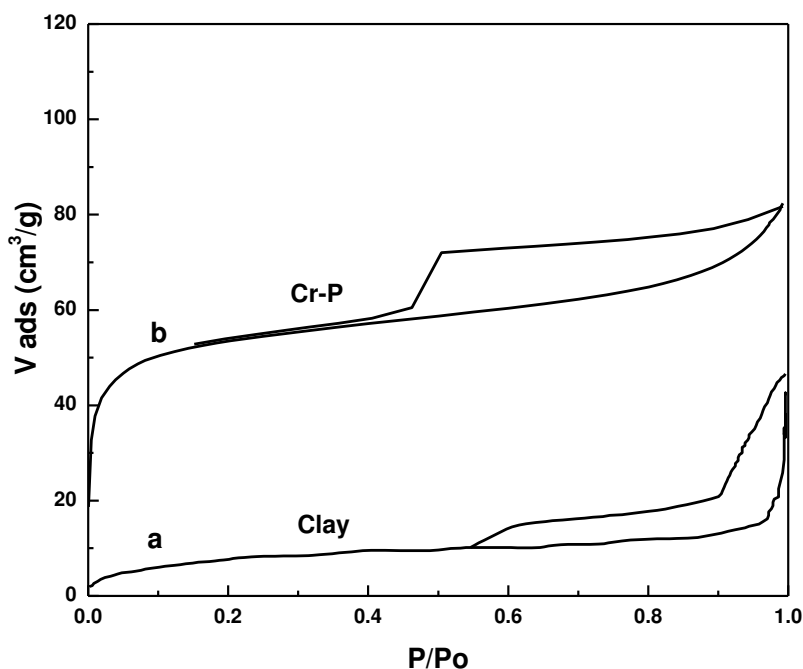


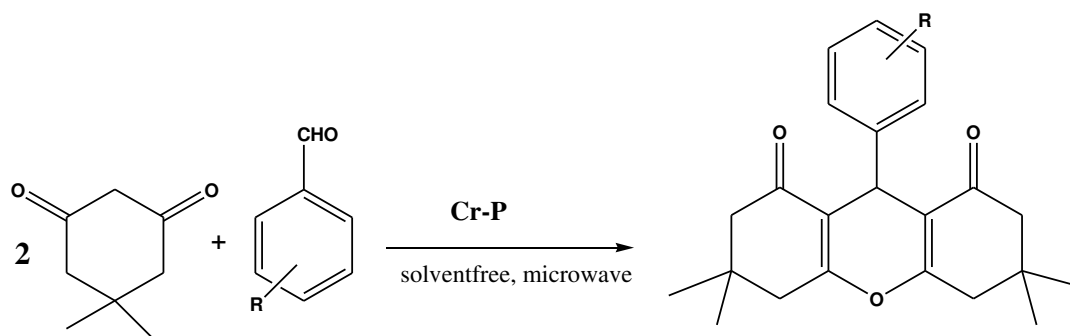
**Figure 3.5** N<sub>2</sub> sorption isotherm of (a) Parent Clay and (b) Cr-P material.

Sychev et al. have studied the intercalation of Cr-oligomeric clusters into the clay interlayer and their subsequent sulfidation to generate chromium sulfide pillars. The Cr- and sulfided Cr-pillared clay materials have been found to exhibit type-I isotherm with H3 type hysteresis typical of microporous layered solid materials. The observation of a type-I isotherm in the present study is in accordance with the earlier studies on Cr-pillared clay available in literature (Pinnavaia *et al.*, 1985a; Tzou and Pinnavaia, 1988; Sychev *et al.*, 1997a; Roulia, 2005). The surface area (272.0 m<sup>2</sup>/g) and pore volume (0.22 cm<sup>3</sup>/g) of the calcined Cr-P is found to be considerably higher than the parent clay materials (the surface area and pore volume are 30.1 m<sup>2</sup>/g and 0.06 cm<sup>3</sup>/g, respectively) (Table 3.1). During the process of pillaring, the expansion in the clay structure and the desegregation of the clay particles largely contributes to the enhancement of the surface area and porosity of the clay materials.

### **3.2.6 CATALYTIC ACTIVITY STUDY**

#### **3.2.6.1 SYNTHESIS OF OCTAHYDROXANTHENES**

The catalytic activity of the calcined Cr-pillared clay material is evaluated for the one pot synthesis of octahydroxanthenes by condensation of dimedone with aryl aldehydes under solvent-free conditions using microwave as energy source (Scheme 3.1). Initially, the condensation of benzaldehyde with dimedone is taken as model reaction and the reaction conditions are optimized for the solvent-free synthesis. It is observed that in the absence of the catalyst, 2,2'-arylmethylene bis(3-hydroxy-5,5-dimethyl 2-cyclohexene-1-one) was obtained as the major product. In the presence of the calcined Cr-pillared clay catalyst, the reaction is found to be significantly expedited with 2,2'-arylmethylene 9-aryl 1,3-dioxooctahydroxanthenes as the sole product.



**Scheme 3.1** One pot synthesis of octahydroxanthenes using Cr-P catalyst.

Various reaction parameters such as catalyst amount, microwave power and exposure duration are varied to obtain the optimized protocol. The detailed results of these catalytic experiments are presented in Fig. 3.6.

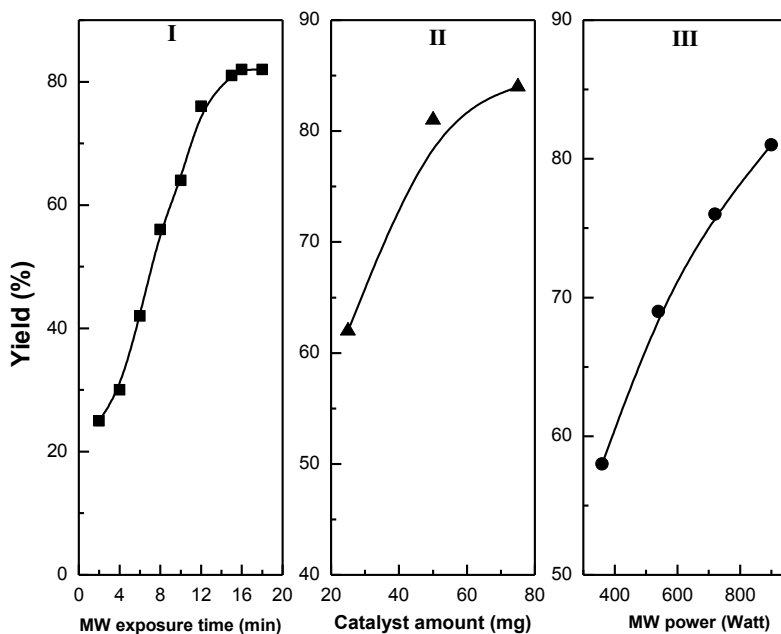


**Figure 3.6** Effect of various reaction parameters on the yield of the product for the reaction of benzaldehyde (1 mmol) with dimedone (2mmol) (I) Effect of reaction time (900 W and 50 mg of catalyst), (II) Effect of catalyst amount (900 W for 15 minutes duration), (III) Effect of microwave power (50 mg catalyst for 15 minutes duration)

It is observed that for the model reaction involving 1 mmol of the aryl aldehyde, 50 mg of the catalyst is ideal for an efficient condensation of the reactants for a microwave exposure time of 15 min at 900 W. A further increase in catalyst amount or the exposure duration does not have any significant impact on the yield of the reaction (Fig. 3.6). Ensuing optimized conditions for this condensation reaction, we explored the scope and limitations of this reaction using different substituted aromatic aldehydes (Table 3.2). Aromatic aldehydes having electron withdrawing groups reacted at faster rate compared to aromatics aldehydes containing electron releasing groups. For reactions involving the same substituent in the aromatic aldehyde, the para substituted aldehydes give improved yields as compared to the ortho substituted aldehydes. This seems to be due to the greater steric hindrance exerted by the ortho substituent than the para substituents. All the products are obtained within 10–20 min of irradiation time at 900 W microwave power.

**Table 3.2** Calcined Cr-P catalyzed synthesis of octahydroxanthenes under solvent free conditions and microwave irradiation

Sl No	R	Time (min)	Yield (%)
1	H	15	81
2	4-NO <sub>2</sub>	12	86
3	2-NO <sub>2</sub>	12	85
4	3-NO <sub>2</sub>	12	87
5	4-Cl	15	88
6	4-Br	15	85
7	2-Cl	15	83
8	3-Cl	15	82
9	4-F	15	86
10	4-OH	20	78
11	2-OH	20	80

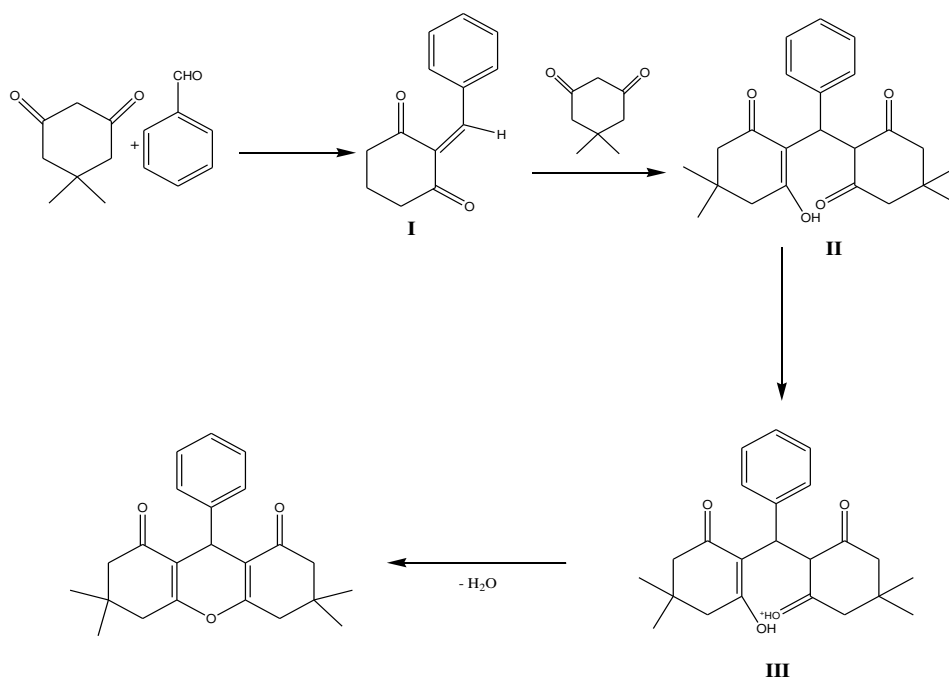


A comparison of the present catalytic method with earlier literature study revealed that the present method is advantageous in terms of less reaction time (Table 3.3). The yield of the products obtained in this study is better than many earlier studied catalytic systems such as 1-methylimidazolium trifluoroacetate ([Hmim]TFA and HClO<sub>4</sub>-SiO<sub>2</sub>, whereas for other system such as molecular iodine and P<sub>2</sub>O<sub>5</sub>/SiO<sub>2</sub> the yields are comparable. However, the present protocol exhibit distinct advantage in terms of the heterogeneous nature of the catalyzed process. Comparing the results of the present work, with SO<sub>4</sub><sup>2-</sup>/Fe-Zr-O heterogeneous catalyst, it is observed that the yields are marginally better in the latter case. However, for a reaction involving 1 mmol of benzaldehyde, 100 mg of SO<sub>4</sub><sup>2-</sup>/Fe-Zr-O catalyst is required for effective condensation where as in the present study 50 mg catalyst is sufficient to get good yield of products.

**Table 3.3 Comparison of the catalytic activity of Cr-P with other catalytic system reported in literature for synthesis of octahydroxanthenes.**

Sl. No	Catalyst	Reaction condition	Yield(%)	Reference
1.	Calcined Cr-P	Solventfree, microwave, 12-15 min	78-88	This work
2.	Molecular iodine	isopropanol, 70–80 °C, 1-2 h	90-96	Mulakayala <i>et al.</i> , 2012
3.	P <sub>2</sub> O <sub>5</sub> /SiO <sub>2</sub>	Solvent free, 80 °C, 1-4 h	76-97	Hasaninejad <i>et al.</i> , 2012
4.	3-(N,N-dimethyldodecylammonium) propanesulfonic acid hydrogen sulfate [DDPA][HSO <sub>4</sub> ]	Water, 100 °C, 1-2 h	87-96	Fang <i>et al.</i> , 2011
5.	1-methylimidazolium trifluoroacetate ([Hmim]TFA)	80 °C, 2.5-4 h	80-94	Dabiri <i>et al.</i> , 2008
6.	HClO <sub>4</sub> -SiO <sub>2</sub>	Neat, 140 °C, 3 h	23-32	Kantevari <i>et al.</i> , 2007
7.	100 mg SO <sub>4</sub> <sup>2-</sup> /10Fe-Zr-O	Solventfree, 12-18 min	75-90	Samantaray <i>et al.</i> , 2013

The mechanistic pathway for the formation of the octahydroxanthenes has been studied earlier in literature (Kantevari *et al.*, 2007; Pore *et al.*, 2010; Hasaninejad *et al.*, 2012; Mulakayala *et al.*, 2012). A plausible mechanism for formation of the octahydroxanthenes over the Cr-pillared clay materials is presented in Scheme 3.2. Initially, the condensations of the aryl aldehyde with the active methylene center of the dimedone takes place resulting in the formation of the Knoevenagel adduct (I). The subsequent addition of a second molecule of dimedone by Michael addition to I results in the formation of 2,2'-arylmethylene bis(3-hydroxy-5,5-dimethyl 2-cyclohexene-1-one) (II). The intermediate II undergoes a cyclodehydration process to yield the 2,2'-arylmethylene- 9-aryl-1,3-dioxooctahydroxanthenes as the final product.

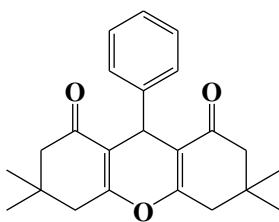


**Scheme 3.2 Probable mechanism for the synthesis of octahydroxanthenes catalyzed by calcined Cr-P catalyst**

The presence of the Cr-pillared clay can significantly expedite the Michael addition and cyclodehydration steps in the reaction mechanism. The enhanced Brønsted sites of the Cr-pillared clays can catalyze the above mentioned steps. The number of acidic sites of the clay

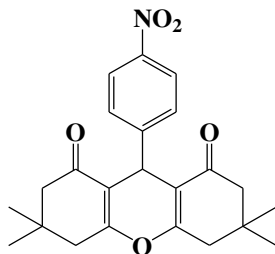
materials has been found to improve significantly upon pillaring with the chromium oligomeric clusters (Table 3.1). The Cr-nanoclusters as pillars can contain defect and coordinatively unsaturated sites in the clay microenvironment, which can contribute to the enhancement in the acidity of pillared clay material. The reusability of the catalyst was tested for three consecutive cycles. After the completion of the reaction, the filtered and dried catalyst was washed with 10 ml of methanol and calcined at 450°C for 2 h to generate the clay catalyst. The regenerated catalyst was used for three successive cycles without any significant change in the catalytic activity (Table 3.2, entry 2, 86, 1<sup>st</sup>, 82, 2<sup>nd</sup>, 79, 3<sup>rd</sup>). **The regenerated catalyst has been studied using XRD and sorptometric methods. No appreciable change in crystallinity is observed from XRD. However, there is a marginal decrease in surface area and porosity after 3<sup>rd</sup> cycle of catalysis study (surface area: 250 m<sup>2</sup>/g, pore volume: 0.19 cm<sup>3</sup>/g). The marginal loss in activity can be assigned to the decrease in the surface area and porosity of the Cr-P material.**

***9-(phenyl)-3,4,6,7-tetrahydro-3,3,6,6-tetramethyl-2H-xanthene-1,8(5H,9H)-dione (Table 3.2, Entry 1)***



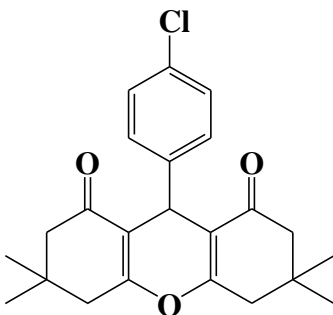
Mp: 200-202°C, IR (KBr): 3037, 2950, 1665, 1460, 1360, 1200, 1198, 1152, cm<sup>-1</sup>; <sup>1</sup>HNMR (400MHz, CDCl<sub>3</sub>): δ1.00 (s, 6H, CH<sub>3</sub>); 1.12 (s, 6H, CH<sub>3</sub>); 2.16 (q, 4H, CH<sub>2</sub>); 2.48 (s, 4H, 2CH<sub>2</sub>); 4.76 (s, 1H, CH); 7.11-7.32 (m, 5H, Ar)

***9-(4-Nitrophenyl)-3,4,6,7-tetrahydro-3,3,6,6-tetramethyl-2H-xanthene-1,8(5H,9H)-dione (Table 3.2, Entry 2)***



Mp: 224-225°C, IR (KBr): 3060, 2952, 1665, 1525, 1460, 1360, 1198, 1152  $\text{cm}^{-1}$ ;  $^1\text{H}$ NMR (400MHz,  $\text{CDCl}_3$ ):  $\delta$ 1.01 (s, 6H,  $\text{CH}_3$ ); 1.12 (s, 6H,  $\text{CH}_3$ ); 2.1-2.2 (q, 4H,  $\text{CH}_2$ ); 2.48 (s, 4H, 2 $\text{CH}_2$ ); 4.75 (s, 1H, CH); 7.28 (d, 2H, Ar); 8.10 (d, 2H, Ar)

***9-(4-Chlorophenyl)-3,4,6,7-tetrahydro-3,3,6,6-tetramethyl-2H-xanthene-1,8(5H,9H)-dione***  
(Table 2, Entry 5)

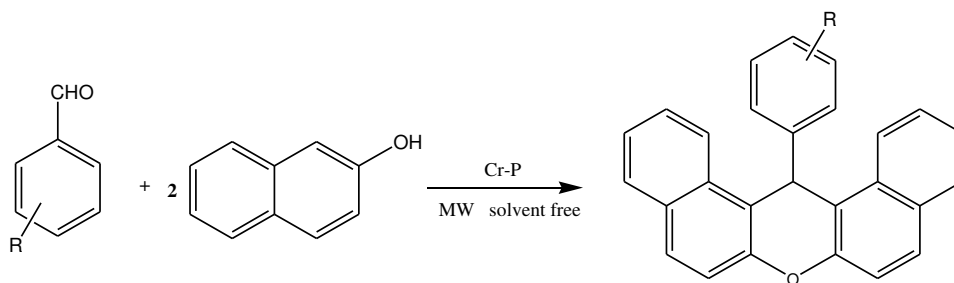


Mp: 231–233 °C, IR (KBr): 3015, 2987, 1682, 1478, 1384, 1194, 1176, 841 $\text{cm}^{-1}$ ,  $^1\text{H}$  NMR ( $\text{CDCl}_3$ , 400 MHz):  $\delta$ 1.02 (s, 6H,  $\text{CH}_3$ ), 1.13 (s, 6H,  $\text{CH}_3$ ), 2.06–2.22 (q, 4H,  $\text{CH}_2$ ), 2.46 (s, 4H,  $\text{CH}_2$ ), 4.62 (s, 1H), 7.24–7.41 (m, 4H, ArH).

### 3.2.6.2 SYNTHESIS OF BENZOXANTHENES

Cr-pillared clay has also been used as an environmentally benign solid acid catalyst for synthesis of aryl-14H-dibenzo[*a,j*]xanthenes by the condensation of  $\beta$ -naphthol and aryl aldehydes (Scheme 3.3). Initially the reaction conditions are optimized by taking the reaction of benzaldehyde and  $\beta$ -Naphthol as a model reaction. The reaction protocol is optimized by varying

the catalyst amount, solvent system and using microwave and conventional oil bath as energy source for the transformation.



### Scheme 3.3 One pot synthesis of benzoxanthenes using Cr-P catalyst.

It is observed that, 50 mg of Cr-P is quite efficient for the condensation of β-naphthol and benzaldehyde to produce the corresponding benzoxanthenes in high yield and purity. The use of solvent free condition and microwave irradiation was found to be beneficial in achieving good yield of product in less time. After optimizing the reaction conditions, the generality of the protocol is ascertained by reacting different aryl aldehydes bearing electron withdrawing and releasing groups with β-naphthol. Table 3.3 shows the yields of the different aryl-14H-dibenzo[*a,j*]xanthenes prepared using the optimized protocol. The reaction is found to proceed rapidly for aryl aldehydes containing electron withdrawing group. The catalyst is found to be highly active to afford all the products in good yields. After completion of the reaction, the reaction mixture is dispersed in 10 ml of ethyl acetate and stirred for 30 min at room temperature. The catalyst particles are filtered from the ethyl acetate suspension and the products are recovered by evaporation of the solvent by gentle heating, which is subsequently recrystallized. The recovered catalyst was regenerated by washing three times with 10 mL portions of methanol followed by heat treatment at 450 °C for 2 h. The regenerated catalyst is reused for three consecutive cycles without any significant loss of activity (Table 3.3, Entry 5, yields, 86%, 1<sup>st</sup>; 82%, 2<sup>nd</sup>; 80%, 3<sup>rd</sup>). Overall, the protocol developed in this study for synthesis

of aryl-14H-dibenzo[*a,j*]xanthenes is advantageous in terms of in high yield and purity of the products, preclusion of toxic solvents, short reaction time and catalyst recyclability.

**Table 3.4 Cr-P catalyzed synthesis of benzoxanthenes under solvent free condition and microwave irradiation**

Sl. No	R	Time (min)	Yield (%)
1	H	10	76
2	4-NO <sub>2</sub>	8	84
3	2-NO <sub>2</sub>	12	79
4	3-NO <sub>2</sub>	9	82
5	4-Cl	11	86
6	4-Br	10	85
7	2-Cl	12	80
8	3-Br	12	81
9	4-F	9	80
10	4-OCH <sub>3</sub>	12	78

Table 3.5 shows the comparison of the catalytic activity of the calcined Cr-P with the earlier literature reported methods for synthesis of benzoxanthenes. It is observed that Cr-P material gives good yield of product within a shorter period of time. The yield observed in this work is similar to the earlier reported methods. However, the method is advantageous in terms of solvenfree synthesis, recyclable catalyst and easy work up conditions compared to the literature reported procedures.

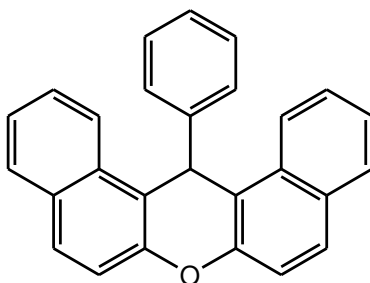
**Table 3.5 Comparison of the catalytic activity of Cr-P with other catalytic systems reported in literature for synthesis of benzoxanthenes.**

Sl. No	Catalyst	Reaction condition	Yield(%)	Reference
1.	Calcined Cr-P	Solvent free, microwave, 8-12 min	76-86	This work
2.	BF <sub>3</sub> .SiO <sub>2</sub>	Chloroform, reflux, sonication for 6 min	85-96	Mirjalili <i>et al.</i> , 2008
3.	Yb(OTf) <sub>3</sub>	Ionic liquid ([BPy]BF <sub>4</sub> ), 110 °C, 3-7 h	80-95	Su <i>et al.</i> , 2008
4.	Cellulose sulfuric acid	Solvent free, 110-115°C, 1-3h	81-97	Madhav <i>et al.</i> , 2009
5.	Ceric ammonium nitrate	Solvent free, 120 °C, 30 min	91-96	Kumar <i>et al.</i> , 2010

*Physical and spectral data of some of the representative compounds*

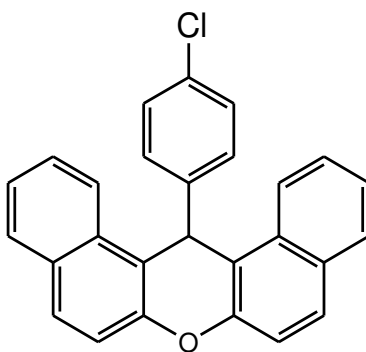
**14-(Phenyl)14H-dibenzo[*a,j*]xanthenes (Table 3.3, Entry 1)**

Mp: 182–184°C; IR (KBr) (cm<sup>-1</sup>): 3068, 3016, 2889, 1621, 1585, 1519, 1452, 1416, 1253, 1074, 959, 809, 739; <sup>1</sup>H NMR (CDCl<sub>3</sub>, 400 MHz)/ δ ppm: 6.51 (s, 1H, CH), 6.99 (t, 1H), 7.16 (t, 2H, Ar), 7.44(t, 2H, Ar),7.44–7.51 (m, 4H, Ar), 7.59 (t, 2H, Ar), 7.86 (d, 2H, Ar), 7.81 (d, 2H, Ar), 8.42 (d, 2H, Ar);



***14-(4-Chlorophenyl)14H-dibenzo[*a,j*]xanthenes (Table 3.3, Entry 5)***

Mp: 288–290 °C; IR (KBr) ( $\text{cm}^{-1}$ ): 3064, 1618, 1594, 1517, 1581, 1435, 1247, 1091, 967, 814, 748;  $^1\text{H}$  NMR ( $\text{CDCl}_3$ , 400 MHz)/  $\delta$  ppm: 6.46 (s, 1H, CH), 7.11–7.15 (d, 2H, Ar), 7.44–7.51 (m, 4H, Ar), 7.59–7.63 (m, 2H, Ar), 8.31 (d, 2H, Ar).





**PART B: SYNTHESIS OF 1,4-DIHYDROPYRIDINES CATALYZED BY  
SILICOTUNGSTIC ACID PARTICLES DISPERSED OVER Cr-PILLARED CLAYS**

### **3.3 INTRODUCTION**

Heteropoly acids (HPAs) are a class of polyoxometallates with interesting tunable acidic and redox properties (Kozhevnikov, 1998; 2009; Misono, 2013). Several types of heteropoly acids with diverse structural and chemical properties have been reported in open and patent literature. From catalysis point of view, Keggin type heteropoly acids display higher structural stability, Bronsted acidity, oxidation potential and resistance to deactivation by hydrolysis. The Keggin type heteropoly acids have been extensively investigated for industrially important chemical reactions (Mizuno and Misono, 1998; Misono, 2013). The chemical formula of a Keggin type heteropoly acid is generally presented as  $X^{n+}M_{12}O_{40}^{(8-n)-}$  where X is a heteroatom from 1<sup>st</sup> row transition elements and main group. The metal cation M such as  $Mo^{+6}$ ,  $W^{+6}$ ,  $V^{+5}$  have the characteristics of high charge and smaller size. The structure of Keggin anion can be described as composed of a central tetrahedron ( $XO_4$ ) surrounded by 12 edge- and corner-sharing metal-oxygen octahedra ( $MO_6$ ). This molecular arrangement is referred to as the primary structure of heteropoly acids (Fig. 3.7). The secondary structure of heteropoly acids is the HPA crystallites composed of heteropoly anions, counter cations and water of hydration. Heteropoly acids such as  $H_3PW_{12}O_{40}$  and  $H_3PMo_{12}O_{40}$  are known to possess well-defined Brønsted acidic sites. The Brønsted acidity of HPAs in solid and liquid state has been studied using several analytical techniques such as indicator titration, TPD, FT-IR study of adsorbed probe molecules, microcalorimetry and NMR spectroscopy (Kozhevnikov, 1998; 2009 Mizuno and Misono, 1998; Misono, 2013). These studies revealed that the Bronsted acidity of HPAs are stronger than most of the conventional solid acids such as  $SiO_2-Al_2O_3$ ,  $H_3PO_4/SiO_2$ , and HX and HY zeolites. The

catalytic activity of HPAs has been studied for esterification, Friedal-Craft alkylation, olefin hydration, condensation, polymerization and liquid phase oxidation [25, 26]. In recent years, there have been extensive efforts to utilize the potential of the HPAs in synthetic organic chemistry such as deprotection of t-butyldimethylsilane, regioselective aerobic oxygenation of nitrobenzene to 2-nitrophenol and oxidation of aliphatic, benzylic and allylic alcohols using dimethyl sulfoxides as oxygen transfer agents, synthesis of quinoxalines, 1,5-benzodiazepines and oxidative sulfurization (Khenkin *et al.*, 2002; 2005; Kishore Kumar and Bhaskaran *et al.*, 2005; Mishra *et al.*, 2006; Alibeik and E.H.-Torkabad 2012; Li *et al.*, 2011 ).

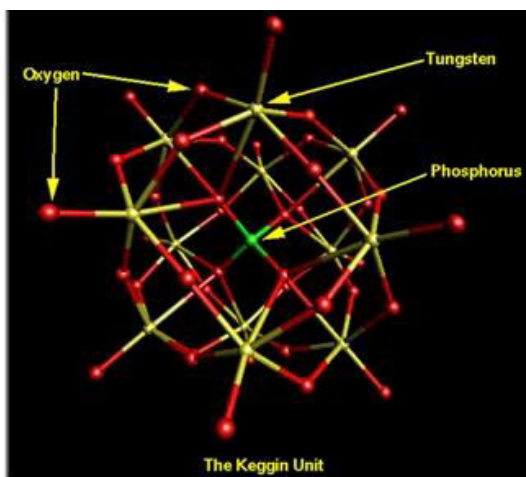


**Figure 3.7** Structure of keggin anion.

Although heteropoly acids display promising surface and catalytic properties, their application in catalysis is limited by their low surface area. This limitation can be overcome by dispersing HPAs on solid supports with high surface area and porous nature (Misono, 2013). In general, heteropoly acids interact strongly with supports at low loading levels, often resulting in grafting of these materials on solid surface. At higher loading, however, the bulk properties of HPAs prevail. Acidic or neutral substances such as  $\text{SiO}_2$ , active carbon and acidic ion-exchange resin are suitable supports employed. Solids having basicity such as  $\text{Al}_2\text{O}_3$  and  $\text{MgO}$  tend to decompose HPAs and are not preferable to be used as support. In recent years, heteropoly acids

supported on silicious porous materials such as MCM-41, SBA-15 and hexagonal mesoporous silicas are being explored for effective utilization of the active protonic sites of these acids (Sawant *et al.*, 2007; Liu *et al.*, 2009). The catalytic activity of the supported HPA system has been evaluated for several industrially important chemical transformations. HPA supported MCM-41 have been found to be effective for liquid phase alkylation of toluene with 1-octane with better selectivity for monoalkylated products (Liu *et al.*, 2009). Esterification of benzyl alcohol with acetic acid has been carried out using 12-silicotungstic acid supported on ZrO<sub>2</sub>/SBA-15 system which shows enhanced activity and stability (Sawant *et al.*, 2007). Earlier investigation in literature shows that the clay based materials served as efficient support for the dispersion and stabilization of the HPA units (Yadav and Badure 2008; Bhorodwaj and Dutta, 2010; 2011; Yadav and More 2011). Moreover, the acidic sites of the clay work synergistically with the acidic sites of the HPA for efficient catalysis process. **K-10 clay has been found as effective support for the phosphotungstic acid. Coumarins were synthesized by the condensation of ethyl acetoacetate with phenol in presence of catalytic amount of PWA/K-10 (Vijaykumar and RangaRao, 2012b).** Acid treated bentonites as well as montmorillonite have been found to be efficient support for phosphotungstic acid for esterification of acetic acid with butanol (Bhorodwaj and Dutta, 2010; 2011). Cs modified HPA supported over K-10 clay efficiently catalyze acylation of 1,3-dibenzyloxybenzene and alkylation of anisole with cyclohexene (Yadav and Badure 2008; Yadav and More 2011). With an objective to explore the catalytic potential of highly dispersed HPA nanoclusters for synthesis of biologically relevant molecules, in this work, we have employed Cr-pillared clay as a support for silicotungstic acid. The catalytic activity of silicotungstic acid nanoparticles dispersed in the micropores of the Cr-pillared clay (STA/Cr-P) has been studied for the synthesis of 1,4-dihydropyridines under solvent free conditions. **The**

rationale behind choosing the Cr-P clay material as support is based on its important physicochemical properties such as higher surface area and good porosity which is ideal for dispersion of the STA species. Moreover, the STA which is thermally more stable and display strong surface acidic sites among different polyoxometallates is ideal for acid catalyzed synthesis of heterocyclic compounds. The synergistic effect between the acidic sites of both Cr-P and STA is expected to efficiently catalyze the synthesis of dihydropyridine molecules.

Dihydropyridines (DHPs) and their derivatives are an important class of bioactive molecules which have been extensively investigated for their application as anticonvulsant, antidiabetic, antidepressive, antitumor, and anti-inflammatory agents (Litvic *et al.*, 2008; Gaudio *et al.*, 1994; Mohammadi *et al.*, 2010). DHPs are also useful compounds for synthesis of neuroprotectants and treatment of Alzheimer's disease due to their cerebral anti-ischemic properties (Mohammadi *et al.*, 2010) The 1,4-dihydropyridines are generally synthesized by Hantzsch method which involves one-pot condensation of  $\beta$ -keto esters, aromatic aldehyde and ammonia under reflux condition in alcoholic media (Litvic *et al.*, 2008; Mohammadi *et al.*, 2010). In the past few years, there have been significant efforts to modify this classical method by employing various acidic/basic catalysts to improve the yield and purity of the synthesized products. Hantzsch process has been modified by using different catalysts such as TMSCl–NaI, ionic-liquids, InCl<sub>3</sub>, ceric ammonium nitrate (CAN), Na- and Cs-exchanged carbons, and metal triflates (Sridhar *et al.*, 2005; Rondon *et al.*, 2006; Sridharan *et al.*, 2007; Debache *et al.*, 2009; Yamuna *et al.*, 2011). However, most of the catalytic protocol reported so far uses homogeneous catalysts, Lewis acidic salts or supported reagents which suffer from the drawback of leaching, separation, recovery and handling of the catalyst. A stable heterogeneous catalytic system which is

recyclable and provide good yield of the product is highly desirable for synthesis of 1,4-dihydropyridines.

### 3.4 RESULTS AND DISCUSSION

#### 3.4.1 XRD STUDY

The XRD patterns of the parent clay along with the calcined Cr-P and STA/Cr-P material in the  $2\theta$  range of  $3-20^\circ$  are presented in Fig. 3.8. The parent clay shows a sharp and intense peak at  $2\theta = 6.8^\circ$  corresponding to the reflection from the (001) planes of the layered materials. The basal spacing and interlayer spacing of the parent clay is calculated to be  $12.9 \text{ \AA}$  and  $3.3 \text{ \AA}$ , respectively. The expansion in the interlayer structure of the clay material is clearly observed after the intercalation of the Cr-pillaring solution. The calcined Cr-P material shows a  $d_{001}$  spacing of  $20.8 \text{ \AA}$ . The interlayer space of the Cr-pillared clay material was found to be retained in the STA/Cr-P material.

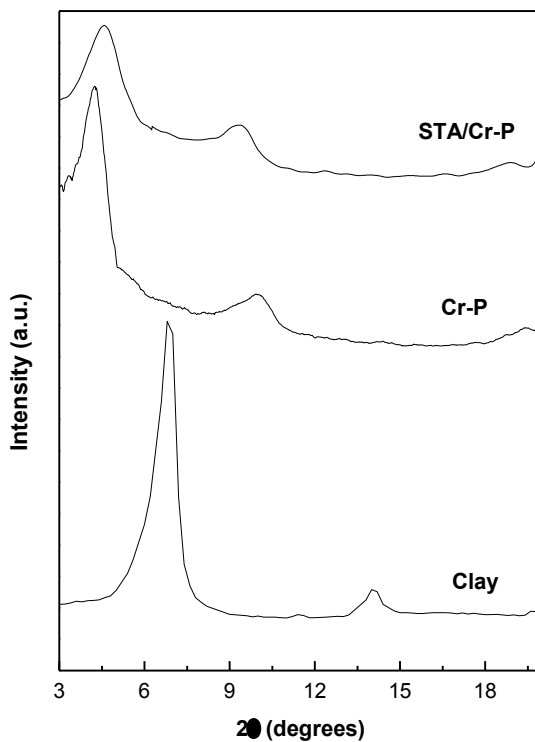


**Figure 3.8** XRD patterns of (a) Clay, (b) Cr-P and (c) STA/Cr-P

The STA/Cr-P material exhibits a broad (001) peak of reduced intensity with a basal spacing of 19.6 Å. This shows that the long range order of the Cr-P material is reduced to a certain extent due to dispersion of STA particles. No characteristic peak of bulk STA is observed in the STA/Cr-P which indicates that STA particles have been finely dispersed in the micropores of the chromia pillared clay.

### 3.4.2 FT-IR STUDY

The FT-IR spectra of different pillared clay materials along with the STA/Cr-P and bulk STA are presented in the Fig. 3.9. All characteristic vibrational features of the clay material are retained in the STA/Cr-P material (Fig. 3.9). However, there is significant enhancement in the band intensity for the structural –OH group after pillaring with Cr-polycations and dispersion of STA clusters.

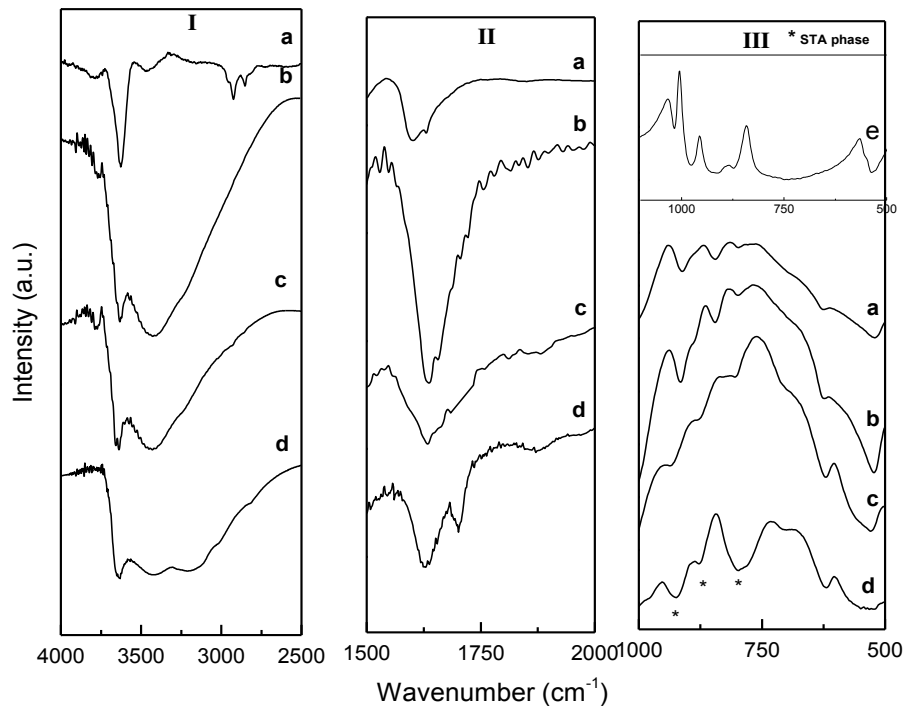


**Figure 3.9** FTIR spectra of (a) Parent clay, (b) air dried Cr-P, (c) calcined Cr-P and (d) STA/Cr-P (Panel III, inset (e) bulk STA)

Since the structural hydroxyl group accounts for the acidic nature of clay materials, this observation indicates the possibility of enhancement of the acidity as a result of Cr-pillaring and subsequent dispersion of the STA clusters. Due to the existence of hydrogen bonds, STA/Cr-P material shows a series of broad peak in the range of 3440–3150  $\text{cm}^{-1}$ . The peak at 3440  $\text{cm}^{-1}$  arises due to stretching vibrations of Si-OH bond (Bodoardo *et al.*, 1994).

Pure STA in its bulk state shows a series of discrete peak in the frequency region of 600–1100  $\text{cm}^{-1}$  (Fig. 3.9 III inset). The IR spectrum of pure STA shows five peaks at 1015, 978, 915, 885, 800  $\text{cm}^{-1}$ . These peaks can be attributed to the symmetric and asymmetric stretching vibrations of W=O bond, Si-O, W-O<sub>c</sub>-W, W-O<sub>e</sub>-W groups, respectively (Brahmkhatri and Patel, 2011). The dispersed STA particles in the Cr-P matrix shows the characteristic STA vibrational features at 985, 972, 875 and 800  $\text{cm}^{-1}$  indicating the structural integrity of the STA cluster in the microenvironment of the Cr-pillared clay.

### 3.4.3 UV-VIS STUDY

The UV–Vis spectra of Cr-pillared clay along with STA/Cr-P and bulk STA are presented in Fig. 3.10. The clay materials show UV absorption due to the transition metal ions present in the interlayer or in the silicate structure. A broad band with maxima at 245 nm is observed for the parent clay which can be assigned to the charge transfer transition  $\text{Fe}^{3+} \leftarrow \text{O}^{2-}$ ,  $\text{OH}^-$  or  $\text{OH}_2$ , for the structural iron present in the octahedral layer of the clay mineral (Fig. 3.10 a) (Mishra and Ranga Rao, 2003). The absorption spectrum is found to be altered on intercalation of the chromium oxyhydroxy species and subsequent thermal treatment. In addition to the characteristic clay peak, two well defined broad bands are observed with maxima at 420–440 nm and 580–600 nm. These peaks can be assigned to the  $A_{2g} \rightarrow T_{1g}$  and  $A_{2u} \rightarrow T_{2g}$  transitions characteristics of Cr(III) ions in octahedral symmetry present in the form of  $\text{Cr}_2\text{O}_3$  nanoclusters in the clay

interlayer (Fig. 3.10 b) (Rombi *et al.*, 2006). For the STA/Cr-P material, an intense band is perceptible with absorption maxima around 270 nm along with a broad shoulder at 345 nm. These UV absorption bands can be assigned to the different oxygen to metal charge transfer transitions arising out of the dispersed STA clusters (Rombi *et al.*, 2006). For bulk STA, the  $W^{6+} \leftarrow O^{2-}$  charge transfer transitions induce two intense and broad bands in the absorption spectrum (Fig. 3.10 d). The band observed at 245 nm can be assigned to  $W^{6+} \leftarrow O_e^{2-}$  (edge shared oxygen) charge transfer transition whereas the 345 nm band is due to  $W^{6+} \leftarrow O^{2-}$  transition from corner shared oxygen (Naik *et al.*, 2011).

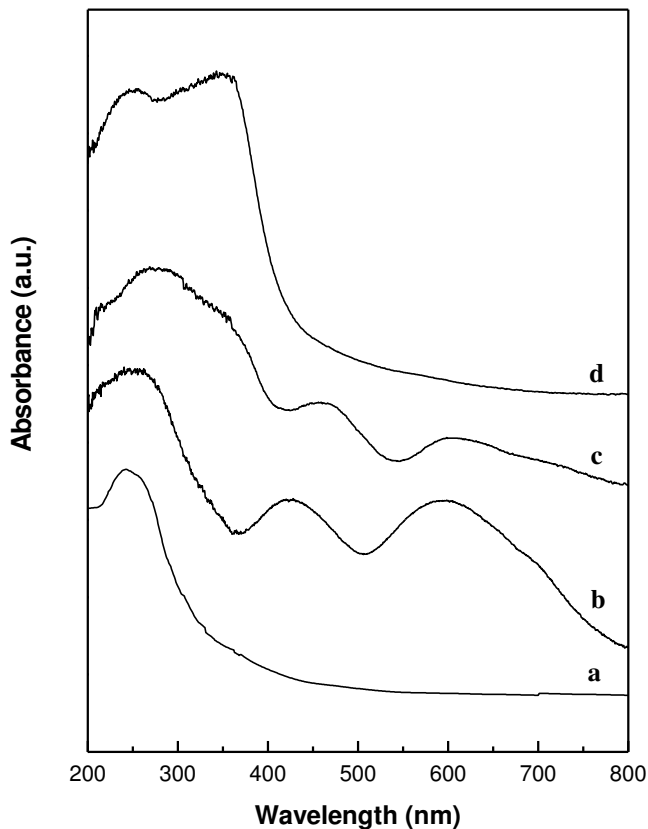


**Figure 3.10** UV-Vis spectra of (a) parent clay, (b) Cr-P calcined, (c) STA/Cr-P and (d) bulk STA.



The absorption feature of pure STA is found to be different from that of STA/Cr-P. The band at 245 nm got red shifted to 270 nm and the intensity of the band at 345 nm is reduced. This reveals that there might be change in co-ordination environment of the oxygen present in the STA clusters. The electronic spectra indicate a possible interaction of the STA clusters with the clay microenvironment leading to their anchoring in the pillared clay lattice.

### 3.4.4 THERMOGRAVIMETRIC ANALYSIS

The TGA/DTG profile of STA/Cr-P materials is illustrated in Fig. 3.11. Two prominent weight loss regions are observed for the STA/Cr-P material in the TG profile. Initial weight loss in the range of 40–160°C is due to removal of physisorbed water and water of crystallization of STA molecules.

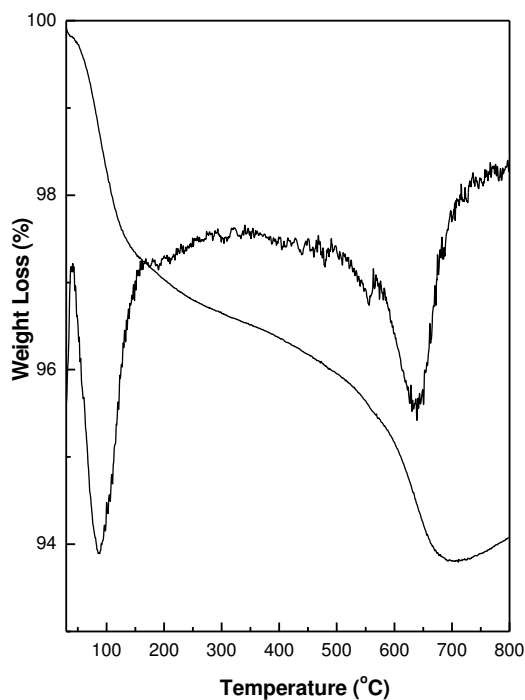


**Figure 3.11** TGA/DTG profile of 10STA/CrP material.

Another weight loss in the range of 520–680°C is due to loss of structural protons from STA molecules (Rajkumar and RangaRao, 2008). At this temperature range, STA clusters get transformed into mixed metal oxides by thermal decomposition. Thus from the TG plot it is interpreted that the prepared STA/Cr-P catalyst is stable up to 500°C.

### 3.4.5 SORPTOMETRIC STUDY

The N<sub>2</sub> sorption isotherm of the STA/Cr-P material along with the Cr-P material is presented in Fig. 3.12. The corresponding surface area and pore volume of the STA/Cr-P materials is presented in Table 3.4. The STA/Cr-P materials shows type I isotherms as per the BDDT classification indicating the presence of micropores in the material (Fig. 3.12 b). The type of hysteresis observed on these materials is H3 type indicating the presence of slit shaped pores.

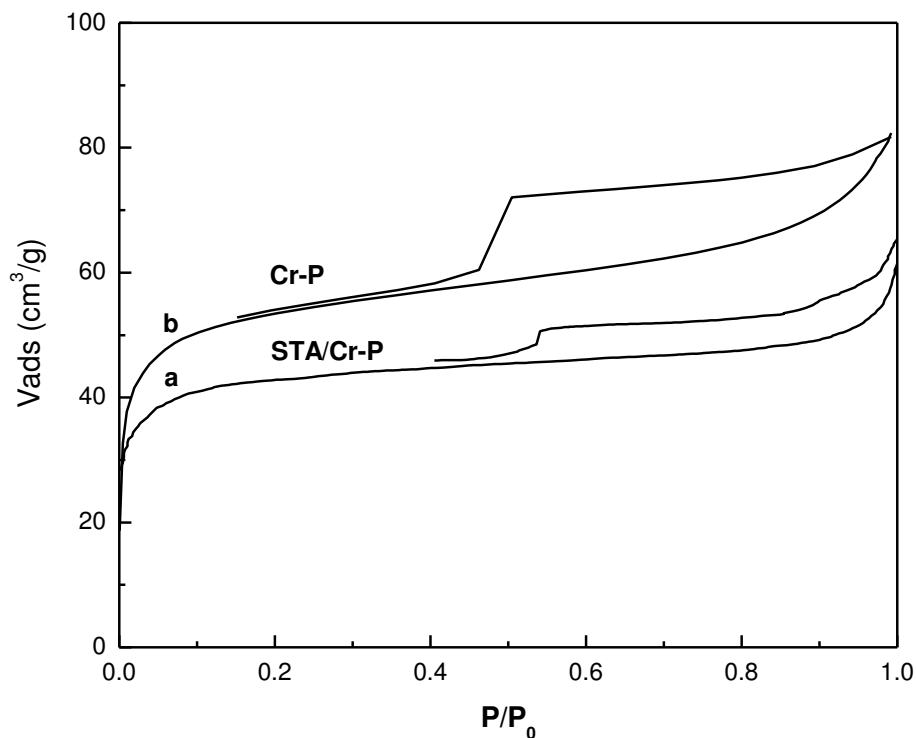


**Figure 3.12** N<sub>2</sub> sorption isotherm of (a) STA/Cr-P and (b) Cr-P.

The calcined Cr-pillared clay materials exhibit a surface area of 272 m<sup>2</sup>/g which is significantly higher than the value of 30 m<sup>2</sup>/g observed for the parent clay material. The STA/Cr-P material exhibit surface area and pore volume of 215 m<sup>2</sup>/g and 0.12 cm<sup>3</sup>/g. The decrease in the surface area and pore volume is due to the partial occupation of the pores of the Cr-pillared clay by STA particles (Fig.3.12 a).

### 3.4.6 SEM STUDY

The scanning electron micrograph of the air dried and calcined Cr-pillared clay along with the STA/Cr-P material is presented in Fig. 3.13.

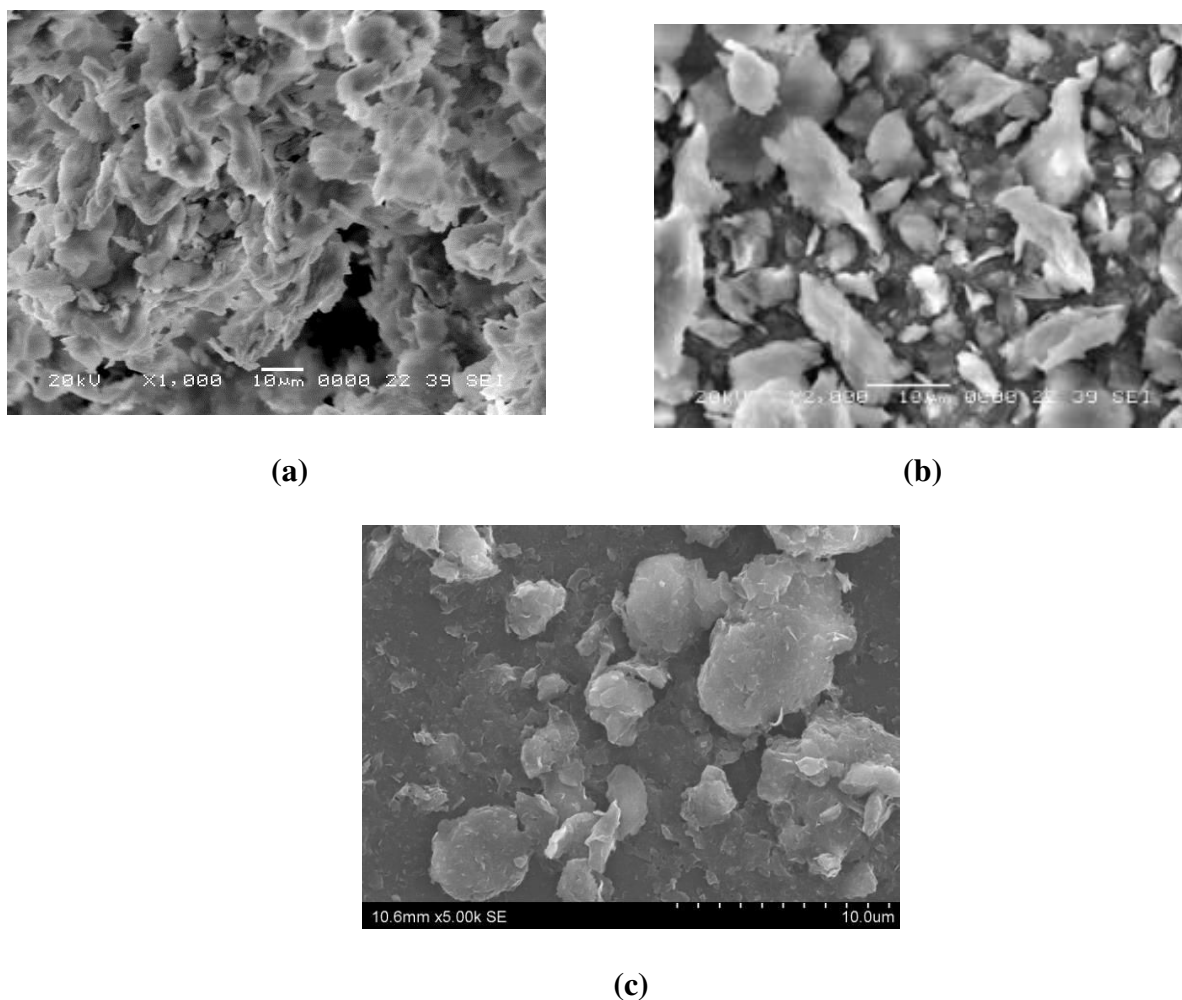


**Figure 3.13** Scanning electron micrograph of (a) Cr-P air dried, (b) Cr-P calcined and (c) STA/Cr-P.

For the air-dried Cr-P materials, lamellar structure is developed due to maximum face to face interaction as the particles are stacked in (001) direction. However on subjecting air dried Cr-P to higher temperature treatment the lamellar structure got distorted due to edge to edge interaction and edge to face interaction (Sychev *et al.*, 1997a; Tomul and Balci, 2009). It is ascribed from SEM image that dispersion of STA particles into Cr-P clay leads to folded morphology most likely due to the interaction of the STA particles with the clay layers.

### 3.4.7 TEM STUDY

The TEM image of the STA/Cr-P material along with the STA/Clay is presented in Fig. 3.14. The TEM picture of STA/Cr-P reveals that the STA particles are present in a well dispersed state and are of irregular shape (Fig. 3.14 a). The particle sizes of the supported STA particles are in the range of 10–20 nm. No agglomeration is found as the STA particles are well separated from each other.

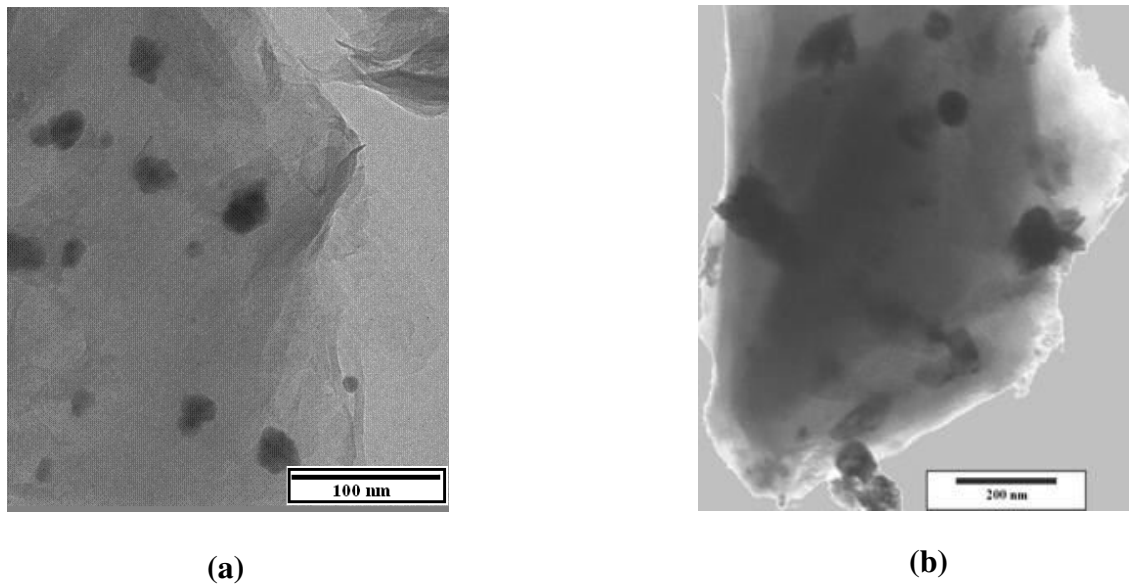


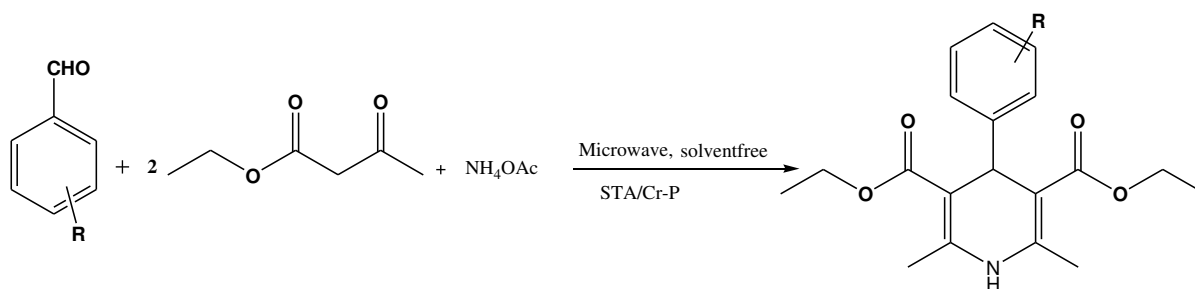
**Figure 3.14** Transmission electron micrographs of (a) STA/Cr-P and (b) STA/Clay

The STA particles dispersed in the parent clay matrix (STA/ Clay), on the other hand, display larger particle (20–40 nm) and inhomogeneity in size distribution (Fig. 3.14 b). This observation

indicates that the Cr-pillared clay material is quite efficient for the dispersion of the STA particles in its matrix. The high surface area and the uniform micropores of the Cr-pillared clay is responsible for the dispersion and separation of the STA particles in the clay structure.

### 3.4.8 CATALYTIC ACTIVITY FOR THE SYNTHESIS OF 1,4-DIHYDROPYRIDINES

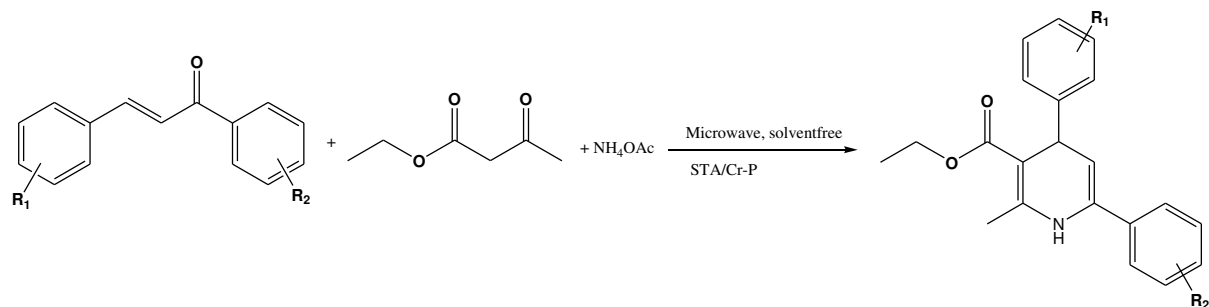
The STA/Cr-P material is used as an efficient and ecofriendly catalyst for the synthesis of 1,4-dihydropyridines by one pot condensation of aldehyde/chalcones, ethylacetoacetate and ammonium acetate under microwave irradiation (Scheme 3.4 and Scheme 3.5). Initially, the catalytic activities of various clay based materials were evaluated taking the multicomponent one pot reaction of benzaldehyde, ethylacetoacetate and  $\text{NH}_4\text{OAc}$  as a model reaction. The physicochemical characteristics and catalytic activity of the clay based materials studied for this condensation reaction are presented in Table 3.4. Parent clay was found to be inactive for the reaction. Pillaring with Cr-oligomeric nanoclusters significantly improves the surface area, pore volume as well as the catalytic activity of the parent clay. Among the supported STA catalysts, the STA/Cr-P material exhibit better yield compared to the STA/Clay material.



**Scheme 3.4 STA/Cr-P catalyzed multicomponent condensation of arylaldehydes, ethylacetoacetate and ammonium acetate.**

The higher surface area and pore volume of the Cr-P material helps in better dispersion of the STA particles compared to the parent clay. The effective utilization of the active sites available on the supported STA clusters as well as the Cr-pillars is responsible for the higher catalytic

activity observed for STA/Cr-P material. The catalytic activity of the clay catalysts is found to correlate well with the surface acidity of these materials determined using TGA of adsorbed n-butyl amine. Since the clay materials exhibit different surface area and acidity, the reaction rate were calculated in terms of unit surface area and acidic sites by estimating the benzaldehyde conversion in the reaction mixture by GC analysis. It was observed that the STA/Cr-P catalyst shows higher reaction rates as compared to other materials. This catalyst also provide better yield of the products at a shorter reaction time compared to the other clay based catalytic materials (Fig. 3.15). Based on the results described in the Table 3.4 and Fig. 3.15, the STA/Cr-P catalyst was selected for further studies.



**Scheme 3.5 STA/Cr-P catalyzed multicomponent condensation of chalcones, ethylacetoacetate and ammonium acetate.**

The catalyst amount in the reaction mixture is varied between 50 mg and 150 mg for a reaction involving 1 mmol of the reactants for the model reaction (Fig. 3.16). It is observed that 100 mg of the STA/Cr-P catalyst is quite proficient for carrying out condensation of aldehyde, ethylacetoacetate and NH<sub>4</sub>OAc. Further increase in the catalyst amount does not have any marked impact on the yield of the product (Fig. 3.16).

**Table 3.6. Physicochemical characteristics and catalytic activity of different clay materials studied for the synthesis of 1,4-Dihydropyridines by multicomponent condensation of benzaldehyde, ethylacetoacetate and NH<sub>4</sub>OAc.**

Clay sample	Basal spacing (Å)	Surface area (m <sup>2</sup> /g)	Pore volume (cc/g)	Acidity <sup>a</sup> (mmol/g)	MW irradiation time (sec)	Yield <sup>b</sup> (%)	Rate <sup>c</sup> (mmolh <sup>-1</sup> g <sup>-1</sup> )	Rate (mmolh <sup>-1</sup> m <sup>-2</sup> )	TOF (h <sup>-1</sup> )
Clay	12.8	30.1	0.06	0.15	600	NR	--	--	-
Cr-P	20.8	272.0	0.22	0.42	480	52	42.7	0.0157	10.1
STA/Cr-P	19.6	215.4	0.12	0.56	300	75	97.2	0.0376	17.3
STA/Clay	12.7	20.6	0.02	0.28	480	38	31.5	0.1529	11.2
Acid activated Montmorillonite <sup>d</sup>	---	135.0	0.15	0.37	480	48	39.7	0.0294	10.7

*a* Calculated from TG analysis of *n*-butyl amine, *b* Refers to pure and isolated yield, *c* Calculated with respect to the benzaldehyde conversion in the reaction mixture analyzed using Gas chromatography, *d* Synthesized by treating the parent clay with 3N sulphuric acid at 80°C for 6h followed by quenching in ice cold water

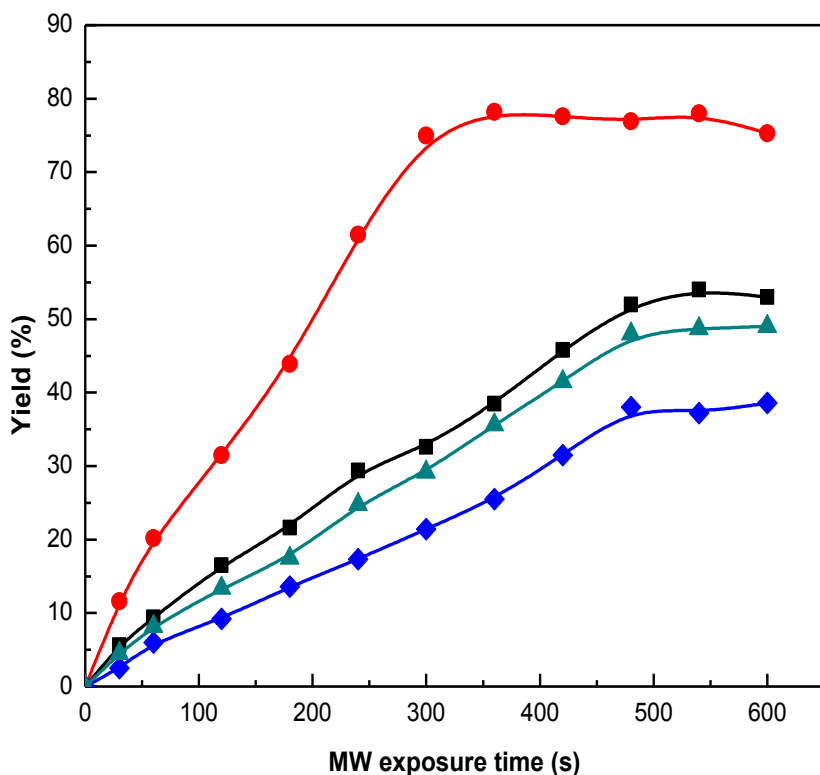


**Figure 3.15** Effect of microwave exposure time on the yield of 1,4-dihydropyridines synthesized by condensation of benzaldehyde (1mmol), ethylacetoacetate (2 mmol) and  $\text{NH}_4\text{OAc}$  (1mmol) . (-●-) STA/Cr-P, (-■-) Cr-P, (-▲-) AAM, and (-◆-) STA/Clay

After optimizing the reaction condition, the applicability of the optimized protocol was evaluated by taking different substituted benzaldehyde as reactants. Table 3.5 illustrates the yield of the various DHPs synthesized using the optimized protocol. It was observed that a variety of aryl aldehydes reacted under the optimized condition to give the corresponding dihydropyridines in high yield and purity. In general, better yield are achieved for aldehydes containing electron withdrawing groups than that of electron donating groups. On completion of reaction the obtained product is dissolved in 10 ml of ethyl acetate, stirred and then filtered to separate the



catalyst particles. The final product is acquired by evaporation of solvent and subsequently recrystallized.

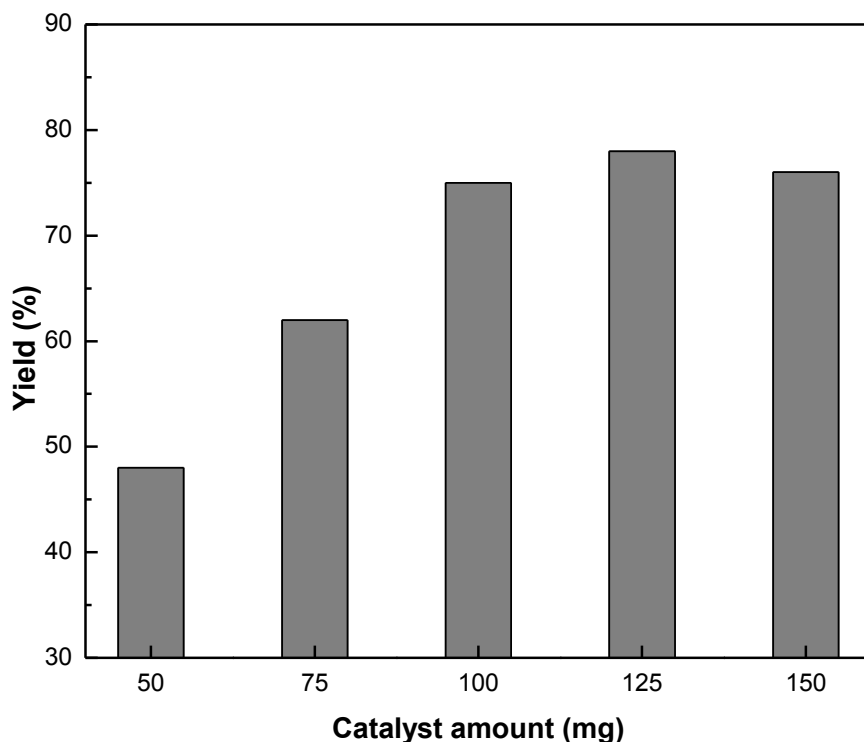


**Figure 3.16** Effect of catalyst weight on the yield of of 1,4-dihydropyridines synthesized by condensation of benzaldehyde (1mmol), ethylacetoacetate (2 mmol) and  $\text{NH}_4\text{OAc}$  (1mmol) using STA/Cr-P catalyst.

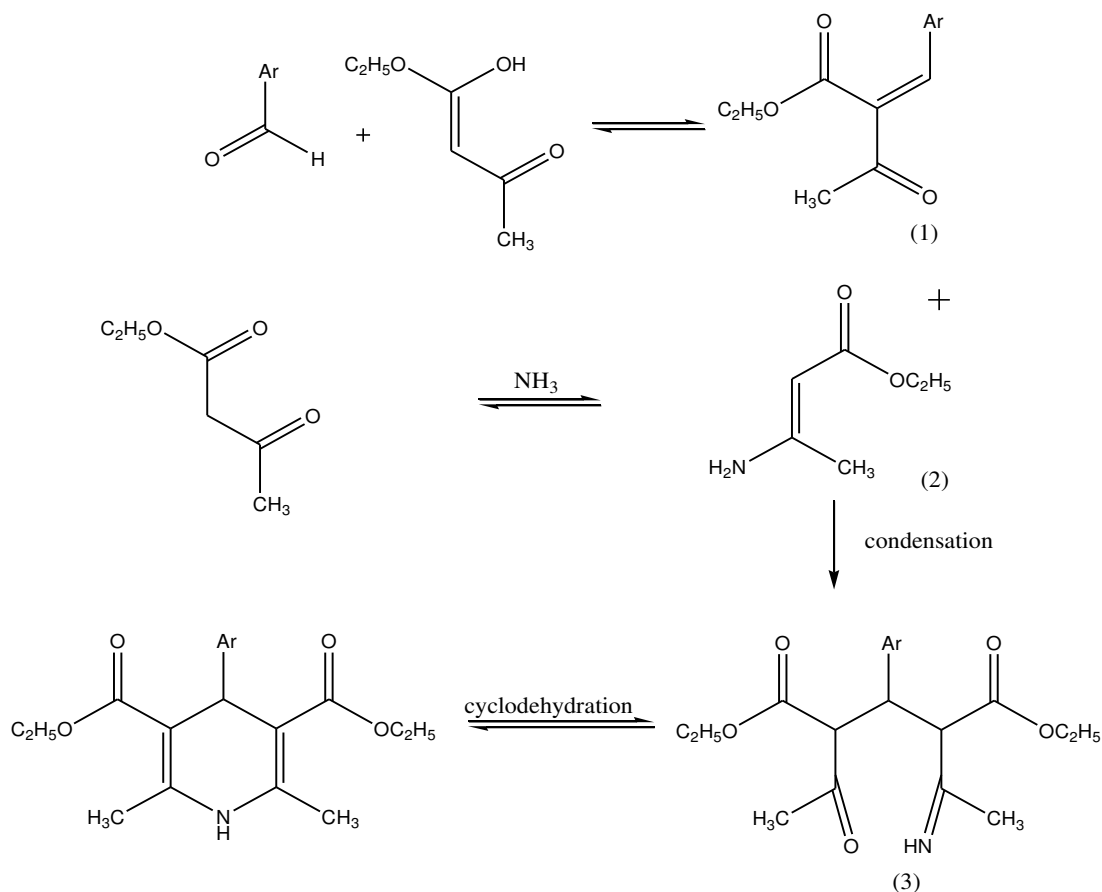
The catalyst is regenerated by three times washing with 10 ml portions of ethyl acetate followed by heat treatment at 250 °C for 1 h. The recyclability of the regenerated catalyst was studied for three consecutively cycles. The catalyst is found to be stable up to three cycles without any significant loss in the catalytic activity (Table 3.5, entry 2, 84, 1st, 82, 2nd, 79, 3rd). The mechanistic aspect of the reaction has been studied earlier in literature (Sridhar and Perumal, 2005; Datta and Pasha, 2011).

**Table 3.7 STA/Cr-P catalyzed one pot synthesis of dihydropyridines by condensation of arylaldehydes (1mmol), ethylacetoacetate (2 mmol) and ammonium acetate (1 mmol).**

Sl. No	R	Time (min)	Yield (%)
1	H	5	75
2	4-NO <sub>2</sub>	6	84
3	2-NO <sub>2</sub>	11	78
4	3-NO <sub>2</sub>	6	75
5	4-Cl	8	82
6	4-Br	9	85
7	2-Cl	6	86
8	4-F	8	74
9	4-OH	10	70
10	2-OH	10	78

Initially, the condensation of ethyl acetoacetate with aromatic aldehyde leads to the formation of Knoevenagel product (1) (Scheme 3.6). A second molecule of  $\beta$ -keto ester reacts with ammonia molecule to form an ester enamine (2). The subsequent condensation of the Knoevenagel product (1) with the ester enamine (2) yield the intermediate (3) which undergo cyclodehydration to form the 1,4-dihydropyridines (Scheme 3.6). The STA/Cr-P catalyst can take part in more than one step in the proposed mechanism to expedite the synthesis of 1,4-dihydropyridines. In the STA/Cr-P catalyst, the  $W^{6+}$  act as Lewis acidic sites where as the structural hydroxyls of the clay sheet as well as the delocalized protons of STA can act as Bronsted acidic sites. The aldehydic

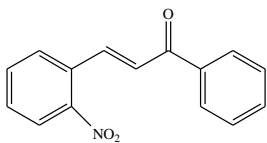
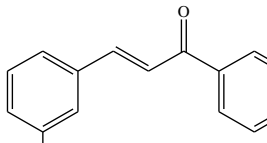
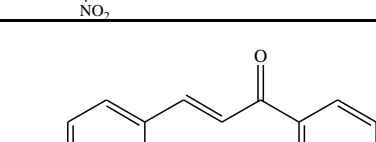
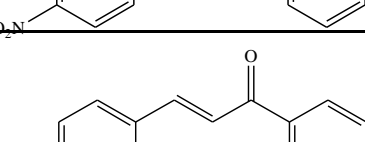
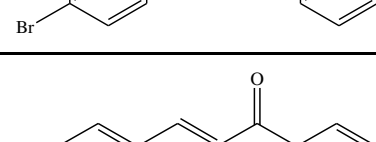
carbonyl group can be activated by adsorption onto the Lewis acidic  $W^{6+}$  sites of STA/Cr-P catalysts. Similarly, the process of enolization of  $\beta$ -keto esters, formation of ester enamine and the cyclodehydration steps can be catalyzed in the presence of the Bronsted acidic sites of the STA/Cr-P catalyst.



**Scheme 3.6 Probable mechanistic path for synthesis of 1,4-Dihydropyridine in the surface of STA/Cr-P catalyst.**

In order to further extend the application of the optimized catalytic protocol, chalcones are used as reactant in place of aldehydes (Scheme 3.5). In case of chalcones, the reaction rates are relatively sluggish and the yield is less as compared to that of aryl aldehydes (Table 3.6).

**Table 3.8 STA/Cr-P catalyzed one pot synthesis of dihydropyridines by condensation of chalcones (1mmol), ethylacetoacetate (1mmol) and ammonium acetate (1mmol).**

Sl.No.	Chalcone	Time(min)	Yield(g)
1.		12	64
2.		12	68
3.		15	75
4.		12	73
5.		10	78

However, under the optimized conditions a variety of chalcones reacted to give the corresponding DHPs. Table 3.9 presents a comparison of the catalytic activity of the STA/Cr-P material with earlier investigated catalytic systems for synthesis of dihydropyridines. The present system exhibit good yield of the product under mild condition and less reaction time compared to literate reported methods. Moreover, the heterogeneous nature of the catalytic system facilitates easy recovery and regeneration of the catalyst particles. Thus in this present investigation, the

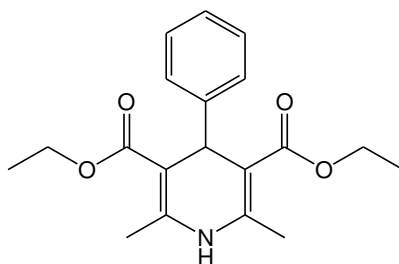
STA/Cr-P is demonstrated as a new environmental friendly and economical heterogeneous catalyst for the synthesis of structurally diverse 1,4-dihydropyridines. The specific advantages of the catalytic protocol developed in this study include solvent free condition, stable and recyclable heterogeneous catalyst, preclusion of toxic solvent, simple experimentation and high yield and purity of the product.

**Table 3.9 Comparison of the catalytic activity of STA/Cr-P with other catalytic systems reported in literature for synthesis of dihydropyridine.**

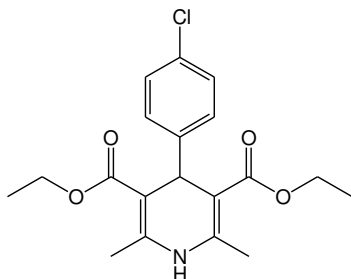
Sl. No	Catalyst	Reaction condition	Yield(%)	Reference
1.	STA/Cr-P	Solvent free, microwave, 5-11 min	70-86	This work
2.	Triphenylphosphine	Ethanol, reflux, 2-5 h	75-95	Debache <i>et al.</i> , 2009
3.	Cerium ammonium nitrate (CAN)	Ethanol, room temp, 1h	61-74	Sridharan <i>et al.</i> , 2007
4.	3,4,5-Trifluorobenzeneboronic acid, ionic liquid	Room temp, 4-6 h	85-93	Sridhar <i>et al.</i> , 2005
5.	Molecular iodine with urea H <sub>2</sub> O <sub>2</sub> adduct	Ethyl acetate, room temp, 0.75-12 h	87-99	Litvic <i>et al.</i> , 2008
6.	Sulfonic acid-functionalized silica	Solvent free, 90 °C, 1h	87-93	Mohammadi <i>et al.</i> , 2010

Physical and spectral data of some selected compounds are given below

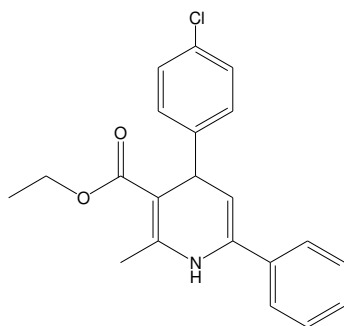
- Diethyl-2,6-dimethyl-4-phenyl-1,4-dihydropyridine-3,5-dicarboxylate (Table 3.5, entry 1):  
M.P. 158–159°C; FT-IR (KBr, cm<sup>-1</sup>): 1694, 3338; <sup>1</sup>H NMR (CDCl<sub>3</sub>, 400 MHz): δ 1.16 (t, 6H), 2.23 (s, 6H), 4.03 (q, 4H), 4.93 (s, 1H), 5.60 (s, 1H), 7.06–7.22 (m, 5H) ppm.



2. Diethyl-2,6-dimethyl-4-(4-chloro-phenyl)-1,4-dihydropyridine-3,5-dicarboxylate (Table 3.5, entry 5): M.P. 144-145°C; IR (KBr,  $\text{cm}^{-1}$ ): 1694, 3332;  $^1\text{H}$  NMR ( $\text{CDCl}_3$ , 400 MHz,):  $\delta$  1.22 (t, 6H), 2.30 (s, 6H), 4.04 (m, 4H), 4.92 (s, 1H), 5.73 (s, 1H), 7.13-7.29 (m, 4H) ppm.



3. Ethyl 4-(4-chlorophenyl)-2-methyl-6-phenyl-1,4-dihydro-3-pyridinecarboxylate (Table 3.6, entry 5): M. P. 254-256; IR(KBr,  $\text{cm}^{-1}$ ): 3340, 1718, 1670;  $^1\text{H}$  NMR ( $\text{DMSO-d}_6$ , 400 MHz)  $\delta$  1.14 (t, 3H), 2.10 (s, 3H), 3.50 (q, 2H), 6.33 (d, 1H), 6.93 (d, 1H), 7.19 (s, 1H, NH), 7.28 (d, 2H), 7.32–7.52 (m, 5H), 7.69 (d, 2H) ppm.



### 3.5 CONCLUSIONS

In this chapter, we have studied the catalytic applications of Cr-pillared clays and STA/Cr-P material for synthesis of biologically important molecules. The intercalation of the chromium oligomeric nanoclusters has been confirmed from the expansion of the interlayer space of the parent clay material. The Cr-pillared clay is microporous in nature and displays higher surface area and pore volume compared to the parent clay material. The IR spectra of the Cr-pillared clays indicates an enhancement of structural hydroxyl group and water retention capacity. UV–

Vis spectra indicate the presence of  $\text{Cr}_2\text{O}_3$  nanoclusters as pillars inside the clay interlayer. The Cr-pillared clay was used as an efficient support for dispersion of silicotungstic acid nanoclusters. The interlayer spacing of the Cr-pillared clay is retained after the dispersion of the STA particles. IR and UV–Vis study reveals the structural integrity STA nanoparticles in the micropores of the Cr-P material. From TEM analysis it is observed that the supported STA particles are of irregular shape with size in the range of 10–20 nm.  $\text{N}_2$  sorptometric study depicts the microporous nature of STA/Cr-P materials. The Cr-PM material has been used as an efficient catalyst for the synthesis of octahydroxanthenes and benzoxanthenes. A series of structurally diverse targeted molecules were synthesized under microwave irradiation using the Cr-P catalyst. Similarly, structurally diverse DHPs are also synthesized in high yield and purity by one pot multicomponent condensation of aldehydes/chalcones, ethylacetoacetate,  $\text{NH}_4\text{OAc}$  using the STA/Cr-P materials as heterogeneous catalyst. The catalytic experiments conducted in this study revealed that the Cr-pillared clay and their modified form are quite promising heterogeneous catalysts for synthesis of biologically important molecules under environmentally benign conditions. Overall, new and efficient protocols have been designed in this study using the Cr-pillared clay based catalyst which is advantageous in terms of simple experimentation, preclusion of toxic solvent, shorter reaction times, catalyst recyclability and high yield and purity of the products.

## CHAPTER 4

# SYNTHESIS AND CATALYTIC APPLICATIONS OF Zr-PILLARED CLAY-POLYMER COMPOSITE MATERIALS

## PART A: SYNTHESIS OF TETRAHYDROPYRIDINES USING POLYPHOSPHORIC ACID-Zr PILLARED CLAY COMPOSITE MATERIALS AS CATALYST

### 4.1 INTRODUCTION

Polymeric acid display molecularly defined catalytically active sites suitable for a variety of organic transformations. However, they possess inherent disadvantages such as low surface area and difficulty in recovery and regeneration when they are used in pristine form. In order to enhance their surface area, stability, and to avoid corrosive property it is desirable to heterogenize these materials by dispersing in inorganic hard matrices by forming nanocomposites. Among inorganic polymers, polyphosphoric acid has promising application potential as catalyst in acid catalyzed organic transformations. The polyphosphoric acid is a oligomeric form of phosphoric acid which contain  $-(\text{PO}_3\text{H})-$  repeating unit in the polymer structure. Compared to other homogeneous corrosive acids, it is less corrosive, mild and exhibit dehydrating properties, which has been successfully exploited to carry out acylation and cyclization reaction of a variety of substrates (Itoh *et al.*, 2011; Sadanandam *et al.*, 2011). PPA is also used as a catalyst for synthesis of heterocyclic compounds. The synthesis of 2-aryl/alkyl substituted benzimidazoles, benzoxazoles and benzothiazoles as well as purine derivatives has been accomplished by using PPA as catalyst (Sadanandam *et al.*, 2011). Although there are reports on the catalytic activity of PPA, its applicability is limited due to disadvantages such as high viscosity and difficulty in separation and handling. In order to extend its effectiveness and to improve its recyclability, PPA has been supported over porous materials having high surface



area such as SiO<sub>2</sub> (Itoh *et al.*, 2011). The PPA–SiO<sub>2</sub> has been used as efficient catalyst for the multicomponent one pot synthesis of polyhydroquinoline derivatives, 1,8-octahydroxanthenes, N,N'-alkylidenebisamide derivatives and structurally diverse 3-benzoylisoxazoles (Kantevari *et al.*, 2007; Itoh *et al.*, 2011; Khojastehnezhad *et al.*, 2011; Shafiee, 2014). Norouzi *et al.* have investigated the catalytic activity of alumina supported PPA for the synthesis of 14-aryl-14H-dibenzoxanthenes (Norouzi *et al.*, 2011). Sachdev and Dubey. have successfully synthesized SBA-15 supported PPA by direct as well as impregnation method and the efficiency of the prepared catalyst has been examined for the acylation of naphthalene in liquid phase using acetyl chloride as acylation agent (Sachdev and Dubey, 2013). In this work, we have utilized the Zr-pillared clay as a host matrix to disperse polyphosphoric acid and studied their catalytic activity for synthesis of tetrahydropyridines. The Zr-pillared clays by virtue of their good surface area, uniform porosity and interlayer space of few molecular dimension (~ 1 nm) is ideal for entrapment of PPA molecular chains. The constrained interlayer space of the Zr-pillared clays can prevent the aggregation of polymeric chain and contribute to more number of exposed active sites. Since, the synthesis of tetrahydropyridine requires Bronsted acidic sites, more number of such sites can be created by dispersing PPA in Zr-P matrix. In this study, different synthetic strategies are adopted to maximize the dispersion of the PPA in the clay and pillared clay matrix. The resulting composite materials are characterized by XRD, IR, FE-SEM, EDX, TGA, UV–Vis and sorptometric techniques.

Piperidine motifs are found in the basic skeleton of various natural alkaloids and pharmaceuticals (Mohite *et al.*, 2012). Synthesis of various substituted piperidines has received considerable attention in recent years because of their antibacterial, anti-inflammatory, anticonvulsant and antimalarial properties (Ramin and Hajar, 2013) Furthermore, these moieties are highly active in

inhibiting the action of cancer causing enzymes farnesyl transferase (Brahmachari and Das, 2012). Hence different strategies are being developed for the synthesis of substituted tetrahydropyridines motifs. One pot multicomponent condensation reaction (MCR) is found to be most favourable way for synthesis of these complex organic molecules within a very short period of time. MCR has certain advantages such as atom economy, shorter reaction time and eluding difficult purification processes. Earlier literature shows that lot of effort are being devoted by the researchers to develop a simple and easy protocol for the synthesis of substituted tetrahydropyridines by using various catalysts such as l-proline/TFA, bromodimethylsulfonium bromide (BDMS), tetrabutylammonium tribromide (TBATB), molecular iodine, ceric ammonium nitrate (CAN),  $ZrOCl_2 \cdot 8H_2O$ ,  $InCl_3$ , picric acid, poly(N,N'-dibromo-N-ethylbenzene-1,3-disulfonamide) [PBBS] and N,N,N',N'-tetrabromobenzene-1,3-disulfonamide [TBBDA] and bismuth nitrate ( $Bi(NO_3)_3 \cdot 5H_2O$ ) (Khan *et al.*, 2008; 2010a; 2010b; Misra *et al.*, 2009; Mishra and Ghosh, 2011; Mukhopadhyay *et al.*, 2011a; Wang *et al.*, 2011; Brahmachari and Das, 2012; Ramin and Hajar, 2013). Although these catalysts have been found to be effective for the multicomponent condensation, they possess limitations in terms of greater reaction time, homogenous nature of the reaction, requirement of higher amount of catalyst and cost ineffectiveness. To overcome such drawbacks we have employed PPA-Zr-pillared clay composite materials as catalyst for synthesis of various substituted tetrahydropyridines under environment benign conditions.

## **4.2 RESULTS AND DISCUSSION**

### **4.2.1 XRD STUDY**

The XRD patterns of the parent clay along with the Zr-pillared clay and clay-PPA composite materials in the  $2\theta$  range of  $3-15^\circ$  are presented in Fig. 4.1. The corresponding basal spacing

values calculated from the XRD profile are presented in Table 4.1. The parent clay shows a sharp and intense peak at  $2\theta = 6.8^\circ$  corresponding to the reflection from the (001) planes of the layered material. The basal spacing of the parent clay is 12.8 Å (Fig. 4.1a). The intercalation of Zr-polyoxocationic clusters leads to the shifting of  $d_{001}$  peak to the lower  $2\theta$  value indicating an expansion in the clay structure due to pillaring (Fig. 4.1b). The as synthesized Zr-pillared clay shows a basal spacing of 20.2 Å. On thermal treatment for 2 h at 500°C, the Zr-pillared clay shows a slight shift in the peak position towards the higher  $2\theta$  value (Fig. 4.1c).

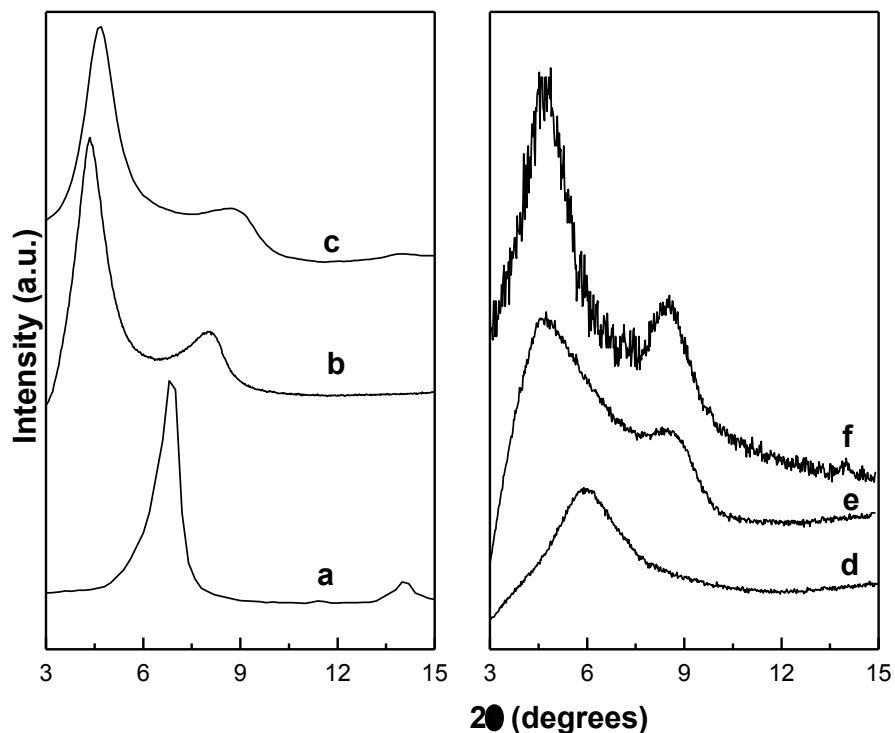


**Figure 4.1** XRD patterns of (a) parent clay, (b) air dried Zr-P, (c) calcined Zr-P, (d) PPA-Clay, (e) PPA-ZrP and (f) ZrP-PPA.

This is due to conversion of the polyoxocations to oxide nanoclusters. However, there is no appreciable difference in the intensity or broadness of the peak indicating the calcined Zr-pillared clay is stable up to 500°C. The  $d_{001}$  value for the calcined Zr-P material is found to be

19.0 Å. From the XRD study it is illustrated that heat treatment up to 500 °C does not noticeably affect the crystallinity and stacking pattern of the pillared clay material. Fig. 4.1d–f shows the XRD patterns of different PPA–clay composite materials. Intercalation of PPA in general leads to the broadening of the peaks as compared to the respective clay materials. The broadening of the peak implies loss of crystallinity to a certain degree upon PPA intercalation. This may be attributed mainly to two factors. First, because of acidic nature of PPA, it can partially hydrolyse the Al-O-Si bond of the clay sheet which may result in disorder clay structure and consequent loss in crystallinity. However, considering the noncorrosive nature of PPA compared to other mineral acid this can occur to a small extent. The second important factor which can contribute to the peak broadening is the formation of a well dispersed intercalated PPA–clay nanocomposite. Since PPA is intercalated to the clay matrix in swelled condition, it is likely that PPA molecules reside in the interlayer region. The presence of PPA molecules can disturb the stacking arrangement of the clay sheets along the [001] axis, which give rise to the disordered structure. The presence of PPA in the interlayer region is further evident from the shifting of peak towards lower  $2\theta$  value for the parent clay intercalated with PPA (PPA–clay). The  $d_{001}$  value observed for PPA–clay is 15 Å (Table 4.1). The XRD pattern of the PPA–ZrP composite is shown in Fig. 4.1e. The XRD peak is broadened indicating a decrease in the crystalline character as compared to pure Zr-P. However, the noticeable point is that when the PPA–clay is crosslinked using Zr-polycation a basal spacing value (19.2 Å) similar to the Zr-pillared clay was obtained (Table 4.1 and Fig. 4.1e). This observation is indicative of the fact that the pillaring process imparts structural rigidity to the PPA–clay structure and the PPA molecules are trapped in the lateral space between the pillars.

**Table 4.1 Basal spacing and surface area of different clay-PPA composite catalysts.**

Material	Basal spacing (Å)	Surface area (m <sup>2</sup> /g)
Clay	12.8	30.2
Zr-P	19.0	176.0
PPA-Clay	15.0	17.5
PPA-CTAB-Clay	18.5	38.0
PPA-ZrP	19.2	95.2
ZrP-PPA	18.8	86.3

In case of ZrP–PPA materials, which is prepared by the dispersion of PPA molecules in the micropores of Zr-P, basal spacing value of 18.8 Å is observed (Fig. 4.1f). However, the XRD peaks corresponding to the ZrP-PPA and PPA-ZrP materials are broad with enhanced noise to signal ratio in comparison to pure ZrP. This observation indicates that the composite materials exhibit lower crystallinity compared to the Zr-P material.

#### 4.2.2 FTIR STUDY

The FTIR spectra of different clay materials are represented in Fig. 4.2. The characteristic vibrational feature of the clay materials are retained in the FTIR spectra of the composite catalytic system. Moreover, there is an enhancement in the intensity of the structural -OH vibration at 3636 cm<sup>-1</sup> after the pillaring process. This observation indicates the generation of new structural hydroxyl centres in the clay material as a result of pillaring (Sposito *et al.*, 1983; Bodoardo *et al.*, 1994; Mishra and Ranga Rao, 2005; Samantaray *et al.*, 2011). The zirconia oligomeric clusters present inside the clay interlayer can contain hydroxyl groups. After the intercalation of the PPA to the clay, noticeable changes are observed in the stretching region of

the FTIR spectra. The -OH stretching peak for PPA intercalated clay (Fig. 4.2b) is very broad that ranges from 3000 to 3600  $\text{cm}^{-1}$ . The broadening of the -OH band can be ascribed to the formation of a variety of hydrogen bonding in presence of PPA inside the clay interlayer. The -OH group of PPA can form hydrogen bond with the OH group of the clay sheet as well as the coordinated water molecule. Since the clay structure contains -OH groups differing in bond strength due to their location and coordination, it is expected that a wide range of hydrogen bonds of different strength can form in clay interlayer. These hydrogen bonds are responsible for broadening of the -OH peak (Chen and Wang, 2006).

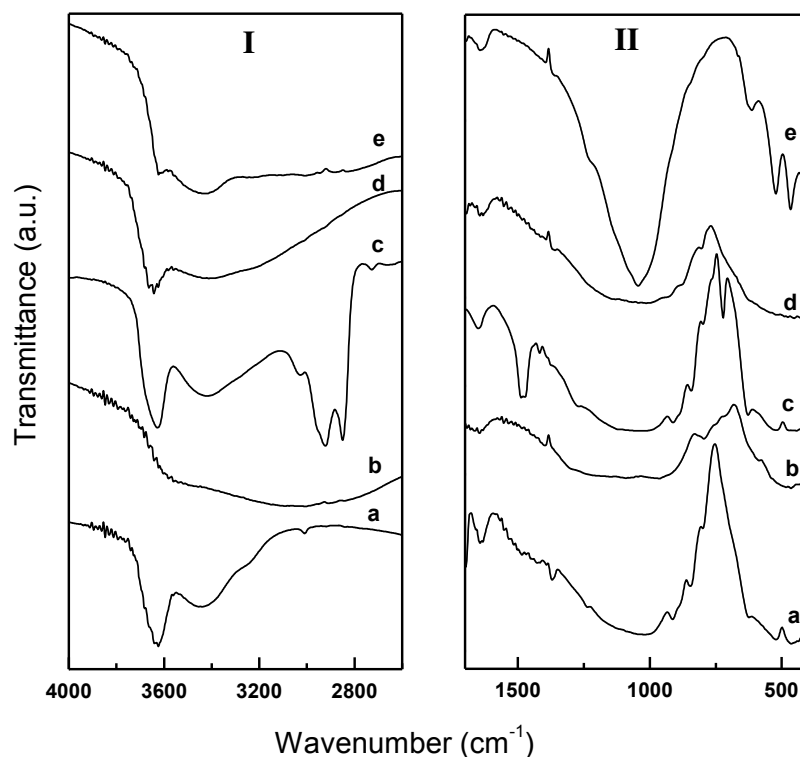


**Figure 4.2** FTIR Spectra of (a) parent clay, (b) PPA-clay (c) CTAB-PPA-clay (d) ZrP-PPA and (e) PPA-ZrP (panel I and panel II in the range of 4000-3000  $\text{cm}^{-1}$  and 1700-400  $\text{cm}^{-1}$ , respectively).

PPA in its bulk state shows a prominent peak at  $1015\text{ cm}^{-1}$  due to the stretching vibrations of P–O–P bond. The asymmetric stretching and bending vibration of P–O–P absorb IR radiation at  $924$  and  $484\text{ cm}^{-1}$ , respectively (Zhang and Yu, 2010). These characteristic peaks with slight shift are observed for the clay–PPA composite materials which support the intercalation of PPA into the clay materials. For CTAB–PPA–clay, in addition to the characteristic peaks corresponding to the clay lattice and PPA, well distinguished peaks for CTAB are observed at  $2851$  and  $2920\text{ cm}^{-1}$  after intercalation of PPA. These peaks are ascribed to symmetric and asymmetric stretching vibrations of C–CH<sub>2</sub> present in the cetyl group of CTAB (Ma *et al.*, 2005). **This observation implies limited uptake of PPA in presence of CTAB. CTAB being an amphiphile generates a hydrophobic environment in the clay matrix which is not conducive for the intercalation of PPA which is predominantly hydrophilic in nature.** This fact is also evident from Table 4.2 which shows CTAB–PPA clay has less phosphorous content as compared to other clay materials.

### 4.2.3 UV-VIS STUDY

The UV–Vis spectra of the parent clay along with other clay polymer composite materials are presented in Fig. 4.3. The band observed at  $247\text{ nm}$  (Fig. 4.3a) is characteristic for montmorillonite clay and attributed to the charge transfer transition for the structural iron present in the octahedral layer of the clay mineral ( $\text{Fe}^{3+} \leftarrow \text{O}^{2-}$ ,  $\text{OH}^-$  or  $\text{OH}_2$ ) (Mishra and Ranga Rao, 2004). Upon incorporation of PPA into the clay matrix the band maxima was found to shift towards the higher wavelength side. The PPA–clay shows absorption maximum at  $265\text{ nm}$  which is attributed to the change in coordination environment in the clay interlayer in presence of the PPA moieties. The same shift in band has also been observed for other composite materials.

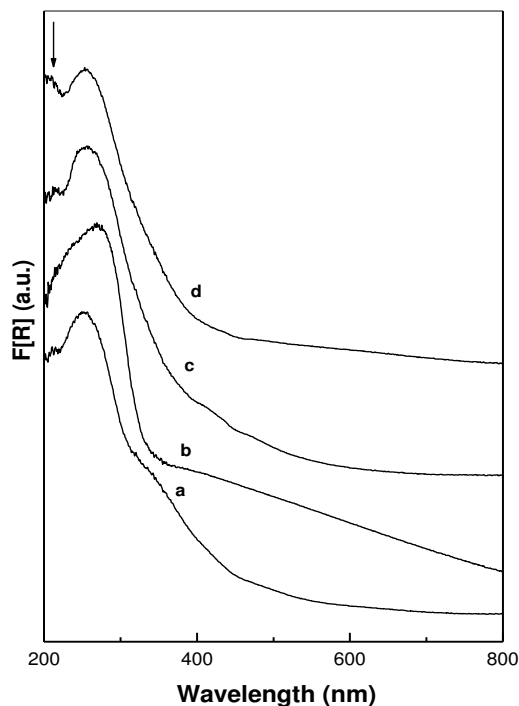


**Figure 4.3** UV-Vis spectra of (a) parent clay, (b) PPA-clay, (c) ZrP-PPA and (d) PPA-ZrP.

All the PPA containing composites shows UV absorption maxima in the range of 255–265 nm. In case of the PPA–ZrP and ZrP–PPA, an additional band is observed at 210 nm. This band can be ascribed to the  $Zr^{4+}$  (4d)  $\leftarrow O^{2-}$  (2p) charge transfer transition from the zirconia nanopillars present in the clay interlayer (Samantaray *et al.*, 2011).

#### 4.2.4 THERMOGRAVIMETRIC ANALYSIS

The TGA profile of the air dried Zr-P, PPA–clay and ZrP–PPA clay materials is depicted in Fig. 4.4. Three major weight loss regions have been observed for the air dried Zr-pillared clay sample in the range of 50–200°C, 400–550°C and >550°C (Fig. 4.4, Panel I). The removal of adsorbed water molecules present in the interlayer region of pillared materials is responsible for the weight loss between 50–200°C. However, the weight loss detected in the range of 400–550°C and >500 °C are accredited to the loss of structural water molecules and dehydroxylation of the pillars as



well as clay sheets, respectively. The weight loss at high temperature region ( $>550^{\circ}\text{C}$ ) is more gradual without any well-defined inflection point (Mishra and Ranga Rao, 2004). For ZrP-PPA three weight loss regions are also observed (Fig. 4.4, Panel III). The weight loss between  $35\text{--}120^{\circ}\text{C}$  is due to the release of water molecules physically adsorbed into the pores of the clay matrix. The second weight loss between  $125\text{--}180^{\circ}\text{C}$  is due to loss of water molecules coordinated to the pillars. These water molecules are in a coordinated state and hence require higher temperature for their removal.

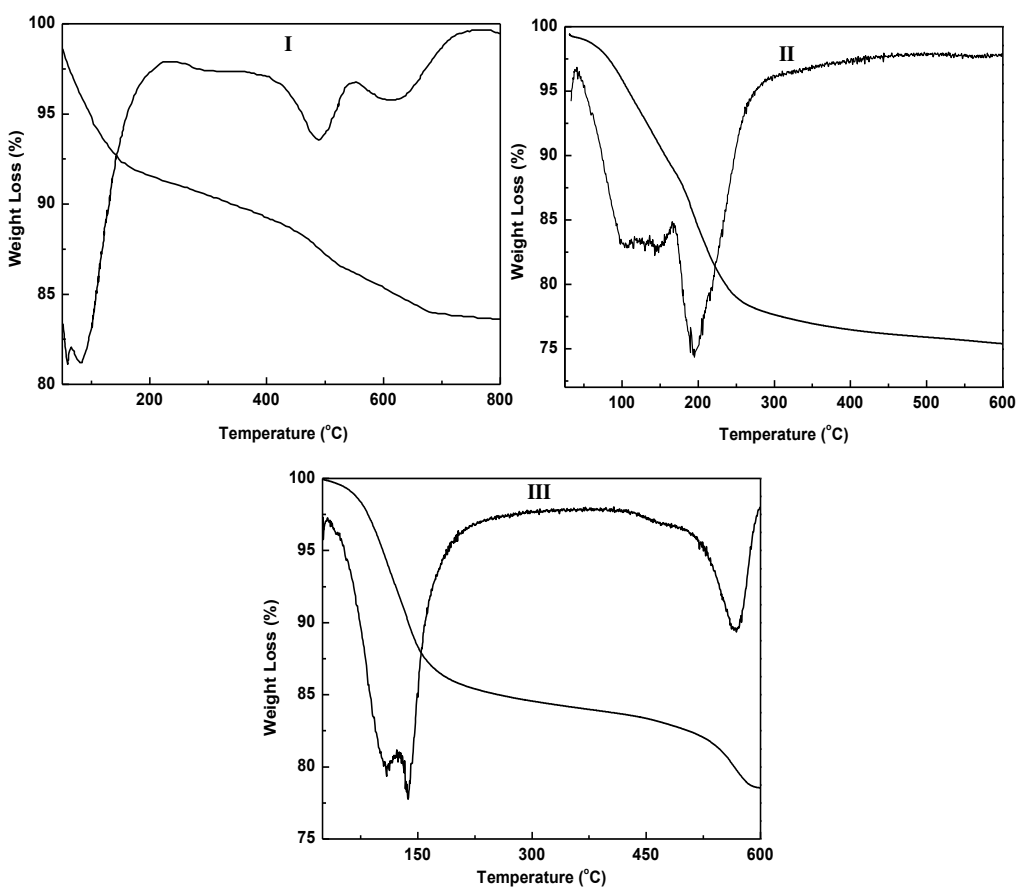


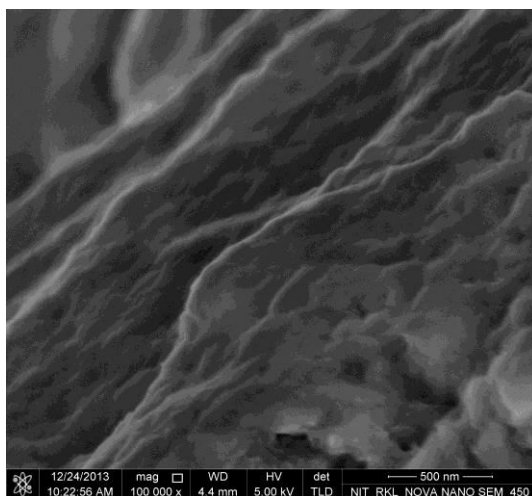
**Figure 4.4** Thermogravimetric profiles of (I) Zr-P, (II) PPA-Clay and (III) ZrP-PPA materials.

The third weight loss region observed in the temperature range 430–580°C is ascribed to the removal of polyphosphoric acid. This weight loss is relatively sharp and can be clearly differentiated from the high temperature weight loss observed for air dried Zr-pillared clay sample. The PPA–clay shows two major weight loss regions in the temperature range of 75–175°C and 180–250°C (Fig. 4.4, Panel II). The low temperature weight loss can be ascribed to the removal of physisorbed water molecules present in the clay interlayer and attached to the clay sheet. The weight loss in the region 180–250°C is probably due to the removal of polyphosphoric acid in its monomeric form. Polyphosphoric acid is a linear polymer which contains mixture of oligomers of orthophosphoric acid up to 14 phosphorous units (Jameson, 1959). Polyphosphoric acid undergo hydrolysis at a very sluggish rate in presence of water to convert to its monomeric form i.e. orthophosphoric acid. The rate of hydrolysis becomes significant at higher temperature in presence of excess of water (Platonov, 2000). It is possible that the hydrophilic environment of the clay interlayer coupled with the constrained interlayer region of the clay can promote the hydrolysis of PPA to orthophosphoric acid (boiling point 160°C) which is released in the temperature range of 180–250°C. This hydrolysis process is suppressed to a greater extent in the Zr-pillared clay matrix. Although the hydrolysis of PPA in Zr-P matrix cannot be ruled out completely, a significant fraction of PPA remains in polymeric form and are removed in the temperature range of 430–580°C which is the normal boiling point range of PPA used in this study.

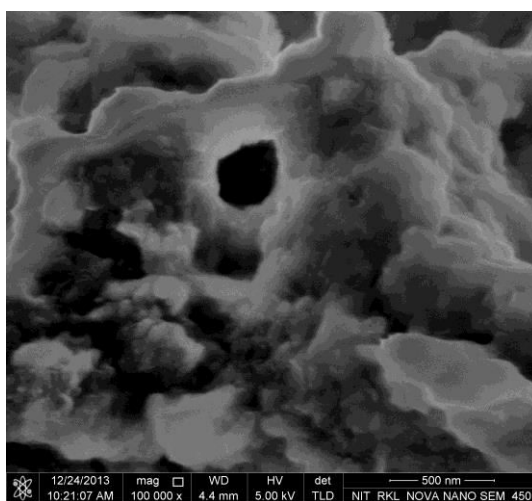
#### **4.2.5 FE-SEM STUDY**

The FE-SEM image of PPA–ZrP and ZrP–PPA composite materials is presented in Fig. 4.5. The PPA–ZrP composite material shows relatively smooth surface extending up to the edge of the

crystallites. The layer to layer orientation of the particles seems to be the favored orientation which leads to the morphology observed in Fig. 4.5a.



(a)



(b)

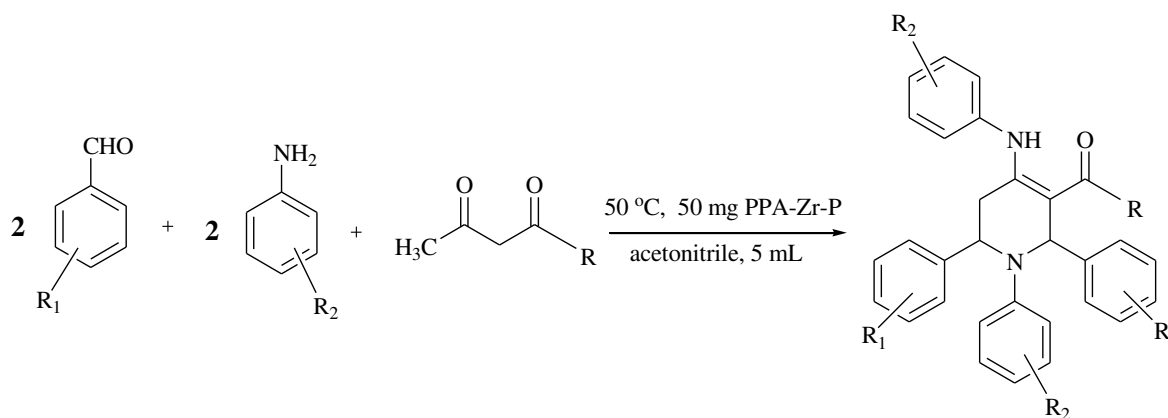
**Figure 4.5** FE-SEM images (a) PPA-ZrP and (b) ZrP-PPA.

In case of the PPA-ZrP composite, the PPA molecules are present in the interlayer space which is sandwiched between the clay sheets. The protons present in the PPA molecules can form an electrical double layer between the clay sheets facilitating the face to face interaction. Where as in case of ZrP-PPA, the pillaring of the clay with the Zr-polycations provides structural rigidity

to the clay lattice. Upon dispersion of the PPA in the Zr-P matrix, the PPA molecules occupy the micropores as well as the external surface. The presence of the PPA and its subsequent interaction with the faces and edges of the Zr-P crystallites distorts the lamellar structure of the clay platelets which results in particles with folded morphology (Fig. 4.5b).

#### 4.2.6 CATALYTIC STUDIES FOR SYNTHESIS OF TETRAHYDROPYRIDINES

The catalytic activity of the clay–polymer composite systems is evaluated for the synthesis of tetrahydropyridines (THP) by one pot multicomponent condensation of aryl aldehydes, substituted aniline and  $\beta$ -dicarbonyl compounds at 50°C using acetonitrile as solvent (Scheme 4.1).



**Scheme 4.1** Synthesis of tetrahydropyridines by multicomponent one pot condensation of arylaldehydes, substituted aniline and  $\beta$ -dicarbonyl compounds.

At first emphasis is led on optimizing the reaction condition. Multicomponent reaction of benzaldehyde, aniline, and ethylacetoacetate served as paradigm reaction for optimization. Initially, different clay–PPA composite materials synthesized in this work are evaluated for their activity using the model reaction. Table 4.2 shows the physicochemical characteristics of different clay–PPA composite systems along with the yield of THP obtained after 5 h of reaction. Among all the composite materials, the PPA–ZrP shows highest yield of the product. This

material also exhibits higher surface area and acidic property compared to other composite materials. Since the composite materials display different physicochemical characteristics, the reaction rates are calculated in terms of unit surface area and per gram of the material which is presented in Table 4.2. It is observed that among all the composite catalyst, the PPA–ZrP shows higher reaction rate per gram of the material. The higher reaction rate per unit surface observed for the PPA–clay composite material is due to the higher density of phosphorous atom per unit area compared to other catalyst. This material contains higher percentage of phosphorous atom as observed from the EDAX analysis. However, in terms of total number of acidic site exposed to the surface, the PPA–clay display less number of sites compared to other catalyst. This is due to the fact that the PPA blocks the micropore of the clay material decreasing its exposed surface significantly.

**Table 4.2 Physicochemical characteristics and catalytic activity of the clay-PPA composite materials.**

Material	Acidic sites <sup>a</sup> (mmolg <sup>-1</sup> )	Phosphorous content (wt%)	Yield <sup>b</sup> (%)	Rate (mmolh <sup>-1</sup> g <sup>-1</sup> )	Rate (mmolh <sup>-1</sup> m <sup>-2</sup> x 10 <sup>-3</sup> )	TOF <sup>c</sup> (h <sup>-1</sup> )
PPA-Clay	0.36	9.6	30.2	2.4	6.9	6.7
PPA-CTAB-Clay	0.46	2.6	36.2	2.9	3.8	6.2
PPA-ZrP	0.73	7.1	83.3	6.7	3.5	9.1
ZrP-PPA	0.63	8.5	65.2	5.2	3.0	8.2

Reaction condition: benzaldehyde:aniline:ethylacetoacetate 2:2:1, temperature 50 °C, 5 mL of acetonitrile, reaction time 5 h.

*a* Calculated from non-aqueous titration.

*b* Refers to pure and isolated yield.

*c* Calculated with respect to the benzaldehyde conversion in the reaction mixture.

Moreover, due to the diffusional constraint the internal sites remain inaccessible for catalysis. The turn over frequency (TOF) calculated for all the composite materials are presented in Table 4.2. The PPA–ZrP shows highest TOF compared to other composite materials. The PPA–ZrP material has been selected for further study for THP synthesis. The amount of catalysts in the reaction mixture is varied between 25 mg and 100 mg. It is observed that for reaction involving 2 mmol of benzaldehyde, the yield of the reaction improves with catalyst amount up to 50 mg. Further increase in the catalyst amount only marginally influences the yield of the products (Fig. 4.6, Panel I). Hence the catalyst amount was fixed at 50 mg. The effect of reaction temperature is studied by varying the temperature in the range of 30–60°C. It is observed that with increase in temperature the THP yield increases significantly up to 50°C. Further increase in temperature to 60°C marginally improves the yield (Fig. 4.6, Panel II).

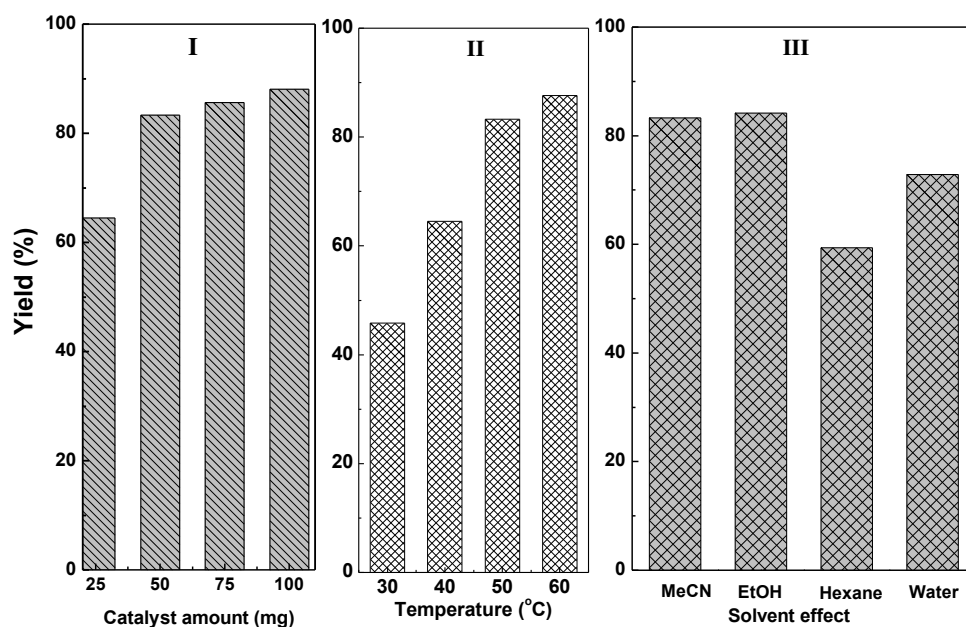


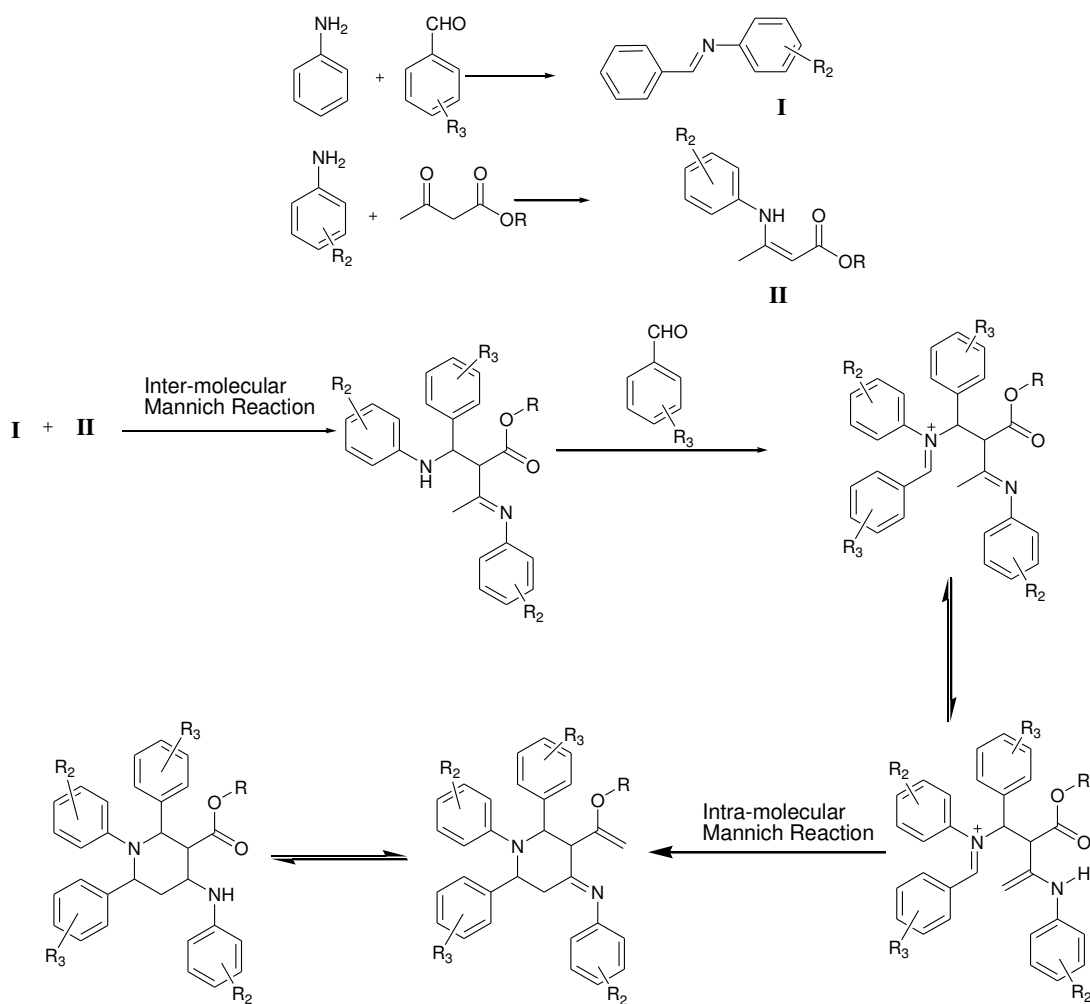
**Figure 4.6** Effect of catalyst amount, temperature and solvent on the yield of the tetrahydropyridine synthesized by one-pot multicomponent reaction of benzaldehyde, aniline and ethylacetoacetate.

Hence in this study, the reaction temperature is fixed at 50°C. In order to study the effect of reaction media on the catalytic activity, solvents with different polarity are used in the optimized reaction protocol. It is noticed that for nonpolar solvent such as hexane the yield of the product is very less. The yield is found to improve upon use of polar solvent. Among different solvent tried for the reaction, comparable yields of the THP are obtained in acetonitrile and ethanol. Hence acetonitrile is used as a solvent for further study (Fig. 4.6, Panel III). After optimizing the reaction conditions, we further investigated the scope and limitation of the optimized protocol using different  $\beta$ -dicarbonyl compounds, substituted aldehydes and substituted anilines (Table 4.3). It is observed that aniline substituted with electron donating groups is more active for the synthesis of THPs. The mechanistic pathway for formation of THP has been reported earlier (Khan, *et al.*, 2010a). The aniline reacts with one mole each of  $\beta$ -dicarbonyl compound and arylaldehyde to form the corresponding enamine and imine, respectively. Subsequently, the enamine undergoes intermolecular Mannich reaction with imine to generate an intermediate. This intermediate reacts with aldehyde followed by cyclization by intramolecular Mannich reaction to form the THPs (Scheme 4.2).

**Table 4.3 Catalytic activity of PPA-ZrP composite materials for the synthesis of tetrahydropyridines by one-pot multicomponent reaction of aryl aldehydes, substituted anilines and ethylacetoacetate.**

Sl No	R	R <sub>1</sub>	R <sub>2</sub>	Yield (%)
1	OCH <sub>3</sub>	4-NO <sub>2</sub>	H	68.1
2	OC <sub>2</sub> H <sub>5</sub>	4-NO <sub>2</sub>	H	74.3
3	C <sub>6</sub> H <sub>5</sub>	4-NO <sub>2</sub>	H	62.7
4	OCH <sub>3</sub>	4-Cl	H	75.3
5	OC <sub>2</sub> H <sub>5</sub>	4-Cl	H	82.4
6	C <sub>6</sub> H <sub>5</sub>	4-Cl	H	68.2
7	OCH <sub>3</sub>	4-F	H	81.2
8	OC <sub>2</sub> H <sub>5</sub>	4-F	H	79.8
9	C <sub>6</sub> H <sub>5</sub>	4-F	H	72.6
10	OCH <sub>3</sub>	H	H	78.5
11	OC <sub>2</sub> H <sub>5</sub>	H	H	83.3
12	C <sub>6</sub> H <sub>5</sub>	H	H	74.5
13	OCH <sub>3</sub>	4-OCH <sub>3</sub>	H	76.6
14	OC <sub>2</sub> H <sub>5</sub>	4-OCH <sub>3</sub>	H	84.5
15	C <sub>6</sub> H <sub>5</sub>	4-OCH <sub>3</sub>	H	68.4
16	OC <sub>2</sub> H <sub>5</sub>	H	4-Cl	78.0
17	OC <sub>2</sub> H <sub>5</sub>	H	2-Cl	72.0
18	OC <sub>2</sub> H <sub>5</sub>	H	3-OH	90.4
19	OC <sub>2</sub> H <sub>5</sub>	H	4-F	70.8
20	OC <sub>2</sub> H <sub>5</sub>	H	4-OCH <sub>3</sub>	88.2
21	OC <sub>2</sub> H <sub>5</sub>	H	4-NO <sub>2</sub>	66.7
22	OC <sub>2</sub> H <sub>5</sub>	H	2-OH	86.2





**Scheme 4.2 Probable mechanistic path for synthesis of tetrahydropyridines catalyzed by PPA-ZrP composite material.**

The presence of electron donating group in the substituted aniline increases the nucleophilicity of the amine group thereby facilitating the formation of enamine and imine. Upon variation of  $\beta$ -dicarbonyl compounds, it is noticed that the yield of the products are better in case of ethylacetoacetate as compared to that of methyl acetoacetate (Table 4.3). The minimum yield is observed when benzoyl acetone is used as  $\beta$ -dicarbonyl compound in the optimized protocol. The higher yield observed for ethylacetoacetate can be attributed to the greater acidic character of the alpha protons which facilitate the formation of the enamine. In case of benzoyl acetone the

COC<sub>6</sub>H<sub>5</sub> group has electron withdrawing tendency and hence display weak acidic protons compared to its ester counterparts. However, for substituted aromatic aldehydes the electronic effect of the electron withdrawing or electron donating groups do not have much impact over the yield of the product. Among all aldehydes, the yield of the THP is less for p-nitrobenzaldehyde as compared to other substituted benzaldehydes. This is due to greater stability of the imine as the conjugation is extended to the NO<sub>2</sub> group. After completion of the reaction, the catalyst particles are filtered from the reaction mixture. The catalyst is washed three times with 10 mL portion of ethanol and subsequently heat treated at 300°C for 2 h to regenerate the catalyst. The recyclability of the catalyst is studied for three consecutive cycles without any significant loss in activity (Table 4.3, entry 11, yields, 83%, 1st; 80%, 2nd; 78%, 3rd).

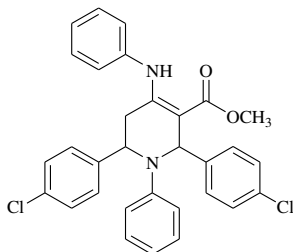
Table 4.4 shows the comparison of the catalytic activity of the PPA-ZrP material with the literature reported methods. The catalytic protocol developed in this work is found to be advantageous in terms of good yield and purity of the products, catalyst recyclability and less reaction time.

**Table 4.4 Comparison of the catalytic activity of PPA-ZrP with other catalytic systems reported in literature for synthesis of tetrahydropyridines.**

Sl. No	Catalyst	Reaction condition	Yield (%)	Reference
1.	PPA-ZrP	Acetonitrile, 50 °C, 5 h	68-90	This work
2.	Bismuth nitrate	Ethanol, room temp, 12-48h	41-81	Brahmachari and Das, 2012
3.	Tetrabutylammonium tribromide (TBATB)	Ethanol, room temp, 8-36h	62-82	Khan <i>et al.</i> , 2010a
4.	L-proline/TFA	Acetonitrile, 20-30 °C, 16-24 h	55-75	Misra <i>et al.</i> , 2009
5.	Cerium ammonium nitrate (CAN)	Acetonitrile, room temp, 15-35 h	55-86	Wang <i>et al.</i> , 2011
6.	N,N,N',N'-tetrabromobenzene-1,3-disulfonamide [TBBDA]	Ethanol, room temp, 7-20 h	68-91	Ramin and Hajar, 2013

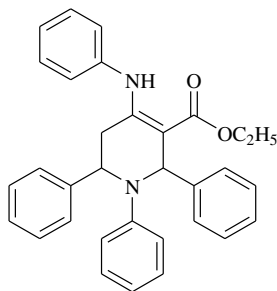
**Physical and spectra data of some representative compounds from Table 4.3**

**Methyl 2,6-bis(4-chlorophenyl)-1-phenyl-4-(phenylamino)-1,2,5,6-tetrahydropyridine-3-Carboxylate (Table 4.3, Entry 4)**



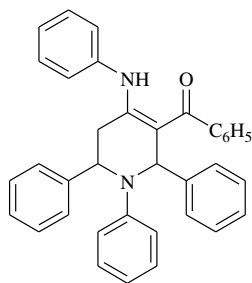
Mp: 187-190 °C, IR (KBr)  $\text{cm}^{-1}$ : 3230, 2942, 1655, 1590, 1490, 1250, 1068,  $^1\text{H}$  NMR ( $\text{CDCl}_3$ )  $\delta$ : 2.75 (1H, dd), 2.80 (1H, dd), 3.90 (3H, s), 5.05-5.07 (1H, m), 6.33 (1H, s), 6.40 (2H, d), 6.48 (2H, d), 6.62 (1H, t), 7.02-7.07 (4H, m), 7.10-7.15 (2H, m), 7.20-7.24 (7H, m), 10.24 (1H, brs).

**Ethyl 1,2,6-triphenyl-4-(phenylamino)-1,2,5,6-tetrahydropyridine-3-carboxylate (Table 4.3, Entry 11)**



Mp: 176-178 °C, IR (KBr)  $\text{cm}^{-1}$ : 3245, 3057, 2978, 1651, 1590, 1500, 1254, 1065,  $^1\text{H}$  NMR ( $\text{CDCl}_3$ )  $\delta$ : 1.48 (3H, t), 2.79 (1H, dd), 2.88 (1H, dd), 4.28-4.39 (1H, m), 4.40-4.50 (1H, m), 5.13-5.15 (1H, m), 6.28-6.30 (2H, m), 6.45 (s, 1H), 6.50 (2H, d), 6.60 (1H, t), 7.03-7.10 (5H, m), 7.17-7.20 (2H, m), 7.25 (1H, d), 7.25-7.30 (5H, m), 7.35 (2H, d), 10.30 (1H, brs).

***1,2,6-Triphenyl-4-(phenylamino) 1,2,5,6-tetrahydropyridin-3-yl phenyl methanone (Table 4.3, Entry 12)***



Mp: 192-194 °C, IR (KBr)  $\text{cm}^{-1}$ : 3064, 3022, 1590, 1576, 1542, 1494, 1323, 1273, 1024,  $^1\text{H}$  NMR ( $\text{CDCl}_3$ )  $\delta$ : 2.82 (2H, d), 5.15 (1H, t), 6.27 (2H, dd), 6.43 (2H, d), 6.53(1H, s), 6.64 (1H, t), 7.02-7.07 (3H, m), 7.09-7.15 (5H, m), 7.14-7.18 (1H, m), 7.19-7.22 (3H, m), 7.30-7.34 (4H, m), 7.44-7.48 (2H, m), 7.74 (2H, dd) 12.91 (1H, brs).

## **PART B: SYNTHESIS OF HEXAHYDROPYRIMIDINES USING Zr-P-SULFONATED PVA COMPOSITE AS HETEROGENEOUS CATALYST**

### **4.3 INTRODUCTION**

Inorganic-organic hybrid materials have attracted a great deal of attention in recent years for their applications in many advanced fields such as optics, electronics, ionics, mechanics, membranes, protective coatings, catalysis, sensors and biology (Sayari and Hamoudi, 2001; Wright and Davis, 2002; Amali and Rana, 2008; Kalbasi and Mosaddegh, 2011; Mittal and Matsko, 2012; Behrendt *et al.*, 2013, Zhang *et al.*, 2013). There are several types of organic-inorganic hybrid materials ranging from functional microporous molecular materials to ordered mesoporous inorganic structures with organic species tethered to the surface to polymer-inorganic nanocomposites (Wright and Davis, 2002; Mittal and Matsko, 2012; Zhang *et al.*, 2013). From catalysis point of view, the inorganic-polymer nanocomposites are most promising. The most widely studied polymer based composite materials are the ordered silica-polymer nanocomposites and clay-polymer nanocomposites. The mesoporous silica based ordered materials such as MCM-41, MCM-48, SBA-1, SBA-15, KIT-6 provide large internal surface and uniform pore structure for dispersion of the polymeric moieties (Xu *et al.*, 2003; Wang *et al.*, 2008; Zhu *et al.*, 2011; Kalbasi and Mosaddegh, 2011; 2012; Li *et al.*, 2012). Different approaches have been adopted in literature to maximize the dispersion of the polymeric components in the inorganic matrices. Zhao and co-workers have prepared polymer-silica and carbon-silica nanocomposites with interpenetrating networks by the evaporation-induced triconstituent co-assembly method (Liu *et al.*, 2006). These authors have used resol polymer as an organic precursor, prehydrolyzed TEOS as an inorganic precursor, and triblock copolymer F127 as template. Rioo and coworkers (Choi *et al.*, 2005) have used free radical polymerization of various vinyl monomers, such as styrene, chloromethyl styrene, 2-hydroxyethyl methacrylate,

and methacrylic acid in conjugation with crosslinkers to yield a uniform coating of the polymer inside the mesopores of SBA-15. These polymeric systems have been subsequently functionalized with catalytically active groups to yield heterogeneous nanocomposite catalysts with excellent activity and selectivity for esterification reaction of benzyl alcohol with hexanoic acid.

Clay-polymer nanocomposites comprise another class of promising materials which have been investigated for their thermal, mechanical, chemical and optical properties (Hetzer and Kee., 2008; Pavlidou and Papaspyrides., 2008; Tămășan *et al.*, 2013; Tokarský *et al.*, 2013). A polymer-clay nanocomposite is typically prepared by incorporating finely dispersed layered silicate materials into a polymer matrix. Broadly, there are two kinds of clay-polymer nanocomposites i.e. intercalated and exfoliated polymer-clay nanocomposites. Intercalated nanostructures are formed when a single extended polymer chain is intercalated between the clay layers where as exfoliated or delaminated clay-polymer nanocomposites are obtained when the clay layers are individually dispersed in the continuous polymer matrix (Hetzer and Kee., 2008; Pavlidou and Papaspyrides., 2008; Chiu *et al.*, 2013). A variety of thermosetting and thermoplastic polymers such as polyamides, polymethyl methacrylate, polystyrene, polybenzoxale, polyolefins, polyethylene terephthalate (PET), polyethylene oxide, poly (vinyl acetate), Poly (vinyl ethylene) and poly(vinyl pyrrolidone) have been used to prepare the clay-polymer nanocomposite materials (Akelah and Moet 1996; Liao *et al.*, 2001; Okamoto *et al.*, 2001; Hsu and Chang, 2002; Sun and Garces, 2002; Jana *et al.*, 2011). Most of the studies reported so far deals with composites where the polymeric species is the major phase and the focus is on improving the physicochemical properties of the polymer with the aid of the clay sheets (Ray and Okamoto; 2003; Alena *et al.*, 2013). In an alternative strategy, for application

pertaining to catalysis, the molecularly defined active sites of the polymeric species in conjugation with the active sites of the clay material can be used for efficient catalytic process where as the clay material provide a robust matrix for dispersion of the polymeric species. Very few works have been reported so far which deals with the catalytic application of clay-polymer composite materials. Hasan et al synthesized polymer/iron phthalocyanine/pillared clay nanocomposites by loading iron phthalocyanine onto the Ti- and V-pillared clay. The iron phthalocyanine loaded pillared clay sample have been used as efficient polymerization catalyst for in situ polymerization of methyl methacrylate (Hassan *et al.*, 2010). Similarly, there have been attempts to immobilize Ziegler–Natta, metallocene, and transition metal catalysts which have been used as olefins polymerization catalyst in order to produce the polyolefin/clay nanocomposites (Liu *et al.*, 2003; He and Zhang, 2007; Scott *et al.*, 2008; Mignoni *et al.*, 2011; Carrero *et al.*, 2012; Abedi and Abdouss, 2014). Contin et al have synthesized noble metal nanoparticles containing poly(N-vinylcaprolactam-co-acetoacetoxyethyl methacrylate) microgel/clay nanohybrids (Contin *et al.*, 2014). The microgel-clay supported metal nanoparticles have been used as an efficient catalyst for Suzuki and Sonogashira cross-coupling reactions. In order to study the catalytic efficiency of the clay-polymer nanocomposite systems for application in organic synthesis, in this work we have synthesized Zr-pillared clay-sulfonated PVA nanocomposite materials (ZrP-SPVA) and studied their catalytic application for synthesis of biologically important hexahydropyrimidines. In order to achieve effective sulfonation of the polymeric species and to facilitate its intercalation inside the clay interlayer, a low molecular weight PVA (Molecular Weight 14000) is chosen for synthesis of the composite material. Two different methods were used to synthesize the composite material. Firstly, the sulfonated PVA was intercalated inside the interlayer of clay, CTAB intercalated clay and Zr-Pillared clay from

aqueous solution. In an alternative approach, the PVA was intercalated inside the clay interlayer and then it was sulfonated inside the clay interlayer using chlorosulfonic acid as sulfonating agent to obtain the composite materials.

Hexahydropyrimidines have received a great deal of attention in recent years for their important biological activities. Hexahydropyrimidines moieties are found in many natural alkaloids such as eudistomidines H, tetraponerines, verbametrine and verbamethin. Different N-substituted hexahydropyrimidines are also used as synthon for spermidine-nitroimidazole drugs for the treatment of A549 lung carcinoma (Mukhopadhyay *et al.*, 2011b; Janati *et al.*, 2013). Owing to their attractive biological activity, the synthesis of this category of compounds has received much attention in recent years. The classical route for synthesis of hexahydropyrimidines involves the condensation of substituted propane-1,3-diamines with aldehydes or ketones. The main limitation associated with this method is the generation of an effective library of compounds being restrained by the availability of appropriately functionalized 1,3-diamines. Mukhopadhyay *et al* have recently developed a facile method for synthesis of hexahydropyrimidines by multicomponent condensation of 1,3-dicarbonyl compounds, amines and formaldehyde catalyzed by  $\text{FeCl}_3$  (Mukhopadhyay *et al.*, 2011b). The other catalytic method which has been successfully developed include the synthesis of spiro-hexahydropyrimidine derivatives using  $\text{In}(\text{OTf})_3$  as catalyst (Dandia *et al.*, 2012). However, to the best of our knowledge no heterogeneous catalytic protocol has been reported so far for synthesis of these important classes of compounds. **Since the synthesis of hexahydropyrimidines require acidic sites, the use of heterogeneous catalyst containing molecularly well-defined strong surface acidic sites is highly desirable. In this work we have used the SPVA-Zr-pillared clay composite materials as environmentally benign heterogeneous catalyst for synthesis of**



structurally diverse hexahydropyrimidines. The sulfonated PVA contain –SOH functional groups in its structure which is a strongly acidic functional group. Moreover, the –OH group of Zr-pillared clay are known to display acidic character. It is expected that the synergistic effect between these acidic sites can help in efficient synthesis of hexahydropyrimidines.

## 4.4 RESULTS AND DISCUSSION

### 4.4.1 XRD STUDY

The XRD patterns of the clay-polymer composite materials are presented in Fig. 4.7 and 4.8. The corresponding basal spacing values calculated from the XRD peaks are presented in Table 4.4. The formation of the Zr-pillared clay upon insertion of the zirconium oligomer clusters inside the clay interlayer was confirmed from the XRD study (section 4.2.1). The calcined Zr-pillared clay shows a basal spacing value of 19.0 Å. The XRD patterns of the Clay-polymer composite materials synthesized by intercalation of the sulfonated polyvinyl alcohol are presented in Fig. 4.7. The Clay-SP material shows an intense XRD peak at  $2\theta = 6.8^\circ$  corresponding to a basal spacing value of 12.8 Å. This value is identical to the basal spacing value observed for the parent clay. In addition to the intense peak at  $6.8^\circ$ , a broad XRD peak is observed at  $2\theta$  value of  $4.4^\circ$ . The  $d_{001}$  spacing corresponding to this broad peak is 20.5 Å. The XRD profile of the Clay-SP material clearly indicates that a major fraction of the parent clay material is not intercalated with the sulfonated polyvinyl alcohol. The polymeric species mostly resides on the external surface of the clay. The CTAB-Clay on the other hand shows a prominent peak at  $3.5^\circ$  corresponding to  $d_{001}$  spacing of 25.2 Å. The enhanced interlayer spacing of the CTAB-Clay indicates intercalation of the SPVA polymeric chains inside the clay interlayer. The CTAB as a structure expanding agent increases the interlayer space of the clay material thereby facilitating the

intercalation of the sulfonated polymer. Moreover, it creates an organophilic environment inside the clay interlayer which is conducive for the intake of the organic polymer.

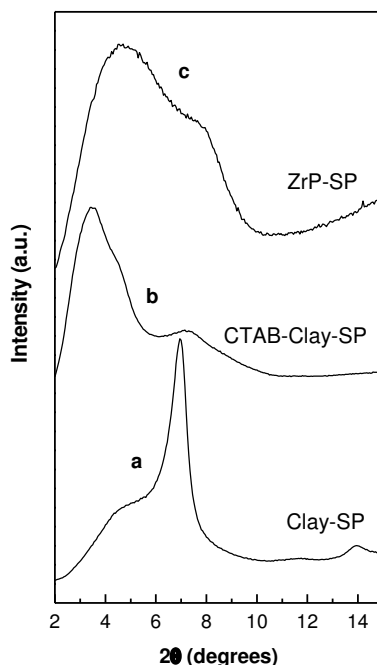


**Figure 4.7** XRD patterns of (a) Clay-SP, (b) CTAB-Clay-SP, (c) ZrP-SP.

When the dispersion of the polymeric chain was carried out inside the interlayer space of Zr-pillared clay a broad XRD peak with basal spacing value of 19.2 Å is observed. This value is identical to the basal spacing value obtained for Zr-pillared clay. This observation indicates that the structurally rigid Zr-pillared clay structure remains unaffected as a result of intercalation of the sulfonated polyvinyl alcohol. The expanded interlayer structure and the open channels of the Zr-pillared clay are capable of accommodating the polymeric chains of the SPVA polymer which is quite evident from the high sulfur content for the ZrP-SP material (Table 4.4). The XRD patterns of the PVA intercalated clays sulfonated inside the clay interlayer using chlorosulfonic acid as sulfonating agent are presented in figure 4.8. The PVA-clay when sulfonated inside the clay interlayer shows a broad and intense peak with basal spacing value of 20.6 Å along with a

less intense but well defined peak with  $d_{001}$  spacing of 48.1 Å. This observation, in contrast to the SPVA intercalated clay, indicates a significant expansion of the clay structure when PVA is intercalated inside the clay followed by sulfonation inside the clay matrix.

**Table 4.5 Physicochemical characteristics and catalytic activity of ZrP-sulfonated PVA composite catalysts for the synthesis of hexahydropyrimidines by multicomponent condensation of ethylacetoacetate (1mmol), aniline (2 mmol) and formaldehyde (3 mmol).**

Sl No	Catalyst	Basal spacing (Å)	Sulfur content (wt %) <sup>a</sup>	Acidity <sup>b</sup> (mmol/g)	MW exposure Time (min)	Yield (%) <sup>c</sup>
1	Clay-SP	12.8 (major) 20.5 (minor)	0.60	0.15	10	42.3
2	CTAB-Clay-SP	25.2	1.78	0.28	10	65.7
3	ZrP-SP	19.2	3.8	0.43	08	76.8
4	Clay-PIS	20.6 (major) 48.1 (minor)	2.12	0.21	10	28.2
5	CTAB-Clay-PIS	14.5 48.1	3.40	0.34	10	58.1
6	ZrP-PIS	21.4 (major) 48.5(minor)	4.15	0.39	10	72.8

*a. Sulfur content calculated from EDAX analysis, b. calculated from non-aqueous titration, c. refers to pure and isolated yield*

The difference observed in the XRD peak position and intensity for the Clay-SP and Clay-PIS material can be related to the nature of the polymer. In case of Clay-SP the sulfonated polymers are intercalated inside the clay interlayer. The intercalation property of this polymer is

completely different from the neutral and hydrophilic polyvinyl alcohol. The PVA uptake is facilitated by the hydrophilic environment created in the interlayer of the clay material. The in situ sulfonation of the PVA was found to be beneficial in terms of efficient sulfonation of PVA as well as structural organization of the clay sheets to accommodate the sulfonated PVA polymeric chains. The sulfonation of the PVA moieties is evident from the sulfur content of the Clay-PIS material presented in Table 4.4.

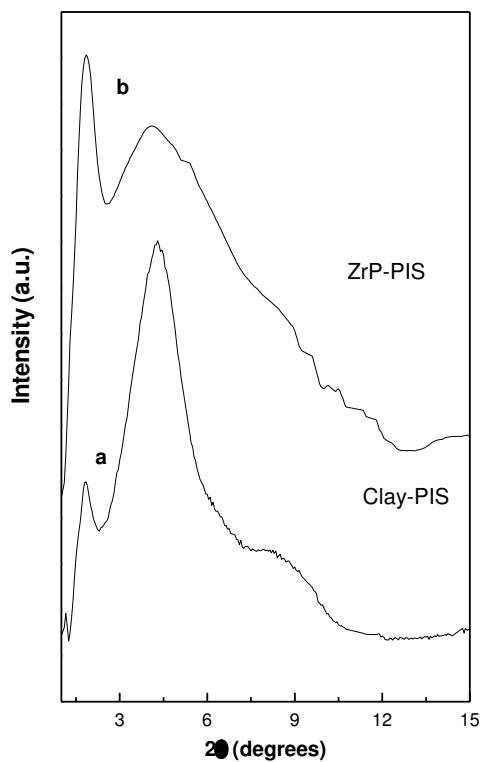


**Figure 4.8 XRD patterns of (a) Clay-PIS, (b) ZrP-PIS.**

The diffraction peak observed at lower  $2\theta$  value for Clay-PIS and ZrP-PIS can be ascribed to the presence of multiple polymeric chains inside the clay interlayer. For ZrP-PIS material the  $d_{001}$  peak is much broadened compared to the ZrP-SP material. This material has been synthesized by sulfonation of the intercalated PVA moieties inside the Zr-Pillared clay interlayer. It is anticipated that the presence of PVA inside the clay matrix may yield pillared material with

inhomogeneous pillar distribution and a consequent broadening in XRD peak. Moreover, the corrosive nature of chlorosulfonic acid can partly destroy the clay sheet resulting in broad peak for the Clay-PIS and ZrP-PIS material as compared to the SP series of materials. Nevertheless, pillaring with the polycations traps the PVA species in the lateral space between the pillars which is helpful for the retention of the PVA species inside the clay matrix.

#### **4.4.2 FT-IR STUDY**

The FTIR spectra of the clay-polymer composite materials synthesized by both methods are presented in figure 4.9 and 4.10. The characteristic vibrational features corresponding to the –OH functionality of the clay sheets are preserved in the composite materials. The structural hydroxyl vibrations at 3630 and 1630  $\text{cm}^{-1}$  significantly gains intensity upon pillaring followed by the dispersion of the polymeric species (Fig. 4.9 Panel I and II) (Sposito *et al.*, 1983; Bodoardo *et al.*, 1994; Mishra and Ranga Rao, 2005; Samantaray *et al.*, 2011). In addition to the O-H stretching vibration, the clay-polymer composite materials show two less intense bands at 2850 and 2920  $\text{cm}^{-1}$  in the stretching region of the FTIR spectrum. These peaks are ascribed to symmetric and asymmetric stretching vibrations of  $\text{CH}_2$  group in the structural skeleton of the polymeric species as well as from the cetyl group of CTAB (Taghizadeh and Sabouri, 2013). In the bending mode region all the composite materials show three IR bands at 912, 840 and 795  $\text{cm}^{-1}$  corresponding to the bending vibration modes of the Al-Al-OH, Al-Mg-OH and Mg-Mg-OH groups, respectively, in the octahedral layer of the montmorillonite. In addition to the characteristics clay vibrations, two additional bands are observed at 1155 and 1030  $\text{cm}^{-1}$  for the clay-polymer composites.

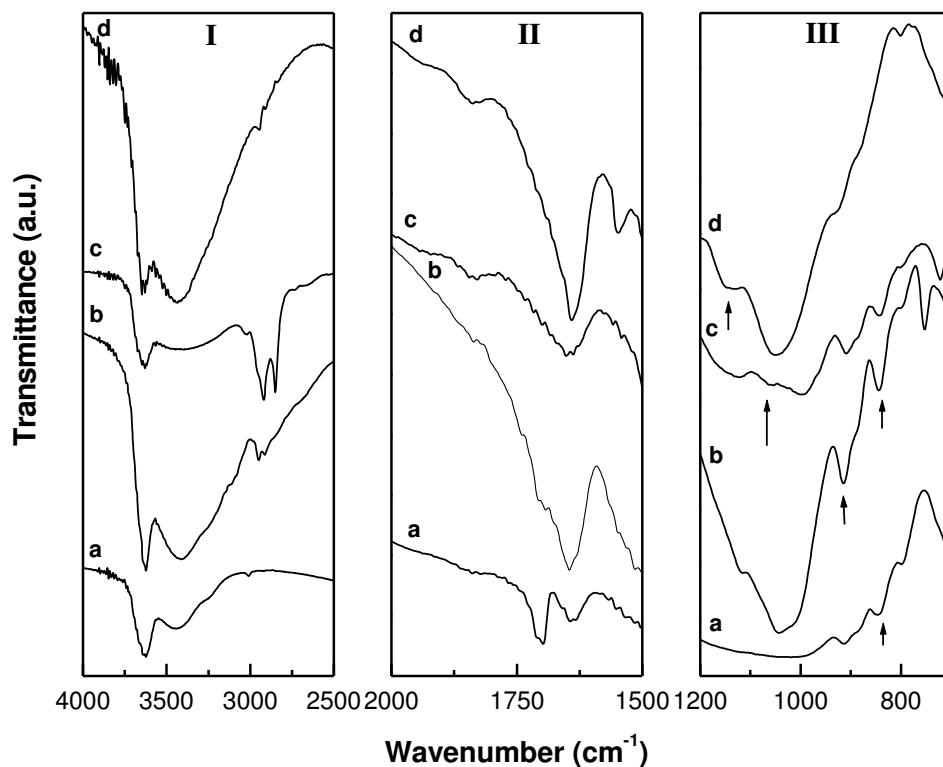


**Figure 4.9** FTIR spectra of (a) Clay, (b) Clay-SP, (c) CTAB-Clay-SP, (d) ZrP-SP.

These bands are ascribed to the S=O and O–S–O vibrations of the sulfonate ( $-\text{SO}_3\text{H}$ ) group present in the polymer skeleton (Cristovan *et al.*, 2006; Zhang *et al.*, 2010). The FTIR study indicates the presence of sulfonated polymeric species in the clay interlayer and the clay material retains its structural integrity in the composite material.

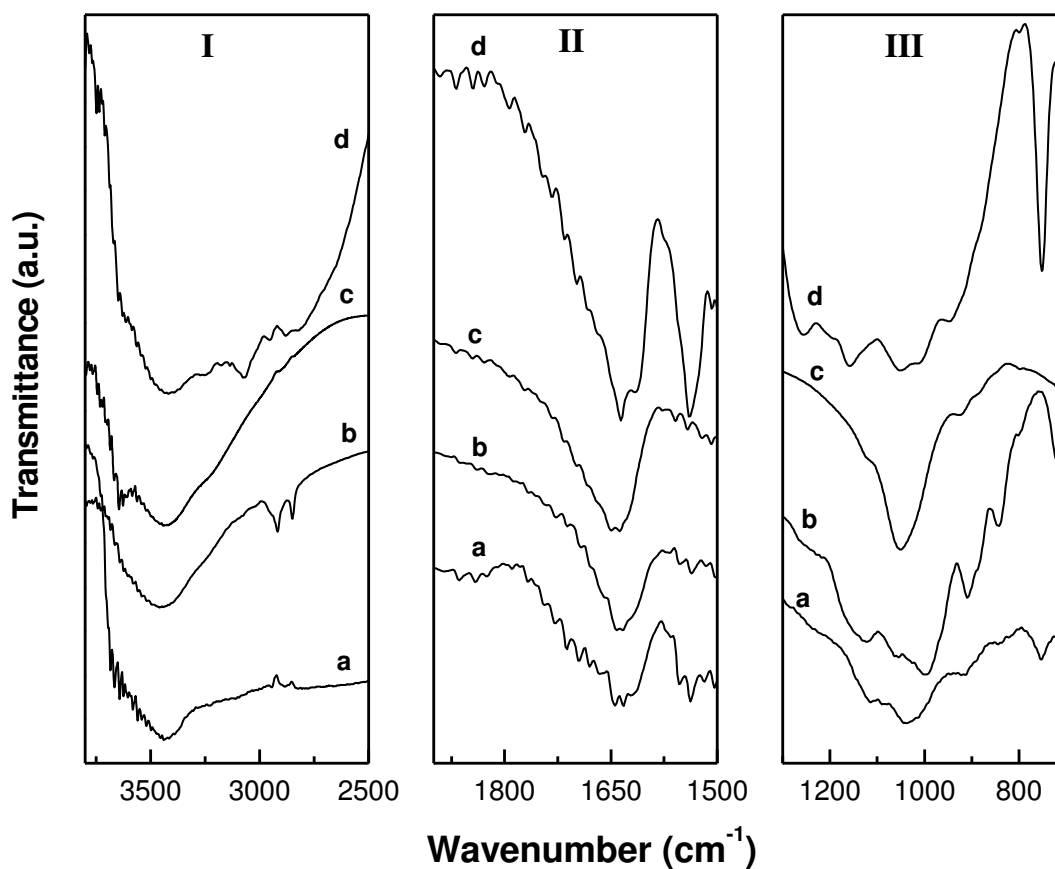


**Figure 4.10 FTIR spectra of (a) Clay-PIS, (b) CTAB-Clay-PIS, (c) ZrP, (d) ZrP-PIS.**

#### **4.4.3 UV-VIS STUDY**

The UV-visible spectra of pure clay material along with the Zr-P, ZrP-SP and ZrP-PIS are presented in figure 4.11. The band observed at 247 nm (Fig. 4.11a) is characteristic for montmorillonite clay and attributed to the charge transfer transition for the structural iron present in the octahedral layer of the clay mineral ( $\text{Fe}^{3+} \leftarrow \text{O}^{2-}$ ,  $\text{OH}^-$  or  $\text{OH}_2$ ) (Mishra and Ranga Rao, 2004).

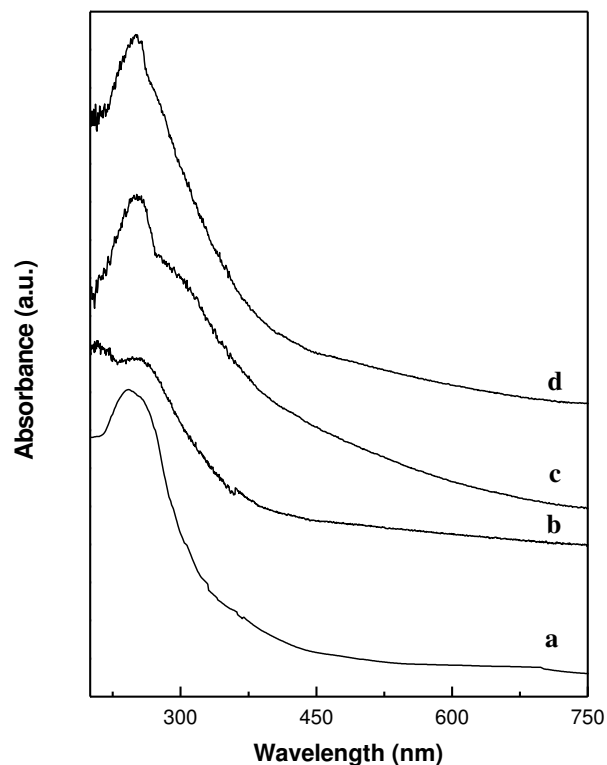


**Figure 4.11** UV-Vis spectra of (a) Clay, (b) Zr-P, (c) ZrP-SP, (d) ZrP-PIS.

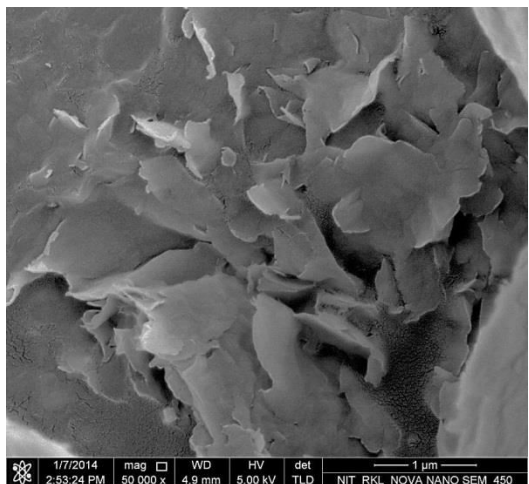
Incorporation of the Zr- nanopillars into the clay interlayer results in a change in the absorption feature of the parent clay. For Zr-P material, an additional band was observed at 210 nm. This band can be assigned to the  $Zr^{4+} \leftarrow O^{2-}$  charge transfer transition arising out of the zirconia nanopillars present in the clay interlayer (Gao *et al.*, 1999). Zirconia is a direct band gap insulator which shows interband transition in the UV region of the electronic spectrum corresponding to the  $O^{2-}(2p) \rightarrow Zr^{4+}(4d)$  transition. Among the polymorphic forms of zirconia, the octacoordinated tetragonal (space group  $Fm\bar{3}m$ ) and cubic (space group  $P42/nmc$ ) phases show UV absorption maxima in the range of 200-210 nm whereas the hepta coordinated monoclinic phase (space group  $P21/c$ ) shows UV maxima around 240 nm (Lo'pezet *al.*, 2001). It has been observed that as the coordination number of  $Zr^{4+}$  ion decreases from 8 to 6 the LMCT absorption maxima progressively shifts to lower energy (higher wavelength) (Gao *et al.*, 1999;



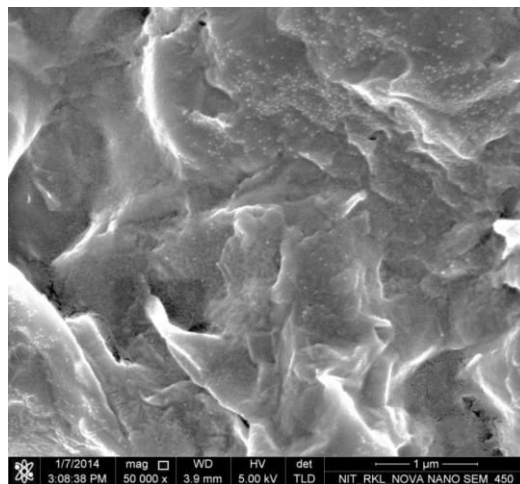
Lo'pez *et al.*, 2001; Li *et al.*, 2001; Zhao *et al.*, 2008). In case of Zr-P material, it is likely that extremely small zirconium dioxide nanoclusters exist as pillars with octacoordination in the clay interlayer. The essential UV-vis spectral feature of the clay material was found to be preserved in case of ZrP-SP and ZrP-PIS materials. However, in both materials an additional broad shoulder was observed in the wavelength range of 340-360 nm. Since, the polymer skeleton does not absorb UV-vis light in the spectral range of 200-800 nm. This broad shoulder can be ascribed to the transition from the hydrated sulfonated clusters of the sulfonated polymer. Similar observation has been noted in case of hydrates nafion polymer which contains sulfonic acid group (Almeida and Kawano, 1997; Swetha and Kumar, 2013). The hydrophilic environment inside the clay interlayer can facilitate the hydration of the sulfonic acid clusters of the sulfonated polyvinyl alcohol polymer. The UV-Vis study supplements the observation from FTIR study towards the presence of sulfonate groups in the composite system in a hydrated state.

#### **4.4.4 FE-SEM STUDY**

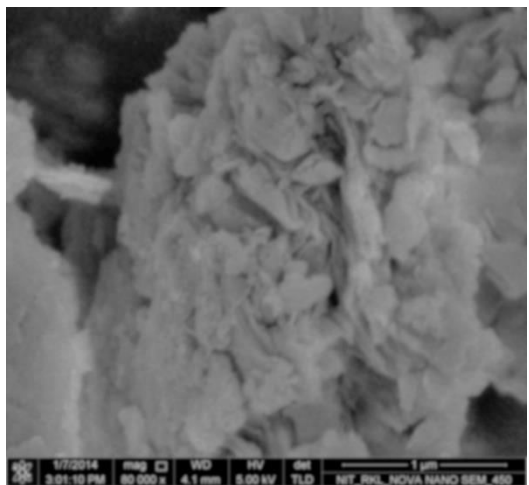
The FE-SEM images of the sulfonated polyvinyl alcohol- clay composite materials are presented in Figure 4.12. The Clay-SP and clay-PIS materials show presence of individual clay sheets randomly oriented in the clay particles. Clay platelets of different dimensions are clearly observed from the FE-SEM images in Figure 4.12(a and b). This observation suggests that upon intercalation of the polymeric species the clay platelets are widely separated from one another resulting in an exfoliated state. In both these materials, the polymeric molecules present in the interlayer considerably reduce the electrostatic forces between the clay platelets resulting in the expansion in the clay lattice and subsequent separation of the clay sheets. Contrary to this observation, both the pillared materials shows particle with folded morphology. The structural rigidity achieved due to pillaring seems to be the factor which is responsible for this morphology.



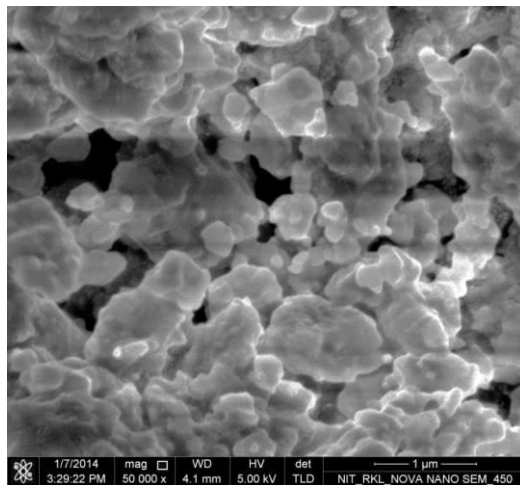
(a)



(b)



(c)



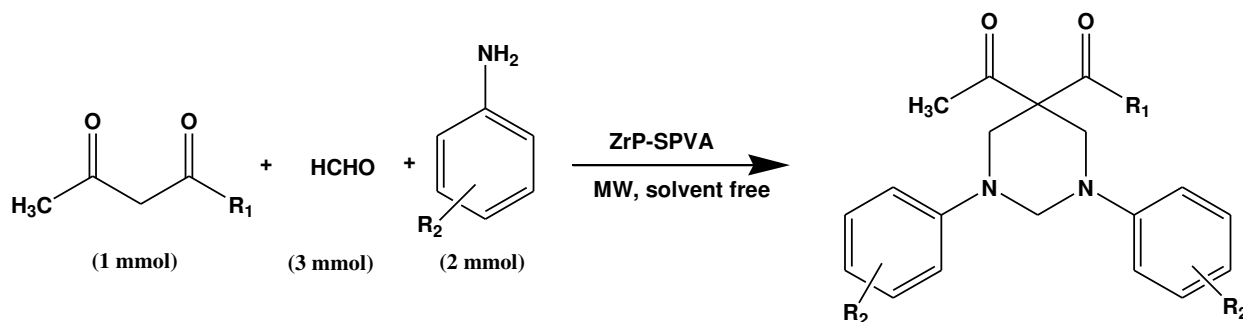
(d)

**Figure 4.12** FE-SEM image of (a) Clay-SP, (b) Clay-PIS, (c) ZrP-SP and (d) ZrP-PIS.

Upon dispersion of the SPVA in the Zr-P matrix, the SPVA species occupy the micropores as well as the external surface. The presence of the SPVA and its subsequent interaction with the faces and edges of the Zr-P crystallites distorts the lamellar structure of the clay platelets which results in particles with folded morphology.

#### 4.4.5 CATALYTIC STUDIES FOR SYNTHESIS OF HEXAHYDROPYRIMIDINES

The catalytic activity of sulfonated polyvinyl alcohol-Zr-pillared clay composite materials has been studied for the synthesis of hexahydropyrimidines (HHP). The HHPs are synthesized by one-pot multicomponent condensation of  $\beta$ -dicarbonyl compounds (1mmol), substituted anilines (2 mmol) and formaldehyde (3mmol) using conventional heating as well as microwave as energy source (Scheme 4.3).



**Scheme 4.3** Synthesis of hexahydropyrimidines by multicomponent one pot condensation of  $\beta$ -dicarbonyl compounds, substituted aniline and formaldehyde.

The reaction conditions are optimized initially by taking the condensation of ethylacetoacetate (1mmol), aniline (2 mmol) and formaldehyde (3 mmol) as a model reaction. The multicomponent reactions are carried out under microwave irradiation at 900 W taking 50 mg of different composite materials as catalyst. The yields of the products obtained from the catalytic studies are presented in Table 4.4. Among all the composite materials, the ZrP-SP material exhibit highest yield of the product (76.8%) within a microwave exposure time span of 8 minutes. The physicochemical properties of the composite materials are also listed in Table 4.4. The yield of the product correlate well with the acidic sites of the materials determined from non-aqueous titration method. A comparison of the catalytic activity for the non-pillared composites with pillared catalytic system indicate that the pillared clay based composite

materials show higher catalytic activity and possess greater number of acidic sites. During the process of pillaring, the expansion in the clay structure and the desegregation of the clay particles increases the accessibility of the catalytically active sites present in the interlayer space of the clay materials. Moreover, the Zr-pillars can contain new acidic sites which are catalytically active. For all the composite materials, a good correlation is observed between the number of acidic sites and the sulphur content. This observation indicate that the sulfonate groups of the polymer and the hydroxy groups of the clay sheet and the pillars act as acidic sites which are responsible for the observed catalytic activity. Among the pillared clay based composite materials, the ZrP-SP material shows marginally better yield of the product compared to the ZrP-PIS materials. Hence the ZrP-SP material was selected for further catalytic studies. Various reaction parameters such as catalyst amount, microwave power and exposure duration are varied to obtain the optimized protocol. The detailed results of these catalytic experiments are presented in Fig. 4.13. It is observed that for the model reaction involving 2 mmol of aniline, 50 mg of the catalyst is ideal for efficient condensation of the reactants for a microwave exposure time of 8 min at 900 W. Further increase in catalyst amount does not have any significant impact on the yield of the product (Fig. 4.13). The microwave power is varied in the range of 450-900 W. With increase in microwave power the yield of the product is found to increase. Hence in this study, 900 W is selected as the preferable microwave power (Fig. 4.13).

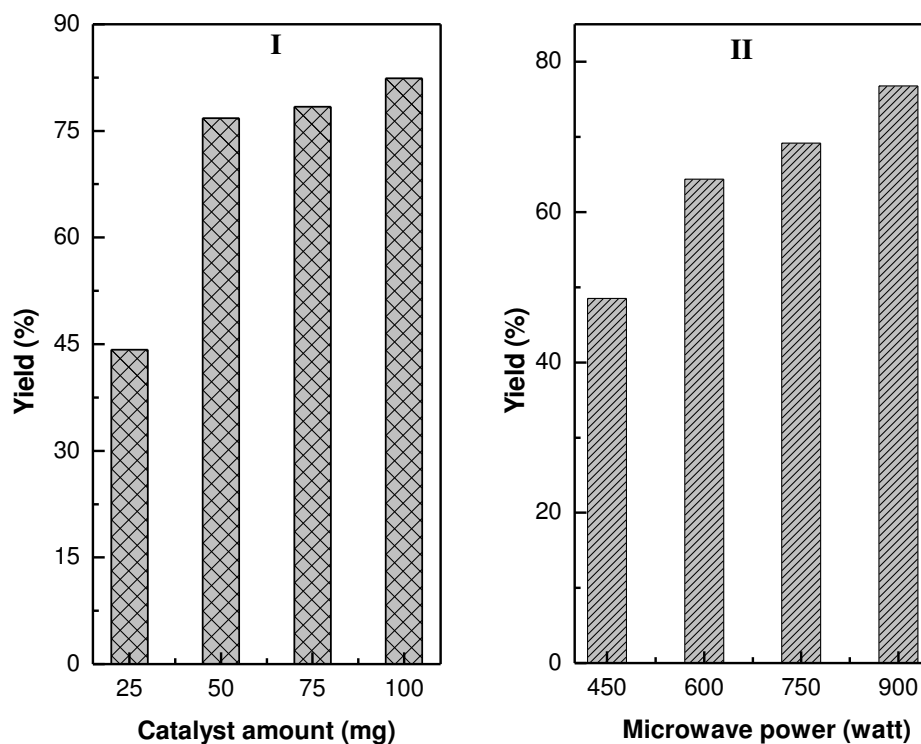


**Figure 4.13 Effect of catalyst amount and microwave power on the catalytic activity of ZrP-SP catalyst for the synthesis of hexahydropyrimidines by multicomponent condensation of ethylacetoacetate (1mmol), aniline (2 mmol) and formaldehyde (3 mmol).**

In order to evaluate the catalytic activity under diverse conditions, hexahydropyrimidines are also synthesized in different reaction media using conventional heating in an oil bath. The reaction stoichiometry employed for this protocol is identical to the one used in the microwave synthesis procedure. Initially, the reaction temperature is optimized for the model reaction by varying temperature in the range of 50-80°C using ethanol as a solvent. It is observed that the yield of the product increases with increase in temperature upto 70°C. Further increase in temperature marginally improves the yield. Hence the temperature of the reaction is fixed at 70°C (Fig. 4.14). In order to study the effect of reaction media on the catalytic activity, solvents

with different polarity are used in the optimized reaction protocol. It is noticed that for nonpolar solvent such as hexane the yield of the product is less. The yield is found to improve upon use of polar solvent. Among different solvent used for the reaction, best yield of the HHP was obtained when ethanol is used as solvent (Fig. 4.14, Panel II). After optimizing the reaction conditions for both conventional as well as microwave heating route, we explored the scope and limitation of the optimized protocol by using different  $\beta$ -dicarbonyl compounds and substituted anilines.

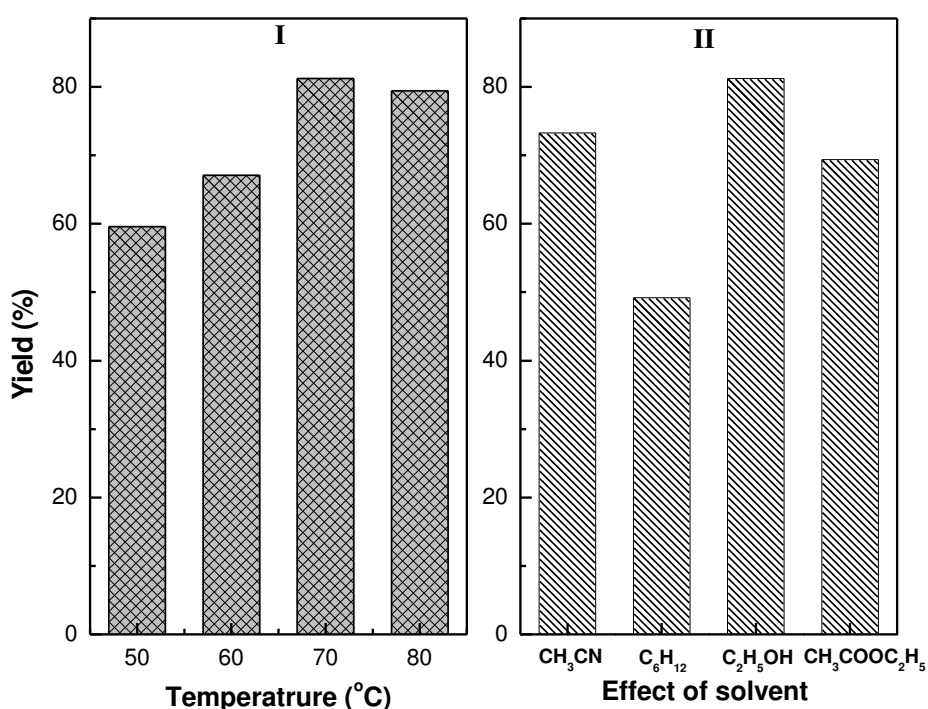


**Figure 4.14** Effect of temperature and reaction media on the catalytic activity of ZrP-SP catalyst for the synthesis of hexahydropyrimidines obtained by multicomponent condensation of ethylacetoacetate (1mmol), aniline (2 mmol) and formaldehyde (3 mmol).

Table 4.5 shows the yield of different substituted hexahydropyrimidines prepared by both conventional as well as microwave heating route. Structurally diverse hexahydropyrimidines are synthesized in high yield and purity using the optimized protocols.

**Table 4.6 Catalytic activity of ZrP-SP composite material for synthesis of hexahydropyrimidines by multicomponent condensation of  $\beta$ -dicarbonyl compounds substituted aniline and formaldehyde.**

Sl. No	R <sub>1</sub>	R <sub>2</sub>	MW assisted synthesis		Conventional route yield (%) <sup>a</sup>
			Exposure time (min)	Yield (%)	
1	OC <sub>2</sub> H <sub>5</sub>	H	8	76.8	81.2
2	OC <sub>2</sub> H <sub>5</sub>	4-Cl	10	72.0	75.5
3	OC <sub>2</sub> H <sub>5</sub>	4-OCH <sub>3</sub>	8	82.5	85.7
4	OC <sub>2</sub> H <sub>5</sub>	4-NO <sub>2</sub>	12	68.3	69.6
5	OCH <sub>3</sub>	H	10	73.2	78.7
6	OCH <sub>3</sub>	4-Cl	10	65.0	65.3
7	OCH <sub>3</sub>	4-OCH <sub>3</sub>	10	74.3	82.1
8	OCH <sub>3</sub>	4-NO <sub>2</sub>	12	63.0	66.0
9	C <sub>6</sub> H <sub>5</sub>	H	14	68.0	72.5
10	C <sub>6</sub> H <sub>5</sub>	4-OCH <sub>3</sub>	14	75.0	80.3

*a. isolated yield obtained after 6 h of reaction time using ethanol as solvent*

Comparing both protocols, although the yields of the products are marginally better in the conventional route, the reaction rate is quite sluggish as compared to the microwave assisted synthesis under solvent free condition. Among different substrates used for the reaction, the substituted anilines containing electron donating group reacts faster in the optimized protocol than the anilines containing electron withdrawing groups. Similarly, the reactivity of the  $\beta$ -dicarbonyl compounds varies in the order ethylacetoacetate > methylacetoacetate > benzoylacetate. A comparison of the catalytic activity of the ZrP-SP material with earlier literature reported system is presented in table 4.7. Among the few catalytic protocols reported

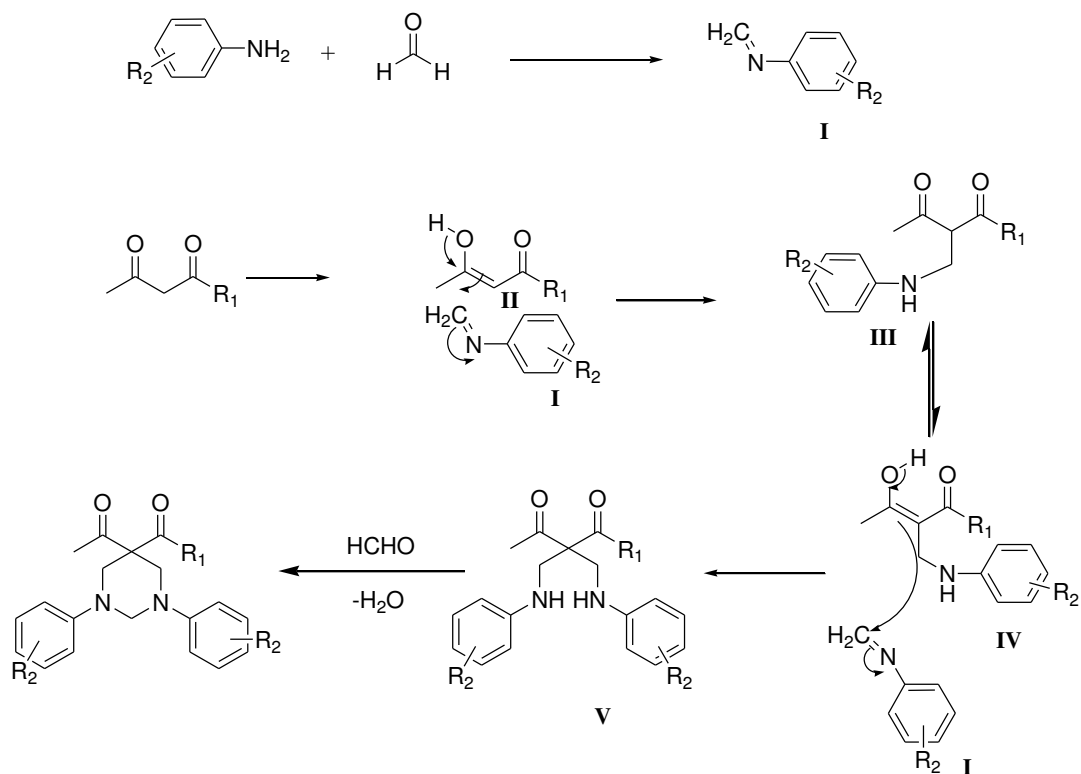
for synthesis of HHPs, the  $\text{FeCl}_3$  and  $\text{In}(\text{OTf})_3$  are homogeneous catalyst which suffer from the drawbacks such as catalyst handling, separation and purification of the products. The  $\text{Fe}_3\text{O}_4$  catalyst although heterogeneous in nature requires higher temperature for synthesis. In the present study, comparable yield of the products are obtained in high purity. Moreover, the use of microwave in conjugation with the ZrP-SP catalyst significantly reduces the reaction time. The present protocol is advantageous in terms of heterogeneous and recyclable catalyst and lower reaction time.

**Table 4.7 Comparison of the catalytic activity of ZrP-SP with other catalytic systems reported in literature for synthesis of hexahydropyrimidines.**

Sl. No	Catalyst	Reaction condition	Yield (%)	Reference
1.	ZrP-SP	(a) Ethanol, 70 °C, 6 h (b) Microwave, 8-14 min	(a) 65-85 (b) 65-82	This work
2.	$\text{FeCl}_3$	Dichloromethane, 25-30 °C, stir, 6 h	63-92	Mukhopadhyay <i>et al.</i> , 2011b
3.	Superparamagnetic $\text{Fe}_3\text{O}_4$	Solvent free, 80 °C, stir, 2-5 h	70-94	Janati <i>et al.</i> , 2013
4.	$\text{In}(\text{OTf})_3$	Dichloromethane, room temp, 4-6 h, stir	50-80	Dandia <i>et al.</i> , 2012

The mechanistic path for the synthesis of hexahydropyrimidines has been reported in the literature (Janati *et al.*, 2013). Initially, one mole of aniline reacts with one mole of formaldehyde to form the enamine (I). The enamine reacts with the enolic form of the  $\beta$  dicarbonyl compound to form the adduct (III). The enolic form of adduct (III) react with another mole of enamine to give (V). The intermediate (V) undergo cyclodehydration reaction in presence of one mole of formaldehyde to form the hexahydropyrimidines (Scheme 4.4).



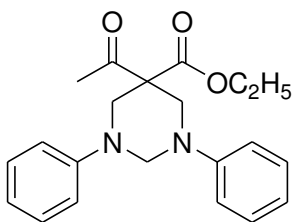


**Scheme 4.4** Probable mechanistic path for synthesis of hexahydropyrimidines catalyzed by ZrP-SP composite material.

The acidic sites of the ZrP-polymer composite material can catalyze the enamine formation, keto-enol tautomerism and cyclodehydration steps in expediting the rate of hexahydropyrimidine formation.

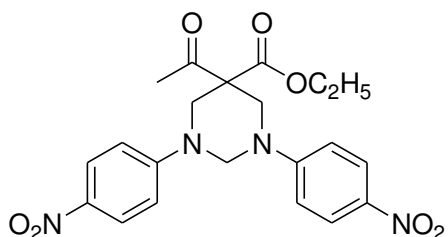
**Physical and spectra data of some representative compounds from Table 4.5**

**5-Acetyl-1,3-diphenyl-hexahydro-pyrimidine-5-carboxylic acid ethyl ester (Table 4.5, entry 1)**



IR (KBr): 3035, 2920, 2840, 1720, 1495, 1380, 1220, 1028 and 940  $\text{cm}^{-1}$   $^1\text{H}$  NMR (400 MHz,  $\text{CDCl}_3$ ): 7.32–7.28 (4H, m, ArH), 7.05 (4H, dd, ArH), 6.95–6.93 (2H, m, ArH), 4.54 (1H, d, equatorial N–CH–N), 4.49 (1H, d, axial N–CH–N), 3.99 (2H, q, O–CH<sub>2</sub>), 3.85–3.79 (4H, m, 2xN–CH<sub>2</sub>), 2.21 (3H, s, CH<sub>3</sub>–CO), 1.17 (3H, t, COOCH<sub>2</sub>CH<sub>3</sub>).

**5-Acetyl-1,3-bis-(4-nitrophenyl)-hexahydropyrimidine-5-carboxylic acid ethyl ester (Table 4.5, entry 4)**



IR (KBr) 3035, 2940, 2825, 1710, 1480, 1354, 1232, 1026, 997  $\text{cm}^{-1}$   $^1\text{H}$  NMR (400 MHz,  $\text{CDCl}_3$ ): 8.11 (4H, d, ArH), 7.51 (4H, d, ArH), 4.42 (1H, d, equatorial N–CH–N), 4.26 (1H, d, axial N–CH–N), 4.06 (2H, q, O–CH), 3.82 (2H, d, N–CH<sub>2</sub>), 3.72 (2H, d, N–CH<sub>2</sub>), 2.28 (3H, s, CH<sub>3</sub>–CO), 1.20 (3H, t, O–CH<sub>2</sub>–CH<sub>3</sub>).

#### 4.5 CONCLUSIONS

In this chapter, we have studied the synthesis, characterization and catalytic application of Zr-pillared clay-polymer composite catalytic systems. Two polymeric species with acidic functionality i.e. polyphosphoric acid and sulfonated polyvinyl alcohol, have been used for the synthesis of the composite materials. Different preparative strategies are adopted to maximize the dispersion and entrapment of the polymeric species in the clay and pillared clay matrix. The use of CTAB as a structure expansion agent is found to be beneficial in terms of the higher uptake of the polymer as compared to the parent clay. The expansion of the layered structure of the clay material is observed as a result of the incorporation of the polymers as well as due to pillaring with the Zr-polycations. In case of the PPA based polymeric composites, the Zr-pillared

clay provides an efficient matrix for dispersion and stabilization of the PPA moieties. The hydrolysis of PPA species to small oligomers is suppressed to a large extent due to the expanded interlayer space of the Zr-pillared clay. In case of SPVA-ZrP composite system, the intercalation behaviour of the polymer was found to be crucial for the final properties of the composite system. The intercalation of hydrophilic PVA polymer inside the clay structure is facilitated by the hydrophilic character of the clay interlayer. The structural integrity and the presence of required functionality in the clay and polymer structure is confirmed from the FTIR and UV-Vis study. The clay sheets are largely present in an exfoliated state in the polymeric composite involving parent clay. However, the insertion of the Zr-pillar imparts structural rigidity and consequent changes in the morphological features as observed from FESEM study. The catalytic activity of the PPA-ZrP composite system is evaluated for synthesis of tetrahydropyridines by one pot multicomponent condensation of aromatic aldehydes, substituted aniline, and  $\beta$ -dicarbonyl compounds. Similarly, the ZrP-SP material is used as an efficient catalyst for synthesis of hexahydropyrimidines by multicomponent condensation of substituted aniline, formaldehyde and  $\beta$ -dicarbonyl compounds. Structurally diverse tetrahydropyridines and hexahydropyrimidines were synthesized in high yield and purity using the composite catalytic systems. This chapter demonstrates the applicability of the clay-polymer composite materials as efficient catalytic system for synthesis of biologically important molecules.

## CHAPTER 5

### CATALYTIC APPLICATION OF Pd AND Pd BASED BIMETALLIC PARTICLES SUPPORTED ON Al-PILLARED CLAY

#### PART A: HYDRODEHALOGENATION OF HALOGENATED PHENOLS OVER Pd/Al-PILLARED CLAY

##### 5.1 INTRODUCTION

Halogenated organic compounds are used as precursors in several industries for the synthesis of herbicides, wood preservatives, dyes, plant regulators, disinfectants and insecticides (Hoke *et al.*, 1992; Molina *et al.*, 2009a; 2009b; 2010). These compounds are highly toxic and non-biodegradable. The halogenated organics can enter into the environment causing imbalance in ecological cycle (Molina *et al.*, 2009a). This has necessitated the treatment of industrial effluents containing halogenated organic pollutants before discarding them into environment. Some prevalent processes for treatment of halogenated organics include super critical water oxidation, wet air oxidation, UV photolysis, incineration, adsorption on activated carbon and biodegradation (Hoke *et al.*, 1992; Keane and Murzin, 2001). However, these processes have certain drawbacks. Incineration and chemical oxidation lead to incomplete decomposition of organic compounds thereby producing lethal substances such as polychlorinated dibenzodioxins and polychlorinated dibenzofurans compounds (Shin and Keane, 1998; Molina *et al.*, 2010). Biodegradation process is cost ineffective as it requires huge reactors, greater retention time and precise environment for carrying out anaerobic oxidation (Keane and Murzin, 2001; Patel and Suresh, 2007; Dı'az *et al.*, 2008). Catalytic hydrodehalogenation (HDH) is one of the promising strategies for the removal of halogen under milder conditions (Molina *et al.*, 2009b). HDH is effectively catalysed by transition and noble metals such as Pd, Pt, Ni and Rh. During catalytic process molecular hydrogen get cleaved to active hydrogen species on the metal surface which play an important role in dissociation of C-Cl bond of the substrate (Patel and Suresh, 2007). Xu *et al.* had studied the gas phase HDH of

chlorobenzene at 573 K using nickel particles supported over TiO<sub>2</sub> as catalyst. Although Ni metal proved to be an efficient catalyst, it requires higher temperature and high pressure for effective dechlorination of chlororganics (Srebowata *et al.*, 2007). Srikanth et al had applied supported ruthenium particles as catalyst for the hydrodechlorination (HDC) of 1,2,4-trichlorobenzene. Ru supported over carbon and SBA-15 exhibit higher catalytic efficiency compared to other supports studied. Better dispersion and smaller particle size of the Ru metal over these supports has been responsible for higher HDC activity (Srikanth *et al.*, 2011). Rh particles supported over reduced graphene oxide is found to be effective for hydrodechlorination of 4-Chlorophenol. The synergistic effect of the smaller size of Rh particles and surface hydroxyl groups of the support has been invoked to explain the HDC activity (Ren *et al.*, 2014). Pt metal supported over Al-pillared clay has been employed as catalyst for HDC of 4-chlorophenol (Molina *et al.*, 2009b). Although supported Pt shows good catalytic activity, it exhibit poor reusability due to formation of carbonaceous materials (Molina *et al.*, 2009a; 2009b). Palladium (Pd) is one of the promising noble metal for hydrodehalogenation process as it has greater selectivity for the replacement of chlorine atom by hydrogen. Moreover, Pd gets less deactivated by the released hydrogen halides which act as catalyst poison. Pd metal in finely dispersed form as well as in supported state on catalytically active functional and porous supports has been studied for hydrodechlorination (HDC) process (Urbano and Marinas, 2001; Amorim *et al.*, 2005; Gopinath *et al.*, 2008; Zhang *et al.*, 2013a). The physicochemical properties of support such as pore structure, surface area, electronic interaction with metal and surface functionality strongly influences the dispersion of the metal particles and control the catalyst deactivation. The dispersion of the Pd nanoparticles is also dependent on the type of metal precursor used and its subsequent interaction with the support (Aramend'ia *et al.*, 1999; Urbano and Marinas, 2001). Certain inorganic supports promote side reactions such as Cl/F exchange thereby causing loss in selectivity. Some support gets deactivated by reaction with the generated hydrogen halides

(Van de Sandt *et al.*, 1998; Urbano and Marinas, 2001). The proper choice of support is highly essential to obtain stable catalytic activity. Pd supported over  $\gamma$ -Al<sub>2</sub>O<sub>3</sub> show greater selectivity for complete hydrodehalogenation of CH<sub>2</sub>F<sub>2</sub> (Juszczak *et al.*, 1997; Urbano and Marinas, 2001). Anwer *et al.* have compared the activity Pd particles supported on Al<sub>2</sub>O<sub>3</sub>, keisulghur, CaCO<sub>3</sub>, BaSO<sub>4</sub> and carbon. The Pd/C shows highest catalytic activity for hydrodechlorination of parachloroanisole. The enhanced catalytic activity for Pd/C has been attributed to the hydrophobicity of the carbon which facilitates the adsorption of substrate on its surface (Anwer *et al.*, 1999). Earlier work reported in literature shows that Pd supported over clay and pillared clay materials have been used as catalyst for several industrially important reactions (Zuo and Zhou, 2008; Wang *et al.*, 2013; Molina *et al.*, 2014; Pizarro *et al.*, 2014). Pillared clay supported noble metals such as Pd and Pt have been explored for catalytic reduction of nitric oxide, propene combustion, combustion of methyl ethyl ketone, hydrogenation of phenyl alkyl acetylenes, hydrogenation of adipic ester, oxidation of aromatic VOCs and deep oxidation of benzene (Gil *et al.*, 2001; Qi *et al.*, 2004; Astorga *et al.*, 2005; Zuo and Zhou, 2006; Figueiredo *et al.*, 2008; Oliveira *et al.*, 2008; Azna' rez *et al.*, 2011).

In this work, we have studied the catalytic application of Pd metal supported Al-pillared clay for the hydrodehalogenation of halogenated organic compounds under mild conditions. Instead of using molecular hydrogen, we have used hydrazine hydrate as a hydrogen transfer agent to carry out the hydrodehalogenation process.

## **5.2 RESULTS AND DISCUSSION**

### **5.2.1 XRD STUDY**

The XRD patterns of the parent clay, Al-P and the Pd/Al-P materials are presented in Fig. 5.1 and the corresponding basal spacing values are given in Table 5.1. The parent clay shows a sharp and intense reflection at  $2\theta = 6.8^\circ$  from the (001) planes corresponding to the basal spacing of 12.9 Å (Fig. 5.1a). The insertion of the Al-polycationic clusters into the clay

interlayer resulted in an expansion of the clay interlayer. The calcined Al-P material shows a  $d_{001}$  spacing of 19.2 Å (Fig. 5.1b). The preparation and characterization of the Al-pillared clay materials have been studied earlier by many authors in the literature (Salerno and Mendioroz, 2002; Sapag and Mendioroz, 2001; Vicente *et al.*, 2003; Moronta *et al.*, 2008). The Al pillaring species are generally prepared by the controlled hydrolysis of  $\text{AlCl}_3 \cdot 6\text{H}_2\text{O}$  at moderately concentrated aqueous solutions. The basal spacing value observed in this study is in accordance with the earlier literature reported value for Al-pillared clay materials (Vicente *et al.*, 2003; Ranga Rao and Mishra, 2007).

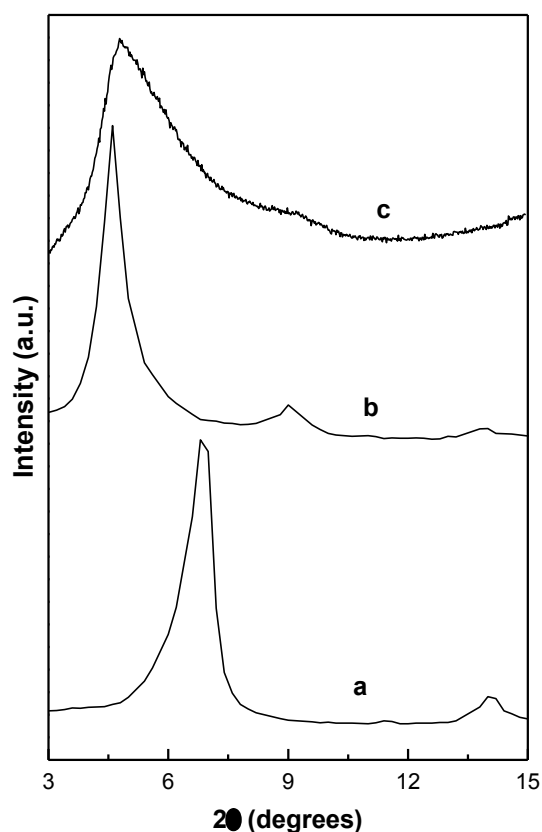


**Figure 5.1** XRD patterns of (a) Clay, (b) Al-P and (c) Pd/Al-P.

After dispersion of the Pd nanoparticles in the Al-pillared clay matrix, the  $d_{001}$  peak is found to be broadened slightly without any significant reduction in intensity. Nevertheless, the Pd/Al-P material exhibit crystalline character with regular stacking of the clay sheet (Fig. 5.1c). Since the Pd particles have been synthesized using mild chemical reduction method, it

is expected that the structural characteristics of the pillared clay will remain unchanged after supporting Pd particles. The Pd/Al-P material shows a basal spacing of 18.6 Å.

**Table 5.1 Physicochemical properties of parent clay, Al-P and Pd/Al-P.**

Sample	Surface area(m <sup>2</sup> /g)	Basal spacing (Å)	Pore Volume(cc/g)
Clay	30	12.9	0.06
Al-P	245	19.2	0.18
Pd/Al-P	186	18.6	0.10

### 5.2.2 FTIR STUDY

The FT-IR spectra of parent clay and Al-pillared clay along with the Pd/Al-P are presented in Fig. 5.2. The characteristics vibrational feature corresponding to the clay sheet is preserved in the supported metallic system (Bodoardo *et al.*, 1994; Mishra and G. Ranga Rao, 2004, Samantaray *et al.*, 2011). Pillaring with Al-polycation significantly enhances the intensity of the structural –OH vibrations. For pillared materials, the band at 3450 cm<sup>-1</sup> also gains intensity indicating an improvement in the water retention capacity of the clay material as a result of pillaring. In the spectral region of 600–1000 cm<sup>-1</sup>, the parent clay and Al- pillared clay shows a series of discrete peaks (Fig. 5.2III). Three bands observed at 915, 845 and 805 cm<sup>-1</sup> are attributed to the bending vibration modes of Al–Al–OH, Al–Mg–OH and Mg–Mg–OH groups, respectively, in the octahedral layer of the montmorillonite clay (Sposito *et al.*, 1983). For the Pd supported pillared clay material the peak positions have been shifted to higher wavenumber by 10-15 cm<sup>-1</sup>. This may be attributed to the orientational changes in the O–H bond present in the octahedral layer. It is believed that the presence of Pd nanoparticles cause steric hindrance to the protruded –OH groups of the octahedral layer. The OH group can change orientation to minimize steric repulsion which resulted in shifting of the bending vibration to higher wave number. Another noticeable change in the IR spectra is the reduction



in the intensity of the OH stretching vibration in case of Pd supported system. It is known from literature that the OH group exist primarily in the edge of the clay sheet, along broken edges as well as attached to surface Al and Si atoms. These locations can serve as sites for anchoring Pd particles in the clay matrix (Molina *et al.*, 2009a; Azna´rez *et al.*, 2011).

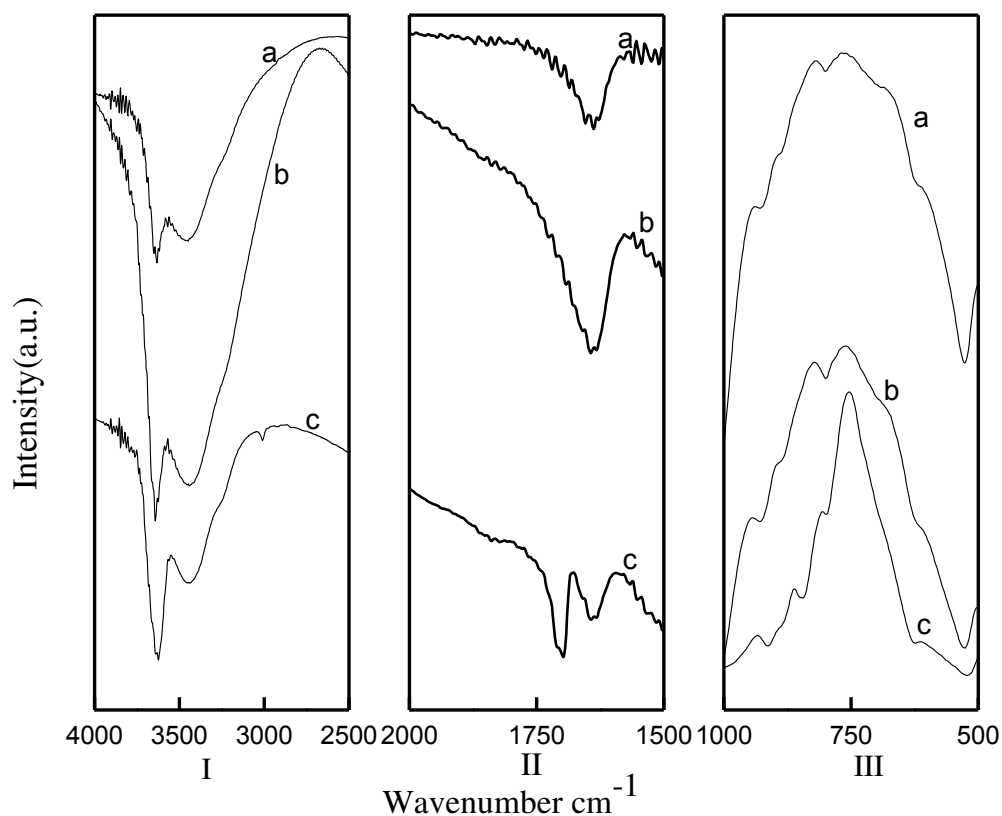


**Figure 5.2 FTIR Spectra of (a) Pd/Al-P, (b) Al-P and (c) clay.**

### 5.2.3 SORPTOMETRIC STUDY

The N<sub>2</sub> sorption isotherm of Al-P and Pd/Al-P is presented in Fig. 5.3. The corresponding surface area and total pore volume obtained from the N<sub>2</sub> sorption studies are given in Table 5.1. Both the pillared clay materials show high initial adsorption and near horizontal plateau which extends up to the relative pressure ~ 0.9. The sorption isotherms observed for these pillared clays are Type I according to the Brunauer, Deming, Deming, Teller (BDDT) classification indicating the presence of micropores (Gil *et al.*, 2000a; Sowmiya *et al.*, 2007; Gil *et al.*, 2011; Jalil *et al.*, 2014 ). The hysteresis loops observed for these materials are H3

type according to IUPAC classification and attributed to slit shaped pores or plate like particles with space between the parallel plates (Gregg and Sing, 1982). The pillaring process has a large impact on the surface area and pore volume of the parent clay (Table 5.1).

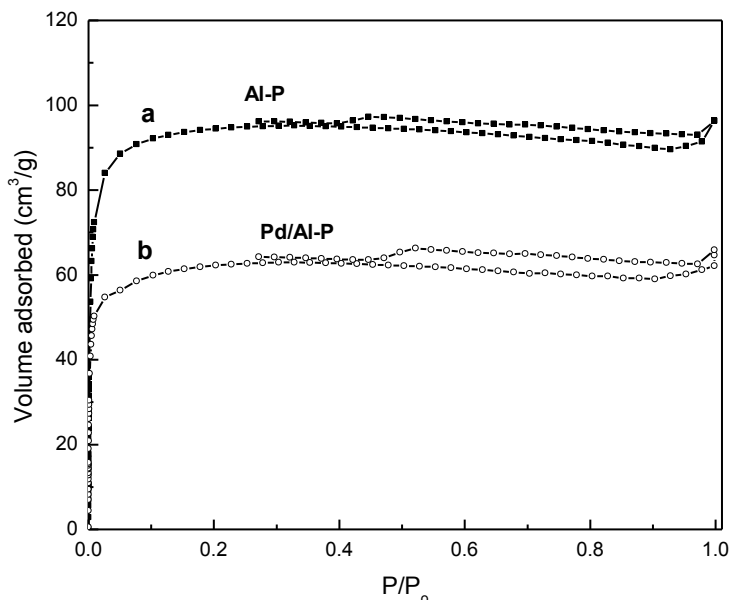


**Figure 5.3**  $N_2$  adsorption-desorption isotherms of (a) Al-P and (b) Pd/Al-P.

The parent clay displays a surface area of  $30 \text{ m}^2/\text{g}$ . After pillaring with the Al-polycations surface area of  $245 \text{ m}^2/\text{g}$  is achieved. During the process of pillaring, the expansion in the clay structure and the desegregation of the clay particles largely contributes to the enhancement of the surface area and porosity of the clay materials. After dispersion of the Pd nanoparticles, the surface area and pore volume of the pillared clay decreases due to the partial blocking of the pores by the Pd particles (Table 5.1).

#### 5.2.4 FE-SEM STUDY

The scanning electron micrographs of the Al-P and Pd/Al-P are presented in Fig. 5.4. The Al-P material shows the presence of disorderly arranged clay lamellae. The individual clay platelets are desegregated and express themselves as exfoliated sheets. The pillars act as rigid crosslinkers which holds the clay sheets apart promoting face to face interaction among the clay platelets stabilizing the lamellar structure. The Pd/Al-P material, on the other hand, shows folded particle shape (Fig. 5.4b). Large agglomerated particles of irregular shape and

size is observed for Pd/Al-P material which may be ascribed to the edge to edge and edge to face interactions.

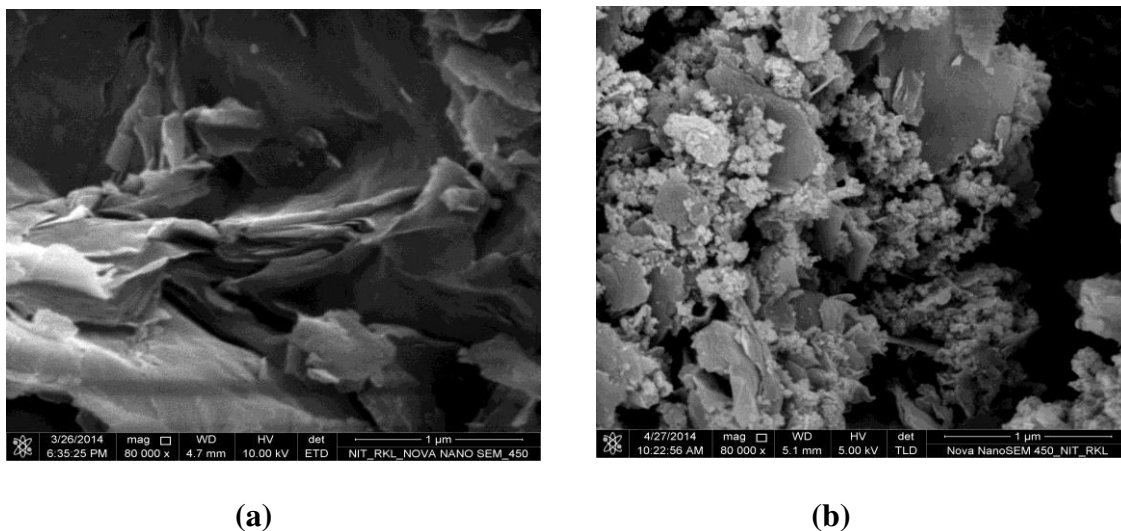


**Figure 5.4** FE-SEM images of (a) Al-P and (b) Pd/Al-P.

### 5.2.5 TEM STUDY

The transmission electron micrograph for Pd nanoparticles supported over Al-P is represented in Fig. 5.5. The TEM study indicates that Pd particles are well dispersed in the pillared clay matrix and separated from one another without any sign of agglomeration.

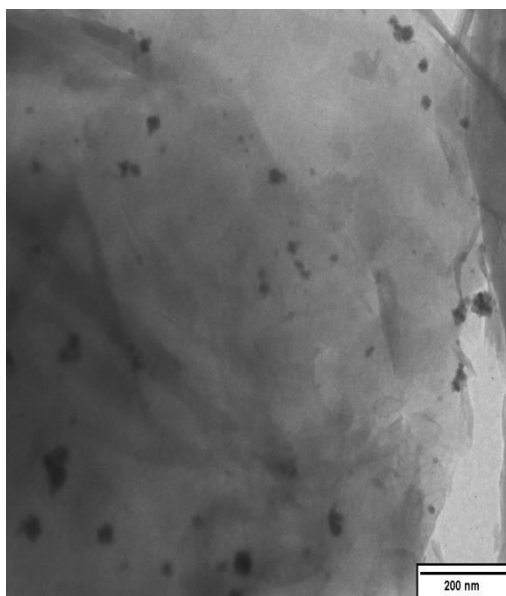


**Figure 5.5** Transmission electron micrograph of Pd/Al-P.

The particle size of Pd particles is in the range 5–30 nm. The well dispersion of the metallic nanoparticles can be ascribed to the enhanced surface area and porosity of the clay material achieved due to the process of pillaring. The Al<sub>2</sub>O<sub>3</sub> nanoclusters inserted into the clay layer act as pillars and hold two clay sheets apart from each other. Significant interlayer expansion and exfoliation takes place during the process of pillaring. This leads to the enhancement of the interlayer spacing and porosity of the Al–P which effectively disperse the Pd nanoparticles in the Al–P clay matrix.

#### **5.2.6 CATALYTIC ACTIVITY OF Pd/Al–P MATERIALS FOR HYDRODEHALOGENATION (HDH) REACTION**

The Pd/Al–P material is used as an efficient heterogeneous catalyst for the HDH of halogenated aromatic phenols. Initially, in order to establish the role of support for the HDH reaction, the Pd metal is dispersed on various intercalated and pillared clays. The catalytic activity of the clay supported systems was evaluated by taking the HDH of p-chlorophenol as a model reaction. Figure 5.6 shows the time vs conversion profile of Pd metal supported on clay, CTAB intercalated clay, Al- and Zr-pillared clay materials. Among all the clay materials used in this study the Pd nanoparticles supported on Al-pillared clay show maximum activity and 100 % selectivity towards the HDC process. In literature two mechanistic pathways have been proposed to explain the HDH activity of supported Pd particles (Kovenklioglu *et al.*, 1992; Gampine and Eyman, 1998; Sainero *et al.*, 2004; Yuan and Keane, 2007; Chaplin *et al.*, 2012). Some studies have proposed that the chlorinated compounds are initially adsorbed on the support surface and then they shift to the Pd particles for the HDH reaction to take place (Gampine and Eyman, 1998). The second mechanism proposed involve the cleavage of the C-X (halogen) bond over support surface and replacement of spill over hydrogen from Pd onto the support for HDH activity. In both the mechanism the support play a major role and effectively controls the HDH activity of Pd particles (Gampine and Eyman, 1998).

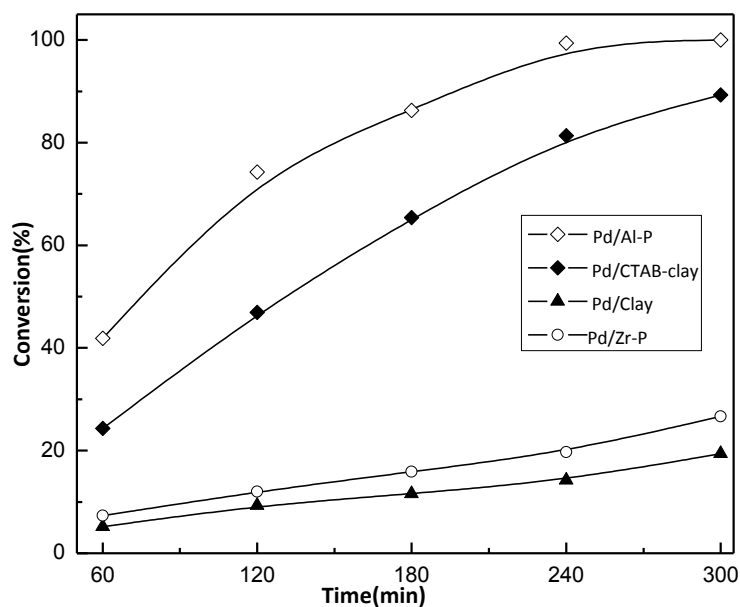


**Figure 5.6 Effect of different supports used for dispersion of 5 wt% Pd particles on the HDC activity for p-Chlorophenol.**

Figure 5.6 reveals that for Pd/Zr–P material the rate of hydrodechlorination is sluggish with 26 % conversion achieved after 5 h of reaction. The Pd/CTAB-clay show improved catalytic efficiency compared to the Pd/Zr–P material possibly due to the organophilic environment generated by CTAB species which helps in the adsorption of the p-chlorophenols by hydrophobic interactions. The Pd metal supported on parent clay show least activity. From the result shown in Fig. 5.6, the Al-pillared clay was chosen as support for Pd nanoparticles for further study. The reaction conditions are further optimized by using different hydrogen transfer agents. Figure 5.7 shows the time vs conversion plot for hydrodechlorination of p-chlorophenol using different hydrogen transfer agents over Pd/Al–P catalyst. Among all hydrogenating agents, hydrazine hydrate is found to be most efficient for HDH of p-chlorophenol.

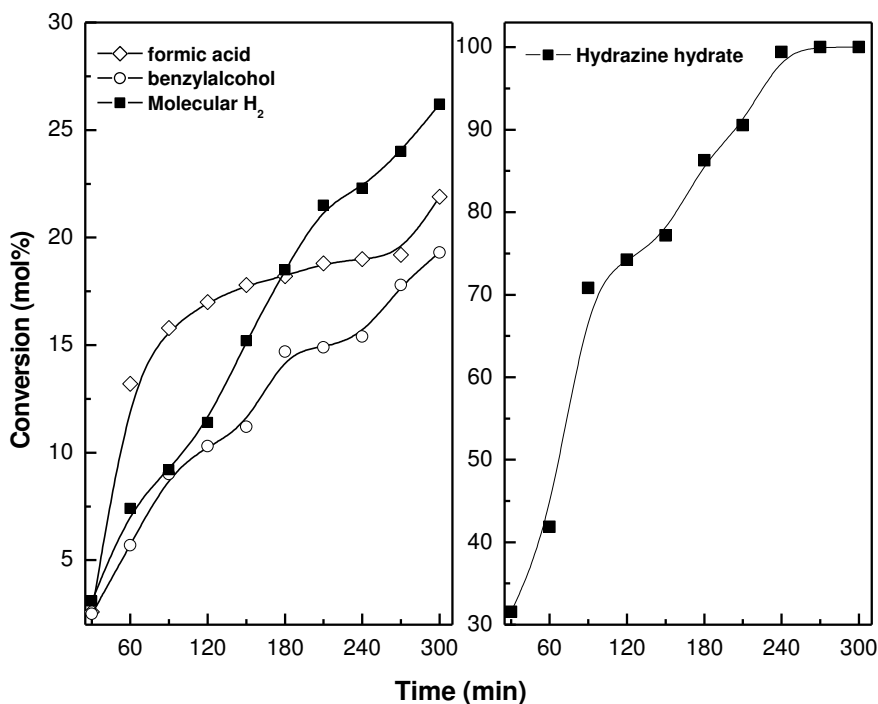


**Figure 5.7** Effect of (a) different hydrogen transfer reagents and (b) hydrazine hydrate as hydrogen donors on the **catalytic activity of Pd/Al-P** for the hydrodechlorination of p-chlorophenol.

The reduction potential and the molecular size of the hydrogen transfer agent are important factors which determine the rate of hydrogen liberation from the molecule. Among different hydrogen transfer agents used in this study, benzyl alcohol and formic acid are bulkier molecules which hinder their adsorption and transport to the Pd surface. The lower activity observed for molecular hydrogen can be ascribed to its limited solubility in aqueous media and lower reduction potential compared to hydrazine hydrate. The best result was observed for hydrazine hydrate with 70 % hydrodechlorination activity after 2 h of reaction. To study the effect of temperature, hydrodechlorination of p-chlorophenol is carried out at three different temperatures and the results are presented in Fig. 5.8. At 40°C and 50°C the rate of conversion is very high as compared to the reaction carried out at 30°C. Within 2 h of reaction time the HDC process get completed at 40°C and 50°C. At 30°C, we observed a gradual increase in rate of reaction and the reaction reaches the completion stage after 5 h

(Fig. 5. 8). Therefore in this study, 30°C was taken as the optimum temperature to study the HDH process.

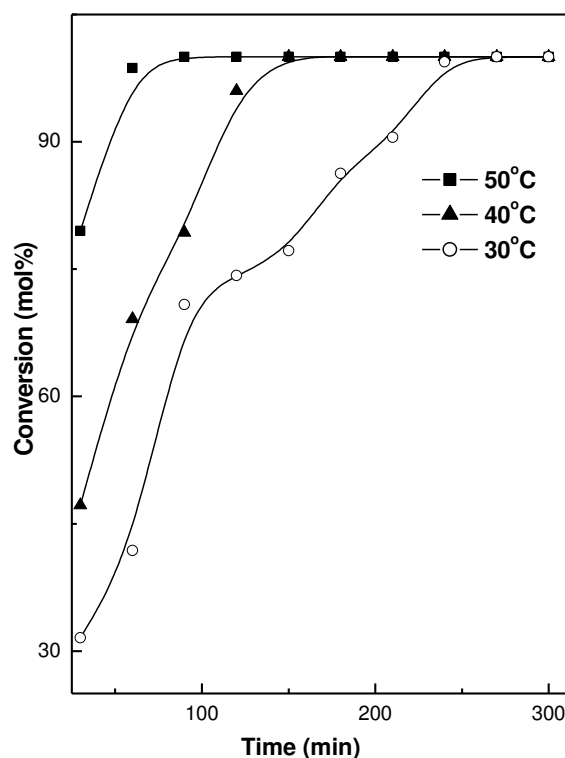


**Figure 5.8 Effect of temperature on the hydrodechlorination activity of p-chlorophenol catalysed by Pd/Al-P catalyst.**

After optimizing the reaction temperature, support and hydrogenating agent, the molar ratio of substrate to hydrazine hydrate was varied to determine the optimum value. Figure 5.9 shows the conversion of p-chlorophenol after 1 h of reaction for different p-chlorophenol to hydrazine hydrate molar ratio. For lower molar ratio, the rate of conversion is less. As molar ratio increases there is a gradual increase in conversion reaching the optimum value at 1:8. Further increase in molar ratio does not have any marked impact on the HDC activity. Hence in this study the molar ratio of 1:8 was chosen as optimum molar ratio of p-chlorophenol and hydrazine hydrate for further study. To study the reactivity of different substituted chlorinated organic compounds, the HDH has been carried out under optimized conditions. The rate of HDH process depends on the types of functional groups and halogen associated with the substrate (Urbano and Marinas, 2001).

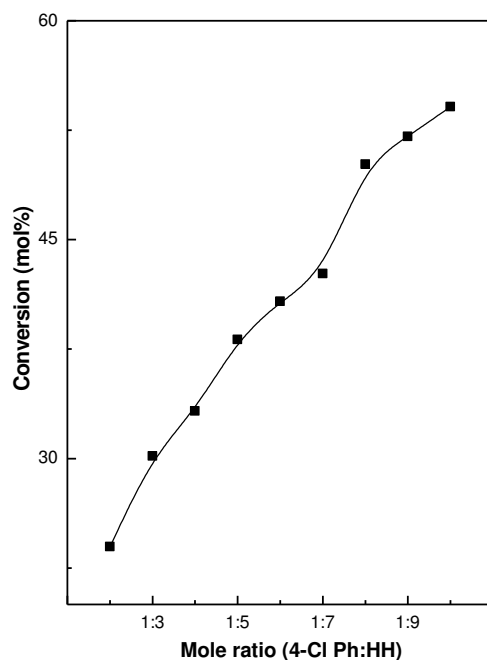


**Figure 5.9** Effect of t molar ratio of p-chlorophenol and hydrazine hydrate on the hydrodechlorination activity of p-chlorophenol catalysed by Pd/Al-P.

Table 5.2 shows HDH activity of Pd/Al-P catalyst for different halogenated compounds after 30 min of reaction time. Among chlorophenols, the ortho substituted phenols have greater reactivity as compared to p-chlorophenol. Figure 5.10 and 5.11 represent the time vs conversion profile of different mono and di substituted chlorophenols along with p-fluorophenol. The exclusion of fluorine from the p-fluorophenol takes place at a slower rate as compared to chlorinated compounds. This is attributed to the greater dissociation energy associated with C–F bond than C–Cl bond. From the Fig. 5.10 it is observed that after 5 h, 79 % of fluorine is removed from p-fluorophenol whereas under identical reaction time 100 % chlorine removal takes place from p-chlorophenol. Chlorine removal is quite spontaneous for ortho substituted phenol which is illustrated in Fig. 5.11. The electron donating O–H group creates more electron rich centre at ortho position than para position. Chloroanilines show greater rate of conversion compared to the chlorophenols. (Fig. 5.10 and 5.11). A comparison of HDH activity of mono and dichlorophenols for a given time period indicates that the dichlorophenols undergo slower dechlorination as compared to monosubstituted phenols.



Among the disubstituted phenols, 2,6-dichlorophenol shows 98.5 % chlorine removal after 3 h of reaction.

**Table 5.2 Dehydrohalogenation of different halogenated organic compounds using Pd/Al-P as catalyst after 30 minutes reaction time.**

Sl No	Halogenated species	Time (min)	Conversion (%)
1	4-Chlorophenol	30	31.6
2	2-Chlorophenol	30	100
3	2,4-Dichlorophenol	30	17.1
4	2,6-Dichlorophenol	30	33.6
5	4-Fluorophenol	30	26.3

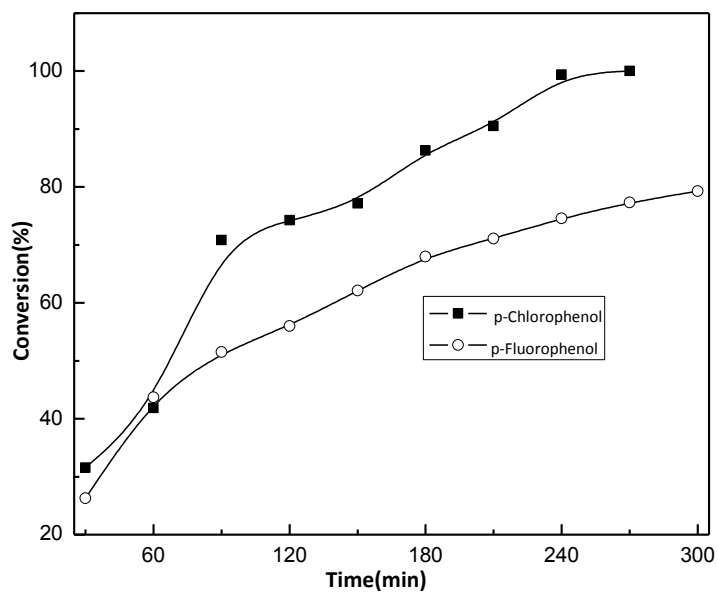


**Figure 5.10 Activity of Pd/Al-P catalyst for the hydrodechlorination of different halogenated organic compounds at 30 °C.**

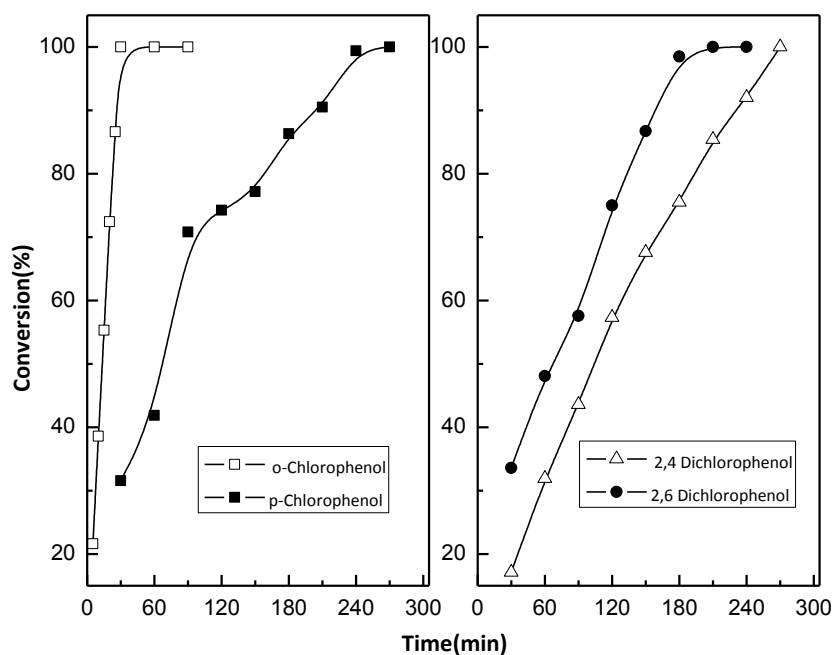


**Figure 5.11 Catalytic activity of Pd/Al-P catalyst for the hydrodechlorination of mono- and di- chlorinated phenols at 30 °C .**

Under similar reaction condition the 2,4- dichlorophenol show 75.5 % chlorine removal. The higher electrophilicity of the o-positions as compared to the p- position is responsible for higher reactivity of the 2,6-disubstituted products. The recyclability of the Pd/Al–P catalyst was evaluated for three consecutive cycles for the HDC of p-chlorophenol at 30°C and 1:8 molar ratio of substrate to hydrazine hydrate for 2 h of reaction time. After completion of each reaction cycles, the catalyst particles were filtered from the reaction mixture, dried and washed with 10 ml portions of ethyl acetate for three times. The catalyst particles were subsequently dried in a vacuum oven at 120 °C and reused for further catalytic studies. The Pd/Al–P catalyst exhibited stable catalytic activity without any significant decrease in the HDC of p-chlorophenol for three consecutive cycles (conversion: 74.2 %, 1st cycle; 71.2 %, 2nd cycle; 69.3 %, 3rd cycle).

## **PART B: HYDRODEHALOGENATION OF HALOGENATED ANILINES OVER Pd-M (M= Cu and Ni)/Al-PILLARED CLAY**

### **5.3 INTRODUCTION**

Catalytic hydrodehalogenation (HDH) is one of the promising strategies for the removal of halogen under mild conditions (Molina *et al.*, 2009a; 2009b). HDH is effectively catalysed by various transition and noble metals such as Pd, Pt, Ni, Ru and Rh (Sun *et al.*, 2011). However, various monometallic systems studied for HDH, possess certain drawbacks such as catalyst poisoning due to metal halides formation, metal sintering, coke deposition, migration of metal, and alteration of metal oxidation state which reduce their stability and activity (Bedia *et al.*, 2012; Seshu Babu *et al.*, 2012). Among monometallic systems studied for HDH, Pd and Ni have been most active. Nickel metal requires higher temperature and high pressure for effective dechlorination of chlororganics (Srebowata *et al.*, 2007). Palladium metal has been widely used for HDH; however, its cost ineffectiveness is a major limitation. Alloying of Pd with a second metallic component is an attractive way to generate bimetallic catalysts which exhibit enhanced activity, selectivity and stability for HDH process. The formation of bimetallic system prevents agglomeration of individual metal particles thereby exposing more number of active sites on the surface. The alloying effect has been explained earlier in terms of structure-activity relationship. The selective occurrence of a metallic component at a particular topology of the surface sites such as low index planes, kinks, corners, edges has also been observed to be advantageous in terms of stability and enhanced catalytic activity (Coq and Figueras, 2001). Different Pd based bimetallic systems such as Pd-Al, Pd-Au, Pd-Pt, Pd-Cu, Pd-Fe and Pd-Ag have been evaluated for their HDH activity (Heinrichs *et al.*, 2001; Golubina *et al.*, 2006; Nutt *et al.*, 2006; Yang *et al.*, 2011; Bedia *et al.*, 2012; Gregori *et al.*, 2014 ). Gregori et al had synthesized Pd-Cu bimetallic particles supported on MCM-41 using different preparative strategies. The dispersion and size of the

metallic particles is controlled by the method of preparation which in turn affect the rate and selectivity of hydrogen assisted dechlorination of  $\text{CF}_3\text{OCFCICF}_2\text{Cl}$  (Gregori *et al.*, 2014). Pd-Yb bimetallics supported on silica was found to be promising catalyst for the gas-phase HDC of chlorobenzene and dichlorobenzene. Yb acts as effective electron donating agent thereby enhancing the catalytic activity (Jujjuri *et al.*, 2006). The hydrodechlorination of trichloroethene have been carried out in presence of Pd/Au nanoparticles. The increase in catalytic activity in presence of the bimetallic particles has been ascribed to the formation of Pd ensembles and Pd-Au mixed sites that serve as adsorption and reaction sites for the substrates (Nutt *et al.*, 2006). The nature of the co-metal, its oxidation state, segregation of either of the two components on the surface and topological distribution of the metal particles are the key factors which affect the catalytic activity (Scott *et al.*, 2011; 2013). The nature of the support also plays an important role in controlling the activity and selectivity of the bimetallic particles (Bedia *et al.*, 2012). The metal-support interaction, porosity and acid-base character of the support are important factors which controls the dispersion and stability of bimetallic particles (Urbano and Marinas 2001). Among Pd based bimetallic systems, Pd-Ni is one of the widely investigated systems (Simagina *et al.*, 2003; Srebowata *et al.*, 2007; Sun *et al.*, 2011; Seshu Babu *et al.*, 2012). Simagina et al have studied the HDC activity of Pd-Ni bimetallic catalyst supported on carbon for hydrodechlorination of hexachlorobenzene. The surface enrichment of Pd metal in the bimetallic catalyst which in turn affects the surface Pd concentration has been correlated to the HDC activity. Isolated Pd particles present near the Ni rich phases have been proposed to be highly active compared to the Pd present in large ensembles (Simagina *et al.*, 2003). Sheshu Babu et al. studied gas phase hydrodechlorination of chlorobenzene employing Pd-Ni supported on  $\text{Al}_2\text{O}_3$  as catalyst. The molar ratio of the two metals i.e. Pd and Ni influence the catalytic activity for HDC. The formation of Pd-Ni interfaces embedded with  $\text{Pd}^{\delta+}$  species has been identified as the active site for the HDC of chlorobenzene (Seshu Babu *et al.*, 2012).

Previous studies in literature show that pillared clays are highly effective as support for catalytically active monometallic and bimetallic systems (Moronta *et al.*, 2006; Barama *et al.*, 2009; Su *et al.*, 2009; Aznárez *et al.*, 2011; Pérez *et al.*, 2014). Various bimetallic particles such as Fe-Ni, Ru-Sn and Ru-Cu supported on modified pillared clays have been investigated respectively for degradation of amoxicillin, hydrogenation of dimethyl adipate and hydrogenolysis of glycerol, (Jiang *et al.*, 2009; Fontana *et al.*, 2011; Weng *et al.*, 2014). In this work we have employed Al-pillared clay as an efficient support for Pd-Ni bimetallic particles for hydrodechlorination of a variety of substrates with major focus on chloroanilines, under milder condition using hydrazine hydrate as hydrogen transfer agent.

## 5.4 RESULTS AND DISCUSSIONS

### 5.4.1 XRD STUDY

The X-Ray diffraction patterns of the Pd-Ni(1:1)/Al-P and Pd-Cu(1:1)/Al-P is presented in Fig. 5.12. The bimetallic systems show broad and intense reflections indicating the materials are crystalline in character. However, the broadening of the peaks indicates a disturbance in the stacking arrangement of the clay sheets along the z-direction for the supported system in comparison to the pure Al-P. The (001) reflection for the supported system occurs at lower  $2\theta$  values indicating structural expansion of clay lattice as a result of pillaring with Al-polycationic clusters. The basal spacing value of the supported metallic systems presented in Table 5.3 are similar to the one observed for the Al-pillared clay material. The basal spacing value observed for the Pd-Ni(1:1)/Al-P and Pd-Cu(1:1)/Al-P materials are 18.3 and 18.7 Å, respectively. The basal spacing value indicates that the interlayer structure of the pillared clay remains intact in the supported catalysts and the supported system are structurally stable.

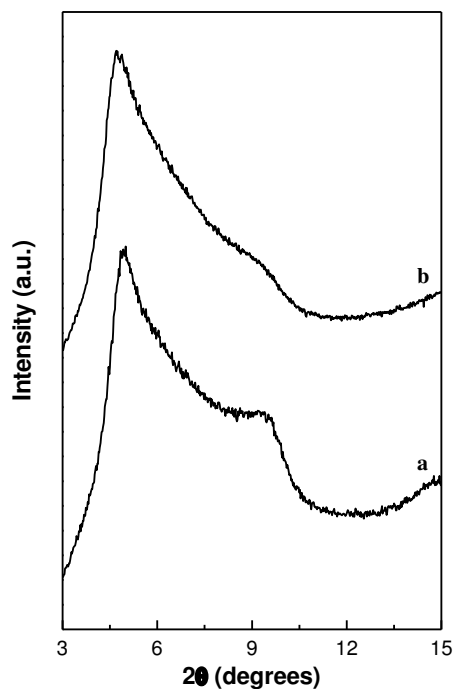


**Figure 5.12** XRD patterns of (a) Pd-Ni(1:1)/Al-P and (b) Pd-Cu(1:1)/Al-P.

**Table 5.3** Physicochemical characteristics of Pd-M/Al-P catalyst.

Sl No	Catalyst	Basal spacing (Å)	Surface area (m <sup>2</sup> /g)
1	Clay	12.9	30
2	Al-P	19.2	245
3	Pd/Al-P	18.6	186
4	Pd-Cu (1:1)/AL-P	18.7	164
5	Pd-Ni (1:1)/AL-P	18.3	172

#### 5.4.2 UV-VIS STUDY

The UV-Vis spectra of parent clay, Al-P, Pd-M/Al-P clay materials along with PdCl<sub>2</sub> and Pd (0) nanoclusters are presented Fig. 5.13. The dilute aqueous solution of PdCl<sub>2</sub> shows two distinguished absorption bands at 304 nm and 413 nm. These bands arise because of spin forbidden d-d transition (<sup>1</sup>A<sub>2g</sub> ← <sup>1</sup>A<sub>1g</sub>) (Alonso *et al.*, 2010). The PdCl<sub>2</sub> solution has been used

for generation of the Pd clusters by chemical reduction method using alkaline formaldehyde as reducing agent. Fig. 5.13 b shows the UV-Vis spectra of PdCl<sub>2</sub> solution reduced using alkaline formaldehyde after 6 h of reaction time. It is observed from the Fig. 5.13b that the two bands which are designated for Pd<sup>2+</sup> are completely absent. This observation implies that Pd<sup>2+</sup> ions have been completely reduced to Pd (0) in presence of the reducing agent (D'Souza *et al.*, 2013). The parent clay displays a broad UV absorption band with maxima at 245 nm. This band is attributed to the Fe<sup>3+</sup>←O<sup>2-</sup>, OH<sup>-</sup> or OH<sub>2</sub> charge transfer transition for the structural iron present in the octahedral layer of the clay sheet (Fig. 5.13c) (Ranga Rao and Mishra, 2005).

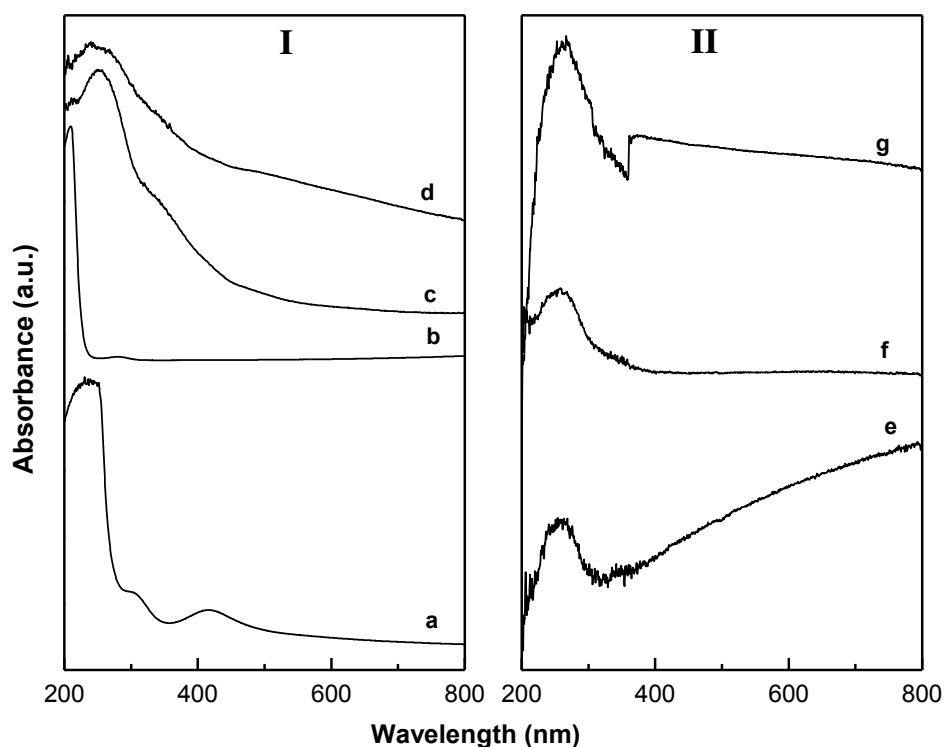


**Figure 5.13** UV-Vis spectra of (a) PdCl<sub>2</sub>, (b) Pd nanoclusters, (c) Clay and (d) Al-P (panel I) and (e) Pd/Al-P, (f) Pd-Ni(1:1)/Al-P and (g) Pd-Cu(1:1)/Al-P (panel II).

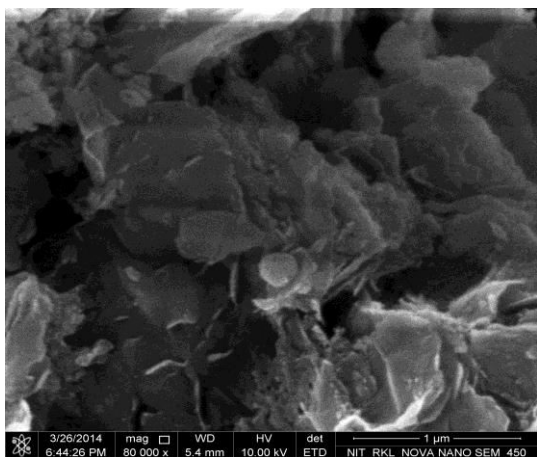
The isomorphous substitution of octahedral Al with Fe is responsible for the characteristic absorption feature of the clay materials. The Al-pillared clay shows similar absorption feature as that of the parent clay which is indicated in Fig. 5.13d. Alumina pillared clay is synthesized

by intercalation of  $[\text{AlO}_4\text{Al}_{12}(\text{OH})_{24}(\text{H}_2\text{O})_{12}]^{7+}$  polyoxocations followed by calcination. On calcination, these polyoxocations are converted to  $\text{Al}_2\text{O}_3$  nanoclusters which are covalently bonded with clay sheets and hold them apart.  $\text{Al}_2\text{O}_3$  being a direct band gap insulator, it does not absorb light in the range of 200-800 nm thereby causing no variation in its absorption feature with respect to parent clay (RangaRao and Mishra, 2007). The UV-Vis spectrum of Pd/Al-P is shown in Fig. 5.15e. This spectrum does not show any additional band corresponding to  $\text{Pd}^{2+}$ . Hence it can be concluded the Pd particles dispersed in the matrix of Al-P is in zero oxidation state. The UV-vis absorption spectra of Cu and Ni nanoparticles have been studied in literature (Xiang *et al.*, 2004; Scaiano *et al.*, 2011). The absorption band from Cu and Ni nanoparticles are observed at 570 and 400 nm, respectively, which has been attributed to the plasmon resonance occurring due to interaction of conduction band electrons with the electromagnetic radiation. However, in the present study the Pd-Cu/Al-P and Pd-Ni/Al-P does not show this absorption feature corresponding to Cu and Ni nanoparticles. This can be ascribed to the enrichment of the Pd metal over the bimetallic particle surface which suppress the plasmon resonance band of the second metal.

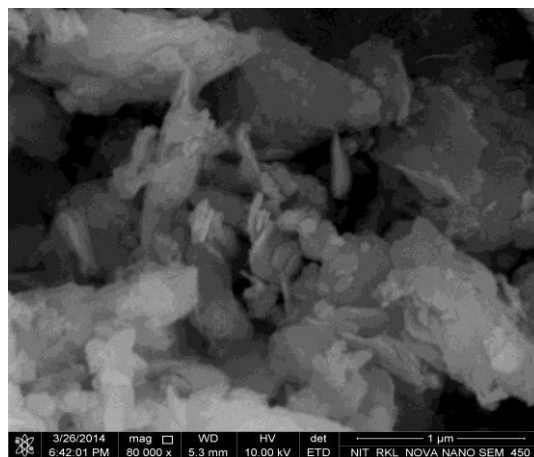
### 5.4.3 FE-SEM STUDY

The field emission scanning electron micrographs of Pd-Cu(1:1)/Al-P and Pd-Cu(1:1)/Al-P materials are presented in Fig. 5.14. Both the materials show the presence of flake like particles of irregular shape and size. This observation is in contrast to the sheet like morphology observed for the Al-pillared clay material (section 5.2.4). This observation indicates morphological changes due to the presence of metallic particles in the pillared clay matrix. The presence of the metallic particles along the broken edges as well as the defect sites of the clay sheets can promote edge to edge and edge to face interaction. This may result in folding of the clay sheet generating particles with irregular shape and morphology.





(c)

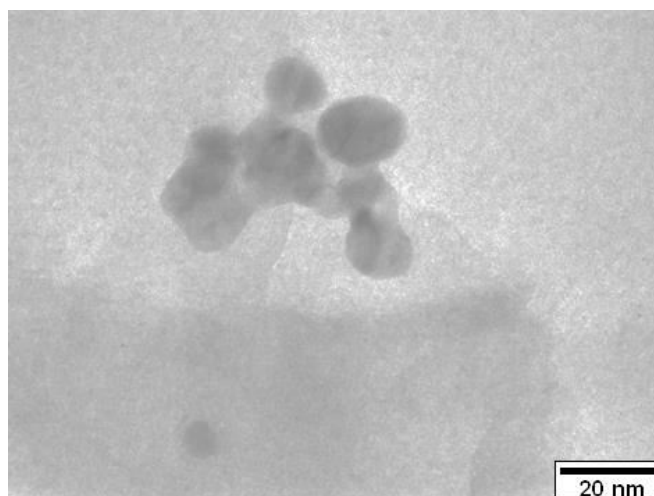


(d)

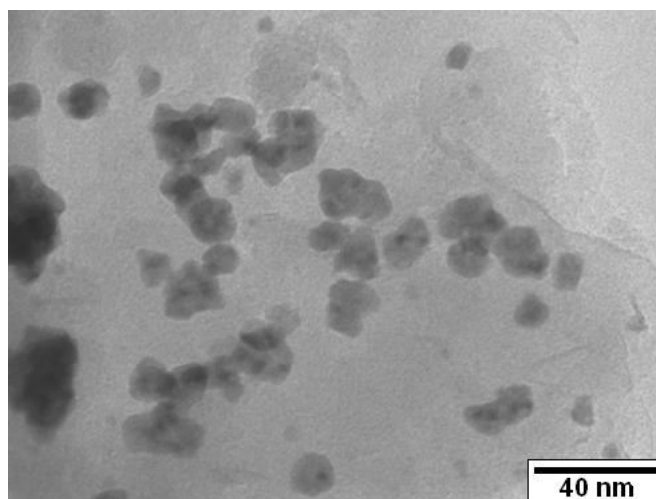
**Figure 5.14** FE-SEM images (a) Pd-Ni (1:1)/Al-P and (b) Pd-Cu(1:1)/Al-P.

#### 5.4.4 TEM STUDY

The transmission electron micrographs Pd and Pd-Ni bimetallic materials supported on Al-pillared clay is presented in figure 5.15. The Pd/Al-P system indicates the presence of Pd nanoparticles with size in the range of 5-30 nm well dispersed in the matrix of the Al-pillared clay (Fig. 5.15a). The TEM image of the Pd-Ni(1:1)/Al-P revealed the presence of particles with size in the range of 5-25 nm embedded in the Al-pillared clay matrix (Fig. 5.15b). The bimetallic particles show two contrasting metallic phases in the Al-pillared clay matrix.



(a)



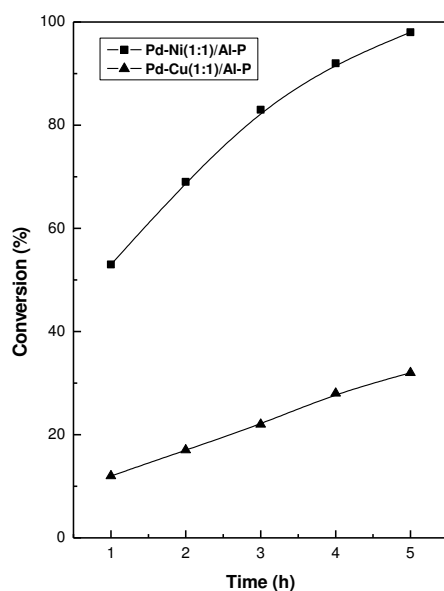
(b)

**Figure 5.15** TEM images (a) Pd/Al-P and (b) Pd-Ni(1:1)/Al-P.

#### **5.4.5 CATALYTIC ACTIVITY FOR HYDRODEHALOGENATION OF ORGANIC COMPOUNDS**

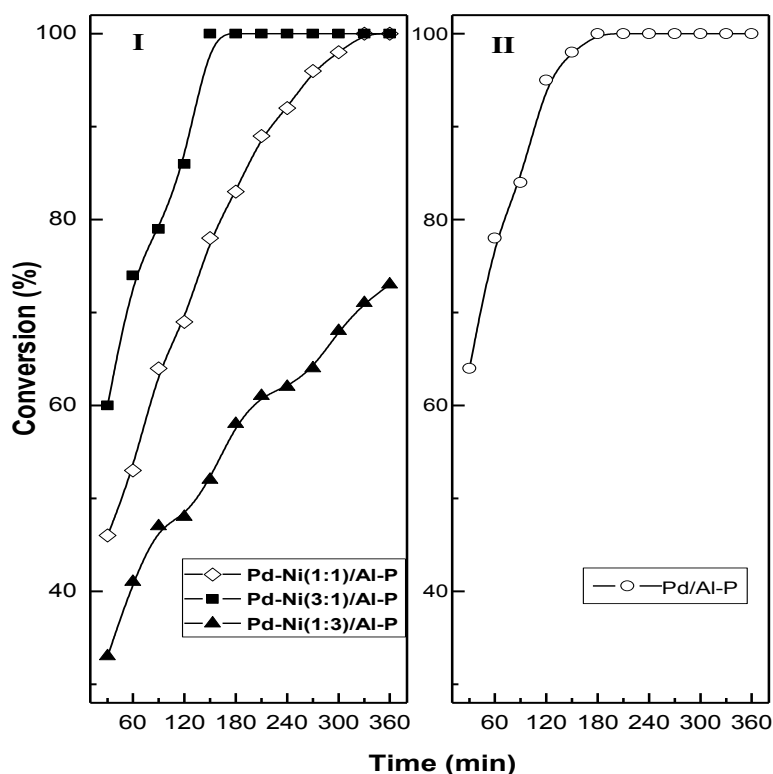
The catalytic activity of the Pd-M/Al-P materials has been examined for the hydrodechlorination of the halogenated aromatic organic compounds with particular focus on chloroanilines under transfer hydrogenation condition. Fig. 5.16 represents the time vs conversion profile of the Pd-Cu (1:1)/Al-P and Pd-Ni(1:1)/Al-P catalyst for hydrodechlorination of 4-Chloroaniline carried out at 40°C. Under the adopted experimental condition, the Pd-Ni(1:1)/Al-P catalyst exhibit higher catalytic activity compared to Pd-Cu (1:1)/Al-P catalyst. Pure Clay and Al-P materials were inactive for the reaction. It can be observed that the activity for HDH increases with time for both the catalyst. The Pd-Ni bimetallic particles exhibit high initial rates and good efficiency for HDC activity. For Pd-Cu on the other hand the increase is more gradual with respect to time. The Pd-Cu system attends 32% conversion after 5 h of reaction where as complete HDH was achieved in case of Pd-Ni bimetallic particles for same reaction time. Pd-Ni supported bimetallic systems have been studied earlier for HDH activity of different aromatic and aliphatic substrate. The Pd metal being primarily responsible for the activity of the catalyst, the selectivity for a particular product is tailored in presence of Ni (Srebowata *et al.*, 2007). Pd metal undergoes surface

segregation in the Pd-Ni bimetallic catalyst (Srebowata *et al.*, 2007). The surface segregation exposes more number of Pd atoms on the surface there by helping in the optimum utilization of the active sites



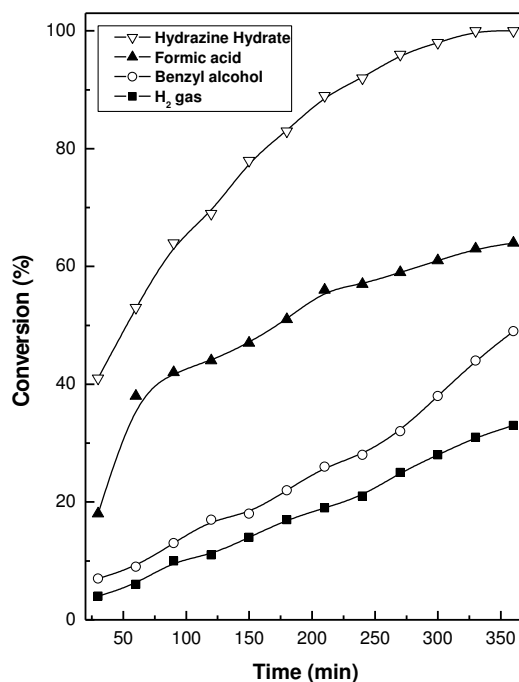
**Figure 5.16 Time vs conversion profile of Pd-Cu(1:1)/Al-P and Pd-Ni(1:1)/Al-P materials for hydrodechlorination of 4-Chloroaniline at 40° C.**

Fig. 5.17 shows the effect of molar ratio of Pd and Ni on the activity of Pd-Ni/Al-P catalyst for the HDH of 4-Chloroaniline. **The hydrodechlorination activity was found to increase with increase in the Pd content in the bimetallic catalyst which is in accordance with the earlier observation in literature (Simagina *et al.*, 2003).** From kinetics consideration, the Pd-Ni(1:1)/Al-P was selected for further study. In order to study the effect of the nature of the hydrogen transfer agent on the catalytic activity of the Pd-Ni(1:1)/Al-P catalyst, different hydrogen transfer agents are used for the HDC activity of 4-Chloroaniline.



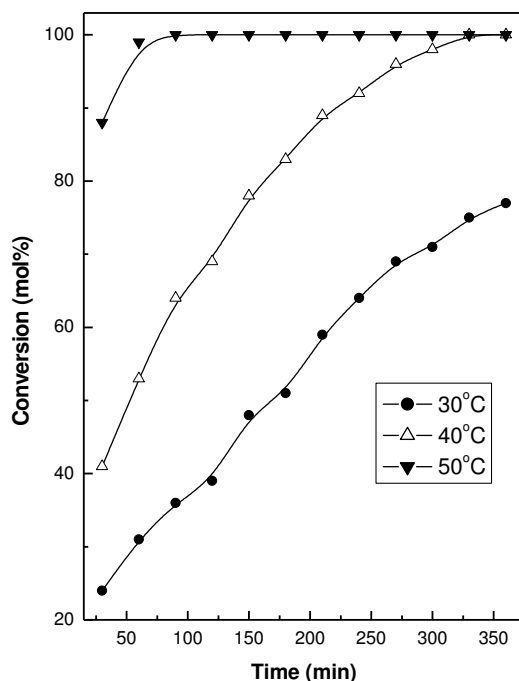
**Figure 5.17 (I) Effect of molar ratio of Pd:Ni on the catalytic activity of Pd-Ni/Al-P catalyst, (II) catalytic activity of Pd/Al-P, for the hydrodechlorination of 4-Chloroaniline.**

Fig. 5.18 shows the time vs conversion plot for hydrodechlorination of 4-Chloroaniline using different hydrogen transfer agents over Pd-Ni(1:1)/Al-P catalyst. Among all hydrogenating agents hydrazine hydrate is found to be most efficient with 98% conversion after 5 hours of reaction. The larger size and low reduction potential of benzyl alcohol hinder its adsorption and transport to the bimetallic surface. The lower activity observed for molecular hydrogen can be ascribed to its limited solubility in aqueous media and lower reduction potential compared to hydrazine hydrate.



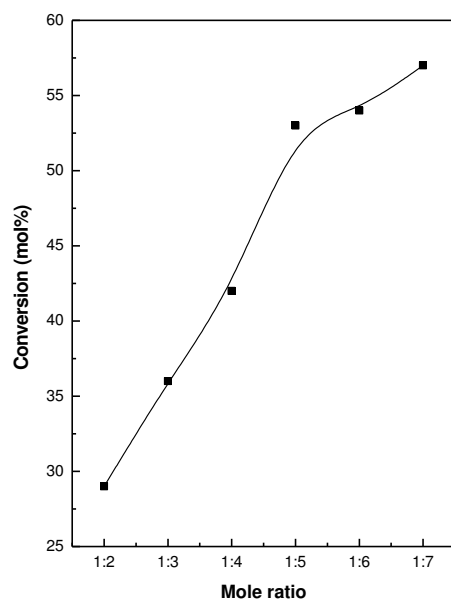
**Figure 5.18 Effect of various hydrogenating agents on the hydrodechlorination activity of 4-Chloroaniline for Pd-Ni(1:1)/Al-P catalyst.**

Further optimization of the HDH of 4-Chloroaniline was carried out by varying the temperature. Fig. 5.19 represents the effect of temperature on the catalytic activity of Pd-Ni(1:1)/Al-P catalyst in the range of 30-50°C. At 30°C, the rate of HDH is very slow and even after 6 hours 77% of hydrodechlorination of the substrate was observed. Similarly, the reaction rates are enhanced significantly at 50°C and the hydrodechlorination process get completed after 1 hour of reaction time. At 40°C the reaction complete conversion takes place after 5 hours of reaction. Hence 40°C is chosen as optimum temperature to carry out further reactions. After optimizing different parameters, the molar ratio of substrate to hydrazine hydrate was varied to determine the optimum value.



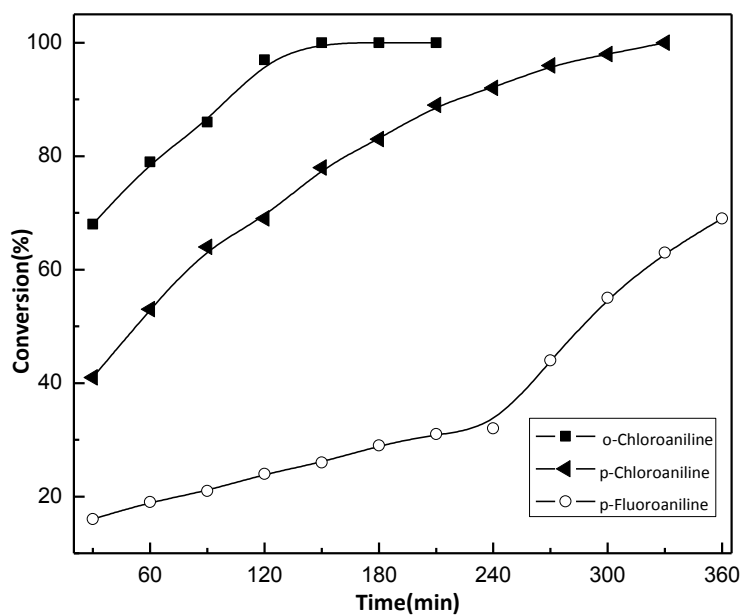
**Figure 5.19 Effect of temperature on hydrodechlorination of 4-Chloroaniline after 1 h of reaction time for Pd-Ni(1:1)/Al-P catalyst.**

Fig. 5.20 shows the HDH activity of Pd-Ni(1:1)/Al-P catalyst for 4-Chloroaniline after 1 h of reaction at different substrate to hydrazine hydrate molar ratio. For lower molar ratio, the rate of HDH is less. As molar ratio increases there is a gradual increase in conversion reaching the optimum value at 1:5. Further increase in molar ratio does not have any marked impact on the HDC activity. Hence in this study the molar ratio of 1:5 was chosen as optimum molar ratio of 4-Chloroaniline and hydrazine hydrate for further study. In order to evaluate the effect of functional groups on the HDC process, various halogenated organics differing in functionality are used in the catalytic study under optimized conditions. Fig. 5.21 and 5.22 show the percentage conversion vs time plot for different ortho and para substituted chloroanilines, chlorotoluene and chlorophenols.



**Figure 5.20** Effect of molar ratio of 4-Chloroaniline and hydrazine hydrate on the hydrodechlorination of 4-Chloroaniline after 1 h of reaction time for PdNi(1:1)/Al-P catalyst at 40 °C.

From Fig. 5.21, it is noted that for the Pd-Ni(1:1)/Al-P, the 2-Chloroaniline is more reactive and shows higher dechlorination rate compared to its para isomer. It can be explained in terms of electronic effect. The presence of electron donating  $-NH_2$  group creates more electron rich centre at ortho position than para position which helps in the cleavage of the C-Cl bond. For 2-Chloroaniline complete dehalogenation takes place after 4 hours of reaction. The rate of HDC is slower for 4-Fluoroaniline due to greater dissociation energy associated with C-F bond. Fig. 5.22 illustrates catalytic activity of Pd-Ni(1:1)/Al-P catalyst for HDC of 4-Chlorophenol and 4-Chlorotoluene. 4-Chlorophenol undergo dechlorination at a marginally lower rate compared to 4-Chloroaniline. However, least reactivity was observed for 4-Chlorotoluene. The 4-Chlorotoluene containing the hydrophobic  $-CH_3$  group is less accessible to the active metallic sites present in the hydrophilic environment of Al-pillared clay matrix.



**Figure 5.21** Catalytic activity of Pd-Ni(1:1)/Al-P catalyst for the hydrodechlorination of different substituted anilines at 40 °C.

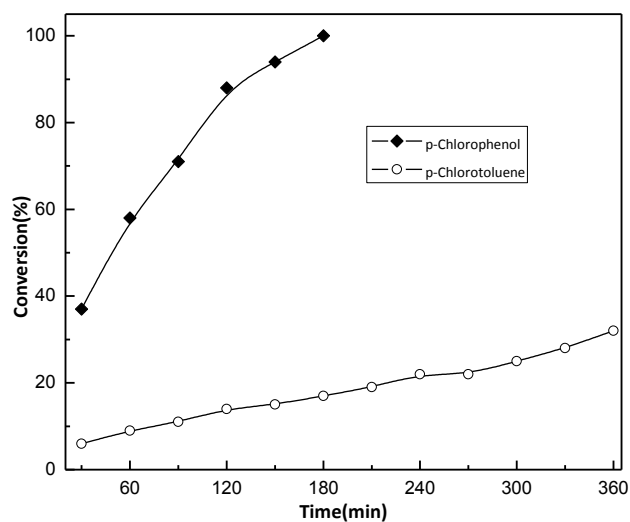


**Figure 5.22** Catalytic activity of Pd-Ni(1:1)/Al-P catalyst for the hydrodechlorination of 4-Chlorophenol and 4-Chlorotoluene at 40 °C.



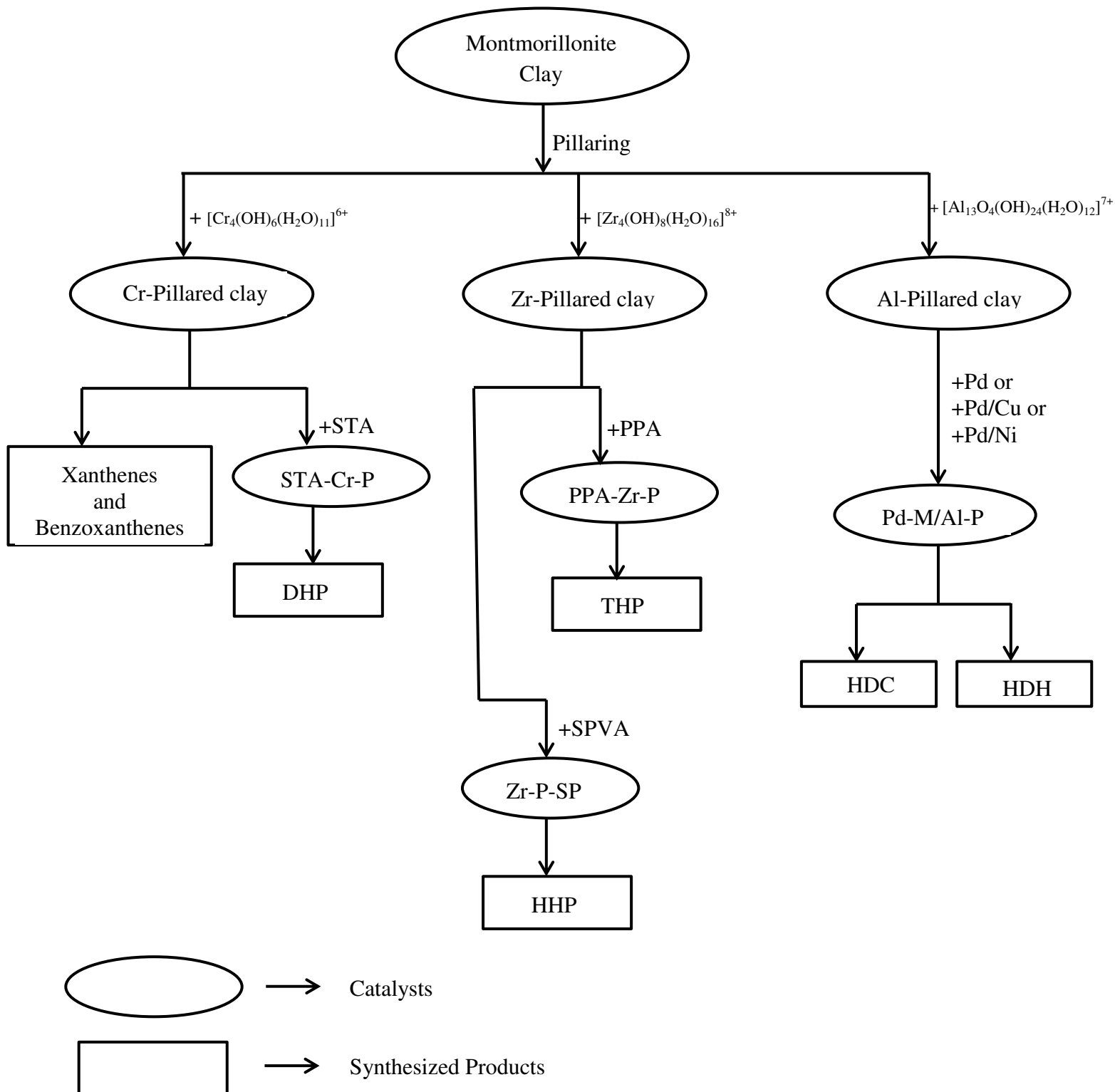
## 5.5 CONCLUSION

In this work, we have explored the synthesis and catalytic application of Pd and Pd-Ni bimetallic nanoparticles dispersed in Al-pillared clay matrix for hydrodechlorination of halogenated aromatics under hydrogen transfer conditions. The pure Pd and Pd-Ni bimetallic nanoparticles were synthesized using chemical reduction method. The expansion of the interlayer space of the clay upon pillaring and its subsequent retention in the supported mono and bimetallic systems is elucidated from XRD study. The Al-pillared clay provides an effective inorganic matrix for the dispersion and stability of the metallic nanoparticles. The IR study indicated the structural integrity of the clay lattice in the supported system. The UV-Vis study revealed complete reduction of the metallic precursor salt and enrichment of Pd on the surface of the bimetallic particles. The changes in the morphological features due to the presence of the metallic particles are apparent from the FESEM study. TEM study of the supported Pd nanoparticles indicated the presence of 5–30 nm size particles well dispersed in the pillared clay structure. The Pd-Ni bimetallic particles as observed by TEM are of irregular shape with size the range of 5-25 nm uniformly dispersed in the Al-pillared clay matrix. The Pd/Al-P and Pd-Ni/Al-P was used as a catalyst for efficient HDH of halogenated organic compounds. Hydrazine hydrate act as an efficient hydrogen transferring agent showing higher HDC activity for a variety of substrates. Among several halogenated substrates it is found that di-substituted substrates undergo HDC at a slower rate as compared to mono substituted halogenated compounds.

## CHAPTER 6

### SUMMARY AND CONCLUSIONS

The summary the research work carried out in this thesis is schematically presented below



In this thesis, the catalytic application of pillared clays and their modified analogues have been evaluated for synthesis of biologically important molecules and hydrodehalogenation of a variety of halogenated aromatic compounds. Three different pillared clays namely Al-, Zr and Cr-pillared clays have been modified using metallic, oxidic and polymeric materials to generate the heterogeneous catalytic systems. The catalytic activity of these pillared clay analogues have been studied for synthesis of biologically important molecules and decontamination of organic contaminants from water. The major conclusions obtained from this works are presented below

### **Major Conclusions**

- The Cr-pillared clay material is used as an efficient catalyst for synthesis of structurally diverse xanthene derivatives. The observed improvement in surface area, microporosity and acidity due to pillaring are the important factors which contribute to the catalytic activity of this material. Compare to literature reported methods, the catalytic protocol developed in this work has been found to be advantageous in term of recyclable catalyst, preclusion of toxic solvent and high yield and purity of the products.
- The Cr-pillared clay is an effective support for dispersing catalytically active silicotungstic acid nanoclusters. The high surface area and microporous nature of the Cr-pillared clay is crucial for well dispersion of the silicotungstic acid.
- The STA/Cr-P materials is catalytically active for the synthesis of 1,4-dihydropyridines (DHPs) by multicomponent reaction of aldehydes/chalcones, ethylacetoacetate and ammonium acetate under solventfree condition. Structurally diverse DHPs are prepared by in high yield and purity using different aryl aldehydes and chalcones as starting materials.
- A novel class of Pillared clay-polyphosphoric acid (ZrP-PPA) nanocomposite materials is synthesized in this work. The constrained interlayer space (~ 1 nm) and high surface area (~

170 m<sup>2</sup>/g) of Zr-pillared clay was used effectively to trap the PPA moieties in the lateral space between the pillars. The trapped PPA moieties in the Zr-P interlayer exhibit good thermal stability and resistance to hydrolysis.

- Structurally diverse tetrahydropyridines were synthesized by multicomponent one pot condensation of aromatic aldehydes, substituted aniline, and  $\beta$ -dicarbonyl compounds using acetonitrile as solvent and ZrP-PPA as heterogeneous catalyst. The catalytic protocol developed using ZrP-PPA catalyst for synthesis of tetrahydropyridines is advantageous in terms of less reaction time, good yield and purity of the products and catalyst recyclability.
- A novel class of inorganic-organic hybrid material containing surface acidic functional groups is synthesized employing Zr-pillared clay as inorganic matrix and sulfonated polyvinyl alcohol as an organic polymer (ZrP-SPVA). The enhanced gallery height and the open channels of the Zr-pillared clay help in intercalation of the polymer. Well dispersion and trapping of the polymeric species in the clay and pillared clay matrix is achieved using CTAB as a structure expanding agent. The intercalation behaviour of the polymer is found to be crucial for the final properties of these composite systems.
- The Z-P-SPVA catalytic system efficiently catalyzes the synthesis of hexahydropyrimidines by one pot condensation of  $\beta$ -dicarbonyl compounds, substituted aniline and formaldehyde. The synergistic effect between the acidic sites of the clay lattice and the  $-\text{SO}_3\text{H}$  group of the polymer is responsible for synthesis of structurally diverse hexahydropyrimidines in good yield under mild conditions.
- The high surface area and microporosity of Al-pillared clay is effectively utilized for supporting Pd metal and Pd-M (M =Cu and Ni) bimetallic nanoparticles. The Al-pillared clay supported Pd nanoparticles exhibit efficient hydrodechlorination activity for a variety of

chlorinated aromatic contaminants under hydrogen transfer condition. The acidic centers of the clay provides adsorption sites for the chlorinated compounds where as the Pd metal is responsible for the hydrodechlorination activity.

- The scope of waste water treatment using supported metallic particles over Al-pillared clay is further broadened in this work by employing supported Pd-Ni bimetallic nanoparticles for dehydrohalogenation of a wide variety of organic contaminants with functional diversity. The Pd metal act as active sites for the dehalogenation reaction where as the Ni metal helps in stability of the bimetallic species.
- For Pd-/Al-P and Pd-Ni/Al-P catalyzed dehydrohalogenation reaction for mono-substituted substrates the reactivity varied in the order chlorotoluene < chlorophenol < chloroaniline. The different in the reactivity has been explained based on the electronic effect exerted by different functional groups present in the substrate. Among different halogenated substrates, di-substituted substrates undergo HDH at a slower rate as compared to mono substituted halogenated compounds.

## REFERENCES

1. **Abedi, S.** and **M. Abdouss** (2014) A review of clay-supported Ziegler–Natta catalysts for production of polyolefin/clay nanocomposites through in situ polymerization. *Applied Catalysis A: General*, **475**, 386–409.
2. **Achma, R. B., A. Ghorbel, A. Dafinov and F. Medina** (2008) Copper-supported pillared clay catalysts for the wet hydrogen peroxide catalytic oxidation of model pollutant tyrosol. *Applied Catalysis A: General*, **349**, 20–28.
3. **Adams, J.M.** and **R.W. M<sup>C</sup> Cabe** (2006) Clay minerals as catalysts. Handbook of clay science Edited by F. Bergaya, B.K.G. Theng and G. Lagaly, *Developments in Clay Science*, **1**, 541–582.
4. **Akçay, M.** (2004) The catalytic acylation of alcohols with acetic acid by using Lewis acid character pillared clays. *Applied Catalysis A: General*, **269**, 157–160.
5. **Akçay, M.**, (2005) The surface acidity and characterization of Fe-montmorillonite probed by in situ FT-IR spectroscopy of adsorbed pyridine. *Applied Catalysis A: General*, **294**, 156–160.
6. **Akelah, A.** and **M. Moet** (1996) Polymer-clay nanocomposites: Free-radical grafting of polystyrene on to organophilic montmorillonite interlayers. *Journal of Material Science*, **31**, 3589–3596.
7. **Akitt, J.W.**, and **A. Farthing** (1981). Aluminium-27 nuclear magnetic resonance studies of the hydrolysis of aluminium III. Part 2. Gel-permeation chromatography. *Journal of the Chemical Society, Dalton Transactions*, **7**, 1606–1608.
8. **Akl, J., T. Ghaddar, A. Ghanem and H. El-Rassy** (2009) Cobalt ferrite aerogels by epoxide sol–gel addition: Efficient catalysts for the hydrolysis of 4-nitrophenyl phosphate. *Journal of Molecular Catalysis A: Chemical*, **312**, 18–22.
9. **Akondi, A.M., R. Trivedi, B. Sreedhar, M. L. Kantam and S. Bhargava** (2012), Cerium-containing MCM-41 catalyst for selective oxidative arene cross-dehydrogenative coupling reactions, *Catalysis Today*, **198**, 35–44.
10. **Alena, K., M. Dagmar, G.J. Francois and S. Miroslav** (2013) Polymer/Clay nanocomposites and their gas barrier properties. *Polymer composites*, 1–7.
11. **Alibeik M.A.- and E.H.-Torkabad** (2012) H<sub>3</sub>PW<sub>12</sub>O<sub>40</sub>/MCM-41 nanoparticles as efficient and reusable solid catalyst for synthesis of quinoxalines. *Comptes Rendus Chimie*, **15**, 517–523.
12. **Almeida, S.H.D.** and **Y. Kawano** (1997) Ultraviolet-visible spectra of Nafion membrane, *European Polymer Journal*, **33**, 1307.
13. **Alonso, L. E.-, K.P. de Jong and B.M. Weckhuysen** (2010) A UV-Vis micro-spectroscopic study to rationalize the influence of Cl<sup>-</sup> (aq) on the formation of different Pd macro-distributions on  $\gamma$ -Al<sub>2</sub>O<sub>3</sub> catalyst bodies. *Physical Chemistry Chemical Physics*, **12**, 97–107.
14. **Álvarez, A., S. Moreno, R. Molina, S. Ivanova, M.A. Centeno and J.A. Odriozola** (2012) Gold supported on pillared clays for CO oxidation reaction: Effect of the clay aggregate size. *Applied Clay Science*, **69**, 22–29.
15. **Amali, A. J.** and **R. K. Rana** (2008) Trapping Pd(0) in nanoparticle-assembled microcapsules: an efficient and reusable catalyst. *Chemical Communications*, 4165–4167.

16. **Amorim, C., G. Yuan, P.M. Patterson and M.A. Keane** (2005) Catalytic hydrodechlorination over Pd supported on amorphous and structured carbon. *Journal of Catalysis*, **234**, 268–281.
17. **Anisia, K.S. and A. Kumar** (2007) Oxidation of cyclohexane with molecular oxygen in presence of characterized macrocyclic heteronuclear FeCu complex catalyst ionically bonded to zirconium pillared montmorillonite clay. *Journal of Molecular Catalysis A*, **271**, 164–179.
18. **Anwer, M. K., D. B. Sherman, J. G. Roney and A. F. Spatola** (1989) Applications of ammonium formate catalytic transfer hydrogenation. 6. Analysis of catalyst, donor quantity, and solvent effects upon the efficacy of dechlorination. *The Journal of Organic Chemistry*, **54**, 1284–1289.
19. **Aouad, A., A. Pineau, D. Tchoubar and F. Bergaya** (2006) Al-pillared montmorillonite obtained in concentrated media. Effect of the anions (nitrate, sulfate and chloride) associated with the Al species. *Clays Clay Miner.* **54**, 626–637.
20. **Aouad, A., T. Mandalia and F. Bergaya** (2005) A novel method of Al-pillared montmorillonite preparation for industrial up-scaling. *Applied Clay Science*, **28**, 175–182.
21. **Aramendia, M. A., V. Bor'au, I. M. Garcia, C. Jimenez, F. Lafont, A. Marinas, J. M. Marinas and F. J. Urbano** (1999) Influence of the reaction conditions and catalytic properties on the liquid-phase hydrodechlorination of chlorobenzene over Palladium-Supported Catalysts: Activity and Deactivation. *Journal of Catalysis*, **187**, 392–399.
22. **Arena, F., R. Dario and A. Parmaliana** (1998) Characterization study of the surface acidity of solid catalysts by temperature programmed methods. *Applied Catalysis A: Gen.*, **170**, 127–137.
23. **Arfaoui, S., N. Frini-Srasra and E. Srasra** (2009) Synthesis and characterization of hydroxy-chromium pillared bentonite. *Surface Engineering and Applied Electrochemistry*, **45**, 239–245.
24. **Auer, H. and H. Hofmann** (1993) Pillared clays: characterization of acidity and catalytic properties and comparison with some zeolites. *Applied Catalysis A: General*, **97**, 23–38.
25. **Awate, S.V., S. B. Waghmode, K. R. Patil, M. S. Agashe and P.N. Joshi** (2001) Influence of preparation parameters on characteristics of zirconia-pillared clay using ultrasonic technique and its catalytic performance in phenol hydroxylation. *Korean Journal of Chemical Engineering*, **18**, 257–262.
26. **Aznárez, A., F.C.C. Assis, A. Gil and S.A. Korili** (2011) Effect of the metal loading on the catalytic combustion of propene over palladium and platinum supported on alumina-pillared clays. *Catalysis Today*, **176**, 328–330.
27. **Aznárez, A., S.A. Korili and A. Gil** (2014a) The promoting effect of cerium on the characteristics and catalytic performance of palladium supported on alumina pillared clays for the combustion of propene. *Applied Catalysis A: General*, **474**, 95–99.
28. **Aznárez, A., R. Delaigle, P. Eloy, E.M. Gaigneaux, S.A. Korili and A. Gil** (2014b) Catalysts based on pillared clays for the oxidation of chlorobenzene. *Catalysis Today*, <http://dx.doi.org/10.1016/j.cattod.2014.07.024>.
29. **Azzouz, A., D. Nistor, D. Miron, A.V. Ursu, T. Sajin, F. Monette, P. Niquette and R. Hausler** (2006) Assessment of acid–base strength distribution of ion-exchanged montmorillonites through NH<sub>3</sub> and CO<sub>2</sub>-TPD measurements. *Thermochimica Acta*, **449**, 27–34.

30. **Baes, C. F. and R.E. Mesmer**, The Hydrolysis of Cations. John Wiley, New York, 1976, xxi, 489 p. ISBN 9780471039853.
31. **Bahranowski, K., R. Grabowski, B. Grzybowska, A. Kielski, E.M. Serwicka, K. Weislo, E. Wisla-Walsh and K. Wodnicka** (2000) Synthesis and physicochemical properties of vanadium-doped zirconia-pillared montmorillonites in relation to oxidative dehydrogenation of propane. *Topics in Catalysis*, **11/12**, 255–261.
32. **Balcha, T., J. R. Strobl, C. Fowler, P. Dash and R. W. J. Scott** (2011) Selective Aerobic Oxidation of Crotyl Alcohol Using AuPd Core-Shell Nanoparticles. *ACS Catalysis*, **1**, 425–436.
33. **Barama, S., C. Dupeyrat-Batiot, M. Capron, E. Bordes-Richard and O. Bakhti-Mohammedi** (2009) Catalytic properties of Rh, Ni, Pd and Ce supported on Al-pillared montmorillonites in dry reforming of methane. *Catalysis Today*, **141**, 385–392.
34. **Barrera-Vargas, M., J. Valencia-Rios, M. A. Vicente, S. A. Korili, and A. Gil** (2005) Effect of the platinum content on the microstructure and micropore size distribution of Pt/alumina-pillared clays, *The Journal of Physical Chemistry B*, **109**, 23461-23465.
35. **Barrault, J., M. Abdellaoui, C. Bouchoule, A. Majesté, J.M. Tatibouët, A. Louloui, N. Papayannakos and N.H. Gangas** (2000) Catalytic wet peroxide oxidation over mixed (Al–Fe) pillared clays. *Applied Catalysis B: Environmental*, **27**, L225–L230.
36. **Bartley, G.J.J.** (1988) Zirconium pillared clays. *Catalysis Today*, **2**, 233-241.
37. **Bedia, J., L.M. Gómez-Sainero, J.M. Grau, M. Busto, M. Martin-Martinez and J.J. Rodriguez** (2012) Hydrodechlorination of dichloromethane with mono- and bimetallic Pd–Pt on sulfated and tungstated zirconia catalysts. *Journal of Catalysis*, **294**, 207–215.
38. **Behrendt, J.M., A.B. Foster, M.C. McCairn, H. Willcock, R.K. O'Reilly and M.L. Turne** (2013) Hybrid inorganic–organic composite nanoparticles from crosslinkable polyfluorenes. *Journal of Materials Chemistry C*, **1**, 3297–3304.
39. **Bekaert, A., J. Andrieux and M. Plat** (1992) New total synthesis of bikaverin. *Tetrahedron Letters*, **33**, 2805–2806.
40. **Benesi, H.A.** (1956) Acidity of catalyst surfaces. I. Acid strength from colors of adsorbed indicators. *Journal of American Chemical Society*, **78**, 5490-5494.
41. **Bergaya, F., G. Lagaly and M. Vayer** (2006a) Chapter 12.10 Cation and anion exchange, *Developments in Clay Science*, **1**, 979-1001.
42. **Bergaya, F., A. Aouad and T. Mandalia** (2006b) Chapter 7.5 Pillared clays and clay minerals. Edited by F. Bergaya, B.K.G. Theng and G. Lagaly, *Developments in clay science*, **1**, 393-422.
43. **Bhattacharyya, K.G. and S. Sen Gupta** (2008) Adsorption of a few heavy metals on natural and modified kaolinite and montmorillonite: A review. *Advances in Colloid and Interface Science*, **140**, 114–131.
44. **Bhorodwaj, S.K. and D.K. Dutta** (2010) Heteropoly acid supported modified montmorillonite clay: An effective catalyst for the esterification of acetic acid with sec-butanol. *Applied Catalysis A: General*, **378**, 221–226.



45. **Bhorodwaj, S.K. and D.K. Dutta** (2011) Activated clay supported heteropoly acid catalysts for esterification of acetic acid with butanol. *Applied Clay Science*, **53**, 347–352.
46. **Biernacka, I. K.-, A.R. Silva, A.P. Carvalho, J. Pires and C. Freire** (2007) Direct immobilisation versus covalent attachment of a Mn(III)salen complex onto an Al-pillared clay and influence in the catalytic epoxidation of styrene. *Journal of Molecular Catalysis A: Chemical*, **278**, 82–91.
47. **Bineesh, K. V., M.-i. Kim, G.-H. Lee, M. Selvaraj, K. Hyun and D.-W. Park** (2012) Production of elemental sulfur and ammonium thiosulfate by the oxidation of H<sub>2</sub>S containing water vapor and ammonia over V/Zr-PILC catalysts. *Journal of Industrial and Engineering Chemistry*, **18**, 1845–1850.
48. **Bineesh, K.V., D.-K. Kim, M.-IL Kim and D.-W. Park** (2011) Selective catalytic oxidation of H<sub>2</sub>S over V<sub>2</sub>O<sub>5</sub> supported on TiO<sub>2</sub>-pillared clay catalysts in the presence of water and ammonia. *Applied Clay Science*, **53**, 204–211.
49. **Bineesh, K.V., M.-i. Kim, G.-H. Lee, M. Selvaraj and D.-W. Park** (2013) Catalytic performance of vanadia-doped alumina-pillared clay for selective oxidation of H<sub>2</sub>S. *Applied Clay Science*, **74**, 127–134.
50. **Binitha, N.N. and S. Sugunan** (2008) Shape selective toluene methylation over chromia pillared montmorillonites. *Catalysis Communications*, **9**, 2376–2380.
51. **Bodman, S.D., W.R. McWhinnie, V. Begon, M. Millan, I. Suelves, M.-J. Lazaro, A.A. Herod and R. Kandiyoti** (2003) Metal-ion pillared clays as hydrocracking catalysts (II): effect of contact time on products from coal extracts and petroleum distillation residues. *Fuel*, **82**, 2309–2321.
52. **Bodoardo, S., F. Figueras and E. Garrone** (1994) IR study of Bronsted acidity of Al-pillared montmorillonite. *Journal of Catalysis*, **147**, 223–230.
53. **Boonamnuayvitaya, V., C. Chaiya, W. Tanthapanichakoon and S. Jarudilokkul** (2004) Removal of heavy metals by adsorbent prepared from pyrolyzed coffee residues and clay. *Separation and Purification Technology*, **35**, 11–22.
54. **Bradley, S.M. and R.A. Kydd** (1993a) A comparison of the catalytic activity of Ga<sub>13</sub>-, Al<sub>13</sub>-, GaAl<sub>12</sub>-, and chromium-pillar interlayered clay minerals and Ga-H-ZSM-5 Zeolite in the dehydrocyclodimerization of propane. *Journal of Catalysis*, **142**, 448-454.
55. **Bradley, S.M. and R.A. Kydd** (1993b) Ga<sub>13</sub>, Al<sub>13</sub>, GaAl<sub>12</sub>, and Cr-pillared montmorillonites: acidity and reactivity for cumene conversion. *Journal of Catalysis*, **141**, 239-249.
56. **Brahmachari, G. and S. Das** (2012) Bismuth nitrate-catalyzed multicomponent reaction for efficient and one-pot synthesis of densely functionalized piperidine scaffolds at room temperature. *Tetrahedron Letters*, **53**, 1479–1484.
57. **Brahmkhatri, V. and A. Patel** (2011) Biodiesel production by esterification of free fatty acids over 12-tungstophosphoric acid anchored to MCM-41. *Industrial & Engineering Chemistry Research*, **50**, 6620–6628.
58. **Breen, C.** (1991) Thermogravimetric and infrared study of the desorption of butylamine, cyclohexylamine and pyridine from Ni and Co-exchanged montmorillonite. *Clay Mineral*, **26**, 487-496.

59. **Brigatti, M.F., E. Galan and B.K.G. Theng** (2013) Chapter 2 – Structure and Mineralogy of Clay Minerals. *Developments in Clay Science*, **5**, 21–81.
60. **Brindley, G.W. and S. Yamanaka** (1979) A study of hydroxy-chromium montmorillonites and the form of the hydroxy-chromium polymers. *American Mineralogist*, **64**, 830-835.
61. **Campos, A., B. Gagea, S. Moreno, P. Jacobs and R. Molina** (2008) Decane hydroconversion with Al–Zr, Al–Hf, Al–Ce-pillared vermiculites. *Applied Catalysis A: General*, **345**, 112–118.
62. **Carr, R.M.** (1985) Hydration States of interlamellar chromium ions in montmorillonite. *Clays and Clay Minerals*, **33**, 357-361.
63. **Carrero, A., R. Grieken, I. Suarez and B. Paredes** (2012) Development of a new synthetic method based on in situ strategies for polyethylene/clay composites. *Journal of Applied Polymer Science*, **126**, 987–997.
64. **Carvalho, A., J. Pires, P. Veloso, M. Machado, M.B. Carvalho and J Rocha** (2003) Nitrate occlusion studies in Y zeolite and in a clay pillared with aluminium oxide. *Microporous Mesoporous Materials*, **58**, 163-173.
65. **Centi, G. and S. Perathoner** (2008) Catalysis by layered materials: A review. *Microporous and Mesoporous Materials*, **107**, 3–15.
66. **Chaabene, S. B., L. Bergaoui and A. Ghorbel** (2004) Zirconium and sulfated zirconium pillared clays: a combined intercalation solution study and solid characterization. *Colloids and Surfaces A: Physicochemical and Engineering Aspects*, **251**, 109–115.
67. **Chaplin, B.P., M. Reinhard, W.F. Schneider, C. Schüth, J.R. Shapley, T.J. Strathmann and C.J. Werth** (2012) Critical review of Pd-based catalytic treatment of priority contaminants in water. *Environmental Science and Technology*, **46**, 3655–3670.
68. **Charan, P.H.K. and G. Ranga Rao** (2013) Investigation of chromium oxide clusters grafted on SBA-15 using Cr-polycation sol. *Journal of Porous Materials*, **20**, 81–94.
69. **Chen, Y. and Q. Wang** (2006) Preparation, properties and characterizations of halogen-free nitrogen-phosphorous flame-retarded glass fiber reinforced polyamide 6 composite. *Polymer Degradation and Stability*, **91**, 2003-2013.
70. **Chen, Z., Z. Luan, J. Fan, and B. Fan** (2007) Effect of thermal treatment on the formation and transformation of Keggin Al<sub>13</sub> and Al<sub>30</sub> species in hydrolytic polymeric aluminum solutions. *Colloids and Surfaces A: Physicochemical and Engineering Aspects*, **292**, 110–118.
71. **Cheng, S.** (1999) From layer compounds to catalytic materials. *Catalysis Today*, **49**, 303-312.
72. **Chidambaram, V. and B. Viswanathan** (2007) Single step catalytic production of diisopropyl ether (DIPE) from acetone feedstock over nickel based catalysts. *Applied Catalysis B: Environmental*, **71**, 32–43.
73. **Chitnis, S.R. and M.M. Sharma** (1997) Industrial application of acid-treated clays catalysts. *Reactive and Functional Polymers*, **32**, 93-115.
74. **Chiu, C., T. Huang, Y. Wang, B.G. Alamani and J. Lin** (2014) Intercalation strategies in clay/polymer hybrids. *Progress in Polymer Science*, **39**, 443–485.

75. **Chmielarz, L., M. Wojciechowska, M. Rutkowska, A. Adamski, A. Wegrzyn, A. Kowalczyk, B. Dudek, P. Boron, M. Michalik and A. Matusiewicz** (2012) Acid-activated vermiculites as catalysts of the DeNO<sub>x</sub> process. *Catalysis Today*, **191**, 25–31.
76. **Choi, M., F. Kleitz, D. Liu, H.Y. Lee, W.-S. Ahn and R. Ryoo** (2005) Controlled polymerization in mesoporous silica toward the design of organic-inorganic composite nanoporous materials. *Journal of the American Chemical Society*, **127**, 1924-1932.
77. **Choudary, B.M. and V.L.K. Valli** (1990) A novel vanadium pillared montmorillonite catalyst for molecular recognition of benzyl alcohols. *Journal of Chemical Society, Chemical Communication*, 1115-1116.
78. **Choudary, B.M., A. DurgaPrasad, V. Bhuma and V. Swapna**, Chromium-pillared clay as a catalyst for benzylic oxidation and oxidative deprotection of benzyl Ethers and benzylamines: A simple and convenient procedure, *Journal of Organic Chemistry*. (1992) **57**, 5841-5844.
79. **Coln, L., J.A., J.A. de los Reyes, A. Vazquez and A. Montoya** (2005) Pillar effects in MoS<sub>2</sub> catalysts supported on Al and Zr pillared clays in a hydrotreatment reaction, A preliminary study. *Applied Surface Science*, **240**, 48–62.
80. **Contin, A., A. Biffis, S. Sterchele, K. Dörmbach, S. Schipmann and A. Pich** (2014) Metal nanoparticles inside microgel/clay nanohybrids: Synthesis, characterization and catalytic efficiency in cross-coupling reactions. *Journal of Colloid and Interface Science*, **414**, 41–45.
81. **Cool, P. and E.F. Vansant** (1996) Preparation and characterization of zirconium pillared laponite and hectorite. *Microporous Material*, **6**, 27-36.
82. **Cool, P. and E.F. Vansant** (1998) Pillared clays: Preparation, characterization and applications. *Molecular Sieves*, **1**, 265-288.
83. **Cool, P., E. F. Vansant, G. Poncelet and R.A. Schoonheydt**, Layered structures and pillared layered structures. Pp 1250-1310 in **K. Sing, J. Weitkamp and F. Schuth** (eds) hand book of porous solids. Wiley-VCH, Germany, 2002.
84. **Coq, B. and F. Figueras** (2001) Bimetallic palladium catalysts: influence of the co-metal on the catalyst performance. *Journal of Molecular Catalysis A: Chemical*, **173**, 117–134.
85. **Costa, F., C.J.R. Silva, M.M.M. Raposo, A.M. Fonseca, I.C. Neves, A.P. Carvalho and J. Pires** (2004) Synthesis and immobilization of molybdenum complexes in a pillared layered clay. *Microporous and Mesoporous Materials*, **72**, 111–118.
86. **Cristovan, F.H., C.M. Nascimento, M.J.V. Bell, E. Laureto, J.L. Duarte, I.F.L. Dias, W.O. Cruz and A. Marletta** (2006) Synthesis and optical characterization of poly(styrene sulfonate) films doped with Nd(III). *Chemical Physics*, **326**, 514–520.
87. **D'Souza, L., M. Noeske, R.M. Richards and U. Kortz** (2013) Polyoxotungstate stabilized palladium, gold, and silver nanoclusters: A study of cluster stability, catalysis, and effects of the stabilizing anions. *Journal of Colloid and Interface Science*, **394**, 157-165.
88. **Dabiri, M., M. Baghbanzadeh and E. Arzroomchilar** (2008) 1-Methylimidazolium trifluoroacetate ([Hmim]TFA): An efficient reusable acidic ionic liquid for the synthesis of 1,8-dioxo-octahydroxanthenes and 1,8-dioxo-decahydroacridines. *Catalysis Communications*, **9**, 939-942.

89. **Dadhania, A.N., V.K. Patel and D.K. Raval** (2012) Catalyst-free sonochemical synthesis of 1,8-dioxo-octahydroxanthene derivatives in carboxy functionalized ionic liquid. *Comptes Rendus Chimie*, **15**, 378–383.
90. **Dandia, A., A.K. Jain and S. Sharma** (2012) Indium triflate catalyzed one-pot multicomponent synthesis of spiro-hexahydropyrimidines explained by multiple covalent bond formation. *Tetrahedron Letters*, **53**, 5270–5274.
91. **Dar, B.A., A. Chakraborty, P.R. Sharma, V. Shrivastava, A. Bhowmik, D. Vyas, P. Bhatti, M. Sharma and B. Singh** (2013) Grinding-induced rapid, convenient and solvent free approach for the one pot synthesis of  $\alpha$ -aminophosphonates using aluminium pillared interlayered clay catalyst. *Journal of Industrial and Engineering Chemistry*, **19**, 732–738.
92. **Datta, B. and M.A. Pasha** (2011) Silica Sulfuric Acid: An Efficient Heterogeneous Catalyst for the One-Pot Synthesis of 1, 4-Dihydropyridines under Mild and Solvent-Free Conditions. *Chinese Journal of Catalysis*, **32**, 1180–1184.
93. **Debache, A., W. Ghalem, R. Boulcina, A. Belfaitah, S. Rhouati and B. Carboni** (2009) An efficient one-step synthesis of 1,4-dihydropyridines via a triphenylphosphine catalyzed three-component Hantzsch reaction under mild conditions. *Tetrahedron Letters*, **50**, 5248–5250.
94. **Di'az, E., J.A. Casas, A'F. Mohedano, L. Calvo, M.A. Gilarranz and J.J. Rodríguez** (2008) Kinetics of the hydrodechlorination of 4-Chlorophenol in water using Pd, Pt, and Rh/Al<sub>2</sub>O<sub>3</sub> catalysts. *Industrial & Engineering Chemistry Research*, **47**, 3840–3846.
95. **Drljaca, A., J.R. Anderson, L. Spiccia and T.W. Turney** (1997) A new method for generating chromium(III) intercalated clays. *Inorganica Chimica Acta*, **256**, 151–154.
96. **Dubbin, W.E. and T.B. Goh** (1999) Permanganate-mediated dissolution of hydroxy-Cr interlayers from montmorillonite. *Applied Clay Science*, **15**, 381–392.
97. **Dultz, S., and B. Riebe** (2012) Organic cation exchanged montmorillonite and vermiculite as adsorbents for Cr(VI): Effect of layer charge on adsorption properties. *Applied Clay Science*, **67–68**, 125–133.
98. **Duong, L., T. Bostrom, T. Kloprogge and R. Frost** (2005) The distribution of Ga in Ga-pillared montmorillonites: A transmission electron microscopy and microanalysis study. *Microporous and Mesoporous Materials*, **82**, 165–172.
99. **Dutta, A., A. K. Patra and A. Bhaumik** (2012) Porous organic–inorganic hybrid nickel phosphonate: Adsorption and catalytic applications. *Microporous and Mesoporous Materials*, **155**, 208–214.
100. **Elkhalifah, A.E.I., S. Maitra, M.A. Bustam and T. Murugesan** (2013) Effects of exchanged ammonium cations on structure characteristics and CO<sub>2</sub> adsorption capacities of bentonite clay. *Applied Clay Science*, **83–84**, 391–398.
101. **Fang, D., J.M. Yang and Z.L. Liu** (2011) Eco-friendly synthesis of 1,8-dioxo-octahydroxanthenes catalyzed by ionic liquid in aqueous media. *Journal of Heterocyclic Chemistry*, **48**, 468–472.
102. **Farfan-Torres, E.M., E. Sham and P. Grange** (1992) Pillared clays: preparation and characterization of zirconium pillared montmorillonite. *Catalysis Today*, **15**, 515–526.

103. **Fatimah, I., D. Rubiyanto and T. Huda** (2014) Effect of sulfation on zirconia-pillared montmorillonite to the catalytic activity in microwave-assisted citronellal conversion. *International Journal of Chemical Engineering*, <http://dx.doi.org/10.1155/2014/950190>.
104. **Fetter, G., V. Herná'ndez, V. Rodri'guez, M.A. Valenzuela, V.H. Lara and P. Bosch** (2003) Effect of microwave irradiation time on the synthesis of zirconia-pillared clays. *Materials Letters*, **57**, 1220–1223.
105. **Figueiredo, F.C.A., E. Jordao and W.A. Carvalho** (2008) Adipic ester hydrogenation catalyzed by platinum supported in alumina, titania and pillared clays. *Applied Catalysis A: General*, **351**, 259–266.
106. **Figueiredo, F.C.A., E. Jordao, R. Landers and W.A. Carvalho** (2009) Acidity control of ruthenium pillared clay and its application as a catalyst in hydrogenation reactions. *Applied Catalysis A: General*, **371**, 131–141.
107. **Figueras, F.** (1988) Pillared clays as catalysts. *Catalysis Review Science and Engineering*, **30**, 457–499.
108. **Fontana, J., C. Vignado, E. Jordao, F.C.A. Figueiredo and W.A. Carvalho** (2011) Evaluation of some supports to RuSn catalysts applied to dimethyl adipate hydrogenation. *Catalysis Today*, **172**, 27–33.
109. **Fraser, A.R. and J.D. Russell** (1969) A spectrophotometric method for determination of cation-exchange capacity of clay minerals. *Clay Minerals*, **8**, 229–230.
110. **Frenkel, M.** (1974) Surface acidity of montmorillonites. *Clays Clay Minerals*, **22**, 435–441.
111. **Fripiat, J.J.** (1988) High resolution solid state NMR study of pillared clays, *Catalysis Today*, **2**, 281–295.
112. **Fripiat, J.J., A.N. Jelli, G. Poncelet and J. Andre** (1965) Thermodynamic properties of adsorbed water molecules and electrical conduction in montmorillonites and silicas. *Journal of Physical Chemistry*, **69**, 2185–2197.
113. **Galeano, L.A., A. Gil and M.A. Vicente** (2010) Effect of the atomic active metal ratio in Al/Fe-, Al/Cu- and Al/(Fe–Cu)-intercalating solutions on the physicochemical properties and catalytic activity of pillared clays in the CWPO of methyl orange. *Applied Catalysis B: Environmental*, **100**, 271–281.
114. **Gallo, J.M.R., S. Teixeira and U. Schuchardt** (2006) Synthesis and characterization of niobium modified montmorillonite and its use in the acid-catalyzed synthesis of  $\beta$ -hydroxyethers. *Applied Catalysis A: General*, **311**, 199–203.
115. **Gampine, A. and D.P. Eyman** (1998) Catalytic hydrodechlorination of chlorocarbons. 2. ternary oxide supports for catalytic conversions of 1,2-Dichlorobenzene. *Journal of Catalysis*, **179**, 315–325.
116. **Gandia, L.M., M.A. Vicente and A. Gil** (2002) Complete oxidation of acetone over manganese oxide catalysts supported on alumina- and zirconia-pillared clays. *Applied Catalysis B: Environmental*, **38**, 295–307.
117. **Gao, X., J.L.G. Fierro and I.E. Wachs** (1999) structural characteristics and catalytic properties of highly dispersed ZrO<sub>2</sub>/SiO<sub>2</sub> and V<sub>2</sub>O<sub>5</sub>/ZrO<sub>2</sub>/SiO<sub>2</sub> catalysts. *Langmuir*, **15**, 3169–3178.

118. **Garrido-Ramirez, E.G., M.V. Sivaiah, J. Barrault, S. Valange, B.K.G. Theng, M.S. U.-Zañartu and M. de la Luz Mora** (2012) Catalytic wet peroxide oxidation of phenol over iron or copper oxide-supported allophane clay materials: Influence of catalyst SiO<sub>2</sub>/Al<sub>2</sub>O<sub>3</sub> ratio. *Microporous and Mesoporous Materials*, **162**, 189–198.
119. **Gaudio, A.C., A. Korolkovas and Y. Takahata** (1994) Quantitative structure–activity relationships for 1,4-dihydropyridine calcium channel antagonists (nifedipine analogues): a quantum chemical/classical approach. *Journal of Pharmaceutical Sciences*, **83**, 1110–1115.
120. **Gil, A. and M. Montes** (1997) Metathesis of propane on molybdenum-aluminum pillared montmorillonite. *Industrial and Engineering Chemistry Research*, **36**, 1431-1443.
121. **Gil, A., F.C.C. Assis, S. Albeniz and S.A. Korili** (2011) Removal of dyes from wastewaters by adsorption on pillared clays. *Chemical Engineering Journal*, **168**, 1032–1040.
122. **Gil, A., L.M. Gandia and M.A. Vicente** (2000a) Recent advances in the synthetic and catalytic applications of pillared clays. *Catalysis Reviews Science and Engineering*, **42**, 145-212.
123. **Gil, A., M.A. Vicente and L.M. Gandia** (2000b) Main factors controlling the texture of zirconia and alumina pillared clays. *Microporous and Mesoporous Materials*, **34**, 115-125.
124. **Gil, A., M.A. Vicente and S.A. Korili** (2006) Effect of the nature and structure of pillared clays in the catalytic behaviour of supported manganese oxide. *Catalysis Today*, **112**, 117–120.
125. **Gil, A., M.A. Vicente, J.-F. Lambert and L.M. Gandia** (2001) Platinum catalysts supported on Al-pillared clays application to the catalytic combustion of acetone and methyl-ethyl-ketone. *Catalysis Today*, **68**, 41–51.
126. **Gil, A., S. A. Korili and M. A. Vicente** (2008) Recent advances in the control and characterization of the porous structure of pillared clay catalysts. *Catalysis Reviews*, **50**, 153-221.
127. **Gil, A., R. Trujillano, M.A. Vicente and S.A. Korili** (2009) Hydrogen adsorption by microporous materials based on alumina-pillared clays. *International Journal of Hydrogen Energy*, **34**, 8611–8615.
128. **Gil, A., S.A. Korili, R. Trujillano, M.A. Vicente**, (Eds.), (2010). Pillared clays and related catalysts. Springer, New York, p:43-63.
129. **Golubina, E.V., E.S. Lokteva, V.V. Lunin, N.S. Telegina, A.Yu. Stakheev and P. Tundo** (2006) The role of Fe addition on the activity of Pd-containing catalysts in multiphase hydrodechlorination. *Applied Catalysis A: General*, **302**, 32–41.
130. **Gonçalves, V.L.C., R.C. Rodrigues, R. Lorençato and C.J.A. Mota** (2007) Assessing the acid strength of solid acid catalysts with the use of linear free energy relationship: H/D exchange with substituted benzene derivatives. *Journal of Catalysis*, **248**, 158–164.
131. **Gopinath, R., N. Seshu Babu, J.V. Kumar, N. Lingaiah and P.S. Sai Prasad** (2008) Influence of Pd precursor and method of preparation on hydrodechlorination activity of alumina supported palladium catalysts. *Catalysis Letters*, **120**, 312–319.
132. **Gregg, S. J. and K. S. W. Sing** Adsorption, surface area and porosity (Academic Press, London, 1982).

133. **Gregori, M., P. Benito, G. Fornasari, M. Migani, S. Millefanti, F. Ospitali and S. Albonetti** (2014) Preparation of Pd/Cu MCM-41 catalysts for hydrodechlorination: Influence of the synthesis procedure. *Microporous and Mesoporous Materials*, **190**, 1–9.
134. **Grieken, R.v, J.M. Escola, J. Moreno and R. Rodríguez** (2009) Direct synthesis of mesoporous M-SBA-15 (M = Al, Fe, B, Cr) and application to 1-hexene oligomerization, *Chemical Engineering Journal*, Volume **155**, 442-450.
135. **Guerra, D.L., C. Airoidi, V.P. Lemos and R.S. Angélica** (2008) Adsorptive, thermodynamic and kinetic performances of Al/Ti and Al/Zr-pillared clays from the Brazilian Amazon region for zinc cation removal. *Journal of Hazardous Materials*, **155**, 230–242.
136. **Guerra, S.R., R.A.S. San Gil and L.C. Dieguez** (2008) Alkylation of benzene with olefins in the presence of zirconium-pillared clays. *Catalysis Today* **133–135**, 223–230.
137. **Guiu, G., A. Gil, M. Montes and P. Grange** (1997) Tantalum pillared montmorillonite I. Synthesis and physicochemical characterization. *Journal of Catalysis*, **168**, 450-462.
138. **Guo, Y., G. Li, C.-W Zhao, Q. Zhao, J. Wang and Z. Luan** (2009). High-concentration  $\epsilon$ -Al<sub>13</sub> nanoclusters sol prepared by chemical synthesis and membrane distillation concentration process. *Separation & Purification Technology*, **69**, 221–223.
139. **Gyftopoulou, M.E., M. Millan, A.V. Bridgwater, D. Dugwell, R. Kandiyoti and J.A. Hriljac** (2005) Pillared clays as catalysts for hydrocracking of heavy liquid fuels. *Applied Catalysis A: General*, **282**, 205–214.
140. **Hachemaoui, A. and M. Belbachir** (2005) Ring-opening polymerization of lactones catalyzed by ion-exchanged clay montmorillonite and the application to well-defined block copolymer synthesis with seven-membered cyclic carbonate. *Materials Letters*, **59**, 3904 – 3908.
141. **Hadjltaief, H.B., P.D. Costa, M.E. Galvez, and M.B. Zina** (2013) Influence of operational parameters in the heterogeneous photo- fenton discoloration of wastewaters in the presence of an iron- pillared clay. *Industrial & Engineering Chemistry Research*, **52**, 16656–16665.
142. **Han, S.W., Y. Kim and K. Kim** (1998) Dodecanethiol-derivatized Au/Ag bimetallic nanoparticles:TEM, UV/VIS, XPS, and FTIR analysis. *Journal of Colloid and Interface Science*, **208**, 272–278.
143. **Hao, Z., H.Y. Zhu and G.Q. Lu** (2003) Zr-Laponite pillared clay-based nickel catalysts for methane reforming with carbon dioxide. *Applied Catalysis A: General*, **242**, 275–286.
144. **Hasaninejad A., M. Dadar and A. Zare** (2012) Silica-supported phosphorus-containing catalysts efficiently promoted synthesis of 1,8-dioxo-octahydroxanthenes under solvent-free conditions. *Chemical Science Transactions*, **1**, 233-238.
145. **Hassan, S.A., F.Z. Yehia, H.A. Hassan, S.A. Sadek and A.S. Darwish** (2010) Various characteristics and catalytic performance of iron (II) phthalocyanine immobilized onto titania- and vanadia-pillared bentonite clay in in situ polymerization of methyl methacrylate An attempt to synthesize novel polymer/iron phthalocyanine/pillared clay nanocomposites. *Journal of Molecular Catalysis A: Chemical*, **332**, 93–105.
146. **Hayashi, E., E. Iwamatsu, M. E. Biswas, Y. Sanada, S. Ahmed, H. Hamid and T. Yoneda** (1999) Characterization of high surface area smectite supported cobalt oxides catalysts for hydrodesulfurization by means of TPR, TPS and ESR. *Applied Catalysis A: General*, **179**, 203-216.

147. **He, F.A. and L.M. Zhang** (2007) New polyethylene nanocomposites prepared by in-situ polymerization method using nickel a-diimine catalyst supported on organo-modified ZnAl layered double hydroxide. *Composites Science and Technology*, **67**, 3226–3232.
148. **He, H.P., J.G. Guo, X.D. Xie and J.L. Peng** (2001) Location and migration of cations in Cu<sup>2+</sup>-adsorbed montmorillonite. *Environment International*. **26**, 347–352.
149. **Heinrichs, B., J. P. Schoebrechts and J.P. Pirard**, Palladium–silver sol–gel catalysts for selective hydrodechlorination of 1,2-dichloroethane into ethylene: III. kinetics and reaction mechanism, *Journal of Catalysis*, **200**, (2001) 309–320.
150. **Herney-Ramirez, J., M.A. Vicente and L.M. Madeira** (2010) Heterogeneous photo-Fenton oxidation with pillared clay-based catalysts for wastewater treatment: A review. *Applied Catalysis B: Environmental*, **98**, 10–26
151. **Hetzer, M. and D. De Kee** (2008) Wood/polymer/nanoclay composites, environmentally friendly sustainable technology: A review. *Chemical Engineering Research and Design*, **86**, 1083–1093.
152. **Hoke, J. B., G.A. Gramiccioni and E.N. Balko** (1992) Catalytic hydrodechlorination of chlorophenols. *Applied Catalysis B: Environmental*, **1**, 285-296.
153. **Hsu, S.L.C. and K.C. Chang** (2002) Synthesis and properties of polybenzoxazole-clay nanocomposites. *Polymer*, **43**, 4097-4101.
154. **Hu, C., T. Peng, X. Hu, Y. Nie, X. Zhou, J. Qu and H. He** (2010) Plasmon-induced photodegradation of toxic pollutants with Ag-AgI/Al<sub>2</sub>O<sub>3</sub> under visible-light irradiation. *Journal of the American Chemical Society*, **132**, 857–862.
155. **Hutson, N.D., M.J. Hoekstra and R.T. Yang** (1999) Control of microporosity of Al<sub>2</sub>O<sub>3</sub>-pillared clays: effect of pH, calcination temperature and clay cation exchange capacity. *Microporous and Mesoporous Materials*, **28**, 447–459.
156. **Issaadi, R. and F. Garin** (2003) Catalytic behaviour of acid catalysts supported palladium: use of Al and Zr-pillared montmorillonite as supports Part II: kinetic study. *Applied Catalysis A: General*, **243**, 367–377.
157. **Issaadi, R., F. Garin and C.-E. Chitour** (2006) Study of the acid character of some palladium-modified pillared clay catalysts: Use of isopropanol decomposition as test reaction. *Catalysis Today*, **113**, 166–173.
158. **Itoh, K., T. Aoyama, H. Satoh, Y. Fujii, H. Sakamaki, T. Takido and M. Kodomari** (2011) Application of silica gel-supported polyphosphoric acid (PPA/SiO<sub>2</sub>) as a reusable solid acid catalyst to the synthesis of 3-benzoylisoxazoles and isoxazolines. *Tetrahedron Letters*, **52**, 6892–6895.
159. **Jagtap, N. and V. Ramaswamy** (2006) Oxidation of aniline over titania pillared montmorillonite clays. *Applied Clay Science*, **33**, 89–98.
160. **Jalil, M.E.R., M. Baschini, E. Rodríguez-Castellón, A. Infantes-Molina and K. Sapag** (2014) Effect of the Al/clay ratio on the thiabendazol removal by aluminium pillared clays. *Applied Clay Science*, **87**, 245–253.



161. **Jameson, R.F.** (1959) The composition of the “strong” phosphoric acids. *Journal of the Chemical Society*, **2**, 752–759.
162. **Jana, S., M.K. Purkait and K. Mohanty** (2011) Clay supported polyvinyl acetate coated composite membrane by modified dip coating method: Application for the purification of lysozyme from chicken egg white. *Journal of Membrane Science*, **382**, 243–251.
163. **Janati, F., M.M. Heravi and A. Mirshokraie** (2013) Superparamagnetic Iron Oxide as an Efficient Catalyst for the One-Pot, Solvent-Free Synthesis of 5,5-Disubstituted Hexahydropyrimidines and Their Spiro Analogues. *Journal of Chemistry*, <http://dx.doi.org/10.1155/2013/214617>.
164. **Jerónimo, D., J.M. Guil, B.M. Corbella, H. Vasques, A. Miranda, J.M. Silva, A. Lobato, J. Pires and A.P. Carvalho** (2007). Acidity characterization of pillared clays through microcalorimetric measurements and catalytic ethylbenzene test reaction. *Applied Catalysis A: General*, **330**, 89–95.
165. **Jha, A. and J. Beal** (2004) Convenient synthesis of 12H-benzo[a]xanthenes from 2-tetralone. *Tetrahedron Letters*, **45**, 8999–9001.
166. **Jha, A., A.C. Garade, M. Shirai and C.V. Rode** (2013) Metal cation-exchanged montmorillonite clay as catalysts for hydroxyalkylation reaction. *Applied Clay Science*, **74**, 141–146.
167. **Jiang, T., Y. Zhou, S. Liang, H. Liu and B. Han** (2009) Hydrogenolysis of glycerol catalyzed by Ru-Cu bimetallic catalysts supported on clay with the aid of ionic liquids. *Green Chemistry*, **11**, 1000–1006.
168. **Jibril, B.Y.** (2004) Propane oxidative dehydrogenation over chromium oxide-based catalysts. *Applied Catalysis A: General*, **264**, 193–202.
169. **Jinjun, L., J. Zheng, H. Zhengping, X. Xiuyan and Z. Yahui** (2005) Pillared laponite clays-supported palladium catalysts for the complete oxidation of benzene. *Journal of Molecular Catalysis A: Chemical*, **225**, 173–179.
170. **Jujjuri, S., E. Ding, E.L. Hommel, S.G. Shore and M.A. Keane** (2006) Synthesis and characterization of novel silica-supported Pd/Yb bimetallic catalysts: Application in gas-phase hydrodechlorination and hydrogenation. *Journal of Catalysis*, **239**, 486–500.
171. **Juszczyk, W., A. Malinowski, M. Bonarowska and Z. Karpinski** (1997) Hydrodechlorination of CF<sub>2</sub>Cl<sub>2</sub> (CFC-12) on Pd/Al<sub>2</sub>O<sub>3</sub> catalysts. *Polish Journal of Chemistry*, **71**, 1314–1320.
172. **Kalbasi, R.J. and N. Mosaddegh** (2011) Synthesis and characterization of poly(4-vinylpyridine)/MCM-48 catalyst for one-pot synthesis of substituted 4H-chromenes. *Catalysis Communications*, **12**, 1231–1237.
173. **Kalbasi, R.J. and N. Mosaddegh** (2012) Palladium nanoparticles supported on poly(2-hydroxyethyl methacrylate)/KIT-6 composite as an efficient and reusable catalyst for Suzuki–Miyaura reaction in water. *Journal of Inorganic and Organometallic Polymers and Materials*, **22**, 404–414.
174. **Kanda, Y., H. Iwamoto, T. Kobayashi, Y. Uemichi and M. Sugioka** (2009) Preparation of highly active alumina-pillared clay montmorillonite-supported platinum catalyst for hydrodesulfurization. *Topics in Catalysis*, **52**, 765–771.

175. **Kantevari, S., R. Bantu and L. Nagarapu** (2007) HClO<sub>4</sub>-SiO<sub>2</sub> and PPA-SiO<sub>2</sub> catalyzed efficient one-pot Knoevenagel condensation, Michael addition and cyclo-dehydration of dimedone and aldehydes in acetonitrile, aqueous and solvent free conditions: Scope and limitations. *Journal of Molecular Catalysis A: Chemical*, **269**, 53-57.
176. **Karthikeyana, G. and A. Pandurangana** (2009) Heteropolyacid (H<sub>3</sub>PW<sub>12</sub>O<sub>40</sub>) supported MCM-41: An efficient solid acid catalyst for the green synthesis of xanthenedione derivatives. *Journal of Molecular Catalysis A: Chemical*, **311**, 36-45.
177. **Katdare, S.P., V. Ramaswamy and A.V. Ramaswamy** (2000) Factors affecting the preparation of alumina pillared montmorillonite employing ultrasonics. *Microporous and Mesoporous Materials*, **37**, 329-336.
178. **Keane, M.A. and D.Y. Murzin** (2001) A kinetic treatment of the gas phase hydrodechlorination of chlorobenzene over nickel/silica: beyond conventional kinetics. *Chemical Engineering Science*, **56**, 3185-3195.
179. **Khan, A.T., M. Lal and Md. M. Khan** (2010a) Synthesis of highly functionalized piperidines by one-pot multicomponent reaction using tetrabutylammonium tribromide (TBATB). *Tetrahedron Letters*, **51**, 4419-4424.
180. **Khan, A.T., Md. M. Khan and K.K.R. Bannuru** (2010b) Iodine catalyzed one-pot five-component reactions for direct synthesis of densely functionalized piperidines. *Tetrahedron*, **66**, 7762-7772.
181. **Khan, A.T., T. Parvin and L.H. Choudhury** (2008) Effects of substituents in the β-position of 1,3-dicarbonyl compounds in bromodimethylsulfonium bromide-catalyzed multicomponent reactions: A facile access to functionalized piperidines. *The Journal of Organic Chemistry*, **73**, 8398-8402.
182. **Khenkin, A.M. and R. Neumann** (2002) Oxygen transfer from sulfoxides: selective oxidation of alcohols catalyzed by polyoxomolybdates. *Journal of Organic Chemistry*, **67**, 7075-7079.
183. **Khenkin, A.M., R. Weiner and L. Neumann** (2005) Selective ortho hydroxylation of nitrobenzene with molecular oxygen catalyzed by the H<sub>5</sub>PV<sub>2</sub>Mo<sub>10</sub>O<sub>40</sub> polyoxometalate *Journal of the American Chemical Society*, **127**, 9988-9989.
184. **Khojastehnezhad, A., F. Moeinpour and A. Davoodnia** (2011) PPA-SiO<sub>2</sub> catalyzed efficient synthesis of polyhydroquinoline derivatives through Hantzsch multicomponent condensation under solvent-free conditions. *Chinese Chemical Letters*, **22**, 807-810.
185. **Kim T. W., S.-J. H., S. H. Jung, J.-S. Chang, H. Park, W Choi and J.-H. Choy** (2008) Bifunctional heterogeneous catalysts for selective epoxidation and visible light driven photolysis: Nickel oxide-containing porous nanocomposite. *Advanced Materials*, **20**, 539-542.
186. **Kim, S.-C. and D.-K. Lee** (2004) Preparation of Al-Cu pillared clay catalysts for the catalytic wet oxidation of reactive dyes. *Catalysis Today*, **97**, 153-158.
187. **Kirksi, I., A. Molnar, I. Palinko, A. Fudala and J. B. Nagy** (1997) Nanoscale redox catalysts: Cr- and Cr, Al-pillared layer clays: Characterization and catalytic activity *Solid State Ionics*, **101-103**, 793-797.
188. **Kishore Kumar, G.D. and S. Bhaskaran** (2005) A Facile, Catalytic, and Environmentally Benign Method for Selective Deprotection of tert-Butyldimethylsilyl Ether Mediated by

- Phosphomolybdic Acid Supported on Silica Gel. *The Journal of Organic Chemistry*, **70**, 4520-4523.
189. **Kloprogge, J.T.** (1998) Synthesis of smectites and porous pillared clay catalysts: A review. *Journal of Porous Materials*, **5**, 5–41.
  190. **Kloprogge, J.T., L.V. Duong and R.L. Frost** (2005) A review of the synthesis and characterization of pillared clays and related porous materials for cracking of vegetable oils to produce biofuels. *Environmental Geology*, **47**, 967–981.
  191. **Komadel, P. and J. Madejova** (2006) Chapter 7.1 Acid activation of clay minerals Handbook of Clay Science. Edited by F. Bergaya, B.K.G. Theng and G. Lagaly, *Developments in Clay Science*, **1**, 263-288.
  192. **Kooli, F., J. Bovey and W. Jones** (1997) Dependence of the properties of titanium-pillared clays on the host matrix: a comparison of montmorillonite, saponite and rectorite pillared materials. *Journal of Material Chemistry*, **7**, 153-158.
  193. **Kovenklioglu, S., Z. Cao, D. Shah, R. J. Farrauto and E. N. Balko** (1992). Direct catalytic hydrodechlorination of toxic organics in wastewater. *AIChE Journal*, **38**, 1003-1012.
  194. **Kozhevnikov I.V.**, (2009) Heterogeneous acid catalysis by heteropoly acids: Approaches to catalyst deactivation. *Journal of Molecular Catalysis A: Chemical*, **305**, Pages 104-111.
  195. **Kozhevnikov, I.V.** (1998) Catalysis by heteropoly acids and multicomponent polyoxometalates in liquid-phase reactions. *Chemical Reviews*, **98**, 171–198.
  196. **Kumar, A., S. Sharma, R.A. Maurya and J. Sarkar** (2010) Diversity oriented synthesis of benzoxanthene and benzochromene libraries via one-pot, three-component reactions and their anti-proliferative activity. *Journal of Combinatorial Chemistry*, **12**, 20–24.
  197. **Lee, J., J. C. Park and H. Song** (2008) A nanoreactor framework of a Au/SiO<sub>2</sub> yolk/shell structure for catalytic reduction of p-Nitrophenol. *Advanced Materials*, **20**, 1523–1528.
  198. **Lenarda, M., R. Ganzerla, L. Storaro, A. Trovarelli, R. Zannoni and J. Kaspar**, Vapour phase hydroformylation of ethylene and propene catalyzed by a rhodium-containing aluminum pillared smectite clay. *Journal of Molecular Catalysis*, **72**, (1992) 75-84.
  199. **León, M.A.D., C.D.L. Santos, L. Latrónica, A.M. Cesio, C. Volzone, J. Castiglioni and M. Sergio** (2014) High catalytic activity at low temperature in oxidative dehydrogenation of propane with Cr–Al pillared clay. *Chemical Engineering Journal*, **241**, 336–343.
  200. **Letar'ef, S., B. Casal, P. Aranda, M.A. Martí'n-Luengo and E. Ruiz-Hitzky** (2003) Fe-containing pillared clay catalysts phenol hydroxylation. *Applied Clay Science*, **22**, 263 – 277.
  201. **Li, B., H. Yuan and Y. Zhang** (2013) Transparent PMMA-based nanocomposite using electrospun graphene-incorporated PA-6 nanofibers as the reinforcement. *Composites Science and Technology*, **89**, 134–141.
  202. **Li, B., Z. Liu, J. Liu, Z. Zhou, X. Gao, X. Pang and H. Sheng** (2011) Preparation, characterization and application in deep catalytic ODS of mesoporous silica pillared clay incorporated with phosphotungstic acid. *Journal of Colloid & Interface Science*, **362**, 450–456.

203. **Li, M., Z. Feng, G. Xiong, P. Ying, Q. Xin and C. Li** (2001) Phase transformation in the surface region of zirconia detected by UV Raman spectroscopy, *Journal of Physical Chemistry B*, **105**, 8107-8111.
204. **Li, N., J.-G. Wang, J.-X. Xu, J.-Y. Liu, H.-J. Zhou, P.-C. Sun and T.-H. Chen** (2012) Synthesis of hydrothermally stable, hierarchically mesoporous aluminosilicate Al-SBA-1 and their catalytic properties. *Nanoscale*, **4**, 2150–2156.
205. **Liao, B., M. Song, H. Liang and Y. Pang** (2001) Polymer-layered silicate nanocomposites. 1. A study of poly(ethylene oxide)/Na<sup>+</sup>-montmorillonite nanocomposites as fillers for reinforcement of polyethylene. *Polymer*, **42**, 10007-10011.
206. **Litvic, M.F., M. Litvic and V. Vinkovic** (2008) An efficient, metal-free, room temperature aromatization of Hantzsch-1,4-dihydropyridines with urea–hydrogen peroxide adduct, catalysed by molecular iodine. *Tetrahedron*, **64**, 5649–5656.
207. **Liu, C., T. Tang, D. Wang and B. Huang** (2003) In situ ethylene homopolymerization and copolymerization catalyzed by zirconocene catalysts entrapped inside functionalized montmorillonite. *Journal of Polymer Science Part A: Polymer Chemistry*, **41**, 2187–2196.
208. **Liu, D., P. Yuan, H. Liu, J. Cai, D. Tan, H. He, J. Zhu and T. Chen** (2013) Quantitative characterization of the solid acidity of montmorillonite using combined FTIR and TPD based on the NH<sub>3</sub> adsorption system. *Applied Clay Science*, **80–81**, 407–412.
209. **Liu, D., P. Yuan, H. Liu, J. Cai, Z. Qin, D. Tan, Q. Zhou, H. He and J. Zhu** (2011) Influence of heating on the solid acidity of montmorillonite: A combined study by DRIFT and Hammett indicators. *Applied Clay Science*, **52**, 358–363.
210. **Liu, R., Y. Shi, Y. Wan, Y. Meng, F. Zhang, D. Gu, Z. Chen, B. Tu, and D. Zhao** (2006) Triconstituent co-assembly to ordered mesostructured polymer-silica and carbon-silica nanocomposites and large-pore mesoporous carbons with high surface areas. *Journal of the American Chemical Society*, **128**, 11652-11662.
211. **Liu, X., J. Cheng, M. Sprik, X. Lu and R. Wang** (2014) Surface acidity of 2:1-type dioctahedral clay minerals from first principles molecular dynamics simulations. *Geochimica et Cosmochimica Acta*, **140**, 410–417.
212. **Liu, Y., L. Xu, B. Xu, Z. Li, L. Jia and W. Guo** (2009) Toluene alkylation with 1-octene over supported heteropoly acids on MCM-41 catalysts. *Journal of Molecular Catalysis A: Chemical*, **297**, 86–92.
213. **Long, R.Q. and R.T. Yang** (2000) The promoting role of rare earth oxides on Fe-exchanged TiO<sub>2</sub>-pillared clay for selective catalytic reduction of nitric oxide by alumina. *Applied Catalysis B: Environmental*, **27**, 87-95.
214. **Lopez, A.J.-, J.M.-Rodriguez, P.O.-Pastor, P.M.-Torres and E.R.-Castellon** (1993) Pillared clays prepared from the reaction of chromium acetate with montmorillonite. *Clays and Clay Minerals*, **41**, 328-334.
215. **López, E.F., V.S. Escribano, M. Panizza, M.M. Carnascialic and G. Busca** (2001) Vibrational and electronic spectroscopic properties of zirconia powders. *Journal of Materials Chemistry*, **11**, 1891-1897.
216. **Louloudi, A., J. Michalopoulos, N.-H. Gangas and N. Papayannakos** (2003) Hydrogenation of benzene on Ni/Al-pillared saponite catalysts. *Applied Catalysis A: General*, **242**, 41-49.

217. **Ma, X., F. Xu, L. Chen, Z. Zhang, Y. Du and Y. Xie** (2005) Magnetic fluids for synthesis of the stable adduct  $\gamma$ -Fe<sub>2</sub>O<sub>3</sub>/CTAB/Clay. *Journal of Crystal Growth*, **280**, 118–125.
218. **Maclennan, A., A. Banerjee and R. W. J. Scott**, Aerobic oxidation of  $\alpha$ - $\beta$  unsaturated alcohols using sequentially-grown AuPd nanoparticles in water and tetraalkylphosphonium ionic liquids. *Catalysis Today*, **207**, (2013) 170–179.
219. **Madhav, J.V., Y.T. Reddy, P.N. Reddy, M.N. Reddy, S. Kuarm, P.A. Crooks and B. Rajitha** (2009) Cellulose sulfuric acid: An efficient biodegradable and recyclable solid acid catalyst for the one-pot synthesis of aryl-14H-dibenzo[a,j]xanthenes under solvent-free conditions. *Journal of Molecular Catalysis A: Chemical*, **304**, 85–87.
220. **Mahdavinia, G. H., S. Rostamizadeh, A. M. Amani and Z. Emdadi** (2009) Ultrasound-promoted greener synthesis of aryl-14-H-dibenzo[a,j]xanthenes catalyzed by NH<sub>4</sub>H<sub>2</sub>PO<sub>4</sub>/SiO<sub>2</sub> in water. *Ultrasonics Sonochemistry*, **16**, 7-10.
221. **Marín-Astorga, N., G. Alvez-Manoli and P. Reyes** (2005) Stereoselective hydrogenation of phenyl alkyl acetylenes on pillared clays supported palladium catalysts. *Journal of Molecular Catalysis A: Chemical*, **226**, 81–88.
222. **Mata, G., R. Trujillano, M.A. Vicente, C. Belver, M. Ferná'ndez-Garci'a, S.A. Korili and A. Gil** (2007) Chromium–saponite clay catalysts: Preparation, characterization and catalytic performance in propene oxidation. *Applied Catalysis A: General*, **327**, 1–12.
223. **Mata, G., R. Trujillano, M.A. Vicente, S.A. Korili, A. Gil, C. Belver, K.J. Ciuffi, E.J. Nassar, G.P. Ricci, A. Cestari and S. Nakagaki** (2009) (Z)-cyclooctene epoxidation and cyclohexane oxidation on Ni/alumina-pillared clay catalysts. *Microporous and Mesoporous Materials*, **124**, 218–226.
224. **M<sup>c</sup> Cabe, R.W.** Clay chemistry. *Inorganic Materials*, 2<sup>nd</sup> Edition, John Wiley and Sons, New York, 313-376, 1996.
225. **Meshram, H.M., P.B. Thakur, B. Madhu Babu and V.M. Bangade** (2012) A convenient, rapid, and general synthesis of  $\alpha$ -oxo thiocyanates using clay supported ammonium thiocyanate. *Tetrahedron Letters*, **53**, 1780–1785.
226. **Mignoni, M.L., J.V.M. Silva, M.O. Souza, R.S. Mauler, R.F. Souza and K.B. Gusmao** (2011) Polyethylene-montmorillonite nanocomposites obtained by in situ polymerization of ethylene with nickel-diimine catalysts. *Journal of Applied Polymer Science*, **122**, 2159–2165.
227. **Mirjalili, B. B. F., A. Bamoniri and A. Akbari** (2008) BF<sub>3</sub>SiO<sub>2</sub>: an efficient alternative for the synthesis of 14-aryl or alkyl-14H-dibenzo[a,j]xanthenes *Tetrahedron Letters*, **49**, 6454-6456.
228. **Mishra, B. G. and G. Ranga Rao** (2003) Influence of synthesis conditions and cerium incorporation on the properties of Zr-pillared clays. *Journal of Porous Materials*, **10**, 93–103.
229. **Mishra, B.G. and G. Ranga Rao** (2004) Physicochemical and catalytic properties of Zr-pillared montmorillonite with varying pillar density. *Microporous and Mesoporous Materials*, **70**, 43-50.
230. **Mishra, B.G. and G. Ranga Rao** (2005) Cerium containing Al- and Zr-pillared clays: Promoting effect of cerium (III) ions on structural and catalytic properties. *Journal of Porous Materials*, **12**, 171–181.

231. **Mishra, B.G., D. Kumar and V.S. Rao** (2006) H<sub>3</sub>PW<sub>12</sub>O<sub>40</sub> catalyzed synthesis of 3,4-dihydro pyrimidin-2(1H)-ones under solvent-free conditions *Catalysis Communications*, **7**, 457–459.
232. **Mishra, S. and R. Ghosh** (2011) Efficient one-pot synthesis of functionalized piperidine scaffolds via ZrOCl<sub>2</sub>.8H<sub>2</sub>O catalyzed tandem reactions of aromatic aldehydes with amines and acetoacetic esters. *Tetrahedron Letters*, **52**, 2857–2861.
233. **Mishra, T. and K. Parida** (1998) Transition metal pillared clay 4. A comparative study of textural, acidic and catalytic properties of chromia pillared montmorillonite and acid activated montmorillonite. *Applied Catalysis A: General* **166**,123-133.
234. **Mishra, T. and K.M. Parida** (2006) Effect of sulfate on the surface and catalytic properties of iron–chromium mixed oxide pillared clay. *Journal of Colloid and Interface Science*, **301**, 554–559.
235. **Mishra, T., K.M. Parida and S.B. Rao** (1996) Transition metal oxide pillared clay 1. A comparative study of textural and acidic properties of Fe(III) pillared montmorillonite and pillared acid activated montmorillonite. *Journal of Colloid and Interface Science*, **183**, 176-183.
236. **Misono M.**, (2013) Chapter 4 – Catalysis of Heteropoly Compounds (Polyoxometalates). *Studies in Surface Science and Catalysis*, **176**, Pages 97–155.
237. **Misra, M., S.K. Pandey, V.P. Pandey, J. Pandey, R. Tripathi and R.P.Tripathi** (2009) Organocatalyzed highly atom economic one pot synthesis of tetrahydropyridines as antimalarials. *Bioorganic & Medicinal Chemistry*, **17**, 625–633.
238. **Mitsudome, T., T. Matsuno, S. Sueoka, T. Mizugaki, K. Jitsukawa and K. Kaneda** (2012) Titanium cation-exchanged montmorillonite as an active heterogeneous catalyst for the Beckmann rearrangement under mild reaction condition. *Tetrahedron Letters*, **53**, 5211–5214.
239. **Mittal, V. and N.B. Matsko** (2012) Chapter 8 Morphology in organic–inorganic composites. In “Analytical Imaging Techniques for Soft Matter Characterization Engineering Materials”, Springer, 97-114.
240. **Mizuno, M. and M. Misono** (1998) Heterogeneous catalysis. *Chemical Reviews*, **98**, 199 -217.
241. **Mnasri, S. and N. Frini-Srasra** (2013) Synthesis, characterization and catalytic evaluation of Zirconia-pillared bentonite for 1,3-dioxalane synthesis. *Surface Engineering and Applied Electrochemistry*, **49**, 336–347.
242. **Mnasri-Ghnimi, S. and N. Frini-Srasra** (2014) Promoting effect of cerium on the characteristic and catalytic activity of Al, Zr, and Al–Zr pillared clay. *Applied Clay Science*, **88–89**, 214–220.
243. **Mohammadi, B., S.M.H. Jamkarani, T.A. Kamali, M. Nasrollahzadeh and A. Mohajeri** (2010) Sulfonic acid functionalized silica: a remarkably efficient heterogeneous reusable catalyst for the one pot synthesis of 1,4-dihydropyridines. *Turkish Journal of Chemistry*, **34**, 613–619.
244. **Mohite, A.R., P.R. Sultane and R.G. Bhat** (2012) BF<sub>3</sub>.Et<sub>2</sub>O and trifluoroacetic acid/triethyl amine-mediated synthesis of functionalized piperidines. *Tetrahedron Letters*, **53**, 30–35.

245. **Mojovic, Z., P. Bankovic, A. Milutinovic-Nikolic, J. Dostanic, N. Jovic-Jovicic and D. Jovanovic** (2009) Al, Cu-pillared clays as catalysts in environmental protection. *Chemical Engineering Journal*, **154**, 149–155.
246. **Mokaya, R. and W. Jones** (1995) Pillared clays and pillared acid-activated clays: A comparative study of physical, acidic and catalytic properties. *Journal of Catalysis*, **153**, 76-85.
247. **Molina, C. B., A. H. Pizarro, M. Gilarranz, J. Casas and J. J. Rodriguez** (2010) Hydrodechlorination of 4-chlorophenol in water using Rh–Al pillared clays. *Chemical Engineering Journal*, **160**, 578–585.
248. **Molina, C.B., A.H. Pizarro, J.A. Casas and J.J. Rodriguez** (2014) Aqueous-phase hydrodechlorination of chlorophenols with pillared clays-supported Pt, Pd and Rh catalysts. *Applied Catalysis B: Environmental*, **148–149**, 330–338.
249. **Molina, C.B., J.A. Casas, J.A. Zazo and J.J. Rodriguez** (2006) A comparison of Al-Fe and Zr-Fe pillared clays for catalytic wet peroxide oxidation. *Chemical Engineering Journal*, **118**, 29–35.
250. **Molina, C.B., L. Calvo, M.A. Gilarranz, J.A. Casas and J.J. Rodriguez** (2009a) Pd–Al pillared clays as catalysts for the hydrodechlorination of 4-chlorophenol in aqueous phase. *Journal of Hazardous Materials*, **172**, 214–223.
251. **Molina, C.B., L. Calvo, M. Gilarranz, J. Casas and J. J. Rodriguez** (2009b) Hydrodechlorination of 4-chlorophenol in aqueous phase with Pt–Al pillared clays using formic acid as hydrogen source. *Applied Clay Science*, **45**, 206–212.
252. **P. L. Brown, E. Curti, B. Grambow.** Chemical Thermodynamics of Zirconium, F. J. Mompeán, J. Perrone, M. Illemassène (Eds.), Elsevier, Volume 8, Amsterdam (2005).
253. **Moreno, S., R. Sun Kou, and G. Poncelet** (1997a) Influence of preparation variables on the structural, textural, and catalytic properties of Al-Pillared smectites. *The Journal of Physical Chemistry B*, **101**, 1569-1578.
254. **Moreno, S., E. Gutierrez, A. Alvarez, N.G. Papayannakos and G. Poncelet** (1997b) Al-pillared clays: from lab syntheses to pilot scale production Characterisation and catalytic properties. *Applied Catalysis A: General*, **165**, 103-114.
255. **Morikawa, Y.** (1992) Catalysis by metal ions intercalated in layer lattice silicates. *Advances in Catalysis*, **39**, 303-327.
256. **Moronta, A., M.E. Troconis, E. Gonzalez, C. Moran, J. Sanchez, A. Gonzalez and J. Quinonez** (2006) Dehydrogenation of ethylbenzene to styrene catalyzed by Co, Mo and CoMo catalysts supported on natural and aluminum-pillared clays Effect of the metal reduction. *Applied Catalysis A: General*, **310**, 199–204.
257. **Moronta, A., T. Oberto, G. Carruyo, R. Solano, J. Sanchez, E. Gonzalez and L. Huerta** (2008) Isomerization of 1-butene catalyzed by ion-exchanged, pillared and ion-exchanged/pillared clays. *Applied Catalysis A: General*, **334**, 173–178.
258. **Mortland, M.M., J.J. Fripiat, J. Chaussidon and J. Uytterhoeven** (1963) Interaction between ammonia and the expanding lattices of montmorillonite and vermiculite. *Journal of Physical Chemistry*, **67**, 248-258.
259. **Mott, C.J.B.** (1988) Clay minerals-an introduction. *Catalysis Today*, **2**, 199-208.

260. **Mrad, I., A. Ghorbel, D. Tichit and J.-F. Lambert** (1997) Optimisation of the preparation of an Al-pillared clay: thermal stability and surface acidity. *Applied Clay Science*, **12**, 349-364.
261. **Muha, G.M. and P.A. Vaughan** (1960) Structure of the complex ion in aqueous solutions of zirconyl and hafnyl oxyhalides. *Journal of Chemical Physics*, **33**, 194-199.
262. **Mukhopadhyay, C., S. Rana, R.J. Butcher and A.M. Schmiedekamp** (2011a) First report of syn isomers in the diastereoselective synthesis of highly functionalized piperidines catalysed by wet picric acid: factors influencing the syn-anti ratios. *Tetrahedron Letters*, **52**, 5835-5840.
263. **Mukhopadhyay, C., S. Rana and R.J. Butcher** (2011b) FeCl<sub>3</sub> catalysed two consecutive aminomethylation at  $\alpha$ -position of the  $\beta$ -dicarbonyl compounds: an easy access to hexahydropyrimidines and its spiro analogues. *Tetrahedron Letters*, **52**, 4153-4157.
264. **Mulakayala, N., P.V.N.S. Murthy, D. Rambabu, M. Aeluri, R. Adepu, G.R. Krishna, C.M. Reddy, K.R.S. Prasad, M. Chaitanya, C.S. Kumar, M.V.B. Rao and M. Pal** (2012) Catalysis by molecular iodine: A rapid synthesis of 1,8-dioxo-octahydroxanthenes and their evaluation as potential anticancer agents. *Bioorganic & Medicinal Chemistry Letters*, **22**, 2186-2191.
265. **Naik, M.A., S. Samantaray and B.G. Mishra** (2011) Phosphotungstic acid nanoclusters grafted onto high surface area hydrous zirconia as efficient heterogeneous catalyst for synthesis of octahydroquinazolinones and  $\beta$ -acetamido ketones. *Journal of Cluster Science*, **22**, 295-307.
266. **Nascimento, F.H. do and J.C. Masini** (2014) Influence of humic acid on adsorption of Hg(II) by vermiculite. *Journal of Environmental Management*, **143**, 1-7.
267. **Nethravathi, C., J.T. Rajamathi, P. George and M. Rajamathi** (2011) Synthesis and anion-exchange reactions of a new anionic clay, a-magnesium hydroxide. *Journal of Colloid and Interface Science*, **354**, 793-797.
268. **Norouzi, H., A. Davoodnia, M. Bakavoli, M. Zeinali-Dastmalbaf, N. Tavakoli-Hoseini, and M. Ebrahimi** (2011) Preparation, characterization and first application of alumina supported polyphosphoric acid (PPA/Al<sub>2</sub>O<sub>3</sub>) as a reusable catalyst for the synthesis of 14-Aryl-14H-dibenzo[a, j]xanthenes. *Bulletin of the Korean Chemical Society*, **32**, 2311- 2315.
269. **Nutt, M.O., K.N. Heck, P. Alvarez and M.S. Wong** (2006) Improved Pd-on-Au bimetallic nanoparticle catalysts for aqueous-phase trichloroethene hydrodechlorination. *Applied Catalysis B: Environmental*, **69**, 115-125.
270. **Occelli, M.L. and R.J. Rennard** (1988) Hydrotreating catalysts containing pillared clays. *Catalysis Today*, **2**, 309-319.
271. **Occelli, M.L., A. Auroux and G.J. Ray** (2000) Physicochemical characterization of a Texas montmorillonite pillared with polyoxocations of aluminum. II. NMR and microcalorimetry results. *Microporous and Mesoporous Materials*, **39**, 43-56.
272. **Ohtsuka, K., Yoshimasa Hayashi and Mitsuru Suda** (1993) Microporous ZrO<sub>2</sub>-pillared clays derived from three kinds of Zr polynuclear ionic species. *Chemistry of Materials*, **5**, 1823-1829.
273. **Okada, K., N. Arimitsu, Y. Kameshima, and K.J.D. MacKenzie** (2006) Solid acidity of 2:1 type clay minerals activated by selective leaching. *Applied Clay Science*, **31**, 185-193.
274. **Okamoto, M., S. Morita and T. Kotaka** (2001) Dispersed structure and ionic conductivity of smectic clay/polymer nanocomposites. *Polymer*, **42**, 2685-2688.



275. **Olaya, A., G. Blanco, S. Bernal, S. Moreno and R. Molina** (2009c). Synthesis of pillared clays with Al-Fe and Al-Fe-Ce starting from concentrated suspensions of clay using microwaves or ultrasound, and their catalytic activity in the phenol oxidation reaction. *Applied Catalysis B: Environmental*, **93**, 56–65.
276. **Olaya, A., S. Moreno and R. Molina** (2009a). Synthesis of pillared clays with Al by means of concentrated suspensions and microwave radiation. *Catalysis Communications*, **10**, 697–701.
277. **Olaya, A., S. Moreno and R. Molina** (2009b) Synthesis of pillared clays with Al(13)-Fe and Al(13)-Fe-Ce polymers in solid state assisted by microwave and ultrasound: characterization and catalytic activity. *Applied Catalysis A: General*, **370**, 7–15.
278. **Oliveira, L.C.A., R.M. Lago, J.D. Fabris and K. Sapag** (2008) Catalytic oxidation of aromatic VOCs with Cr or Pd-impregnated Al-pillared bentonite: Byproduct formation and deactivation studies. *Applied Clay Science*, **39**, 218–222
279. **Pan, J., C. Wang, S. Guo, J. Li and Z. Yang** (2008) Cu supported over Al-pillared interlayer clays catalysts for direct hydroxylation of benzene to phenol. *Catalysis Communications*, **9**, 176–181.
280. **Patel, U. D. and S. Suresh** (2007) Dechlorination of chlorophenols using magnesium–palladium bimetallic system. *Journal of Hazardous Materials*, **147**, 431–438.
281. **Pavlidou, S. and C.D. Papaspyrides** (2008) A review on polymer–layered silicate nanocomposites. *Progress in Polymer Science*, **33**, 1119–1198.
282. **Pérez, A., M. Montes, R. Molina and S. Moreno** (2014) Modified clays as catalysts for the catalytic oxidation of ethanol. *Applied Clay Science*, **95**, 18–24.
283. **Pinnavaia, T.J.** (1983) Intercalated clay catalysts. *Science*, **220**, 365–371.
284. **Pinnavaia, T.J., M.S. Tzou and S.D. Landau** (1985a) New chromia pillared clay catalysts. *Journal of American Chemical Society*, **107**, 4783–4785.
285. **Pinnavaia, T.J., S.D. Landaum M-N. Tzou and I.D. Johnson** (1985b) Layer cross-linking in pillared clays. *Journal of American Chemical Society*, **107**, 7222–7224
286. **Pizarro, A.H., C.B. Molina, J.A. Casas and J.J. Rodriguez** (2014) Catalytic HDC/HDN of 4-chloronitrobenzene in water under ambient-like conditions with Pd supported on pillared clay. *Applied Catalysis B: Environmental*, **158–159**, 175–181.
287. **Platonov, V.A.** (2000) Properties of polyphosphoric acid. *Fibre Chemistry*, **32**, 325–329.
288. **Plee, D., F. Borg, L. Gataineau and J.J. Fripiat** (1985) High resolution solid-state  $^{27}\text{Al}$  and  $^{29}\text{Si}$  nuclear magnetic resonance study of pillared clays. *Journal of American Chemical Society*, **107**, 2362–2369.
289. **Pore, D.M., T.S. Shaikh, N.G. Patil, S.B. Dongare, and U. V. Desai** (2010) Envirocat EPZ-10: a solid acid catalyst for the synthesis of 1,8-dioxo-octahydroxanthenes in aqueous medium. *Synthetic Communications*, **40**, 2215–2219.
290. **Poupelin, J.P., G. S.-Ruf, O. F.-Blanpin, G. Narcisse, G. U.-Ernouf and R. Lacroix** (1978) Synthesis and antiinflammatory properties of bis (2-hydroxy-1-naphthyl) methane derivatives. *European Journal of Medicinal Chemistry*, **13**, 67–71.

291. **Qi, G., R. T. Yang and L. T. Thompson** (2004) Catalytic reduction of nitric oxide with hydrogen and carbon monoxide in the presence of excess oxygen by Pd supported on pillared clays. *Applied Catalysis A: General*, **259**, 261–267.
292. **R.A.P. Castanheiro, M.M.M. Pinto, S.M.M. Cravo, D.C.G.A. Pinto, A.M.S. Silva and A. Kijjoa** (2009) Improved methodologies for synthesis of prenylated xanthenes by microwave irradiation and combination of heterogeneous catalysis (K10 clay) with microwave irradiation. *Tetrahedron*, **65**, 3848–3857.
293. **Rajamathi, M., G.S. Thomas and P. Vishnu Kamath** (2001) The many ways of making anionic clays. *Proceedings of Indian academy of Sciences (Chemical Sciences)*, **113**, 671-680.
294. **Rajkumar, T. and G. RangaRao** (2008) Synthesis and characterization of hybrid molecular material prepared by ionic liquid and silicotungstic acid. *Materials Chemistry and Physics*, **112**, 853–857.
295. **Ramaswamy, V., M. S. Krishnan and A.V. Ramaswamy** (2002) Immobilization and characterization of copper chlorophthalocyanine on alumina-pillared montmorillonite. *Journal of Molecular Catalysis A: Chemical*, **181**, 81–89.
296. **Ramaswamy, V., S. Malwadkar and S. Chilukuri** (2008) Cu–Ce mixed oxides supported on Al-pillared clay: Effect of method of preparation on catalytic activity in the preferential oxidation of carbon monoxide. *Applied Catalysis B: Environmental*, **84**, 21–29.
297. **Ramin, G.-V. and S. Hajar** (2013) Highly efficient one-pot synthesis of tetrahydropyridines. *Comptes Rendus Chimie*, **16**, 1047–1054.
298. **Ranga Rao, G. and B.G. Mishra** (2005). A comparative UV–vis-diffuse reflectance study on the location and interaction of cerium ions in Al- and Zr-pillared montmorillonite clays. *Materials Chemistry and Physics*, **89**, 110–115.
299. **Ranga Rao, G. and B.G. Mishra** (2007) Al-pillared clay supported CuPd catalysts for nitrate reduction. *Journal of Porous Materials*, **14**, 205-212.
300. **Ranga Rao, G., H.R. Sahu and B.G. Mishra** (2003) Vapor phase reduction of cyclohexanone to cyclohexanol on  $Ce_xZr_{1-x}O_2$  solid solutions. *Reaction Kinetics & Catalysis Letters*, **78**, 151-159.
301. **Ravindra Reddy, C., G. Nagendrappa and B.S. Jai Prakash** (2007) Surface acidity study of  $Mn^+$ -montmorillonite clay catalysts by FT-IR spectroscopy: Correlation with esterification activity. *Catalysis Communications*, **8**, 241–246.
302. **Ravindra Reddy, C., Y.S. Bhat, G. Nagendrappa and B.S. Jai Prakash** (2009) Brønsted and Lewis acidity of modified montmorillonite clay catalysts determined by FT-IR spectroscopy. *Catalysis Today*, **141**, 157–160.
303. **Ray, S.S. and M. Okamoto** (2003) Polymer/layered silicate nanocomposites: a review from preparation to processing, *Progress in Polymer Science*, **28**, 1539–1641.
304. **Ren, Y., G. Fan and C. Wang** (2014) Aqueous hydrodechlorination of 4-chlorophenol over an Rh/reduced graphene oxide synthesized by a facile one-pot solvothermal process under mild conditions. *Journal of Hazardous Materials*, **274**, 32–40.

305. **Rhodes, N.C. and D.R. Brown** (1993) Surface properties and porosities of silica and acid-treated montmorillonite catalyst supports: Influence on activities of supported ZnCl<sub>2</sub> alkylation catalysts. *Journal of Chemical Society, Faraday Transactions*, **89(9)**, 1387-1391.
306. **Rivallan, M., G. Berlier, G. Ricchiardi, A. Zecchina, M. T. Nechita and U. Olsbye** (2008) Characterisation and catalytic activity in de-NO<sub>x</sub> reactions of Fe-ZSM-5 zeolites prepared via ferric oxalate precursor. *Applied Catalysis B: Environmental*, **84**, 204–213.
307. **Rombi, E., M.G. Cutrufello, S. De Rossi, M.F. Sini and I. Ferino** (2006) Catalytic nitrooxidation of 1-methylnaphthalene I. Preparation, characterisation and NO-surface interactions of chromia/alumina-based catalysts. *Journal of Molecular Catalysis A: Chemical*, **247**, 171–181.
308. **Romero-Pérez, A., A. Infantes-Molina, A. Jiménez-López, E.R. Jalil, K. Sapag and E. Rodríguez-Castellón** (2012) Al-pillared montmorillonite as a support for catalysts based on ruthenium sulfide in HDS reactions. *Catalysis Today*, **187**, 88–96.
309. **Rondon, P., V.C. Casilda, R.M.M. Aranda, B. Casal, C.J.D. Valle and M.L.R. Cervantes** (2006) Catalysis by basic carbons: preparation of dihydropyridines. *Applied Surface Science*, **252**, 6080–6083.
310. **Rosa-Brussin, M.F.** (1995) The use of clays for the hydrotreatment of heavy crude oils. *Catalysis Review Science & Engineering*, **37**, 1-100.
311. **Rossi, S.D., M.P. Casaletto, G. Ferraris, A. Cimino and G. Minelli** (1998) Chromia/zirconia catalysts with Cr content exceeding the monolayer. A comparison with chromia/alumina and chromia/silica for isobutane dehydrogenation. *Applied Catalysis A: General*, **167**, 257-270.
312. **Roulia, M.** (2005) Synthesis and characterization of novel chromium pillared clays. *Materials Chemistry and Physics*, **91**, 281–288.
313. **Ruiz-Hitzky, E., P. Aranda, M. Darder and G. Rytwo** (2010) Hybrid materials based on clays for environmental and biomedical applications. *Journal of Materials Chemistry*, **20**, 9306–9321.
314. **Sachdev, D. and A. Dubey** (2013) Mesoporous silica/polyphosphoric acid (SBA-15/PPA) nanocomposites for acylation of naphthalene. *Catalysis Communications*, **39**, 39–43.
315. **Sadanandam, P., V. Jyothi, M. A. Chari, P. Das and K. Mukkanti** (2011) Synthesis and characterization of 9-methyl-2-morpholin-4-yl-8-substituted phenyl-1H-purine derivatives using polyphosphoric acid (PPA) as an efficient catalyst. *Tetrahedron Letters*, **52**, 5521–5524.
316. **Sadykov, V., T. Kuznetsova, V. Doronin, R. Bunina, G. Alikina, L. Batuev, V. Matyshak, A. Rozovskii, V. Tretyakov, T. Burdeynaya, V. Lunin and J. Ross** (2006) NO<sub>x</sub> SCR by decane and propylene on Pt+Cu/Zr-pillared clays in realistic feeds: Performance and mechanistic features versus structural specificity of nanosized zirconia pillars. *Catalysis Today*, **114**, 13–22.
317. **Sainero, L.M. G.-, X.L. Seoane and A. Arcoya** (2004) Hydrodechlorination of carbon tetrachloride in the liquid phase on a Pd/carbon catalyst: kinetic and mechanistic studies. *Applied Catalysis B: Environmental*, **53**, 101–110.
318. **Salerno, P. and S. Mendioroz** (2002) Preparation of Al-pillared montmorillonite from concentrated dispersions. *Applied Clay Science*, **22**, 115 – 123.

319. **Salerno, P., M.B. Asenjo** and **S. Mendioroz** (2001) Molybdenum species identification on pillared clays by temperature programmed reduction. *Thermochimica Acta*, **379**, 111-115.
320. **Samantaray, S., S.K. Sahoo** and **B.G. Mishra** (2011) Phosphomolybdic acid dispersed in the micropores of sulfate treated Zr-pillared clay as efficient heterogeneous catalyst for the synthesis of  $\beta$ -aminocarbonyl compounds in aqueous media. *Journal of Porous Materials*, **18**, 573–580.
321. **Samantaray, S., P. Kar, G. Hota,** and **B.G. Mishra** (2013) Sulfate Grafted Iron Stabilized Zirconia Nanoparticles as Efficient Heterogeneous Catalysts for Solvent-Free Synthesis of Xanthenediones under Microwave Irradiation. *Industrial & Engineering Chemistry Research*, **52**, 5862–5870.
322. **Sanabria, N.R., R. Molina** and **S. Moreno** (2009a) Effect of ultrasound on the structural and textural properties of Al-Fe pillared clays in a concentrated medium. *Catalysis Letters*, **130**, 664–671.
323. **Sanabria, N.R., M.A. Centeno, R. Molina** and **S. Moreno** (2009b) Pillared clays with Al-Fe and Al-Ce-Fe in concentrated medium: synthesis and catalytic activity. *Applied Catalysis A: General*, **356**, 243–249.
324. **Sapag, K.** and **S. Mendioroz** (2001) Synthesis and characterization of micro-mesoporous solids: pillared clays. *Colloids and Surfaces A: Physicochemical and Engineering Aspects*, **187–188**, 141–149.
325. **Sawant, D.P., A. Vinu, J. Justus, P. Srinivasu** and **S.B. Halligudi** (2007) Catalytic performances of silicotungstic acid/zirconia supported SBA-15 in an esterification of benzyl alcohol with acetic acid. *Journal of Molecular Catalysis A: Chemical*, **276** 150–157.
326. **Sayari, A.** and **S. Hamoudi** (2001) Periodic mesoporous silica-based organic-inorganic nanocomposite materials. *Chemistry of Materials*, **13**, 3151-3168.
327. **Scaiano, J.C., J.C. N.-Ferreira, E. Alarcon, P. Billone, C.J. B.Alejo, C-O L. Crites, M. Decan, C. Fasciani, M. G.-Béjar, G.H.-Tapley, M. Grenier, K.L. McGilvray, N.L.Pacioni, A. Pardoe, L.R.-Boisneuf, R.S.-Narbonne, M. J. Silvero, K.G. Stamplecoskie** and **T.-L. Wee** (2011) Tuning plasmon transitions and their applications in organic photochemistry. *Pure and Applied Chemistry*, **83**, 913–930.
328. **Scott, S.L., B.C. Peoples, C. Yung, R.S. Rojas, V. Khanna, H. Sano, T. Suzuki** and **F. Shimizu** (2008) Highly dispersed clay–polyolefin nanocomposites, via in situ polymerization of  $\alpha$ -olefins by clay-supported catalysts. *Chemical Communications*, 4186–4188.
329. **Sdiri, A., T. Higashi, T. Hatta, F. Jamoussi** and **N. Tase** (2011) Evaluating the adsorptive capacity of montmorillonitic and calcareous clays on the removal of several heavy metals in aqueous systems. *Chemical Engineering Journal*, **172**, 37–46.
330. **Seshu Babu, N., N. Lingaiah** and **P.S. Sai Prasad** (2012) Characterization and reactivity of Al<sub>2</sub>O<sub>3</sub> supported Pd-Ni bimetallic catalysts for hydrodechlorination of chlorobenzene. *Applied Catalysis B: Environmental*, **111–112**, 309–316.
331. **Shabtai, J., M. Rossel** and **M. Tokarz** (1984) Cross-linked smectites. III. Synthesis and properties of hydroxy-aluminum hectorites and fluorhectorites. *Clays Clay Minerals*, **32**, 99-107.

332. **Shafiee, M.R.M.** (2014) One-pot preparation of N,N'-alkylidene bisamide derivatives catalyzed by silica supported polyphosphoric acid (SiO<sub>2</sub>-PPA). *Journal of Saudi Chemical Society*, **18**, 115–119.
333. **Shakibaei, G. I., P. Mirzaei and A. Bazgir** (2007) Dowex-50W promoted synthesis of 14-aryl-14H-dibenzo[a,j]xanthene and 1,8-dioxo-octahydroxanthene derivatives under solvent-free conditions *Applied Catalysis A: General*, **325**, 188-192.
334. **Shen, B., H. Ma, C. He and X. Zhang** (2014) Low temperature NH<sub>3</sub>-SCR over Zr and Ce pillared clay based catalysts. *Fuel Processing Technology*, **119**, 121–129.
335. **Shimizu, K.-i., T. Higuchi, E. Takasugi, T. Hatamachi, T. Kodama and A. Satsuma** (2008) Characterization of Lewis acidity of cation-exchanged montmorillonite K-10 clay as effective heterogeneous catalyst for acetylation of alcohol. *Journal of Molecular Catalysis A: Chemical*, **284**, 89–96.
336. **Shin, E.-J. and M. A. Keane** (1998) Gas phase catalytic hydrodechlorination of chlorophenols using a supported nickel catalyst. *Applied Catalysis B: Environmental*, **18**, 241-250.
337. **Simagina, V., V. Likhobov, G. Bergeret, M.T. Gimenez and A. Renouprez** (2003) Catalytic hydrodechlorination of hexachlorobenzene on carbon supported Pd-Ni bimetallic catalysts. *Applied Catalysis B: Environmental*, **40**, 293–304.
338. **Singh, V., V. Sapehiya and G.L. Kad** (2004a) Ultrasound and microwave activated preparation of ZrO<sub>2</sub>-pillared clay composite: catalytic activity for selective, solventless acylation of 1,n-diols. *Journal of Molecular Catalysis A: Chemical*, **210**, 119–124.
339. **Singh, V., V. Sapehiya and G. L. Kad** (2004b) Novel heterogeneously catalysed selective, solventless monotetrahydropyranylation of different symmetrical 1,n-diols and various alcohols using ZrO<sub>2</sub>-pillared clay. *Catalysis Communications*, **5**, 463–468.
340. **Singh, V., V. Sapehiya, V. Srivastava and S. Kaur** (2006) ZrO<sub>2</sub>-pillared clay: An efficient catalyst for solventless synthesis of biologically active multifunctional dihydropyrimidinones. *Catalysis Communications*, **7**, 571–578.
341. **Singhal, A., L. M. Toth, J. S. Lin and K. Affholter** (1996) Zirconium(IV) tetramer/octamer hydrolysis equilibrium in aqueous hydrochloric acid Solution. *Journal of the American Chemical Society*, **118**, 11529-11534.
342. **Sis, H. and T. Uysal** (2014) Removal of heavy metal ions from aqueous medium using Kuluncak (Malatya) vermiculites and effect of precipitation on removal. *Applied Clay Science*, **95**, 1–8.
343. **Sivaiah, M.V., S. Petit, J. Brendlé and P. Patrier** (2010) Rapid synthesis of aluminium polycations by microwave assisted hydrolysis of aluminium via decomposition of urea and preparation of Al-pillared montmorillonite. *Applied Clay Science*, **48**, 138–145.
344. **Skoularikis, N.D., R.W. Coughlin, A. Kostapapas, K. Carrado and S.L. Suib** (1988) Catalytic performance of iron(III) and chromium(III) exchanged pillared clays, *Applied Catalysis*, **39**, 61–76.
345. **Sowmiya, M., A. Sharma, S. Parsodkar, and B.G. Mishra** (2007) Nanosized sulfated SnO<sub>2</sub> dispersed in the micropores of Al-pillared clay as an efficient catalyst for the synthesis of some biologically important molecules. *Applied Catalysis A: General*, **333**, 272–280.

346. **Sposito, G., R. Prost and J.P. Gaultier** (1983) Infrared spectroscopic study of adsorbed water on reduced-charge Na/Li-montmorillonites. *Clays and Clay Minerals*, **31**, 9-16.
347. **Srebowata, A., W. Juszczak, Z. Kaszkur and Z. Karpinski** (2007) Hydrodechlorination of 1,2-dichloroethane on active carbon supported palladium–nickel catalysts. *Catalysis Today*, **124**, 28–35.
348. **Sridhar, R. and P.T. Perumal** (2005) A new protocol to synthesize 1,4-dihydropyridines by using 3,4,5-trifluoro benzene boronic acid as a catalyst in ionic liquid: synthesis of novel 4-(3-carboxyl-1H-pyrazol-4-yl)-1,4-dihydropyridines. *Tetrahedron*, **61**, 2465–2470.
349. **Sridharan V., P.T. Perumal, C. Avendano and J.C. Menendez** (2007) A new three component domino synthesis of 1,4-dihydropyridines. *Tetrahedron*, **63**, 4407–4413.
350. **Srikanth, C.S., V.P. Kumar, B. Viswanadham and K.V.R. Chary** (2011) Hydrodechlorination of 1,2,4-trichlorobenzene over supported ruthenium catalysts on various supports. *Catalysis Communications*, **13**, 69–72.
351. **Storaro, L., R. Ganzerla, M. Lenarda, R. Zanoni, A.J. Lopez, P.O.-Pastor and E.R. Castellon** (1997) Catalytic behavior of chromia and chromium-doped alumina pillared clay materials for the vapor phase deep oxidation of chlorinated hydrocarbons. *Journal of Molecular Catalysis A: Chemical*, **15**, 329-338.
352. **Su, H., S. Zeng, H. Dong, Y. Du, Y. Zhang and R. Hu** (2009) Pillared montmorillonite supported cobalt catalysts for the Fischer–Tropsch reaction. *Applied Clay Science*, **46**, 325–329.
353. **Su, W., D. Yang, C. Jin and B. Zhang** (2008) Yb(OTf)<sub>3</sub> catalyzed condensation reaction of β-naphthol and aldehyde in ionic liquids: a green synthesis of aryl-14H-dibenzo[a,j]xanthenes *Tetrahedron Letters*, **49**, 3391-3394.
354. **Sun Kou, M.R., S. Mendioroz and M.I. Guisjarro** (1998) A thermal study of Zr-pillared montmorillonite. *Thermochimica Acta*, **323**, 145-157.
355. **Sun, C., Z. Wu, Y. Mao, X. Yin, L. Ma, D. Wang and M. Zhang** (2011) A highly active Pd on Ni–B bimetallic catalyst for liquid-phase hydrodechlorination of 4-chlorophenol under mild conditions. *Catalysis Letters*, **141**, 792–798.
356. **Sun, T. and J.M. Garces** (2002) High-performance polypropylene-clay nanocomposites by in-situ polymerization with metallocene/clay catalysts. *Advanced Materials*, **14**, 128-130.
357. **Swetha, P. and A.S. Kumar** (2013) Phosphomolybdic acid nano-aggregates immobilized nafion membrane modified electrode for selective cysteine electrocatalytic oxidation and anti-dermatophytic activity. *Electrochimica Acta*, **98**, 54– 65.
358. **Sychev, M., N. Kostoglod, E.M. van Oers, V.H.J. de Beer, R.A. van Santen, J. Kornatowski and M. Rozwadowsk** (1995) Synthesis, characterization and catalytic activity of chromia pillared clays. *Studies in Surface Science and Catalysis*, **94**, 39–46.
359. **Sychev, M.V., V.H.J. De Beer and R.A. Van Santen** (1997a) Chromia and chromium sulfide pillared clays differing in pillar density. *Microporous Materials*, **8**, 255-265.
360. **Sychev, M., V. H. J. (San) de Beer, A. Kodentsov, E.M. van Oers, and R.A. van Santen** (1997b) Chromia- and chromium sulfide-pillared clays: Preparation, characterization, and catalytic activity for thiophene hydrodesulfurization. *Journal of Catalysis*, **168**, 245–254.

361. **Taguchi, A.** and **F. Schuth** (2005) Ordered mesoporous materials in catalysis. *Microporous and Mesoporous Materials*, **77**, 1–45.
362. **Tămășan, M., T. Radu** and **V. Simon** (2013) Spectroscopic characterisation and in vitro behaviour of kaolinite polyvinyl alcohol nanocomposite. *Applied Clay Science*, **72**, 147-154.
363. **Thomas, B., V.G. Ramu, S. Gopinath, J. George, M. Kurian, G. Laurent, G.L. Drisko** and **S. Sugunan** (2011) Catalytic acetalization of carbonyl compounds over cation ( $\text{Ce}^{3+}$ ,  $\text{Fe}^{3+}$  and  $\text{Al}^{3+}$ ) exchanged montmorillonites and  $\text{Ce}^{3+}$ -exchanged Y zeolites. *Applied Clay Science*, **53**, 227–235.
364. **Thomas, V., G. Jose, G. Jose, P.I. Paulose** and **N.V. Unnikrishnan** (2002) Spectroscopic characterization of chromium in sol–gel derived silica *Materials Chemistry and Physics*, **77**, 826–830.
365. **Timofeeva, M.N., V.N. Panchenko, A. Gil, V.P. Doronin, A.V. Golovin, A.S. Andreev** and **V.A. Likholobov** (2011a) Effect of the acid–base properties of Zr, Al-pillared clays on the catalytic performances in the reaction of propylene oxide with methanol. *Applied Catalysis B: Environmental*, **104**, 54–63.
366. **Timofeeva, M.N., V.N. Panchenko, A. Gil, Yu A. Chesalov, T.P. Sorokina** and **V.A. Likholobov** (2011b) Synthesis of propylene glycol methyl ether from methanol and propylene oxide over alumina-pillared clays. *Applied Catalysis B: Environmental*, **102**, 433–440.
367. **Tokarský, J., L. Kulhánková, V. Stýskala, K.M. Kutlákova, L. Neuwirthová, V. Matějka** and **P. Čapková** (2013) High electrical anisotropy in hydrochloric acid doped polyaniline/phyllsilicate nanocomposites: Effect of phyllosilicate matrix, synthesis pathway and pressure. *Applied Clay Science*, **80–81**, 126-132.
368. **Tomul, F.** (2011) Effect of ultrasound on the structural and textural properties of copper-impregnated cerium-modified zirconium-pillared bentonite. *Applied Surface Science*, **258**, 1836– 1848.
369. **Tomul, F.** and **S. Balci** (2009) Characterization of Al, Cr-pillared clays and CO oxidation, *Applied Clay Science*, **43**, 13-20.
370. **Toranzo, R., M. A. Vicente** and **M. A. Bañares-Muñoz** (1997) Pillaring of a saponite with aluminum-chromium oligomers. Characterization of the solids obtained. *Chemistry of Materials*, **9**, 1829-1836.
371. **Tyagi, B., C.D. Chudasama** and **R.V. Jasra** (2006) Characterization of surface acidity of an acid montmorillonite activated with hydrothermal, ultrasonic and microwave techniques. *Applied Clay Science*, **31**, 16 – 28.
372. **Tzou M.S.** and **T.J. Pinnavaia** (1988) Chromia pillared clays. *Catalysis Today*, **2**, 243-259.
373. **Urbano, F.J.** and **J.M. Marinas** (2001) Hydrogenolysis of organohalogen compounds over palladium supported catalysts. *Journal of Molecular Catalysis A: Chemical*, **173**, 329–345.
374. **Vaccari, A.** (1998) Preparation and catalytic properties of cationic and anionic clays. *Catalysis Today*, **41**, 53-71.
375. **Vaccari, A.** (1999) Clay and catalysis: A promising future. *Applied Clay Science*, **14**, 161-198.

376. **Valtchev, V. and L. Tosheva** (2013) Porous nanosized particles: preparation, properties, and applications. *Chemical Reviews*, **113**, 6734–6760.
377. **Van de Sandt, E. J. A. X., A. Wiersma, M. Makkee, H. Van Bekkum and J.A. Moulijn** (1998) Selection of activated carbon for the selective hydrogenolysis of CCl<sub>2</sub>F<sub>2</sub> (CFC-12) into CH<sub>2</sub>F<sub>2</sub> (HFC-32) over palladium-supported catalysts. *Applied Catalysis A: General*, **173**, 161-173.
378. **Varma, R.S.** (2002) Clay and clay-supported reagents in organic synthesis. *Tetrahedron*, **58**, 1235-1255.
379. **Vaughan, D.E.W.** (1988) Pillared clays—a historical perspective. *Catalysis Today*, **2**, 187–198.
380. **Vicente, M.A., A. Gil and F. Bergaya** (2013) Chapter 10.5, Pillared Clays and Clay Minerals, *Developments in Clay Science*, **5A**, 523–557.
381. **Vicente, M.A., A. Meyer, E. González, M.A. Bañares-Muñoz, L.M. Gandía and A. Gil** (2002) Dehydrogenation of ethylbenzene on alumina–chromia-pillared saponites. *Catalysis Letters*, **78**, 99-103.
382. **Vicente, M.A., C. Belver, M. Sychev, R. Prihod’ko and A. Gil** (2009) Relationship between the surface properties and the catalytic performance of Al-, Ga-, and AlGa-pillared saponites. *Industrial Engineering Chemistry Research*, **48**, 406–414.
383. **Vicente, M.A., C. Belver, R. Trujillano, M.A. Bañares-Munoz, V. Rives, S.A. Korili, A. Gil, L.M. Gandia and J.-F. Lambert** (2003) Preparation and characterisation of vanadium catalysts supported over alumina-pillared clays. *Catalysis Today*, **78**, 181-190.
384. **Vijayakumar, B. and G. Ranga Rao** (2012a) Synthesis of 3,4-dihydropyrimidin-2(1H)-ones/thiones using ZrOCl<sub>2</sub>/mont K10 under microwave assisted solvent-free conditions. *Journal of Porous Materials*, **19**, 491–497.
385. **Vijayakumar, B. and G. Ranga Rao** (2012b) PWA/montmorillonite K10 catalyst for synthesis of coumarins under solvent-free conditions. *Journal of Porous Materials*, **19**, 233–242
386. **Volzone, C.** (1995) Hydroxy-chromium smectite: Influence of Cr added. *Clays and Clay Minerals*, **43**, 377-382.
387. **Volzone, C.,** (2001) Pillaring of different smectites members by chromium species (Cr-PILCs). *Microporous and Mesoporous Materials*, **49**, 197-202.
388. **Volzone, C., A.M. Cesio, R.M.T. Sanchez and E. Pereira** (1993) Hydroxy-chromium smectite. *Clays and Clay Minerals*, **41**, 702-706.
389. **Wang, H.-J., L.-P. Mo and Z.-H. Zhang** (2011) Cerium ammonium nitrate-catalyzed multicomponent reaction for efficient synthesis of functionalized tetrahydropyridines. *ACS Combinatorial Science*, **13**, 181–185.
390. **Wang, J.-Q. and R.G. Harvey** (2002) Synthesis of polycyclic xanthenes and furans via palladium catalyzed cyclization of polycyclic aryltriflate esters. *Tetrahedron*, **58**, 5927-5931.
391. **Wang, N., Y. Shao, Z. Shi, J. Zhang and H. Li** (2008) Influence of MCM-41 particle on mechanical and morphological behavior of polypropylene. *Materials Science and Engineering A*, **497**, 363–368.



392. **Wang, S., H.Y. Zhu and G. Q. (Max) Lu** (1998) Preparation, characterization and catalytic properties of clay-based nickel catalysts for methane reforming. *Journal of Colloid & Interface Science*, **204**, 128-134.
393. **Wang, T., J. Su, X. Jin, Z. Chen, M. Megharaj and R. Naidu** (2013) Functional clay supported bimetallic nZVI/Pd nanoparticles used for removal of methyl orange from aqueous solution. *Journal of Hazardous Materials*, **262**, 819–825.
394. **Weng, X., Q. Sun, S. Lin, Z. Chen, M. Megharaj and R. Naidu** (2014) Enhancement of catalytic degradation of amoxicillin in aqueous solution using clay supported bimetallic Fe/Ni nanoparticles. *Chemosphere*, **103**, 80-85.
395. **Wright, A.P, and M.E. Davis** (2002) Design and preparation of organic–inorganic hybrid catalysts. *Chemical Reviews*, **102**, 3589–3614.
396. **Xiang, X., X.T. Zu, S. Zhu and L.M. Wang** (2004) Optical properties of metallic nanoparticles in Ni-ion-implanted  $\alpha$ -Al<sub>2</sub>O<sub>3</sub> single crystals. *Applied Physics Letters*, **84**, 52-54.
397. **Xu, X., C. Song, J.M. Andresen, B.G. Miller and A.W. Scaroni** (2003) Preparation and characterization of novel CO<sub>2</sub> “molecular basket” adsorbents based on polymer-modified mesoporous molecular sieve MCM-41. *Microporous and Mesoporous Materials*, **62**, 29–45.
398. **Yadav, G.D. and O.V. Badure** (2008) Selective acylation of 1,3-dibenzyloxybenzene to 3,5-dibenzyloxyacetophenone over cesium modified dodecatungstophosphoric acid (DTP) on clay. *Applied Catalysis A: General*, **348**, 16–25.
399. **Yadav, G.D. and S.R. More** (2011) Green alkylation of anisole with cyclohexene over 20% cesium modified heteropoly acid on K-10 acidic montmorillonite clay. *Applied Clay Science*, **53**, 254–262.
400. **Yadav, M.K., C.D. Chudasama and R.V. Jasra** (2004) Isomerisation of  $\alpha$ -pinene using modified montmorillonite clays. *Journal of Molecular Catalysis A: Chemical*, **216**, 51–59.
401. **Yamanaka, S. and G.W. Brindley** (1979) High surface area solids obtained by reaction of montmorillonite with zirconyl chloride. *Clays and Clay Minerals*, **27**, 119-124.
402. **Yamuna, E., M. Zeller and K.J.R. Prasad** (2011) InCl<sub>3</sub>-catalyzed four-component reaction: a novel synthesis of N-carbazolyl dihydropyridines. *Tetrahedron Letters*, **52**, 6805–6808.
403. **Yang, B., S. Deng, G. Yu, H. Zhang, J. Wu and Q. Zhuo** (2011) Bimetallic Pd/Al particles for highly efficient hydrodechlorination of 2-Chlorobiphenyl in acidic aqueous solution. *Journal of Hazardous Materials*, **189**, 76–83.
404. **Yapar, S., R. Torres-Sa´nchez, M. Emreol, P. Weidler and K. Emmerich** (2009) Microwave irradiation used for all steps of pre-pillaring Al-montmorillonite. *Clay Minerals*, **44**, 267–278.
405. **Yuan, G. and M.A. Keane** (2007) Aqueous-Phase hydrodechlorination of 2,4-Dichlorophenol over Pd/Al<sub>2</sub>O<sub>3</sub>:reaction under controlled pH. *Industrial & Engineering Chemistry Research*, **46**, 705-715.
406. **Yurdakoc, M. , M. Akcay, Y. Tonbul, F. Ok and K. Yurdakoc** (2008) Preparation and characterization of Cr- and Fe-pillared bentonites by using CrCl<sub>3</sub>, FeCl<sub>3</sub>, Cr(acac)<sub>3</sub> and Fe(acac)<sub>3</sub> as precursors. *Microporous and Mesoporous Materials*, **111**, 211–218.

407. **Zhang, D., C.-H. Zhou, C.-X. Lin, D.-S. Tong and W.-H. Yu** (2010) Synthesis of clay minerals. *Applied Clay Science*, **50**, 1–11.
408. **Zhang, F. and J. Yu** (2010) The research for high-performance SBR compound modified asphalt. *Construction and Building Materials*, **24**, 410–418.
409. **Zhang, M., D.B. Bacik, C.B. Roberts and D. Zhao** (2013a) Catalytic hydrodechlorination of trichloroethylene in water with supported CMC-stabilized palladium nanoparticles. *Water Research*, **47**, 3706–3715.
410. **Zhang, X., G. Dou, Z. Wang, L. Li, Y. Wang, H. Wang and Z. Hao** (2013b) Selective catalytic oxidation of H<sub>2</sub>S over iron oxide supported on alumina-intercalated Laponite clay catalysts. *Journal of Hazardous Materials*, **260**, 104–111.
411. **Zhao, H., C.H. Zhou, L.M. Wu, J.Y. Lou, N. Li, H.M. Yang, D.S. Tong and W.H. Yu** (2013) Catalytic dehydration of glycerol to acrolein over sulfuric acid-activated montmorillonite catalysts. *Applied Clay Science*, **74**, 154–162.
412. **Zhao, Y., S. Fu, H. Li, X. Tian and C. Nie** (2008) An investigation into the surface phase of nanostructured zirconia by conventional UV spectroscopy. *Materials Letters*, **62**, 2207–2210.
413. **Zhou, J., P. Wu, Z. Dang, N. Zhu, P. Li, J. Wu and X. Wang** (2010) Polymeric Fe/Zr pillared montmorillonite for the removal of Cr(VI) from aqueous solutions. *Chemical Engineering Journal*, **162**, 1035–1044.
414. **Zhou, S., C. Zhang, X. Hu, Y. Wang, R. Xu, C. Xia, H. Zhang and Z. Song** (2014) Catalytic wet peroxide oxidation of 4-chlorophenol over Al-Fe-, Al-Cu-, and Al-Fe-Cu-pillared clays: Sensitivity, kinetics and mechanism. *Applied Clay Science*, **95**, 275–283.
415. **Zhu, J., K. Kailasam, X. Xie, R. Schomaecker and A. Thomas** (2011) High-surface-area SBA-15 with enhanced mesopore connectivity by the addition of poly(vinyl alcohol). *Chemistry of Materials*, **23**, 2062–2067.
416. **Zuo, S. and R. Zhou** (2006) Al-pillared clays supported rare earths and palladium catalysts for deep oxidation of low concentration of benzene. *Applied Surface Science*, **253**, 2508–2514.
417. **Zuo, S. and R. Zhou** (2008) Influence of synthesis condition on pore structure of Al pillared clays and supported Pd catalysts for deep oxidation of benzene. *Microporous and Mesoporous Materials*, **113**, 472–480.
418. **Zuo, S., Q. Huang, J. Li and R. Zhou** (2009) Promoting effect of Ce added to metal oxide supported on Al pillared clays for deep benzene oxidation. *Applied Catalysis B: Environmental*, **91**, 204–209.
419. **Zuo, S., R. Zhou and C. Qi** (2011) Synthesis and characterization of aluminum and Al/REE pillared clays and supported palladium catalysts for benzene oxidation. *Journal of Rare Earths*, **29**, 52–57.

## LIST OF PUBLICATIONS

### Refereed Journals

1. **Purabi Kar, B.G. Mishra, S.R. Pradhan**, Polyphosphoric acid–zirconia pillared clay composite catalytic system for efficient multicomponent one pot synthesis of tetrahydropyridines under environmentally benign conditions, *Journal of Molecular Catalysis A: Chemical* 387 (2014) 103–111.
2. **Purabi Kar and B. G. Mishra**, Hydrodehalogenation of Halogenated Organic Contaminants from Aqueous Sources by Pd Nanoparticles Dispersed in the Micropores of Pillared Clays Under Transfer Hydrogenation Condition, *Journal of Cluster Science* 25 (2014) 1463-1478.
3. **Purabi Kar, B.G. Mishra**, Silicotungstic acid nanoparticles dispersed in the micropores of Cr-pillared clay as efficient heterogeneous catalyst for the solventfree synthesis of 1,4-dihydropyridines, *Chemical Engineering Journal* 223 (2013) 647–656.
4. **Purabi Kar, Satish Samantaray, B. G. Mishra**, Catalytic application of chromia-pillared montmorillonite towards environmentally benign synthesis of octahydroxanthenes, *Reaction Kinetics Mechanism & Catalysis* 108 (2013) 241–251.

### Manuscript under review

5. **Purabi Kar and B.G. Mishra**, Potential application of Pd based bimetallic nanoparticles dispersed in Al-pillared clay matrix as catalyst for the hydrodehalogenation of halogenated aromatics under environmentally benign conditions. Communicated.
6. **Purabi Kar, A. Nayak, and B.G. Mishra**, Catalytic application of Zr-Pillared clay-sulfonated polyvinyl alcohol composite catalytic system for one pot multicomponent synthesis of hexahydropyrimidines, Communicated

### Other publications

7. **S. Samantaray, P. Kar, G. Hota, and B. G. Mishra**, Sulfate Grafted Iron Stabilized Zirconia Nanoparticles as Efficient Heterogenous Catalysts for Solvent-Free Synthesis of Xanthenediones under Microwave Irradiation, *Industrial Engineering & Chemistry Research*, 2013, 52, 5862–5870.

### In Conferences/symposia

1. **Purabi Kar and B.G. Mishra**, Novel synthesis of tetrahydropyridines using polyphosphoric acid intercalated zirconia pillared montmorillonite, *16th CRSI National Symposium in Chemistry (NSC-16)*, 7th -9th February, 2014, Department of Chemistry, IIT Bombay, Mumbai, India.

2. **Purabi Kar and B. G. Mishra**, Treatment of halogenated organic compounds using supported Pd bimetallics dispersed in the micropores of Al-pillared clay, *3rd International Conference on Advanced Nanomaterials & Nanotechnology*, 1st-3rd December 2013, Department of Chemistry, IIT Guwahati, India.
3. **Purabi Kar, Satish Samantaray, B. G. Mishra**, Chromium pillared clays and its modified analogues as efficient heterogeneous catalyst for synthesis of Xanthene derivatives and Dihydropyridines, *14th CRSI National Symposium in Chemistry*, 3rd - 5th February 2012, National Institute for Interdisciplinary Science and Technology (NIIST), Thiruvananthapuram, Kerala, India.
4. **Purabi Kar, B. G. Mishra**, Preparation, characterization and catalytic application of vanadia supported Cr-pillared clay for oxidation of aniline, *Silver Jubilee Annual Conference of Orissa Chemical Society & National Conference on Molecule*, 24-26th December 2011, Department of Chemistry, Sambalpur University, Burla, Odisha, India.
5. **Satish Samantaray, Purabi Kar, Prabhat kumar Subudhi and B. G. Mishra**, Selective synthesis and stability of t-zirconia nanoparticles; structural properties, *13th CRSI NSC and 5th CRSI RSC symposium in chemistry 4-6th February 2011*, Department of Chemistry, NISER and KIIT university, Bhubaneswar, India.